

©2009

Eric Andrew Balint

ALL RIGHTS RESERVED

DEVELOPMENT OF A FIBER-REINFORCED MENISCUS SCAFFOLD

by

ERIC ANDREW BALINT

A Dissertation submitted to the

Graduate School-New Brunswick

Rutgers, The State University of New Jersey

And

The Graduate School of Biomedical Sciences

University of Medicine and Dentistry of New Jersey

In partial fulfillment of the requirements

For the degree of

Doctor of Philosophy

Graduate Program in Biomedical Engineering

Written under the direction of

Charles J. Gatt, Jr., M.D.

And approved by

---

---

---

---

New Brunswick, New Jersey

October, 2009

## ABSTRACT OF THE DISSERTATION

### Development of a Fiber-Reinforced Meniscus Scaffold

By ERIC ANDREW BALINT

Dissertation Director:  
Charles J. Gatt Jr., M.D.

The meniscus provides protection to the articular cartilage of the knee by transmitting loads through the joint, distributing high peak stresses on the underlying surfaces, providing shock absorption, and aiding in joint lubrication. It is well accepted that significant loss of meniscal tissue leads to degenerative changes in the joint. Treatment alternatives for patients suffering from severe meniscal deficiency are limited, and thus far have not been shown to offer long-term protection to the underlying cartilage.

This dissertation describes the development of a tissue engineered meniscus scaffold comprised of a chemically crosslinked type I collagen sponge reinforced with resorbable polymer fibers. The long-term goal of this work is to develop a resorbable scaffold which promotes the growth of fibrocartilaginous-like tissue while preventing or delaying degenerative changes in the underlying articular surfaces.

Preliminary evaluation was completed on several potential designs varying in fiber orientation, collagen sponge density, and overall geometry. Two were

chosen to evaluate a series of hypotheses related to their biomechanical properties, *in vitro* biocompatibility, and *in vivo* biocompatibility. Both designs were found to possess the structural properties necessary to function as a load-bearing device in the knee. Furthermore, they were fabricated from resorbable materials which supported the proliferation of fibrochondrocytes *in vitro*. A non-functional evaluation in a rabbit model demonstrated the scaffold to elicit a biological response appropriate for a resorbable device. From the results of these experiments, one design was chosen for functional evaluation in a large animal model.

Scaffolds were implanted at the site of a total meniscectomy in a sheep knee. Short-term results demonstrated that scaffolds incorporated into the joint and elicited an appropriate biological response. However, observed neo-tissue did not possess the high organization inherent to fibrocartilaginous tissues. Furthermore, scaffolds were found to have a limited protective effect on the articular cartilage as variable levels of degenerative changes were observed for all subjects. Results from this evaluation showed proof of principle for this type of scaffold for the treatment of significant meniscal deficiency. However, further optimization of the device is required before it can proceed to clinical evaluation.

## **Acknowledgements**

First and foremost, thank you to my family, especially Mom and Dad, for their continued love, support, and advice; my sister, Erin, for always being there for me; my brother, Andy, for keeping me laughing no matter what; and my new brother Joe, for taking care of the best little sister a guy could ask for.

Thank you to my friends, who have always been there for me and kept me grounded, especially the four biggest jerks I know: Chia, Dvir, Nate, and Jai ... I love you guys. Thank you also to Joey, Charmaine, Keren “Cheese Sandwich!”, and Cindy for their friendship. And thank you to Theresa for being there at the start. I wish you were there at the finish.

Thank you to my advisors, Charles Gatt and Michael Dunn, for their advice and direction to get me started on the project, their optimism and encouragement when things got tough, and their patience when I screwed up. And thank you to the rest of my dissertation committee, Noshir Langrana and Michael Jaffe, for their support and guidance.

A big thank you to Ida Snyder, Mary Barrett, Barbara Perry, Eleanor Kehoe, and John Kehoe for going the extra mile for me when I really needed it. Thank you to Dr. Marion Gordon, Rita Hahn, and John Beloni for their invaluable help with last portion of the study. Thank you also to Joachim Kohn and Sanjeeva Murthy for providing the polymer fiber for this project. And thank you to Dr. Parisa Javidian for help with the histology.

Thank you to the past and present Ortho crew for their friendship and putting up with me and my occasional lapses of maturity: Mark “The Nose” Ohan, Jay “Dr. J” Saleh, Andrea “HEY!” Caruso, Jordan Katz, Nick Tovar, Elaina “Panas” Panas, Aaron “se-TO!” Seto, and Aaron “Wild Spirit” Merriam.

Thank you to all the members of the 108<sup>th</sup> Civil Engineer Squadron – “Ride the Bull!” – especially my commander, Lt Col Paul Novello, for his constant support and mentorship; and also my fellow Scummers, who have done their best over the years to completely destroy my liver (it’s still kickin’!).

To anyone else I forgot (hopefully you know who you are), thank you for making me laugh, for being a positive influence in my life, and for making me get up and walk when I just wanted to sit.

This work was supported by funding from the National Institute of Arthritis and Musculoskeletal and Skin Diseases (NIAMS), National Institutes of Health (NIH), grant# R21 AR052118; the Center for Military Biomaterials Research (CeMBR), The New Jersey Center for Biomaterials; The Armed Forces Institute of Regenerative Medicine (AFIRM); the UMDNJ NJCST Technology Commercialization Fund; and summer fellowships from the New Jersey Center for Biomaterials.

# Table of Contents

TITLE PAGE .....	i
ABSTRACT OF DISSERTATION .....	ii
ACKNOWLEDGEMENTS .....	iv
TABLE OF CONTENTS.....	vi
LIST OF TABLES .....	xi
LIST OF FIGURES.....	xii
1. INTRODUCTION.....	1
1.1. The Meniscus .....	1
1.1.1. Gross Anatomy .....	1
1.1.2. Vasculature .....	2
1.1.3. Microscopic Anatomy.....	3
1.1.3.1. Extracellular Matrix (ECM) .....	3
1.1.3.2. Cells .....	6
1.1.4 Structure and Function.....	6
1.1.4.1. Function.....	6
1.1.4.2. Geometry .....	7
1.1.4.3. Tissue Attachments .....	7
1.1.4.4. Structural Mechanics .....	8
1.1.4.5. Material Properties .....	10
1.2. Injury to the Meniscus .....	13
1.2.1. Options After a Meniscus Injury .....	14
1.3. Tissue Engineering Strategies for the Meniscus.....	15
1.3.1. Functional Tissue Engineering .....	15

1.3.2. Meniscus Allografts .....	18
1.3.3. Meniscus Scaffold .....	19
1.3.3.1. Permanent Prostheses .....	20
1.3.3.2. Resorbable, Synthetic Polymer Scaffolds .....	20
1.3.3.3. Collagen-Based Scaffolds .....	21
1.4 Rationale and Design for Proposed Meniscus Scaffold .....	22
1.4.1. Collagen Matrix .....	23
1.4.2. Fiber Reinforcement .....	25
1.4.2.1.....	25
1.4.2.2. Organizational Pattern of Embedded Fibers .....	26
1.5 Study Overview.....	29
Phase I.....	30
Phase II.....	31
Phase III.....	32
<b>2. METHODS .....</b>	<b>34</b>
<b>Phase I: Preliminary Development of Fiber Reinforced Meniscus Scaffolds (FRMS)</b>	
<b>2.1. First Generation FRMSs .....</b>	<b>34</b>
<b>2.1.1. Mechanical Characterization of First Generation FRMSs .....</b>	<b>36</b>
<b>2.2 Second Generation FRMSs.....</b>	<b>37</b>
<b>2.2.1. Rationale for Design Modifications .....</b>	<b>37</b>
<b>2.2.2. Increasing the Amount of Reinforcing Polymer Fibers.....</b>	<b>38</b>
<b>2.2.3. Fabrication Procedure of Second Generation FRMSs .....</b>	<b>40</b>
<b>2.2.3.1. Materials .....</b>	<b>41</b>
<b>2.2.3.2. Scaffold Fabrication.....</b>	<b>42</b>
<b>2.2.4. Projected Mechanical Properties of Second Generation FRMSs .....</b>	<b>46</b>
<b>Phase II: <i>In Vitro</i> Characterization of the FRMS</b>	

2.3. Mechanical Characterization of Meniscal Scaffolds .....	48
2.3.1. Conversion of Axial Compressive Loads to Tensile Hoop Stresses..	48
2.3.1.1. Setup of Dual Instron Mechanical Testing System .....	48
2.3.1.2. Experimental Testing Protocol Using Dual Instron System.....	50
2.3.2. Pressure Distribution on Tibial Plateau .....	51
2.3.3. Circumferential Tensile Testing.....	53
2.4. Characterization of <i>In Vitro</i> Biological Response to Scaffolds .....	55
2.4.1. Cell Line Harvest and Culture .....	55
2.4.2. Scaffold Preparation.....	56
2.4.3. Cell Seeding of Scaffolds .....	57
2.4.4. Cell Viability Biochemical Analysis .....	57
2.4.5. Histological Analysis .....	59
<b>Phase III: <i>In Vivo</i> Evaluation of the FRMS</b>	
2.5. Preliminary <i>In Vivo</i> Evaluation of FRMS in Rabbit Model .....	60
2.5.1. Overview of Experimental Design .....	60
2.5.2. Scaffold Preparation.....	60
2.5.3. Surgery .....	61
2.5.4. Analysis.....	62
2.6. Functional <i>In Vivo</i> Evaluation of FRMS in Ovine Model.....	64
2.6.1. Overview of Experimental Design .....	64
2.6.2. Surgical Implantation Procedure .....	65
2.6.3. Gross Evaluation .....	67
2.6.4. Biomechanical Analysis .....	68
2.6.4.1. Tensile Testing.....	68
2.6.4.2. Unconfined Compression Testing .....	69
2.6.5. Standard Histological Analysis.....	69

2.6.6. Immunofluorescence Staining .....	69
<b>3. RESULTS .....</b>	<b>72</b>
<b>Phase I: Preliminary Development of Fiber Reinforced Meniscus Scaffolds</b>	
3.1. Mechanical Characterization of First Generation FRMSs .....	72
3.2. Second Generation FRMSs .....	74
3.2.1. Projected Structural Properties .....	74
<b>Phase II: <i>In Vitro</i> Characterization of FRMS</b>	
3.3. Mechanical Characterization of Second Generation FRMSs .....	75
3.3.1. Axial Comp. Loads Converted to Circumferential Tensile Loads .....	75
3.3.2. Evaluation of Load Distribution on Tibial Plateau .....	79
3.3.3. Circumferential Tensile Testing .....	84
3.4. <i>In Vitro</i> Cell Compatibility of FRMS .....	85
3.4.1. Cell Line Harvest and Culture .....	85
3.4.2. Cell Viability Biochemical Analysis .....	86
3.4.3. Historical Analysis .....	86
<b>Phase III: <i>In Vivo</i> Evaluation of FRMS</b>	
3.5. Preliminary <i>In Vivo</i> Evaluation in Rabbit Model .....	89
3.6. Functional <i>In Vivo</i> Evaluation in Ovine Model .....	96
3.6.1. Gross Evaluation .....	96
3.6.2. Biomechanical Analysis .....	100
3.6.2.1. Tensile Testing .....	100
3.6.2.2. Unconfined Compression Testing .....	101
3.6.3. Standard Histological Analysis .....	102
3.6.4. Immunofluorescence Staining .....	112
<b>4. DISCUSSION .....</b>	<b>118</b>
4.1. First Generation Meniscus Scaffolds .....	119

4.2. Second Generation Meniscus Scaffolds.....	120
4.2.1. Design Considerations .....	120
4.3. Mechanical Characterization of Meniscus Scaffolds .....	122
4.3.1. Axial Comp. Loads Converted to Circumferential Tensile Loads.....	123
4.3.2. Pressure Distribution on Tibial Plateau .....	125
4.3.3. Circumferential Tensile Testing.....	128
4.4. <i>In Vitro</i> Cell Compatibility of Meniscus Scaffolds .....	130
4.5. Preliminary <i>In Vivo</i> Evaluation in Rabbit Model .....	133
4.6. Functional <i>In Vivo</i> Evaluation in Ovine Model.....	137
4.6.1. Gross Evaluation .....	138
4.6.2. Surgical Implantation .....	139
4.6.3. Posterior Horn Attachment .....	142
4.6.4. Scaffold Shrinkage .....	143
4.6.5. Biomechanics .....	143
4.6.6. Tissue Incorporation .....	144
4.6.7. Immunofluorescence Staining .....	147
4.6.8. Cartilage Degeneration.....	148
4.6.9. Limitations.....	150
4.7. Future Directions .....	151
5. CONCLUSION .....	153
6. REFERENCES.....	157
APPENDICES.....	169
CURRICULUM VITA.....	171

## List of Tables

<b>Table 2.1.</b>	Projected Structural Properties of Second Generation Scaffolds.....	40
<b>Table 2.2.</b>	Standard Curve for Time Points of Cell Viability Assay.....	58
<b>Table 2.3.</b>	Grading System Used By Pathologist to Qualitatively Evaluate Biological Response to Meniscus Scaffold Wedges Implanted Intrarticularly.....	63
<b>Table 3.1.</b>	Yield Load and Stiffness of First Generation FRMSs Compared to Respective Calculated Values from Published Data.....	73
<b>Table 3.2.</b>	Measured Yield and Ultimate Load of p(DTD DD) Single Fibers and Projected Yield and Ultimate Loads of MS500 and MS1000 FRMSs.....	74
<b>Table 3.3.</b>	Minimum, Maximum, and Range of Tensile Loads Measured at the Anterior and Posterior Anchor Attachments of FRMSs.....	77
<b>Table 3.4.</b>	Calculated Percentage of Axial Compressive Load Converted to Circumferential Tensile Load for Select Load Ranges.....	79
<b>Table 3.5.</b>	Average Peripheral Height of Scaffolds Before and After Compressive Loading.....	83
<b>Table 3.6.</b>	Post-Operative Timeline of Sheep After Implantation of FRMS.....	97
<b>Table 3.7.</b>	Observations of Meniscal Scaffold Made at Sacrifice.....	97

## List of Figures

<b>Figure 1.1.</b>	Illustration of Tibial Plateau with Lateral and Medial Menisci .....	2
<b>Figure 1.2.</b>	Illustration of the Arrangement of the Collagen Fiber Network in the Normal Meniscus .....	4
<b>Figure 1.3.</b>	Micrographs of an Ovine Meniscus Showing Circumferentially Arranged Collagen Fibers.....	4
<b>Figure 1.4.</b>	Micrographs of an Ovine Meniscus Showing Radial Tie Fibers Among Circumferentially Arranged Collagen Fibers .....	5
<b>Figure 1.5.</b>	Free Body Diagram of Meniscus .....	9
<b>Figure 1.6.</b>	Young's Modulus of the Human Lateral and Medial Meniscus.....	11
<b>Figure 1.7.</b>	Poly(desaminotyrosyl-tyrosine dodecyl ester dodecanoate)(12,10).....	26
<b>Figure 1.8.</b>	Assembly of Collagen/Synthetic Fiber Ring Scaffold .....	28
<b>Figure 1.9.</b>	Quasi-Circumferential Pattern Reinforcement .....	29
<b>Figure 2.1.</b>	Sketch of First Generation FRMS.....	34
<b>Figure 2.2.</b>	Synthetic Fibers Wrapped in Quasi-Circumferential Pattern.....	35
<b>Figure 2.3.</b>	Two First Generation Meniscus Scaffolds Next to Two Canine Menisci .	35
<b>Figure 2.4.</b>	Sketch of Second Generation FRMS.....	38
<b>Figure 2.5.</b>	Illustration of Base Plate for Wrapping Polymer Fibers.....	41
<b>Figure 2.6.</b>	Fiber Weaving Pattern Used for Second Generation Scaffolds .....	42
<b>Figure 2.7.</b>	Pictorial Summary of Second Generation FRMS Fabrication Process....	45
<b>Figure 2.8.</b>	Free Body Diagram of FRMS Tested in Tension .....	46
<b>Figure 2.9.</b>	Front and Rear Views of Dual Instron Mechanical Testing System .....	50
<b>Figure 2.10.</b>	Picture of Cellophane Wrapped Pressure Sensitive Film Loaded into Customized Mechanical Tester Jig.....	53

<b>Figure 2.11.</b>	Illustration of Sample Orientation During Tensile Testing .....	54
<b>Figure 2.12.</b>	Illustration of FRMSs Sectioned into Wedges for Cell Seeding.....	56
<b>Figure 2.13.</b>	Sketch of Sectioned Scaffolds for Non-Functional <i>In Vivo</i> Evaluation.....	61
<b>Figure 2.14.</b>	Pictures from Surgical Implantation of FRMS Wedge into Surgically Created Pocket in Rabbit Knee Joint.....	62
<b>Figure 2.15.</b>	Overview of Surgical Implantation Protocol .....	66
<b>Figure 3.1.</b>	Structural Properties of First Generation FRMSs Mechanically Tested in Tension .....	73
<b>Figure 3.2.</b>	Applied Compressive Load as Compared to 10X the Measured Tensile Load for Each Scaffold Under Each Cyclic Loading Condition.....	76
<b>Figure 3.3.</b>	Relationship Between the Applied Compressive Load and the Measured Tensile Load .....	78
<b>Figure 3.4.</b>	Images of Pressure Sensitive Film After Compressive Loading.....	80
<b>Figure 3.5.</b>	Representative Pressure Distribution Profile on Tibial Plateau After Compressive Loading of Either 100 N or 250 N .....	82
<b>Figure 3.6.</b>	Contact Area on Tibial Plateau After Compressive Loading .....	83
<b>Figure 3.7.</b>	Structural Properties of FRMSs and Native Ovine Meniscal Tissue Tested in Tension to Failure.....	84
<b>Figure 3.8.</b>	Fibrochondrocytes from Rabbit Meniscus Growing in Culture .....	85
<b>Figure 3.9.</b>	Number of Viable Fibrochondrocytes Cultured on FRMSs .....	87
<b>Figure 3.10.</b>	Micrographs of Fibrochondrocyte-Seeded FRMSs after 4, 8, and 16 Days Culture .....	88
<b>Figure 3.11.</b>	Histological Sections of MS500 FRMSs at 4 Weeks Post-Implantation ..	91
<b>Figure 3.12.</b>	Histological Sections of MS1000 FRMSs at 4 Weeks Post-Implantation.	92
<b>Figure 3.13.</b>	Histological Sections of MS500 FRMSs at 8 Weeks Post-Implantation ..	93
<b>Figure 3.14.</b>	Histological Sections of MS1000 FRMSs at 8 Weeks Post-Implantation.	94

<b>Figure 3.15.</b>	Comparison of Graded Histological Samples .....	95
<b>Figure 3.16.</b>	Meniscal Scaffolds at 8 Weeks Post-Implantation .....	99
<b>Figure 3.17.</b>	Meniscal Scaffolds at 16 Weeks Post-Implantation .....	99
<b>Figure 3.18.</b>	Excised Meniscal Scaffolds and Ovine Lateral Meniscus .....	100
<b>Figure 3.19.</b>	Structural Tensile Properties of Meniscus Scaffolds Pre-Implantation, 8 Weeks Post-Implantation, and 16 Weeks Post-Implantation as Compared to the Native Ovine Medial Meniscus .....	101
<b>Figure 3.20.</b>	Compressive Modulus of Meniscus Scaffolds .....	102
<b>Figure 3.21.</b>	MS1000 FRMSs After 8 Weeks Implantation in an Ovine Knee .....	105
<b>Figure 3.22.</b>	MS1000 FRMSs in the Bone Tunnel After 8 Weeks Implantation in an Ovine Knee .....	106
<b>Figure 3.23.</b>	Medial Femoral Condyles from Control and Experimental Knees After 8 Weeks Implantation.....	106
<b>Figure 3.24.</b>	MS1000 FRMSs After 16 Weeks Implantation in an Ovine Knee .....	107
<b>Figure 3.25.</b>	MS1000 FRMSs in the Bone Tunnel After 16 Weeks Implantation in an Ovine Knee .....	108
<b>Figure 3.26.</b>	Medial Femoral Condyles from Control and Experimental Knees After 16 Weeks Implantation.....	109
<b>Figure 3.27.</b>	Histological Trends of Biological Response to MS1000 Scaffolds .....	111
<b>Figure 3.28.</b>	Immunofluorescence Staining of Type I Collagen.....	113
<b>Figure 3.29.</b>	Immunofluorescence Staining of Type II Collagen.....	114
<b>Figure 3.30.</b>	Immunofluorescence Staining of Type III Collagen.....	115
<b>Figure 3.31.</b>	Immunofluorescence Staining of Type XII Collagen .....	116
<b>Figure 3.32.</b>	Individual Reactivities of Antibodies with FRMS .....	117

# **1. INTRODUCTION**

## **1.1. The Meniscus**

### **1.1.1. Gross Anatomy**

The menisci of the knee are two C-shaped discs of fibrocartilage found between the condyles of the femur and the tibial plateau that are essential for proper joint function and health. The tissue provides protection to the articular cartilage of the knee by transmitting loads through the joint, distributing high peak stresses on the underlying surfaces, providing shock absorption, aiding in joint lubrication, and contributing to overall joint stability<sup>4-21</sup>. The meniscus covers roughly 2/3 of the tibial plateau with the distal surface (tibial surface) being flat and the proximal surface (femoral surface) being concave. The cross section of each meniscus is triangular, with the larger side at the periphery, or outer rim, and the apex at the inner rim. This geometry allows the meniscus to essentially fit a round surface (femoral head) to a flat surface (tibial plateau).

The tissue can be divided into three zones: the anterior horn, which is the front third of the meniscus; the posterior horn, or the back third; and the body, which is the middle third. The lateral and medial menisci have attachments to the tibial plateau at the anterior and posterior horns, and attach to the joint capsule at the outer rim (Figure 1.1). The medial and lateral menisci are also connected anteriorly by the transverse ligament<sup>22, 23</sup>. The entire periphery of the medial meniscus is attached to the joint capsule, while there is a break in the peripheral attachment of the lateral meniscus, thereby granting access to the passage of the popliteal tendon<sup>15, 22, 23</sup>. The implication for this is that the lateral meniscus is not attached as rigidly as the medial meniscus, allowing it to deform more under high stresses and leaving the medial meniscus more vulnerable to injury.

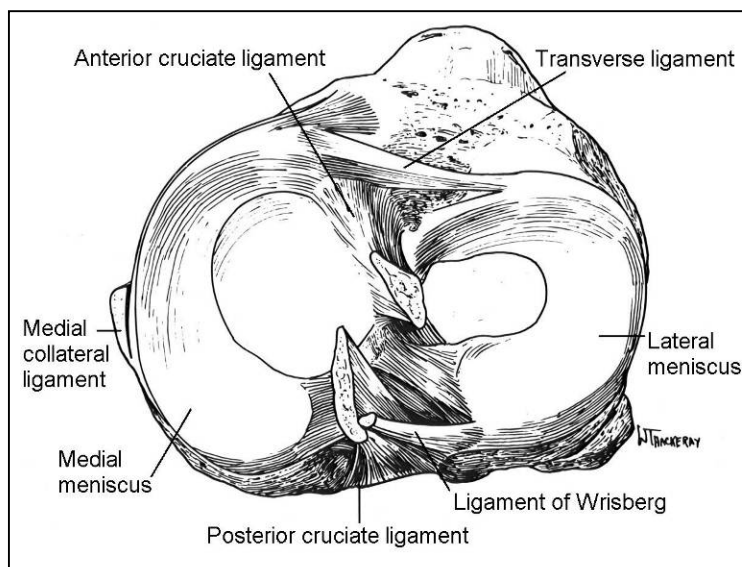


**Figure 1.1: Illustration of Tibial Plateau with Lateral and Medial Menisci.**  
From Arnoczky et al. <sup>1</sup>

### 1.1.2. Vasculature

The outer 10-30% of the medial meniscus is vascularized while the outer 10-25% of the lateral meniscus is vascularized <sup>1, 24</sup>. The remainder of the tissue is avascular and relies on diffusion or mechanical pumping for nutrients and waste removal <sup>24</sup>. The vasculature of the meniscus plays a critical role in its ability to heal after trauma. A lesion in the vascularized zone is called a red-red tear and, because of the available blood supply, has the ability to heal. A tear which includes areas of both the peripheral region as well as the central region is called a red-white tear. Since these injured areas are in contact with a blood supply, they should, in theory, heal <sup>1, 25-27</sup>. The third type of lesion occurs completely in the avascular zone of the meniscus and is called a white-white tear. Given that the injured area is cut off from any blood supply, it does not have the capacity to heal. Injuries to the menisci and the responses to these injuries will be discussed in later sections.

### 1.1.3. Microscopic Anatomy

#### 1.1.3.1. Extracellular Matrix (ECM)

The material and structural properties of the meniscus relate directly to the layout of its extracellular matrix (ECM). The components of the ECM of normal menisci include collagen, elastin, proteoglycans, non-collagenous matrix proteins, and water with various dissolved solutes (about 75% of wet weight)<sup>3, 28-33</sup>. Due to the nature of the meniscus and how it responds to loads, it exhibits characteristics of both fibrous connective tissues, such as tendons and ligaments, and cartilaginous tissue. As a result, the meniscus is often termed a fibrocartilaginous tissue.

Collagen makes up about 75% of the dry weight of the tissue, with type I being the predominant (~90%). Other collagen types include types II, III, V, and VI<sup>3, 30, 32</sup>. The arrangement of the collagen fibers within the meniscus dictates how the tissue functions under applied loads. The distribution and organization of collagen differs based on its location within the tissue (Figure 1.2). The surface of the meniscus contains collagen fibers (predominantly type I with some type II interspersed) arranged randomly<sup>3, 32</sup>. Moving deeper into the meniscus, the orientation of the collagen fibers is mostly circumferential (Figure 1.3 a-b). These fibers are arranged in the direction of the force felt by the tissue. When a compressive load is applied, the tissue is forced out of the joint capsule. Since the menisci are anchored to the tibial plateau at the anterior and posterior horns, tensile stresses are generated in the circumferential direction (hoop stresses)<sup>2, 3, 32</sup>. Radial tie fibers are also found deep in the meniscus (Figure 1.4 c-d). These fibers are thought to function in keeping the circumferentially arranged fibers bundled together, as well as increasing the stiffness of the tissue<sup>3, 32, 34</sup>.

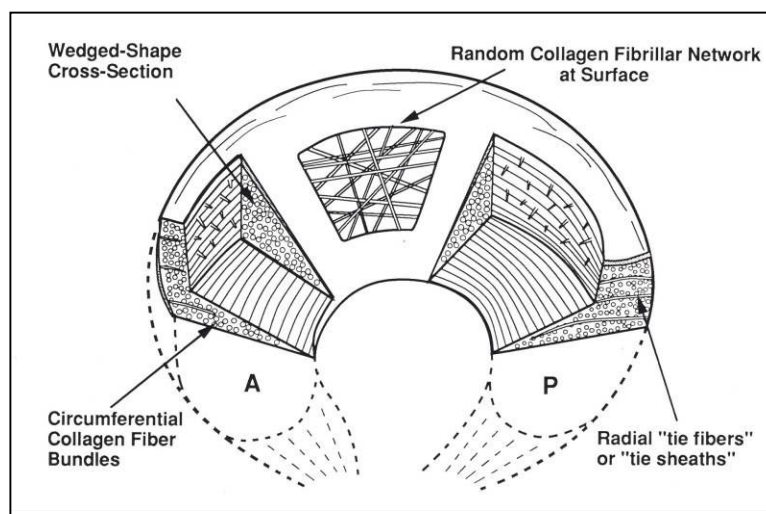


**Figure 1.2: Illustration of the Arrangement of the Collagen Fiber Network in the Normal Meniscus.** The surface of the tissue is comprised of a network of unorganized type I and type II collagen fibers. Deeper in the tissue, collagen fibers are arranged in a circumferential pattern with intermittent radial tie fibers. From Mow et.al.<sup>2</sup>.

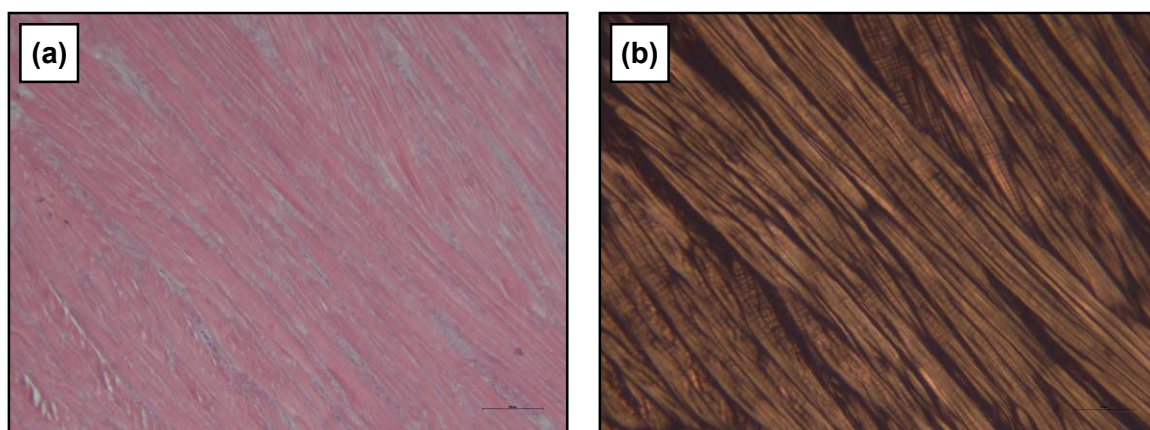


**Figure 1.3: Micrographs of an Ovine Meniscus Showing Circumferentially Arranged Collagen Fibers.** Sections are stained with Haematoxylin and Eosin (H&E) at 40X magnification under (a) regular light and (b) polarized light. Cuts were made along the horizontal plane to view the circumferentially arranged collagen fibers. Under polarized light, the anisotropic fiber arrangement is highlighted.

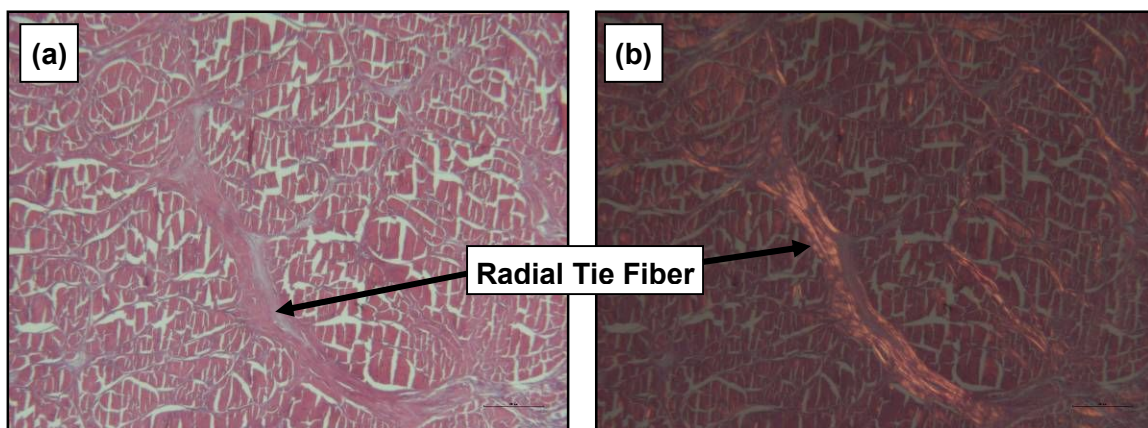


**Figure 1.4: Micrographs of an Ovine Meniscus Showing Radial Tie Fibers Among Circumferentially Arranged Collagen Fibers.** Sections are stained with Haematoxylin and Eosin (H&E) at 40X magnification under (a) regular light and (b) polarized light. Cuts were made along the sagittal plane to view the radial tie fibers (indicated by arrows) as well as the cross-section of the circumferential fibers. Under polarized light, radial tie fibers fluoresce.

The presence of proteoglycans in the ECM also has a significant impact on the properties of the meniscus. These highly hydrophilic molecules are responsible for the viscoelastic behavior of the meniscus and are essential for joint lubrication as well as transportation of nutrients to cells and removal of their waste<sup>31-33</sup>. About 3% of the dry weight of a normal meniscus are proteoglycans – although this percentage depends on the age of the tissue<sup>2</sup>. The predominant type found in meniscal tissue (as well as hyaline cartilage) are large aggregating proteoglycans<sup>2, 31, 32, 35, 36</sup>. In these molecules, chondroitin sulfate and keratan sulfate chains are attached to a protein core which has a specific binding site for hyaluronic acid (HA). When many protein cores containing glycosaminoglycan chains attach to the same HA molecule, an aggregate is formed. Chondroitin sulfate and keratan sulfate chains are composed of repeating sulfate and carboxyl groups that become dissociated and charged in the interstitial fluid of the meniscus. The closely spaced negative charges of the sulfate groups produce repulsive forces within the molecule, causing it to assume an extended configuration and generate internal stresses within the collagen matrix. To counteract the negative charge and

maintain electro-neutrality in the tissue, high concentrations of counter-ions (i.e. Na<sup>+</sup>) carried by the interstitial fluid are required - which translates to an increase in osmotic pressure within the tissue. Thus, the molecular behavior of proteoglycans is essential in maintaining tissue hydration, firmness, and viscoelasticity in the meniscus<sup>2, 3, 32, 37</sup>.

### **1.1.3.2. Cells**

The cells of the meniscus synthesize and organize the extracellular matrix of the tissue. Since it is the ECM which dictates the mechanical properties of the meniscus, the proper function of these cells is vital for the good health of the joint. In the past, researchers were unsure as to how to accurately name the cells of the meniscus<sup>38</sup>. Because of the fibrous nature of the meniscus and the predominant protein secretion (type I collagen), the cells were considered as fibroblasts<sup>39-41</sup>. However, the rounded morphology of the cells, the presence of a pericellular matrix around the cell, and the synthesis of proteoglycans in the ECM are all suggestive of a chondrocytes phenotype<sup>38, 39, 42</sup>. Because the cells of the meniscus have traits similar to fibroblasts and chondrocytes, they have been termed fibrochondrocytes.

## **1.1.4. Structure and Function**

### **1.1.4.1. Function**

The menisci play a crucial role in joint stability, load transmission and distribution, lubrication, and shock absorption in the knee<sup>4-21</sup>. Fukubayashi et al. demonstrated the load distribution function of the meniscus with a study using pressure sensitive film<sup>9</sup>. The investigators showed that with the knee at 0 degrees, the peak pressures on the tibia nearly doubled after the meniscus was removed. In another study demonstrating the load transmission function of the meniscus, it was shown that normal menisci transmit between 70 and 99% of the total load through the joint<sup>21</sup>. In degenerative or

torn menisci, the ability of the tissue to transmit loads was maintained so long as circumferential continuity was preserved. Furthermore, another study has shown that if continuity is completely removed (i.e., radial incision through tissue), the load transmission through the joint is equivalent to that of a joint without any meniscal tissue<sup>20</sup>.

The geometry, tissue attachments, composition, and ultrastructure of the meniscus all contribute to how the tissue responds to mechanical loading. The geometry and tissue attachments provide physical constraints which determine the structural mechanics of the tissue, while the composition and ultrastructure of the meniscus define the material properties of the meniscus.

#### **1.1.4.2. Geometry**

The meniscus is a C-shaped tissue which has anterior and posterior attachments to the tibial plateau. The cross-sectional area of the tissue is triangular, with the apex at the inner margin and the base at the periphery (Figure 1.5). This geometry serves to increase the articulating surface area of the joint by essentially ‘fitting’ the rounded condyles of the femur to the flat tibial plateau. Therefore, when a load is applied through the knee joint, it is distributed evenly on the tibial surface and stress concentrations detrimental to the health of articular cartilage are avoided<sup>7, 9, 14, 43</sup>.

#### **1.1.4.3. Tissue Attachments**

The meniscus has anterior and posterior attachments to the tibial plateau and attaches to the joint capsule around the periphery of the tissue. The tibial attachments are composed of fibrocartilage, calcified cartilage, and subchondral bone<sup>44, 45</sup>. The size, orientation, and strength of these attachments dictates how an axial load is transmitted through the tissue<sup>2, 46</sup>.

As discussed earlier in the anatomy section, the entire periphery of the medial meniscus is attached to the joint capsule while there is a break in the peripheral attachment of the lateral meniscus for passage of the popliteal tendon<sup>15, 22, 23</sup>. The medial meniscus is therefore secured to the joint capsule more firmly than the lateral meniscus and, as a result, the lateral meniscus is able to shift significantly more than the medial meniscus when exposed to high loads – about 1 cm versus 1 mm, respectively. Consequently, the medial meniscus is much more prone to injury than the lateral meniscus<sup>1, 14, 15, 47</sup>.

#### 1.1.4.4. Structural Mechanics

When an axial load is applied to the joint, the geometry of the meniscus causes the tissue to be extruded from the joint. The strong anterior and posterior attachments resist this displacement by developing tensile hoop stresses in the circumferential direction<sup>2, 3, 46</sup>. A more detailed analysis of this behavior is shown in Figure 1.5 and explained below.

Due to its geometry, compressive axial loads applied by the femoral condyles are directed perpendicularly to the femoral surface of the tissue ( $\mathbf{F}$  from Figure 1.5). Because the tibial plateau is a relatively flat surface, the reaction force ( $\mathbf{R}_z$ ) is directed upward, perpendicularly to the tibial surface of the meniscus (this analysis assumes friction to be negligible).  $\mathbf{F}$  can be broken down into two components in the  $\mathbf{z}$  and  $\mathbf{r}$  (radial) directions:  $\mathbf{F}_z$  and  $\mathbf{F}_r$ . Under static conditions, all forces in the  $\mathbf{z}$  direction must sum to zero and likewise for those in the radial direction. Therefore,  $\mathbf{R}_x$  is equal and opposite to  $\mathbf{F}_z$ . However, there is no reaction force from the tibial side of the meniscus to cancel out  $\mathbf{F}_r$ . Reaction forces develop at the anterior and posterior attachments:  $\mathbf{F}_a$  and  $\mathbf{F}_p$  respectively. Consequently, a tensile stress is generated in the circumferential direction to prevent tissue extrusion from the joint capsule. This circumferentially

directed tensile stress is termed hoop stress ( $F_h$ ).  $F_h$  can be broken down into two perpendicular components:  $F_{rh}$  and  $F_{th}$ . The radial forces from the hoop stress cancel out the radial stress from the axial load:  $F_r = 2F_{rh}$ . The circumferential stresses,  $F_{th}$ , also cancel each other out and equilibrium of the meniscus is maintained <sup>2, 3, 46</sup>.

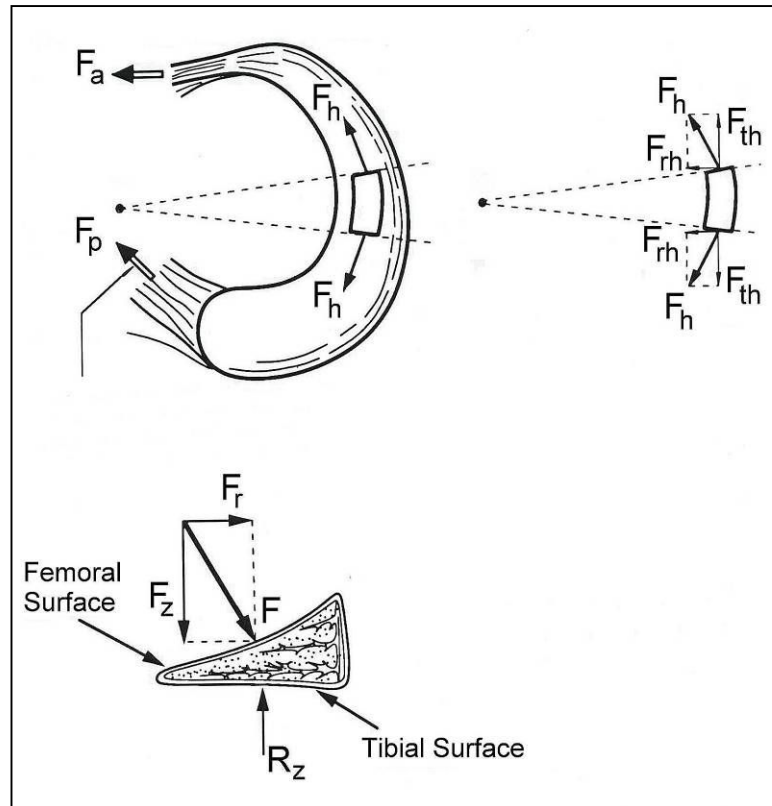


**Figure 1.5: Free Body Diagram of Meniscus.** An applied axial force,  $F$ , is converted to a circumferentially arranged tensile load,  $F_h$ . From Mow et al. <sup>2</sup>

#### 1.1.4.5. Material Properties

The material properties of the meniscus are determined by its composition and ultrastructure. The principal components of the menisci are collagen, proteoglycans, and water. Due to the complex arrangement of the ECM, the meniscus is considered to be highly anisotropic with material properties that vary with depth and location within the tissue<sup>2, 46</sup>. Under normal physiological loading conditions, tensile and compression are the primary loading modes experienced by the meniscus.

##### *Tension*

Type I collagen, the main collagen type found in the tissue, is oriented primarily in the circumferential direction. This organization provides a high degree of tensile strength to the tissue in this direction and is essential for the resistance of hoop stresses generated during loading of the knee<sup>48, 49</sup>. The radial tie fibers are also made of type I collagen and are thought to enhance load transfer between fiber bundles and resist longitudinal tears in the tissue<sup>34, 49</sup>.

When tested in tension, the stress-strain curve of the meniscus is similar to other collagenous tissues. Initially, there is a domain of low stiffness and small strain termed the “toe region”, followed by a linear stress-strain relationship at higher loads and deformations<sup>46</sup>. The tensile strength of the tissue depends not only on the direction of the sample (i.e., circumferential or radial), but also on the location within the tissue. At the surface, the collagen network of the tissue has a random orientation. Consequently, the tensile properties are nearly isotropic (properties the same in any direction)<sup>46</sup>. Deeper in the tissue, the collagen network becomes organized, making this region of the tissue highly anisotropic. Generally, for the normal meniscus, the tissue is significantly stronger in the circumferential direction as opposed to the radial direction. The exception can occur when mechanical test samples in the radial direction contain

complete radial tie fibers. In this case, the circumferential and radial samples have comparable strengths<sup>34, 46</sup>.

Experimentally, the meniscus has been shown to vary in tensile strength along the circumference of the tissue<sup>2, 3</sup>. As seen in Figure 1.6, the weakest section is the medial-posterior region of the medial meniscus, which is a common site of tears. Fithian et al, showed the regional differences in the elastic modulus were due most likely to ultrastructural changes (i.e., fiber bundle direction and collagen crosslinking) and not biochemical differences (i.e., collagen-proteoglycan content and concentration)<sup>3</sup>. Polarized light microscopy has been used to correlate larger collagen fiber bundle orientation to areas of greater strength and stiffness – further supporting the theory that regional differences in stiffness are due to ultrastructural changes<sup>50</sup>.

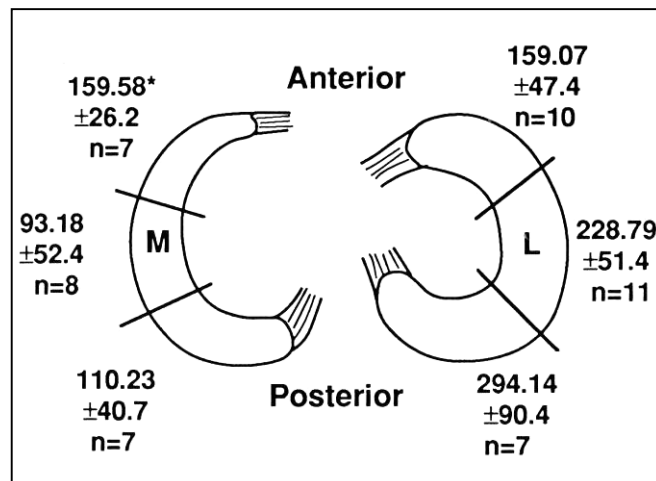


**Figure 1.6: Young's Modulus of the Human Lateral and Medial Meniscus.** Values are reported for the anterior, posterior, and middle third of the tissue. From Fithian et al.<sup>3</sup>

### *Compression*

The meniscus has been shown to be a tissue with a relatively low compressive stiffness and low permeability. Both of these qualities aid it in functioning as a highly

efficient shock absorber. Furthermore, they impart the tissue with relatively high elastic deformability, which is essential for redistribution of loads across the knee <sup>2, 3, 51, 52</sup>.

The compressive properties of the meniscus are primarily dictated by the organization of its two major ECM components – collagen and proteoglycans. The relationship between these two components determines the amount of water in the tissue and its distribution throughout it. Under compressive loading conditions, the ECM resists fluid flow through the matrix, resulting in a viscoelastic (VE) response. The viscoelasticity governs the creep and stress-relaxation responses to loads, which are important in the distribution of stresses on the articular surfaces <sup>2, 3</sup>. Under normal loading conditions, hydrostatic pressure is developed due to the inherent low permeability of the matrix to fluid flow. Initially, the pressure causes the load to be distributed evenly throughout the tissue as the fluid flow supports the majority of the load. As time progresses, the fluid is redistributed within and without the meniscus, resulting in temporary tissue deformations. Consequently, the contact surfaces of the articular cartilage and menisci increase, resulting in enhanced load distribution across the articular surfaces. When the load is removed, the interstitial fluid flows back into the hydrophilic tissue and its normal size and shape are restored. The fluid exudation/imbibition during mechanical loading is thought to be vital to the lubrication of the joint as well as to nutrient transportation to meniscal cells <sup>2, 3, 46</sup>.

### *Shear*

The meniscus has a relatively low shear modulus. Compared to articular cartilage, the shear properties of the meniscus are about 1/10. This allows the tissue to deform easily under loads and accommodate the articulating surfaces of the knee joint. As a result, loads are evenly distributed along the femoral and tibial surfaces and high, unhealthy contact stresses are avoided. Furthermore, the tissue is able to provide better

shock absorption to the joint. Experimental work has demonstrated the anisotropic shear behavior of meniscal tissue – most likely due to the collagen fiber orientation. The shear behavior of the tissue was also found to be non-linear and compression dependent<sup>2, 53</sup>. Other experiments have shown the tissue to be 20-33% stiffer when the test plane is perpendicular to the collagen fiber bundles as opposed to parallel<sup>3</sup>.

Although the meniscus behaves quite differently in tension, shear, and compression, there are several points concerning the tissue that are common to all modes of loading. First, the tissue behaves as a fiber-reinforced, porous-permeable composite which fluid flows through. The flow of the interstitial fluid through the matrix is a significant part of the mechanical response of the tissue to normal loads. Second, the material properties are determined primarily by the organization of the ECM and not by its biochemical content. In other words, regional differences in mechanical properties are not due to differences in collagen or proteoglycan concentrations, but rather to how the molecules interact together. Lastly, because the meniscus is ideally suited to provide load distribution, shock absorption, and stability across the knee joint, any changes to its normal geometry, tissue attachments, loading conditions, or ECM can be expected to have deleterious, and oftentimes irreversible, effects on overall meniscal function and joint health.

## **1.2. Injury to the Meniscus**

Damage to the meniscus usually occurs as a result of traumatic injuries or degenerative processes, or a combination of both. Traumatic injuries, or tears, in younger, active people (13 - 40 years of age) can occur during athletic activities requiring running, cutting, or physical contact<sup>54</sup>. Sports such as basketball, football, soccer, wrestling, and skiing are activities where participants are particularly vulnerable

to knee injury due to the high rotational movements of the knee during loading. However, isolated traumatic incidents such as car accidents or falls can also cause severe damage to the tissues of the knee. Essentially, any activity in which rotational movements of the knee joint are coupled with weight bearing forces leaves a person susceptible to meniscus injuries.

### **1.2.1. Options After a Meniscus Injury**

For tears that exhibit either mechanical or non-mechanical clinical symptoms, the first treatment option is to repair the lesion. Repairing a torn meniscus is typically accomplished through an arthroscopic procedure in which the torn segment is sutured to the main body of the tissue<sup>54</sup>. When considering repair as an option after a meniscal injury, it is important to take into account the extent of the damage to the tissue. A tear which causes too little damage may not be reparable since the tissue may heal on its own, or the act of repairing the tissue may cause more damage than the tear itself. A tear which causes too much damage may not be suitable for repair because the ultrastructure of the tissue is so impaired that even after a repair, the meniscus will not perform well biomechanically<sup>54</sup>. The capacity of meniscal tissue to heal is also important when considering the viability of the repair option. Tears that can be repaired include red-red tears and some red-white tears since they have an available blood supply to initiate the wound healing response<sup>54</sup>.

If it is decided that the meniscus injury is not suitable for repair – either due to the extent of damage or the location of the tear – then excision of the damaged portion is the next option. As discussed previously, if excision is the only alternative available, then preservation of as much tissue as possible is of paramount importance when considering the overall health of the joint<sup>54</sup>. Therefore, the surgeon will usually opt to perform a partial meniscectomy if at all possible. This procedure involves the surgical

excision of any torn, mobile fragments of tissue – typically found near the inner margin. This procedure leaves the periphery intact, thereby preserving the biomechanical function of the meniscus and maintaining joint health. Some degradation in joint mechanics is often observed as the contact area between the femur and tibia decreases, while the local peak stresses on the cartilage increase (typical values are 10% and 65%, respectively). However, the long-term outcome of this procedure is generally satisfactory<sup>6</sup>.

For a meniscus that is too severely damaged, a total meniscectomy may be the only viable option. The degenerative effects of a total meniscectomy were first observed by King in 1936<sup>12</sup>, and later by Fairbank in 1948<sup>8</sup>. Baratz et al, used pressure-sensitive film to show that complete removal of the meniscus resulted in a 75% decrease in contact area between the femur and tibia, and a 235% increase in local peak stresses on the articular cartilage<sup>55</sup>. Unfortunately, this leaves the joint vulnerable to osteoarthritis as contact stresses on the cartilage increase and overall joint stability decreases<sup>5, 7, 9, 13, 54-57</sup>. Long-term clinical data of total and subtotal meniscectomies has shown that pain from osteoarthritic changes in the knee force many patients to undergo lifestyle changes such as a decrease or cessation of physical/sports activities, and even career changes<sup>58, 59</sup>.

To prevent the potential onset of osteoarthritis, several tissue engineering based alternatives are being developed for patients after a total meniscectomy.

### **1.3. Tissue Engineering Strategies for the Meniscus**

#### **1.3.1. Functional Tissue Engineering**

Tissue Engineering (TE) is a field of study in which diseased body tissues/organs are repaired, replaced, or reconstructed by delivering any combination of scaffolds, cells, pharmacologicals, growth factors, and/or genes to the injury site<sup>60-64</sup>. The ultimate goal

is to quickly and effectively produce a tissue/organ which performs at (or above) the level of a normal, healthy one. TE combines concepts from various disciplines such as physiology, anatomy, pharmacology, cellular biology, molecular biology, biochemistry, genetics, materials science, and biomechanics. The use of TE techniques in the development of treatment alternatives for various Orthopaedic maladies has become a popular strategy for researchers.

As the field of Tissue Engineering progresses, several concerns have been identified regarding tissues which serve a biomechanical function. For example, one strategy for tendon or ligament repair is to create a new tissue by implanting cells into a collagen gel<sup>65-68</sup>. After a certain culture time – and in some cases, the application of mechanical stimulation<sup>66, 68</sup> – the new tissue is analyzed for cell phenotype, gene expression, protein synthesis, and/or mechanical strength. While the biological data for experiments such as these is promising, the tissue produced has mechanical properties far lower than that of normal tendons or ligaments. If implanted at the site of an injury (e.g., ACL tear), the neo-tissue would likely fail prematurely under relatively low loads. This type of problem is encountered heavily in the orthopaedic field, where most tissues undergo regular cycles of loading and unloading. With this concern in mind, a subset of the Tissue Engineering field was proposed: Functional Tissue Engineering (FTE)<sup>60, 61</sup>. Functional Tissue Engineering stresses the importance of creating tissue engineered solutions (scaffolds, reconstruction, or repair) which meet the mechanical and structural requirements to restore normal function of the damaged tissue<sup>60, 61</sup>. This concept is especially relevant to orthopaedic tissue engineers, many of whom actively work toward developing constructs for load-bearing tissues such as bone, cartilage, tendons, ligaments, and menisci. By implanting a construct that restores function to the injured area, a mechanical environment is established which is conducive to the overall recovery process. Consider a simple example in which a scaffold has been designed to

replace a ruptured tendon. When implanted at the injury site, the construct restores function to the point where the patient can resume normal activities of daily living (ADL). After implantation, cells infiltrate the scaffold and begin to experience the same types of loads they would experience in a normal tendon (i.e., uniaxial cyclic tensile loads). Mechanochemical transduction pathways within these cells are initiated, causing them to actively modify their surroundings to conform to the mechanical load (i.e., cells within tendon analog will exhibit a fibroblastic phenotype, begin synthesizing and laying down organized type I collagen, and secrete proteases which break down the scaffold). Combine this with the right combination (timing and quantity) of other TE tools such as drug, growth factor, or gene delivery, and the overall process can be accelerated so that a new, functional tendon is quickly formed.

The challenge for tissue engineers is the optimization of all these variables to find the gold standard in tissue repair. To create a biomechanically sound implant, Butler et al. identified several concerns researchers need to address during its design and optimization <sup>61</sup>:

- What mechanical loads the tissues normally experience,
- The mechanical properties of these tissues under normal ADL conditions as well as under failure conditions,
- Which of these properties are relevant to the design of a tissue-engineered construct,
- Prioritization of the relevant mechanical properties,
- Establishment of standards to judge the effectiveness of a design, and
- How mechanical signals affect cells *in vitro* (i.e. bioreactor) and *in vivo*.

Besides the biomechanical requirement for a tissue-engineered replacement or repair, other factors also need to be considered and optimized. For growth factors,

drugs, and gene therapy, several factors must be considered in the optimization process: type, amount, timing of release, necessity, and delivery vehicle. Other factors associated with tissue-engineered constructs include biocompatibility, degradation products, degradation profile of resorbable implants, surgical procedure required for implantation, sterilization, storage, and availability of raw materials. To further complicate matters, a TE solution needs to be customized to the type of tissue it is replacing or repairing, as well as to the individual needs of the patient. With all these variables, the design of a tissue-engineered device can be a daunting task.

Below are several examples of tissue engineering strategies currently being pursued by investigators.

### **1.3.2. Meniscus Allografts**

One alternative for patients after total meniscectomy is the implantation of allogenic tissue to replace the missing meniscus. These procedures are relatively new and are still being investigated further in animal models and clinical trials<sup>43, 69-90</sup>. Although the short-term results have been promising, several significant problems exist: fixation of the graft tissue in the joint<sup>70, 85, 86, 91-94</sup>; attaining proper alignment of the leg<sup>70, 75, 87</sup>; joint instability<sup>70, 75</sup>; tissue/implant site size mismatch<sup>82, 86, 92, 95</sup>; preservation of allograft tissue<sup>70, 72, 81, 82, 89, 90, 92</sup>; potential for immune response to allograft<sup>74, 96</sup>; limited cell repopulation of the tissue<sup>71, 73, 74, 76, 96</sup>; abnormal remodeling of extracellular matrix<sup>77</sup>; and risk of disease transmission<sup>74, 80</sup>. Perhaps the most discouraging problem associated with the use of allogenic tissue is the lack of satisfactory long-term data<sup>70, 71, 75, 77, 79, 80, 83, 89, 97</sup>.

In the short- and mid-term, the use of allogenic tissue for meniscal replacement has been shown to alleviate joint pain and slow down the initial degenerative processes associated with complete removal of the meniscus<sup>43, 69, 70, 76, 77, 80, 82, 95, 98</sup>. While

protection of the articular cartilage was demonstrated <sup>99</sup>, even in the short term the allograft did not provide protection to the same degree that normal meniscal tissue did <sup>43, 78</sup>. Furthermore, in joints with allografts, histological evidence of degenerative changes in the cartilage were observed as early as 12 weeks <sup>78</sup>. With respect to the graft itself, several investigators observed a decrease in cellularity in the allogenic tissue as well as alterations in the biochemical makeup of the tissue <sup>71, 73, 74, 83</sup>. Since the proper function of the meniscus is highly dependent on its biochemical composition, such alterations could significantly alter the mechanics of the tissue, leading to graft failure and/or joint damage.

While the use of allogenic tissue remains a promising alternative for treatment of a meniscus deficient joint, the alleviation of pain and short-term protection of the articular cartilage are not enough to consider these procedures successful. A significant amount of research needs to be accomplished to deal with the numerous issues associated with allograft implantation and optimize the use of this tissue. Overall, the delay or prevention of degenerative arthritis in the long-term must be demonstrated before these procedures can be considered clinically successful <sup>88</sup>.

### **1.3.3. Meniscal Scaffolds**

The use of a tissue-engineered scaffold to replace significant portions of damaged meniscal tissue is an attractive option currently being researched in the Orthopaedic field. It has the potential to overcome many of the obstacles associated with allografts including tissue/implant site size mismatch; preservation of the graft; potential for immune response; and risk of disease transmission. Due to the variety of options available to tissue engineers concerning the design and implementation of a meniscal scaffold, a considerable amount of basic science research is needed to obtain a device that has the potential for clinical success.

Three types of meniscus implants will be discussed in the following section: (1) permanent prostheses; (2) resorbable, synthetic polymer scaffolds; and (3) collagen-based scaffolds.

#### **1.3.3.1. Permanent Prostheses**

Early research focused on designing a meniscal scaffold comprised of non-resorbable materials such as Dacron, Teflon, or Polyvinyl Alcohol-Hydrogel (PVA-H) <sup>100-111</sup>. These methods proved to be ineffectual as significant amount of degenerative changes were seen in the articular cartilage. Furthermore, problems such as low resistance to fatigue and wear, inability to retain shape, and attachment difficulties were common in these types of implants <sup>102</sup>. And because these implants are made up of non-resorbable materials, they need to be able to maintain the appropriate mechanical properties necessary for proper function of a meniscus-like device in the long-term. No published research was able to demonstrate the long-term success of these meniscus prostheses. In a review article on permanent meniscal prostheses, Messner states that “the concept of a permanent meniscal prosthesis does not seem clinically applicable at the moment” <sup>102</sup>. In more recent years, much of the focus for a meniscal device has therefore shifted away from a permanent implant to one that is resorbable.

#### **1.3.3.2. Resorbable, Synthetic Polymer Scaffolds**

Recent research has focused on the development of meniscal replacements derived from various biomaterials. A potential scaffold for a meniscal replacement should meet several criteria <sup>112</sup>. An ideal scaffold should:

- Induce cellular ingrowth and promote new fibrocartilage formation,
- Have a porous structure that allows for cellular ingrowth and diffusion of nutrients,
- Be biodegradable with a degradation profile that closely matches neo-tissue formation and remodeling,

- Be composed of a material that can be used for delivery of drugs and/or growth factors, and
- Have initial mechanical properties that allow the implant to withstand normal loads in the joint without losing structural integrity until neo-tissue can assume load-bearing capacity.

Several types of resorbable scaffolds are currently being developed and characterized by investigators. Polyurethane based polymers have been used to create meniscus shaped foams/sponges for use as scaffolds <sup>113-125</sup>. These devices have met with varying degrees of success regarding articular cartilage protection, promotion of neo-fibrocartilaginous tissue, and polymer degradation. One potential issue may be the amorphous structure of the foam, which inhibits the formation of tensile hoop stresses found in the native meniscus. Chiari et al. and Kon et al. have published short-term results on tissue integration involving a polymer sponge meniscus scaffold reinforced with a small amount of polymer fiber <sup>126, 127</sup>. No mechanical data was reported in these studies; and while tissue synthesis was observed, so was the degeneration of the underlying articular cartilage. Another type of synthetic scaffold design being explored uses polymer meshes to form meniscus implants <sup>128-130</sup>. Results from these studies are limited to *in vitro* experimentation data and small animal data. Further evaluation in a large animal model must be conducted before the efficacy of this type of scaffold can be determined.

#### **1.3.3.3. Collagen-Based Scaffolds**

Collagen based devices also fit the meniscal scaffold criteria set forth by Arnoczky <sup>112</sup> (see above section). One scaffold recently designed and evaluated by Stone et al. is a type I collagen sponge crosslinked by glutaraldehyde and mixed with hyaluronic acid and chondroitin sulfate <sup>112, 131-134</sup>. In an analysis of preliminary data, the

investigators demonstrated the scaffold to be implantable and safe over a three-year period <sup>135</sup>. Second-look arthroscopy in some cases revealed new tissue replacing the implant as it was absorbed. Despite promising preliminary data <sup>136-139</sup>, this product has not been widely accepted by the orthopaedic community <sup>140</sup>. Problems with this type of implant include the cytotoxic byproducts of the glutaraldehyde crosslinking of the collagen <sup>141</sup>, scaffold shrinkage <sup>142</sup>, and the overall mechanical properties of the device, which may be too low for the load bearing environment of the knee <sup>143</sup>. As with the synthetic polymer foam scaffolds, the collagen implants have an amorphous microstructure, which impedes conversion of compressive axial loads to tensile hoop stresses. Even with strong crosslinking, the collagen sponge has material properties less than those of the polyurethane foams.

#### **1.4. Rationale of Design for Proposed Meniscus Scaffold**

With regard to tissue-type, the meniscus can be viewed as a combination of organized fibrous connective tissue predominant at its periphery (i.e., tendon/ligament) merging with cartilaginous tissue at its inner margin. Therefore, from a functional tissue engineering standpoint, it is logical to consider scaffolding technologies from both these areas when designing an implant. The concept of a collagen-based scaffold reinforced with synthetic polymer fibers was therefore proposed and developed in this study.

The collagen provides the cytocompatible matrix portion of the scaffold, while the embedded fibers provide structural support for tensile stresses/strains experienced during joint loading. The major design variables associated with this type of scaffold are as follows:

- Collagen matrix:
  - Type
  - Pore size and structure

- Crosslinking method
- Fiber reinforcement:
  - Polymer Selection
    - Mechanical properties
    - Degradation profile
    - Byproducts of degradation
  - Amount of fibers to use
  - Organizational pattern of embedded fibers
- Structure:
  - Mechanics
  - Geometry
  - Attachments

To simplify the problem and reduce the number of variables to be studied in this project, certain assumptions and decisions were made regarding the design of this scaffold. Many of these decisions were based on data collected over the years from the Robert Wood Johnson Department of Orthopaedics Research Laboratory<sup>144-149</sup>. Others were based on work from other researchers as well as criteria set forth by tissue engineers working on other scaffolding technologies<sup>60, 61, 112, 143</sup>.

#### **1.4.1. Collagen Matrix**

Collagen is an attractive biomaterial for musculoskeletal tissue engineering applications due to its unique biochemical and mechanical properties<sup>150</sup>. Its high cellular affinity makes it an ideal coating material for synthetic polymers, which lack cell-recognition signals. Furthermore, its degradation products have chemotactic properties which play a role in wound healing<sup>151-154</sup>. The mechanical strength, degradation profile, and porosity of collagen implants can be controlled by various methods of processing and crosslinking<sup>155</sup>. Also, the sequence homology of the protein between different species causes a weak immunological response which can be considered negligible.

Collagen-based materials can also be used as vehicles for controlled drug release and gene delivery in the body<sup>156-159</sup>.

Crosslinking of collagen-based analogs is required to enhance the mechanical properties necessary for certain load-bearing applications and to control the degradation rate of the implants. Several crosslinking options exist for collagen-based devices including glutaraldehyde, 1-ethyl-3-(dimethyl aminopropyl) carbodiimide (EDC), exposure to ultraviolet (UV) radiation, and dehydrothermal (DHT) crosslinking. When deciding on a crosslinking method for the collagen matrix portion of the meniscus scaffold, several key factors need to be considered. First, the cytocompatibility of the byproducts from the crosslinking procedure need to be favorable. Harmful substances released by the crosslinking reaction can lead to inflammation and/or encapsulation of the scaffold. Second, the degradation profile of a crosslinked implant should be considered. For crosslinkers that heavily denature the collagen, the degradation rate may be too quick for a scaffold implanted at the site of a meniscal injury. Next, the uniformity of crosslinking must be taken into account. Non-uniform crosslinking of the scaffold may lead to weaker regions which fail or degrade more quickly than the rest of the implant. And last, the added strength of the collagen must be considered – however, since the embedded fibers will be carrying a majority of the load, this is not especially important.

For this study, collagen sponges were chemically crosslinked by EDC. The main by-product of EDC crosslinking is urea, which is non-cytotoxic and easily rinsed away<sup>160-163</sup>. Glutaraldehyde crosslinking typically results in cytotoxic by-products difficult to completely remove – often resulting in encapsulation and inflammation at the site of implantation<sup>141, 163-165</sup>. Denaturation of collagen proteins has been shown to be minimal with EDC crosslinking, as opposed to DHT and UV crosslinking<sup>147, 160, 166</sup>. Because the sponge is being soaked in an EDC solution, the crosslinking will be uniform, as opposed

to UV crosslinking, which cannot penetrate the full thickness of the device. While crosslinking by EDC does not yield the strongest device when compared to the other options, the mechanical strength is adequate, considering the synthetic fibers will be absorbing the vast majority of the load experienced by the scaffold.

Therefore, for a meniscus scaffold, EDC crosslinking was considered the favorable method due to the biocompatibility of the resultant collagen device, the uniformity in crosslinking, the lack of significant denaturation, and the overall increase in strength of the matrix of the implant.

## **1.4.2. Fiber Reinforcement**

### **1.4.2.1. Polymer Selection**

Of the large index of biocompatible polymers screened, one that is currently being studied further for application in Orthopaedics is poly(desaminotyrosyl-tyrosine dodecyl ester dodecanoate)(12,10) – abbreviated as p(DTD DD) or poly(12,10). This polymer is part of a family of tyrosine-derived polyarylates developed by Kohn et al.<sup>167</sup>,<sup>168</sup> and studied by Jaffe et al.<sup>169, 170</sup>.

The repeating unit of this polymer consists of a diacid component and an aromatic diphenol component (Figure 1.7). The diphenol component is made of a tyrosine molecule bonded to a desaminotyrosyl (3-(4'-hydroxyphenyl) propionic acid) molecule. This aromatic backbone imparts added strength and stiffness to the polymer<sup>167</sup>. These polymers can be abbreviated as poly(**R**,**Y**), where **R** and **Y** refer to the number of methylene units of the diacid and alkyl side chain, respectively<sup>170</sup>. Variations in these values yield polymers with differing properties. For Orthopaedic applications, where strength and *in vivo* polymer stability are important, poly(12,10) shows the most potential in this family of polyarylates.

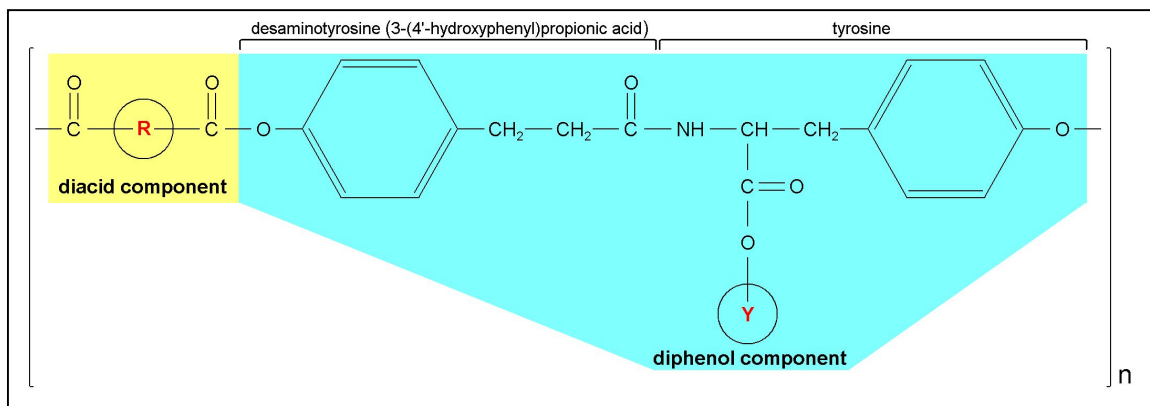


**Figure 1.7: Poly(desaminotyrosyl-tyrosine dodecyl ester dodecanoate)(12,10).** Basic repeating unit of tyrosine-based polyarylate polymer developed by Kohn. The diphenol component is composed of tyrosine bonded with desaminotyrosine (3-(4'-hydroxyphenyl) propionic acid).

#### 1.4.2.2. Organizational Pattern of Embedded Fibers

Several fiber distribution patterns were considered for the meniscus scaffold:

- (1) Layered Fiber Disc Pattern
- (2) Circumferential Ring Pattern
- (3) Mesh Pattern
- (4) Quasi-Circumferential Pattern

The fiber patterns were chosen based on the normal collagen fiber organization in the meniscus. Several criteria were considered for each of these patterns:

- Anticipated mechanical properties
  - The fiber reinforcement must increase the circumferential strength of the scaffold. Increases in compressive strength and radial strength would be beneficial, but are not considered to be as critical as an increase in the tangential properties.
- Ease of construction
  - Scaffolds of a certain design must be relatively easy to construct, and their properties (strength, modulus, porosity, uniformity, etc) must be reproducible.
- Fitting the pattern to physical parameters of the meniscus

- The pattern must be able to be incorporated into a construct that has strong anchor attachments and mimics the geometry of the normal meniscus. This is essential for proper mechanical function of the construct when implanted.

The first distribution pattern explored, the layered fiber disc pattern, was made by creating collagen sponge sheets with fiber inlaid. Fiber imbedding was done prior to lyophilization of the collagen dispersion. The difficulty and tediousness of this pattern made it impractical as a design, and it was therefore rejected early in the design process.

The next pattern, the circumferential ring pattern, was made by creating fiber reinforced collagen rings of differing diameter, and then assembling them into a larger construct. Briefly, fibers were wound around a glass tube of a certain diameter. During winding, the tube was repeatedly dipped in a collagen dispersion. After a given amount of windings, the glass tube (wrapped in synthetic fibers and soaked in a collagen dispersion) was frozen and then lyophilized – resulting in a fiber-reinforced collagen ring. This was repeated using different sized glass tubes, yielding four rings which were then assembled. This assembly was soaked in a collagen dispersion, frozen, and lyophilized to yield a complete device. This procedure was used to make the first prototype meniscus scaffold (Figure 1.8). For ease of fabrication, the prototype was created on a larger scale (~2X greater). When a scaffold was fabricated on a smaller scale (1:1 ratio with that of a canine meniscus), the size constraint added a significant level of difficulty which caused severe deformations in the collagen rings. This made the collagen ring pattern impractical for further scaffold development and it was eliminated from further consideration in the design process.



**Figure 1.8: Assembly of Collagen/Synthetic Fiber Ring Scaffold.** Collagen-synthetic fiber rings (left). Rings are then assembled, soaked in a collagen dispersion, frozen, and lyophilized to get the finished construct (right).

The next pattern considered was the mesh pattern. Polymer meshes were made by hot pressing fibers arranged in a criss-cross pattern (similar to a screen), and then cutting out 'donut' circular sections corresponding to the lateral cross-section of the scaffold. A mold was constructed for the scaffold consisting of a plastic base plate, an outer glass tube, and an inner glass tube. Meshes were stacked on one another in the mold with collagen dispersion between them until the proper scaffold dimensions were achieved. The mold was then frozen in an ethanol bath and lyophilized. While this distribution pattern made scaffold assembly relatively easy and provided added strength to the device, it was difficult to incorporate it into the semilunar, wedge shaped construct. Furthermore, creating anchor attachments – thus allowing the fibers to convert axial compressive loads to tensile hoop stresses – proved to be impractical since only a small percentage of the fibers could be anchored; the rest would hang free, consequently carrying no load and having little function. Therefore, it was decided to eliminate the mesh pattern from further consideration.

The final pattern considered was the quasi-circumferential pattern. In this pattern, a continuous length of fiber is wrapped around points of a circle at varying angles. The result is an organized mesh pattern that has fibers laid in the

circumferential and radial directions. This pattern can be repeated as necessary to achieve the desired fiber reinforcement. Figure 1.9 shows an example of this pattern.

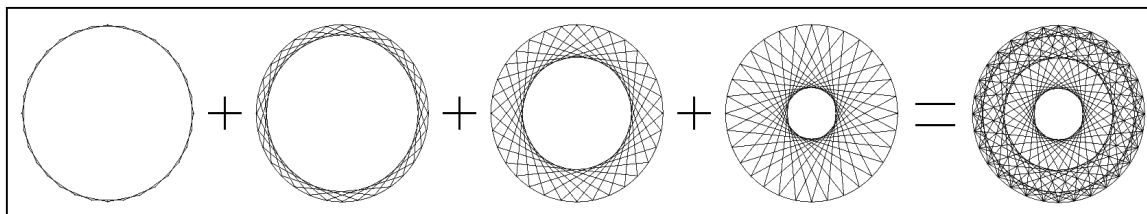


**Figure 1.9: Quasi-Circumferential Pattern Reinforcement.** Fibers were wrapped at angles of  $11.250^\circ$ ,  $28.125^\circ$ ,  $50.625^\circ$ , and  $73.125^\circ$ . Combining these yields a pattern which has circumferentially- and radially-oriented fibers.

This pattern was found to be the most promising as it met all of the established criteria for the fiber reinforcement pattern. Based on the fiber orientation, it has the ability to increase the circumferential strength of the scaffold. Additionally, this pattern is relatively easy to create, making fabrication of scaffolds with reproducible properties possible. This pattern can also be incorporated into the physical parameters of a meniscus scaffold. The angle at which the fiber is bent can be altered to create a 3-dimensional pattern with a triangular cross-section. Furthermore, a single continuous fiber can be used which wraps around nodes at the two ends of a semi-circle, creating stable tissue attachments for the device.

### 1.5. Study Overview

The overall goal of this research is to develop a resorbable meniscus scaffold which will induce neo-fibrocartilaginous tissue growth at the site of a total or subtotal meniscectomy while preventing the onset of degenerative changes in the underlying articular cartilage. The purpose of the experiments presented in this dissertation was to develop and test the feasibility of at least one potential scaffold design. To this end, the study was subdivided into three phases: Phase I: Preliminary development of fiber

reinforced meniscus scaffolds (FRMSs); Phase II: *In vitro* characterization of FRMSs; and Phase III: *In vivo* characterization of FRMSs. The objective of Phase I was to isolate at least two scaffold designs for further *in vitro* and *in vivo* testing in the following phases. For Phases II and III, specific hypotheses were tested to determine the potential of these scaffolds to function as a meniscus scaffold.

### **Phase I: Preliminary Development of Fiber Reinforced Meniscus Scaffolds (FRMS)**

The objective of this phase was to establish a reproducible procedure for fabricating a fiber reinforced meniscus scaffold which has mechanical properties appropriate for load-bearing applications in the knee and is composed of biomaterials shown to be biocompatible.

To reduce the number of variables associated with this goal, several assumptions were made. First, the matrix portion of this scaffold would be a type I collagen sponge crosslinked with EDC. Second, a synthetic biodegradable polymer fiber would be used to provide structural reinforcement. Third, a quasi-circumferential fiber pattern would be used to add circumferential and radial strength to the construct. Finally, fibers would be wrapped in such a way as to replicate the geometry of the normal meniscus and have two strong anchor attachments corresponding to the anterior and posterior horns of the meniscus. The unknown variable in this phase was the amount of fiber reinforcement required to produce a scaffold with the necessary mechanical properties.

Four different first generation scaffold designs – varying in the amount of reinforcing fiber – were tested mechanically in tension until failure. Results were compared against published mechanical data of the meniscus to determine at least two viable scaffold designs which could perform as temporary meniscal substitutes. These

two designs were incorporated into the second generation scaffold design and evaluated further in Phases II and III of this research.

### **Phase II: *In Vitro* Characterization of the FRMS**

The goal of this phase was to characterize the mechanical properties of second generation FRMSs and determine their *in vitro* cytocompatibility. In the biomechanical portion of this phase, three hypotheses were evaluated:

- (II-1) Fiber-reinforced meniscus scaffolds would convert a portion of an axial compressive load to a circumferential tensile load,
- (II-2) Fiber-reinforced meniscus scaffolds would cause an increase in contact area and overall pressure distribution on the tibial plateau after compressive loading,
- (II-3) Fiber-reinforced meniscus scaffolds would possess tensile properties on par with those of the normal ovine meniscus,

Due to the complexity of the meniscus, a customized mechanical testing protocol was developed for evaluating the FRMS designs. Each scaffold was tested for compression-to-tensile load conversion, followed by the evaluation of the pressure distribution profile on the tibial plateau. After these non-destructive tests, scaffolds were pulled in tension to failure to determine the tensile properties of second generation FRMSs and verify calculated results from Phase I.

The *in vitro* cytocompatibility of scaffolds was determined by seeding them with harvested rabbit fibrochondrocytes. Two hypotheses were evaluated in this portion of Phase II:

- (II-4) Fibrochondrocytes seeded onto fiber-reinforced meniscus scaffolds would exhibit a normal growth curve and

- (II-5) Fibrochondrocytes seeded onto MS500 fiber-reinforced meniscus scaffolds would infiltrate further than into MS1000 scaffolds after 16 days.

Cellular viability was determined by biochemical assay and cellular distribution/infiltration was determined by standard histological analysis.

For a scaffold design to proceed to further *in vivo* evaluation, it first had to demonstrate that it had structural properties on par with those of the normal meniscus, while providing a biocompatible substrate for cells to infiltrate in and proliferate on.

### **Phase III: *In Vivo* Evaluation of the FRMS**

The goal of this phase of the study was to evaluate the *in vivo* performance of FRMSs. The first experiment in this phase utilized a rabbit model for non-functional evaluation and comparison of two scaffold designs. Three hypotheses were tested:

- (III-1) Fiber-reinforced meniscus scaffolds would promote cellular and tissue infiltration into the scaffold,
- (III-2) The collagen and fiber portions of the scaffold would exhibit significant degradation between 4 and 8 weeks post-implantation, and
- (III-3) Fiber-reinforced meniscus scaffolds with a higher fiber content would impede cellular and tissue ingrowth within the scaffolds, exhibit slower incorporation, and degrade slower than lower fiber content scaffolds.

Based on the preceding evaluation and in conjunction with data from the previous two phases, one scaffold design was chosen for evaluation in a sheep model. This FRMS design had demonstrated the required mechanical and biocompatible properties necessary for load-bearing devices in the joint. FRMSs were implanted at the site of a total meniscectomy and then evaluated through a series of biomechanical and

histological methods to evaluate the quality of neo-tissue synthesized in the implant. Additionally, the surrounding tissues were evaluated for signs of joint degeneration, specifically the underlying articular cartilage, to determine any protective effect the scaffold may have had in preventing or delaying the onset of osteoarthritis. The following hypotheses were tested in this portion of Phase III:

- (III-4) Fiber-reinforced meniscus scaffolds would promote cellular and tissue infiltration into the scaffold,
- (III-5) The collagen and fiber portions of the scaffold would exhibit significant degradation between 8 and 16 weeks post-implantation, and
- (III-6) The replacement of a surgically removed medial meniscus with a fiber-reinforced meniscus scaffolds would prevent or delay the onset of degenerative changes in the articular surfaces.

## 2. METHODS

### Phase I: Preliminary Development of Fiber Reinforced Meniscus Scaffolds (FRMS)

#### 2.1. First Generation FRMSs

For ease of fabrication and preliminary mechanical evaluation, first generation scaffolds were constructed in a 'donut' shape with the following dimensions – based on those of a typical ovine meniscus (Figure 2.1).

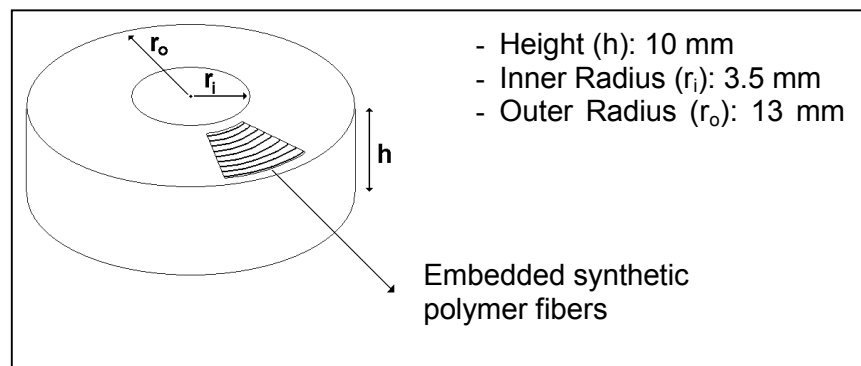


**Figure 2.1: Sketch of First Generation FRMS.** Given dimensions are based those of a meniscus from a quadruped weighing 30 – 60 kg.

A plastic base plate had a series of 32 pins embedded in a circle corresponding to the outer circumference of the scaffold. A continuous length of polymer fiber was repeatedly wrapped around the pins at varying angles (quasi-circumferential pattern – see Figure 1.9). For first generation scaffolds, four fiber angles (with relation to the tangent) were used to construct the devices:  $11.25^\circ$ ,  $28.125^\circ$ ,  $50.625^\circ$ , and  $73.125^\circ$ . For each angle, the corresponding lengths between pivot points (pins) were 0.507 cm, 1.256 cm, 2.014 cm, and 2.485 cm, respectively. There were 32 pivot points, yielding a total fiber length of 199.38 cm for a completed pattern. Using this information in conjunction

with the calculated linear density of p(DTD DD), the approximate mass of each complete pattern was calculated:

$$\text{Length [m] per pattern} * \text{linear density, } \lambda, \text{ [mg/m]} = \text{mass per pattern [mg]}$$

$$0.19938 \text{ m} * 6.20 \text{ mg/m} = 1.24 \text{ mg per pattern}$$

Complete patterns were repeated until the desired synthetic polymer-to-collagen weight ratio was reached. After the fibers were all wrapped around the pins, they were teased up to form a uniform distribution of fiber with a height of approximately 10 mm, corresponding to the height of the scaffold (Figure 2.2).

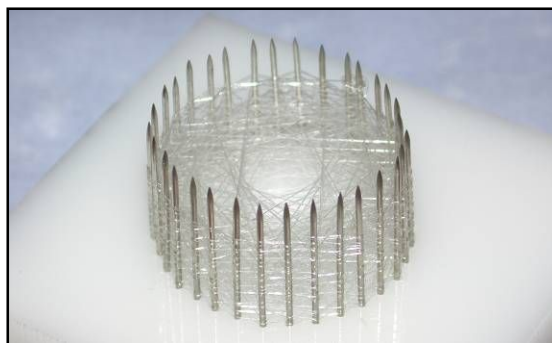


**Figure 2.2: Synthetic Fibers Wrapped in Quasi-Circumferential Pattern.**

Glass tubes with diameters corresponding to the inner and outer surfaces of the scaffold were placed on the base plate and the appropriate amount of collagen dispersion was poured over the fibers. The entire assembly was then frozen and lyophilized, yielding a complete scaffold. Figure 2.3 shows two completed first generation scaffolds as compared to two normal canine menisci.



**Figure 2.3: Two First Generation Meniscus Scaffolds Next to Two Canine Menisci.** Scaffolds are reinforced with polymer fibers arranged in a quasi-circumferential pattern.

### 2.1.1. Mechanical Characterization of First Generation FRMSs

Preliminary mechanical testing of first generation scaffolds was completed on devices with the quasi-circumferential fiber distribution pattern. For this evaluation, four different designs were investigated, varying in synthetic polymer-to-collagen weight ratio:

- Group I: 0% Synthetic polymer, 100% collagen matrix (control group) (n=8)
- Group II: 25% Synthetic polymer, 75% collagen matrix (n=5)
- Group III: 50% Synthetic polymer, 50% collagen matrix (n=5)
- Group IV: 75% Synthetic polymer, 25% collagen matrix (n=5)

Scaffolds were cut in half to form two semi-circular test samples. To prevent slippage from the Instron grips, the ends of each half were soaked in polyurethane glue and allowed to dry in a vacuum chamber. This resulted in a sample with a test section of the following average dimensions: length of 5.8 mm, width of 7.9 mm, and thickness of 5.8 mm. Samples were stored under vacuum until crosslinking.

Scaffolds were crosslinked using a protocol similar to that used previously in our lab for collagen devices<sup>146, 147</sup>. Briefly, the constructs were submerged in a crosslinking solution (10 mM 1-ethyl-3-(dimethyl aminopropyl) carbodiimide (EDC) and 5 mM N-Hydroxysuccinimide (NHS) in deionized water) for 24 hours. Scaffolds were then rinsed thoroughly for 10 minutes in deionized water (repeated three times). Next, scaffolds were submerged in a 0.1 M Na<sub>2</sub>HPO<sub>4</sub> solution for 2 hours to hydrolyze any residual EDC<sup>171, 172</sup>, followed by a rinse in deionized water for 24 hours. Finally, scaffolds were immersed in 70% ethanol for 6 hours for disinfection. Scaffolds were re-hydrated in saline for about 30 minutes prior to mechanical evaluation.

Each sample was loaded into pneumatic grips of an Instron mechanical testing system (Model #4202) and then pulled to failure at a crosshead speed of 10 mm/min. The time (seconds) and load voltage (volts) were recorded. The following structural properties were determined for each group: yield load (N), yield deformation (mm),

ultimate load (N), ultimate deformation (mm), and stiffness (N/mm). The following equations were used to calculate these values:

$$\text{deformation (d) [mm]} = \text{time (t) [sec]} * \text{crosshead speed (v) [mm/sec]}$$

$$\text{load (F) [N]} = \text{voltage (V)} * \text{max load (F}_{\text{max}}) \text{ [N]} / \text{max voltage (V}_{\text{max}}) \text{ [V]}$$

The data in this portion of the study was analyzed using one-way analysis of variance (ANOVA). For data sets that failed the normality test, the Kruskal-Wallis one-way ANOVA on Ranks was performed. All pairwise comparisons were accomplished with the Student-Newman-Keuls test.

## **2.2. Second Generation FRMSs**

Based on the results from the First Generation FRMS evaluation (See Results section 3.1, pg 71), two Second Generation designs were developed for further investigation in Phases II and III of this research.

### **2.2.1. Rationale for Design Modifications**

While the material properties of the meniscus fibrocartilage are important in how the tissue responds to various stresses and strains, its geometry and tissue attachments also play a critical role in its response to load. It is the geometry which causes the tissue to be pushed out of the joint cavity under compressive loads. The tissue attachments then cause tensile hoop stresses along the circumferential collagen fibers to be generated, resisting tissue extrusion. If the embedded synthetic fibers are to take over the role of generating hoop stresses, the scaffold must have a shape that supports its extrusion under loads and the fibers must be anchored.

There were two major modifications to the scaffold design that made these second generation constructs better suited for a meniscus analog. First, the fibers were

arranged such that the semilunar, wedge shape of the normal meniscus was replicated. Next, at the ends of the scaffold, fibers were extended to form anchor attachments for fixation to the tibial plateau at, or near, the insertion points of the anterior and posterior horns. These fibers remained continuous with the reinforcing fibers in the body of the scaffold. In theory, when the scaffold was loaded, the geometry would cause it to be extruded out of the joint capsule. The fibers in the body of the construct would be restrained by the anchors at its anterior and posterior points. Tensile stresses would develop in these fibers, resisting the load and thus, imitating the structural function of the normal meniscus.

The dimensions of a second generation scaffold were based on measurements from harvested ovine menisci and are shown below in Figure 2.4.

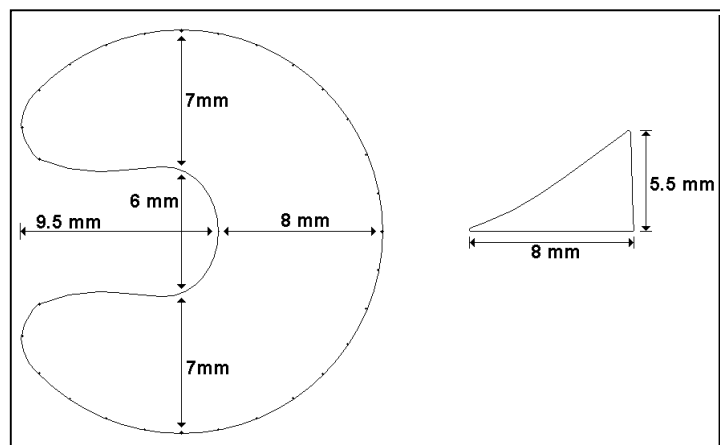


**Figure 2.4: Sketch of Second Generation FRMS.** Dimensions are based on of an ovine meniscus

### 2.2.2. Increasing the Amount of Reinforcing Polymer Fibers

Based on mechanical data collected from first generation scaffold mechanical characterization, it was determined that designing FRMSs based on polymer-to-collagen weight ratio would not yield a structurally viable scaffold (See Results section 3.1, pg 71). Dramatically increasing the amount of reinforcing polymer fiber was necessary to create an implant which would be able to take over the load-bearing role of the

meniscus. Therefore, the relationship between the number of fibers intersecting a given cross-section of first generation FRMSs and its structural properties was calculated, resulting in the following equations:

(1) Yield Load,  $F_y$

$$F_y = 0.317 (N_{ts\_total}) + 2.874 \quad R^2 = 0.998$$

(2) Maximum Load,  $F_{max}$

$$F_{max} = 0.331 (N_{ts\_total}) + 3.978 \quad R^2 = 0.996$$

(3) Stiffness,  $S$

$$S = 0.114 (N_{ts\_total}) + 0.503 \quad R^2 = 0.999$$

From these equations, the structural properties of scaffolds with a higher fiber content were extrapolated (Table 2.1). Based on the diameter of the fibers as well as hands-on experience in fabricating this quasi-circumferential pattern, it was determined that the maximum number of cross-sectional fibers possible in a meniscus scaffold of the dimensions noted above was approximately 1,000.

It should be noted that these values were based on a quasi-circumferential wrapping pattern which used only four wrapping angles. To further increase the structural integrity of FRMSs and create a more uniform fiber distribution within the body of the implant, two additional fiber wrapping angles were included in second generation designs.

While increasing the fiber content to the limit of the physical constraints of the scaffold would significantly increase the tensile strength of the device, the high fiber density may impede biological incorporation into the implant. Therefore, another design was developed which contained about half of the reinforcing fibers of the 1,000 fiber scaffolds. The two scaffold designs considered for further evaluation were:

1. FRMSs containing approximately 1,000 fibers, MS1000, and
2. FRMSs containing approximately 500 fibers, MS500.

**Table 2.1. Projected Structural Properties of Second Generation Scaffolds**

	<b>Number of Fibers, n</b>	<b>Scaffold Shape</b>	<b>Yield Load (N)</b>	<b>Maximum Load (N)</b>	<b>Stiffness (N/mm)</b>
<b>Known:</b>	0	donut	1.06	1.19	0.54
<b>Known:</b>	39	donut	14.81	16.06	5.30
<b>Known:</b>	117	donut	45.82	50.80	15.19
<b>Known:</b>	352	donut	114.32	119.67	40.96
<b>Unknown:</b>	344	Semi-lunar, wedge	112.16	118.00	39.84
<b>Unknown:</b>	478	Semi-lunar, wedge	154.73	162.41	55.16
<b>Unknown:</b>	603	Semi-lunar, wedge	194.45	203.85	69.46
<b>Unknown:</b>	720	Semi-lunar, wedge	231.62	242.63	82.83
<b>Unknown:</b>	969	Semi-lunar, wedge	310.73	325.16	111.31

### 2.2.3. Fabrication Procedure of Second Generation FRMSs

For the experiments outlined in Phases II and III, the second generation fiber reinforced meniscus scaffold design was used. Two specific types of scaffolds were fabricated differing in cross-sectional fiber count: 500 fiber scaffolds (MS500) and 1,000 fiber scaffolds (MS1000). The size and geometry of the implants was based on measurements taken from several harvested canine and ovine menisci. The resultant device had dimensions consistent with those of a quadruped weighing between 30 and 60 kg.

### 2.2.3.1. Materials

The raw materials for the construct were type I, acid-insoluble bovine dermal collagen (Nitta Casings, Somerville, NJ) and poly(desaminotyrosyl-tyrosine dodecyl ester dodecanoate)(12,10), or p(DTD DD). The raw polymer was supplied by Dr. Joachim Kohn and Dr. Sanjeeva Murthy, (Rutgers University, Department of Biomedical Engineering, NJ Center for Biomaterials). The fiber extrusion was completed by Dr. Murthy.

The mold for the scaffold was made up of a plastic base plate and 24 standard straight pins. The dimensions of the base plate were 4 cm x 4 cm x 6 mm. Twenty-four holes ( $\Phi = 0.05$  mm) were drilled through the large face of the plate. Twenty-two holes at equal intervals formed a semi-circle with the remaining two holes opposite the center of the semi-circle. Twenty-four pins were pushed through the holes (Figure 2.5). This pattern allows for a semi-lunar shape to be formed along with two lengths of fibers at each horn for formation of the anchors attachments.

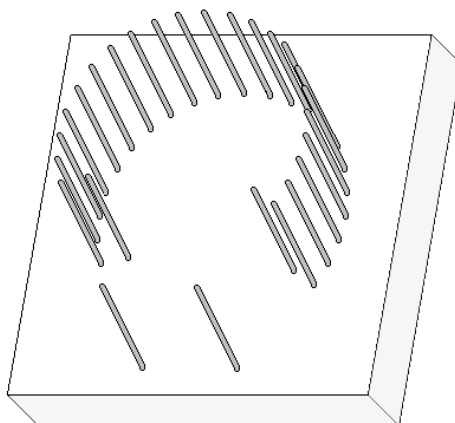


**Figure 2.5: Illustration of Base Plate for Wrapping Polymer Fibers.** The pattern contains 24 standard clothing pins pushed through a plastic base plate in a semi-circular fashion.

### 2.2.3.2. Scaffold Fabrication

Figure 2.6 illustrates the quasi-circumferential pattern used to fabricate second generation FRMSs. For each pattern number, fibers were wrapped around a given node (or pin) at a specific angle relative to the tangent. This was repeated until all nodes were wrapped.

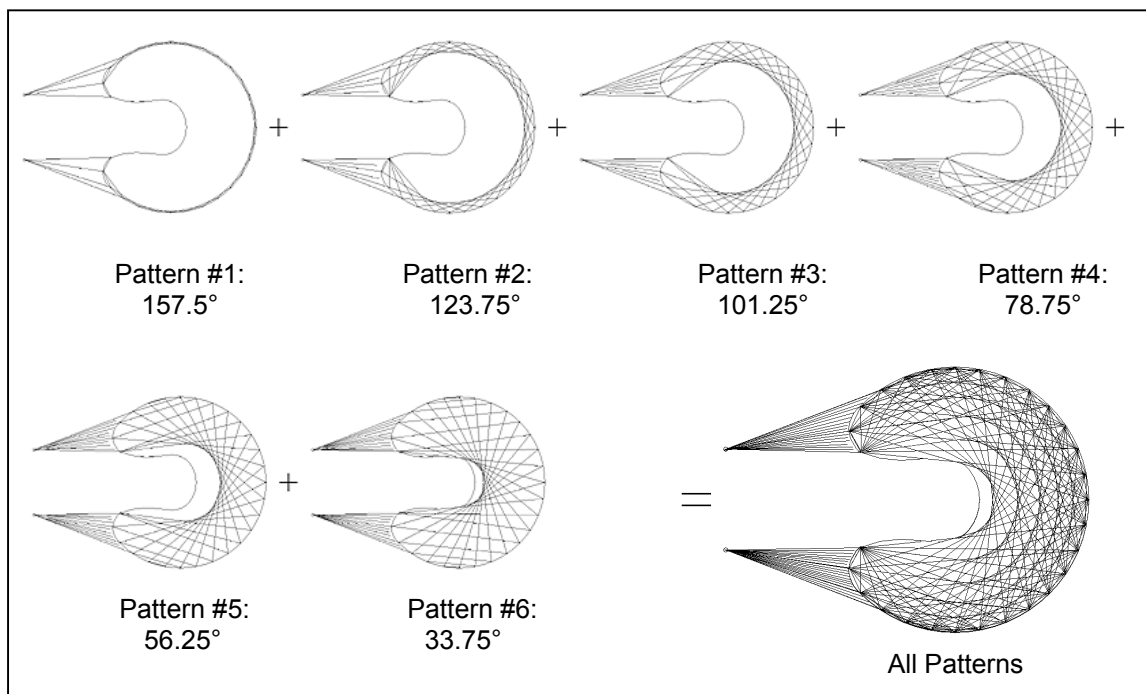


**Figure 2.6: Fiber Weaving Pattern Used for Second Generation Scaffolds.** The given measurement for each pattern is the angle at which the fiber bends around each node.

Figure 2.7 shows a step-by-step pictorial of scaffold fabrication process. For each scaffold, two spools of polymer fiber were used (Figure 2.7C). Starting from the anchor, the two continuous lengths of fiber were repeatedly wrapped in a quasi-circumferential pattern (Figure 2.7B-C). The specific pattern layout and distribution for each type of scaffold can be found in Appendix 1. After wrapping is complete, the fibers are teased up to form a wedge shaped cross-section (Figure 2.7D). The fiber wrapped

assembly is then stored in a low humidity chamber until the collagen dispersion is ready for the molding step.

A collagen dispersion was made by swelling lyophilized type I bovine collagen in an acid solution (pH 2.4). The appropriate amount of collagen was added to a volume of acid (e.g. for 1% dispersion, 1.0 g collagen added to 100ml acid). The collagen/acid mixture was then homogenized using a high speed blender (pulse blending to reduce possible heat denaturation effects on collagen) (Figure 2.7E). After about five minutes of pulse blending (mix ~5 seconds, wait for ~1 minute), the mixture was deaerated under vacuum for five minutes. About 8 ml of the dispersion was drawn up into a syringe using a 20 gauge needle – to prevent large, non-homogenized chunks of collagen from entering scaffold. A peripheral mold was formed using aluminum foil around the periphery of the fiber assembly (Figure 2.7F). The collagen dispersion was the injected into the mold, ensuring no air bubbles were introduced into the scaffold body (Figure 2.7G). The assembly was then wrapped in a thin plastic bag and submerged in an ethanol-dry ice bath (~ -30 °C) for about 10 minutes (Figure 2.7H). The resultant solid was then transferred to a standard freezer for about an hour to ensure complete freezing. After the entire assembly is frozen completely, it was lyophilized in a Freezone 1L system (Labconco, Kansas City, MO) overnight to ensure complete dehydration (Figure 2.7I).

After lyophilization, the pins are removed from the bottom of the base plate, releasing the scaffold from it. Using a standard clothing pin with an eye needle, a continuous length of polymer fiber (double strand) was threaded through the peripheral holes created by the straight pins eight times (Figure 2.6 J). The purpose of this last peripheral stitch was to secure the nodes of scaffold and increase the structural integrity

of the device. Ethibond suture (size 5) was also threaded twice through each horn attachment for anchoring during surgery.

Scaffolds were then crosslinked by EDC using a protocol used previously in our lab<sup>146, 147</sup> (Figure 2.7K). Briefly, the devices were submerged in an EDC solution (10 mM EDC and 5 mM N-Hydroxysuccinimide in deionized water) for 24 hours and then rinsed thoroughly for 10 minutes in deionized water (three rinses). Next, scaffolds were submerged in a 0.1 M  $\text{Na}_2\text{HPO}_4$  solution for 2 hours. Finally, the devices were rinsed in deionized water for 24 hours (changing water every 6 hours). Scaffolds were again wrapped in a thin plastic bag, submerged in a dry-ice ethanol bath, and then lyophilized. The resultant implants were transferred to sealable pouches and sterilized with E-beam (25 kGy) (Figure 2.7L). Sterile scaffolds were stored in a dark vacuum chamber until use.

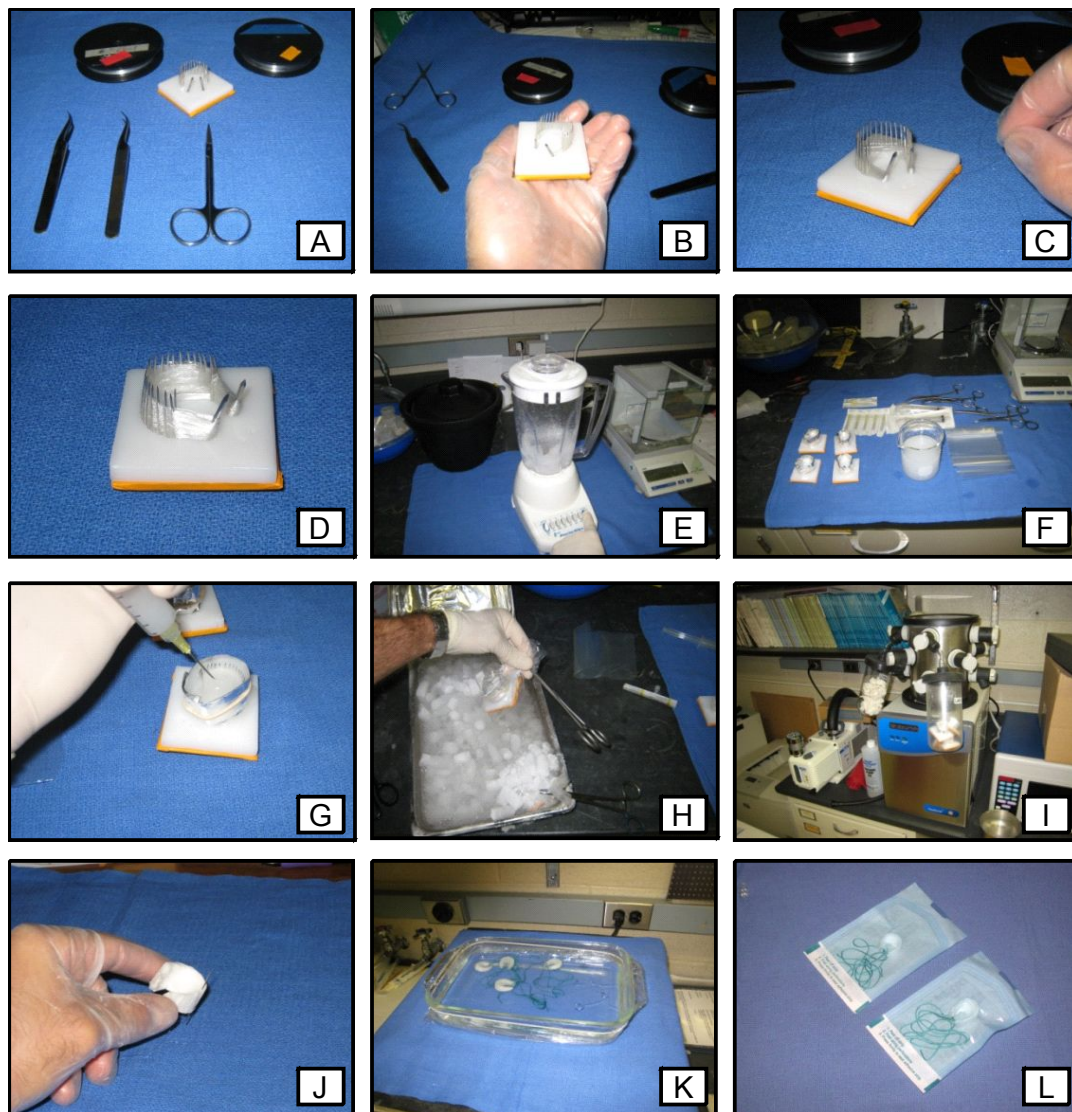


**Figure 2.7: Pictorial Summary of Second Generation FRMS Fabrication Process.** Polymer fibers are wrapped around the scaffold mold as per the pattern illustrated in Figure 2.6. The completed fiber assembly is wrapped in foil and then injected with a 1% type I collagen dispersion. It is then wrapped in a thin plastic bag and submerged in a dry ice-ethanol bath. The frozen scaffolds are lyophilized overnight. Scaffolds are removed from the base plate and a stitch is repeatedly weaved through the periphery of the device. Scaffolds are crosslinked in an EDC solution, frozen, and again lyophilized. They are then transferred to airtight pouches and sterilized with e-beam. Packaged scaffolds are then stored in a cover vacuum chamber until use.

#### 2.2.4. Projected Mechanical Properties of Second Generation FRMSs

The theoretical tensile strength of second generation FRMSs was calculated to validate that this design would possess initial tensile properties on par with those of the normal meniscus.

To calculate the theoretical structural tensile strength of FRMS designs, the relevant material properties of polymer fibers were required. The fiber yield load was obtained from single fiber testing data collected throughout the study to verify consistency of material properties between fiber batches. Briefly, single fibers of p(DTD DD) at a gauge length of 50 mm were pulled in tension to failure at a crosshead speed of 10 mm/min. Data was collected from six batches, each with 5 samples.

For structural property calculations, it was assumed that a uniform tensile load was applied to the scaffold from the anterior and posterior halves. Additionally, it was assumed that fibers at each node were fixed. Mechanical analysis was completed for a small cross-section of the scaffold (Figure 2.8).

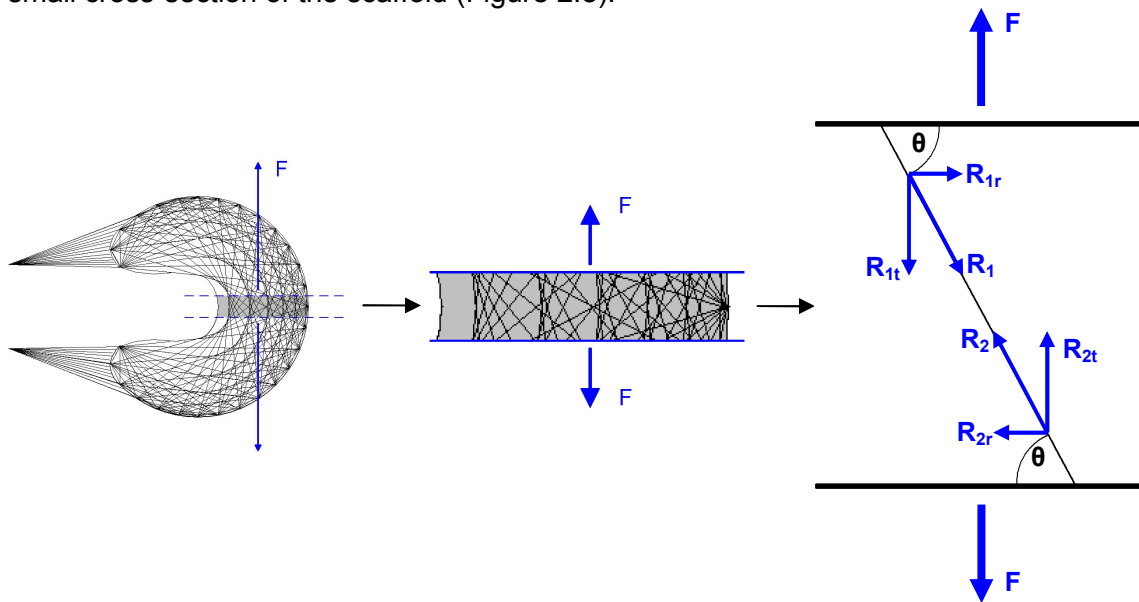


**Figure 2.8: Free Body Diagram of FRMS Tested in Tension.** A uniform tensile load is applied to a scaffold at the anterior and posterior halves. A small area of the scaffold at a  $0^\circ$  radial line is considered for analysis. For a single fiber at an angle,  $\theta$ , the radial and tangential components of the radial force are calculated.

For a force,  $F$ , is applied to the fiber at its ends, the reaction force,  $R$ , generated in the fiber can be broken down into two components in the tangential,  $R_t$ , and radial,  $R_r$ , directions. The radial components,  $R \cos \theta$ , are equal and add up to apply a shear force to the sample. However, for any given fiber, there is another which is oriented at its supplementary angle (not shown in Figure 2.8). The radial components of these two fibers cancel each other out and the resultant shear force is not applied to the whole structure. The tangential components of each fiber,  $R \sin \theta$ , are equal and opposite. Therefore, for a fiber at an angle,  $\theta$ , from the applied force, the tangential yield load of a fiber at an angle,  $\theta$ , can be described as:

$$\text{➤ Single Fiber Tangential Yield Load } [P_{ty}] = \text{Fiber Yield Load } [F_y] * \sin \theta$$

Due to the semi-lunar shape of the FRMS, the fiber orientation was not the same at different angles. Therefore, three radial angles were considered during modeling:  $0^\circ$ ,  $45^\circ$ , and  $90^\circ$ . To calculate the total yield strength of the entire structure, the tangential yield load of each fiber at these three radial angles was calculated and summed together.

$$\text{➤ FRMS Yield Load} = \sum_i (P_{ty(i)} * \sin(\theta_{(i)}))$$

Scaffold designs possessing circumferential yield strength on par with those of the normal meniscus proceeded to further *in vitro* evaluation in Phase II of this project.

## **PHASE II: *In Vitro* Characterization of the FRMS**

### **2.3. Mechanical Characterization of Meniscal Scaffolds**

Biomechanically, the meniscus is a complex tissue, with material properties similar to those of tendons, ligaments and cartilaginous tissues. The purpose of the experiments outlined in this phase was to characterize the structural properties of this meniscus scaffold and determine the potential utility of such a device as a biomechanically relevant meniscal implant.

#### **2.3.1. Conversion of Axial Compressive Loads to Tensile Hoop Stresses**

The ability of the meniscal implant to convert axial, compressive load to tensile, circumferential loads was evaluated in this experiment. The following mechanical testing protocol was based partly on one used previously in the RWJ Orthopaedic Laboratory<sup>173</sup>. It was developed for *in situ* testing of strain in the human meniscus and employs the use of a differential voltage reluctance transducer (DVRT) strain gauge. However, it was found that the DVRT was not a viable option for evaluating the circumferential deformation of a fiber reinforced collagen sponge. The barbs of the gauge essentially got caught in the sponge portion of the implant and did not accurately measure the fiber elongation. Therefore, the testing protocol was altered to directly measure the circumferential, tensile loads experienced by the implant at its attachment points after the application of an axial compressive load.

##### **2.3.1.1. Setup of Dual Instron Mechanical Testing System**

Two Instron Mechanical Testing Systems (Norwood, MA) were used in this experiment: (1) Model #5569, 10 kN load cell, Bluehill software and (2) Model #5542, 100 N load cell, Merlin software. The Instron 5569 was used to apply a compressive

load to the meniscal scaffold at a constant crosshead speed. The Instron 5542 was used to measure any circumferential tensile forces generated in the scaffold as a result of the compressive loading.

A customized jig was fabricated for use with the Instron 5569. The distal and proximal four inches of a sheep femur and tibia, respectively, were harvested and stripped of all soft tissues. The bones were dehydrated for one week in a vacuum chamber and then embedded in Elmer's polyurethane glue. The midline of each was drilled out for insertion of a 1/2" threaded steel rod. This rod screws into aluminum frames which couple with the 10 kN load cell used in the Instron 5569. These frames were fabricated for the DVRT evaluation and previously described by Richards, CJ <sup>173</sup>. Two bone tunnels ( $\Phi$ : 6 mm) were drilled through the tibia, originating at the anterior and posterior horn attachments on the tibial plateau, respectively, and exiting out the lateral aspect of the tibial shaft. These bone tunnels were used for insertion and fixation of the meniscus scaffold to the tibial plateau.

For each test run, the femoral and tibial jigs were loaded into the Instron 5569 at a 30° angle. The anterior and posterior horns of the meniscus scaffold were inserted into the respective bone tunnels of the tibial jig. The suture from the scaffold horn attachment was fed through the opposite side of the tibia and secured to a light-weight, high strength steel cable ( $\Phi$ : 1/32", 3x7 hollow-core, McMaster-Carr, Robbinsville, NJ). This cable was fed through a high precision pulley (McMaster-Carr, Robbinsville, NJ) attached to the bottom plate of the Instron 5542, and secured to its 100 N load cell. Once loaded into the mechanical testing system, scaffolds were pre-tensioned to 2 N by jogging the Instron 5542 crosshead up or down. The vertical position of the Instron 5569 crosshead was adjusted such that the femoral jig was just above the meniscal scaffold. Figure 2.9 shows the setup of the dual Instron system prior to testing.

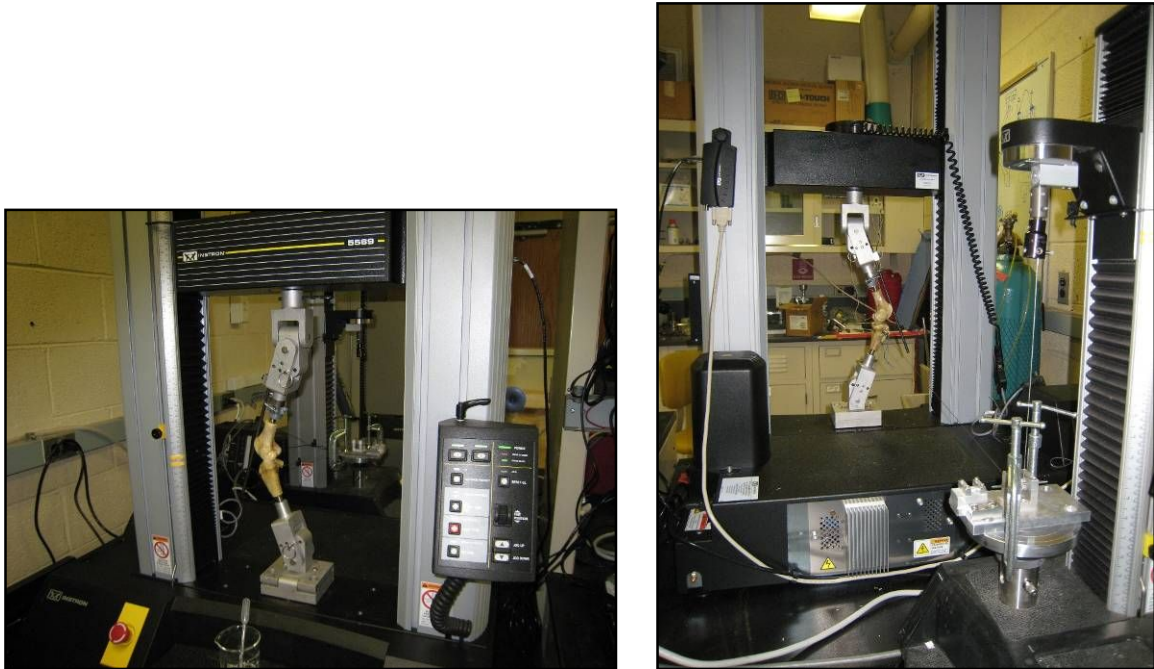


**Figure 2.9: Front and Rear Views of Dual Instron Mechanical Testing System.** The Instron Model #5569 (left image) applies a compressive load at a constant rate, while the Instron Model #5542 (right image) measures any tensile loads transmitted through the steel cable.

### 2.3.1.2. Experimental Testing Protocol Using Dual Instron System

The following procedure was followed under four conditions:

- (1) With MS1000 meniscus scaffolds (n=4),
- (2) With MS500 meniscus scaffolds (n=4),
- (3) With non-fiber reinforced collagen sponges (n=4), and
- (4) With no scaffold loaded onto the tibial jig (n=1)

All scaffolds were hydrated in Phosphate Buffered Saline (PBS) for at least 20 minutes prior to testing.

The Instron #5569 was used to apply two cyclic loading regiments to each scaffold. The first test run was for 5 cycles with minimum and maximum loads of 10 N and 100 N, respectively. The second run was for 5 cycles ranging between 10 N and 250 N. Between runs, scaffolds were rehydrated with PBS, repositioned, and retensioned. The Instron #5569 collected time and compressive load data while the

Instron #5542 collected time and tensile load data. Measurements were taken every 0.1 seconds. Immediately following this test, scaffolds were prepared for the next evaluation.

As a negative control, this procedure was also performed in the presence of no scaffold. The steel rope was secured to the tibia jig through the anterior and posterior bone tunnel. The purpose of this was to identify any contributions to the measured tensile load by deformation of the tibial jig.

The relationship between the compressive load and tensile load was plotted to determine any correlation between the two. For the 100 N cyclic loading run, the average measured tensile values at 10 N (compression) and 100 N (compression) were recorded. Likewise, the tensile values at 10 N and 250 N were recorded for the 250 N cyclic run. Finally, the average percentage of the compressive load converted to a tensile load was calculated in 25 N intervals up to 100 N, and in 50 N intervals between 100 N and 250 N.

All data was analyzed statistically using a one-way analysis of variance (ANOVA). All pairwise multiple comparisons were made using the Student-Newman-Keuls Method with p values < 0.05 considered statistically significant.

### **2.3.2. Pressure Distribution on Tibial Plateau**

In this experiment, pressure sensitive film was used to determine the extent to which a meniscus scaffold could distribute a compressive load on the tibial plateau. Pressurex low film (Sensor Products Inc, Madison, NJ), which measures pressures in the range of 2.4 to 9.7 MPa, releases a red dye when mechanically loaded. The shade of this dye can be correlated to a specific pressure, with darker shades corresponding to higher pressures, and vice versa.

The same experimental setup utilized in the previous evaluation was used in this one. However, before pretensioning of the scaffold, a section of pressure sensitive film was placed between the scaffold and the tibial plateau (Figure 2.10). Each section had dimensions corresponding to the medial half of the tibial plateau and was wrapped in cellophane to avoid moisture contact, which could distort results.

The following procedure was performed under four scaffold conditions:

- (1) With MS1000 meniscus scaffolds (n=4),
- (2) With MS500 meniscus scaffolds (n=4),
- (3) With non-fiber reinforced collagen sponges (n=4), and
- (4) With no scaffold loaded onto the tibial jig (n=4)

The peripheral height of hydrated scaffolds was recorded. They were then loaded into the mechanical tester as described earlier – positioned, secured, and pretensioned. A compressive load of 100 N was applied to each scaffold and then released. The pressure-sensitive film was then replaced, and scaffolds were rehydrated, repositioned, and retensioned. A compressive load of 250 N was then applied and released. Immediately following testing, each section of film was removed from the cellophane wrapping and stored in a clean, dry, dark area until further analysis. Scaffolds were removed from the testing jig and the peripheral height was again measured. Scaffolds were then transferred to a standard freezer until further use.

Data from the film was quantified using the Topaq® Tactile Force Analysis System (Sensor Products Inc., Madison, NJ). From this, the pressure distribution profile on the tibial plateau, as well as the corresponding histogram, were obtained.

To calculate the contact area on the tibial plateau, raw film images were first scanned and converted to high resolution digital images. Artifact film data was cropped out. Pictures were converted to black and white images and the total contact area for each run was defined by the total number of black pixels per image.

All data was statistically analyzed using a one way ANOVA with pairwise multiple comparisons made using the Student-Newman-Keuls Method. P values < 0.05 were considered statistically significant.

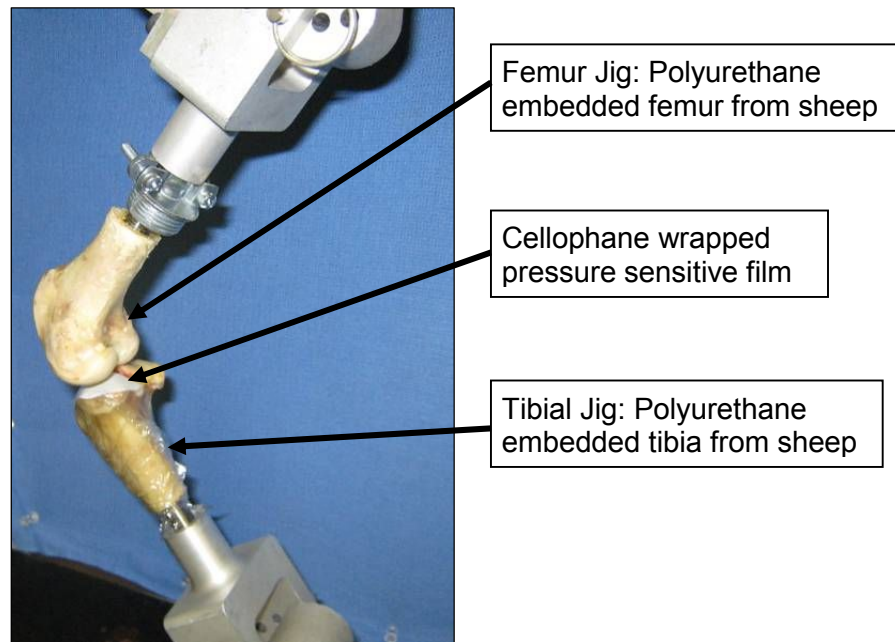


**Figure 2.10: Picture of Cellophane Wrapped Pressure Sensitive Film Loaded into Customized Mechanical Tester Jig.**

### 2.3.3. Circumferential Tensile Testing

The purpose of this experiment was to quantify the tensile strength of each type of meniscus scaffold for comparison to the normal ovine meniscus. All testing was performed using an Instron Model #5569 with a 10 kN load cell. The following groups were evaluated in this experiment:

- (1) MS500 meniscus scaffolds (n=4),
- (2) MS1000 meniscus scaffolds (n=4),
- (3) Medial menisci from knee of skeletally mature sheep (n=9), and
- (4) Lateral menisci from knee of skeletally mature sheep (n=9).

All test samples were soaked in PBS for 20 minutes prior to testing, or until samples were hydrated and at room temperature. To mitigate failure by crack propagation in the native meniscus samples, 1-2 mm of the translucent tissue at the inner margin was trimmed away.

Approximately 5 mm of each sample was loaded into cryogenic freeze clamps (Enduratec, Eden Prairie, MN) in an orientation illustrated in Figure 2.11.

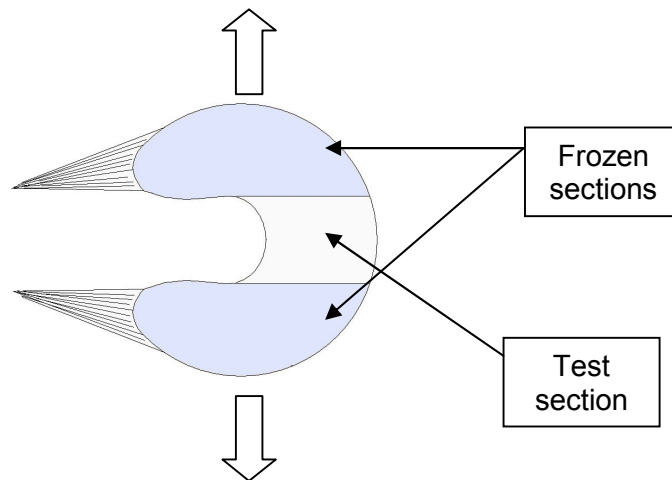


**Figure 2.11: Illustration of Sample Orientation During Tensile Testing.** Shaded areas are loaded into grips and frozen. They function as rigid portions of the scaffold for gripping during the application of a tensile load.

While freezing, samples were pretensioned to 2 N, resulting in a gauge length between 8 and 12 mm. While the testable area remained unfrozen, samples were pulled until failure at a constant rate of 10 mm/min. For each test run, the time, deformation, and tensile load were recorded every 0.1 seconds.

Data was analyzed statistically with a one-way ANOVA and multiple pairwise comparisons determined using the Student-Newman-Keuls Method. P values < 0.05 were considered statistically significant.

## 2.4. Characterization of *In Vitro* Biological Response to Scaffolds

For a scaffold to function as intended, it must retain its biomechanical function while allowing for cellular infiltration, proliferation, protein synthesis, and protein deposition. In this experiment, the *in vitro* cytocompatibility of MS500 (n=7) and MS1000 (n=7) scaffolds were evaluated through biochemical assay as well as standard histology.

### 2.4.1. Cell Line Harvest and Culture

A fibrochondrocyte cell line harvested from the menisci of New Zealand white (NZW) rabbits was used in this experiment. Cells were harvested using protocols used previously in our lab<sup>174, 175</sup> combined with those developed by other investigators<sup>176, 177</sup>. Menisci were harvested aseptically from the knees of NZW rabbits and transferred to Hank's Buffered Salt Solution (HBSS) on ice. The tissue was transported to a cell culture hood for the remainder of the processing. Meniscal tissue was dissected into ~2 mm chunks by a pair of scalpels (size 15 blades). The tissue chunks were transferred to a culture plate with an enzyme solution containing Dulbecco's Modified Eagle Medium (DMEM), 2 mg/ml bacterial collagenase, and 0.15 mg/ml DNAase and left overnight in an incubator at 37 °C, 5% CO<sub>2</sub>, and 95% humidity. The next day, the tissue/enzyme solution was pipetted aggressively several times to break up large tissue chunks and then transferred to a 50 ml centrifuge tube. The solution was centrifuged and the supernatant removed. Complete media – containing DMEM/F-12 media (50/50 mix), 2 mmol glutamine, 10% fetal bovine serum (FBS), 100 units/ml penicillin, 100 µg/ml streptomycin, and 2.5 µg/ml fungizone (all purchased from Gibco, Carlsbad, CA) – was added to the resultant pellet. The media and remaining cell pellet were briefly vortexed and the resultant solution was transferred to a culture plate. The cell line was maintained in an incubator at 37 °C, 5% CO<sub>2</sub>, and 95% humidity until its second or third passage.

### 2.4.2. Scaffold Preparation

Approximately two hours before seeding, sterile scaffolds were divided into six sections; four body sections and two horn sections (Figure 2.12). Sections 1 – 4 were randomly assigned to one of four time point groups: 4 hours, 4 days, 8 days, or 16 days. The two horn sections were either used as back-up in the event one of the body sections became contaminated, or assigned to the 8 or 16 day time point group.

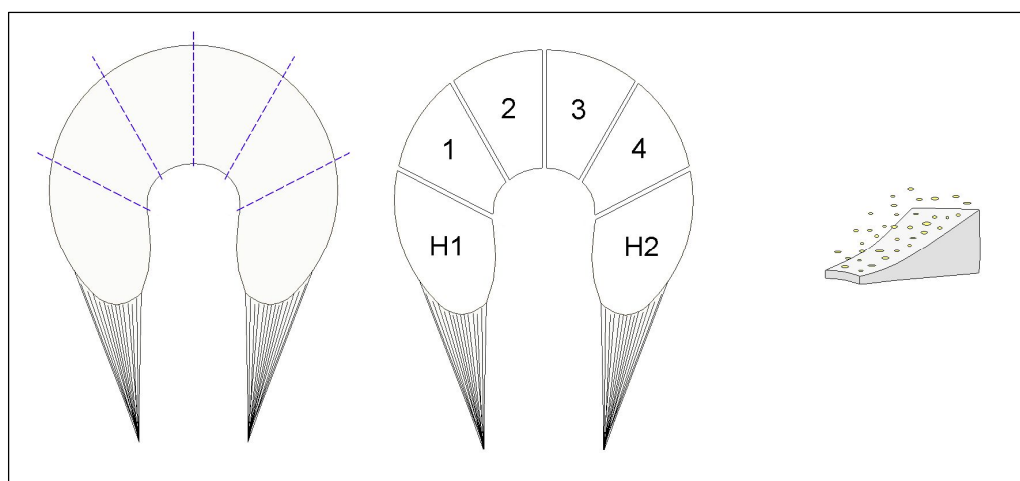


**Figure 2.12: Illustration of FRMSs Sectioned into Wedges for Cell Seeding.** Scaffolds were cut into 6 sections. Sections 1-4 were approximately the same size. The horn sections, H1 and H2, were used as substitutes in case one of the previous sections became contaminated. If this was not the case, they were used in the 8 or 16 day group. Cells were seeded on the top area of each section.

Each section was then transferred to one well of a sterile, 6 well cell culture plate. Scaffold wedges were soaked in Dulbecco's PBS (Gibco, Carlsbad, CA) containing 100 units/ml penicillin, 100  $\mu$ g/ml streptomycin, 2.5  $\mu$ g/ml fungizone, and 40  $\mu$ g/ml gentamicin for one hour, followed immediately by a one hour soak in complete media with 50  $\mu$ g/ml. Immediately prior to seeding, media from the well was removed and the dimensions of the hydrated scaffolds were recorded.

### 2.4.3. Cell Seeding of Scaffolds

Five confluent flasks of fibrochondrocytes were trypsonized and combined into one centrifuge tube. Cells were pelletized by centrifugation at 600 rpm for five minutes, followed by removal of the supernatant and then addition of 20 ml of complete media. The cell concentration was determined manually using a hemocytometer (counted 3x per tube). Dilutions were calculated to give a cell/media solution of  $1.0 \times 10^5$  cells per 40  $\mu$ l. Prepared scaffold wedges were then seeded uniformly on the anterior surface with  $1.0 \times 10^5$  cells (Figure 2.12). After four hours, complete media with ascorbic acid (50  $\mu$ g/ml) was added to the well to completely submerge the scaffold section. Cell seeding was broken up into two days with three of each scaffold type on day 1 and four on day 2.

### 2.4.4. Cell Viability Biochemical Analysis

Cell viability was determined using the CellTiter 96<sup>®</sup> AQueous Non-Radioactive Cell Proliferation Assay (Promenade Corp., Madison, WI) with the manufacturer's recommended protocol<sup>178</sup>. In this assay, viable cells convert MTS tetrazolium salt to formazan via dehydrogenase enzymes. Formazan is a water soluble compound whose absorbance can be measured at 490 nm. This absorbance is directly proportional to the number of viable, metabolically active cells in culture and can be used to determine an approximate cell number by comparison to a standard curve.

Immediately prior to running the assay on the scaffolds, two standard curves were created. Each standard curve was created from three confluent flasks of cells. As described above, cells were trypsonized, pelletized, and then counted manually with a hemocytometer. A twelve point standard curve was created and the cell solution was brought to the appropriate concentration. The number of cells per standard curve point differed depending on the time point. Table 2.2 shows the standard curve used for each time point:

**Table 2.2. Standard Curve for Time Points of Cell Viability Assay**

Time Point	Number of Cells per Standard Curve Point											
	1	2	3	4	5	6	7	8	9	10	11	12
4 hours:	blank	0	4.0E+03	8.0E+03	2.0E+04	4.0E+04	6.0E+04	8.0E+04	1.0E+05	1.2E+05	1.6E+05	2.0E+05
4 days:	blank	0	4.0E+03	8.0E+03	2.0E+04	4.0E+04	6.0E+04	8.0E+04	1.0E+05	1.2E+05	1.6E+05	2.0E+05
8 days:	blank	0	8.0E+03	2.0E+04	4.0E+04	8.0E+04	1.2E+05	1.6E+05	2.0E+05	2.4E+05	2.8E+05	3.2E+05
16 days:	blank	0	6.0E+03	2.4E+04	7.2E+04	1.2E+05	1.8E+05	2.4E+05	3.0E+05	4.2E+05	5.4E+05	6.0E+05

Two standard curves were plated twice in a 24-well plate. Each well contained the desired number of cells in 1000  $\mu$ l of complete media. Standard curves were then set aside while the scaffold sections were prepared for analysis. Media was pipetted out of the appropriate scaffold section well and the dimensions of the wedges were recorded. They were then transferred to a 24-well plate. It was assumed that each scaffold wedge retained approximately 200  $\mu$ l of media. To bring the level of media to that of the standard curves, 800  $\mu$ l of complete media was added to each scaffold well.

Because the MTS solution is light sensitive, the following preparation steps were completed in minimal, indirect light. 200  $\mu$ l of MTS was added to each standard curve well and each scaffold wedge well. The 24-well plates were then transferred to the incubator for 3-4 hours, or until an obvious color gradient was observed in the standard curve. After incubation, 100  $\mu$ l of the MTS/media solution from each standard curve well was transferred to 96-well plate (twice per standard curve, for a total of four standard curves per 96-well plate). Similarly, 100  $\mu$ l of solution from each scaffold well was transferred to the 96-well plate. The absorbance at 490 nm was read by an Emax Precision Microplate Reader (Molecular Devices, Union City, CA).

The absorbance of each unknown was compared against the standard curve to get an approximate cell number. Data was analyzed using a two-way ANOVA with pairwise comparisons using the Student-Newman-Keuls Method.

#### **2.4.5. Histological Analysis**

One scaffold per time point was fixed in Carson's Buffered Formalin. Scaffolds were processed histologically and stained with H&E. For each section, the extent of cellular proliferation into the scaffold, predominant substrate attachment of cells (collagen sponge vs synthetic polymer), and overall cell distribution over the scaffold will be qualitatively analyzed.

For meniscal scaffold designs to be considered for further *in vivo* evaluation, they had to demonstrate the ability to mimic the structural behavior of the meniscus under load. Furthermore, the scaffold needed to support proliferation of fibrochondrocytes in culture.

## Phase III: *In Vivo* Evaluation of the FRMS

### 2.5. Preliminary *In Vivo* Evaluation of FRMS in Rabbit Model

If an implant is to degrade and eventually be replaced by fibrocartilaginous tissue that functions as a meniscus, it must allow for cellular infiltration, proliferation, protein synthesis, and protein deposition. Data from previous experiments conducted in our lab has shown that materials are infiltrated and degrade at different rates depending on the implantation site<sup>144, 145</sup>. For many biological implants, the harsh synovial environment<sup>179, 180</sup> leads to a decrease in cellular infiltration and an increased rate in scaffold degradation. In this experiment, the *in vivo* biological response to MS500 (n=5) and MS1000 (n=5) meniscal scaffolds implanted intraarticularly was evaluated at two time points: 4 weeks (n=5) and 8 weeks (n=5). All surgeries were performed under an Institutional Animal Care and Use Committee (IACUC) approved protocol.

#### 2.5.1. Overview of Experimental Design

Skeletally mature New Zealand white (NZW) rabbits (8-10 lbs) were used in this experiment and assigned to either the 4 week group (n=5) or the 8 week group (n=5). Both knees of each animal were used. A MS500 scaffold wedge was implanted in the left leg and a MS1000 scaffold wedge in the right, for a total of 10 animals in this experiment.

#### 2.5.2. Scaffold Preparation

Immediately prior to surgery, two small sections were cut from the mid-body region of each of the meniscus analogs. Each section was assigned to either the 4 week time point group or the 8 week. The dimensions of each implant are given in Figure 2.13.

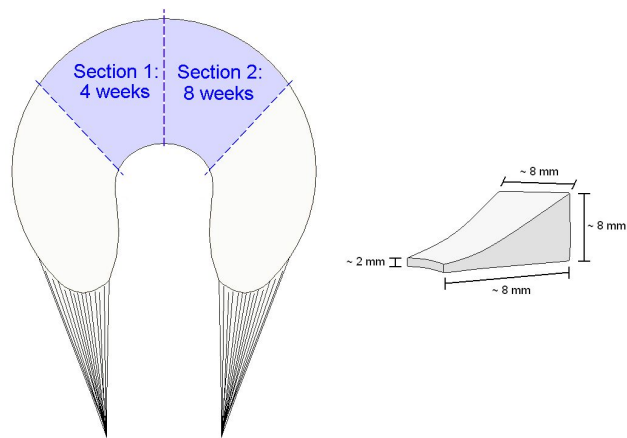


**Figure 2.13: Sketch of Scaffolds Sectioned for Non-Functional *In Vivo* Evaluation.** Two sections were cut from each scaffold and assigned to either the 4 or 8 week group. Approximate dimensions of each wedge are given.

### 2.5.3. Surgery

Approximately one hour prior to surgery, rabbits were given a relatively low dose (0.03 mg/kg) of Buprenorphine (Henry Schein, Melville, NY). Animals were anesthetized with a cocktail containing 35 mg/kg ketamine and 5 mg/kg xylazine (both from Henry Schein, Melville, NY). A face mask was placed on the animal to administer oxygen and, if needed, further anesthesia (Isoforane). The legs of the rabbit were then shaved and scrubbed with betadine and a sterile drape was placed over the animal to create a sterile field.

The surgeon created a mid-line incision over the knee joint, followed by a sharp dissection carried down through the subcutaneous tissue to the extensor mechanism. A medial parapatellar arthrotomy was made, creating a pocket for the implant between the muscle and the medial aspect of the knee joint (Figure 2.14a). The implant was placed in the pocket and secured with suture (Figure 2.14b). The arthrotomy was then closed with interrupted stitches of 2-0 Vicryl suture, the subcutaneous tissue re-approximated with interrupted stitches of 4-0 Vicryl suture, and the skin closed primarily with a running subcuticular 4-0 Monocryl stitch. The animals were returned to their cages and allowed

unrestricted movement. Post-operative pain management included administering of 0.05 mg/kg, every 12 hours for 24 hours. This surgical procedure allows for the implant to be exposed to the synovial fluid without impeding joint function or being mechanically stressed.

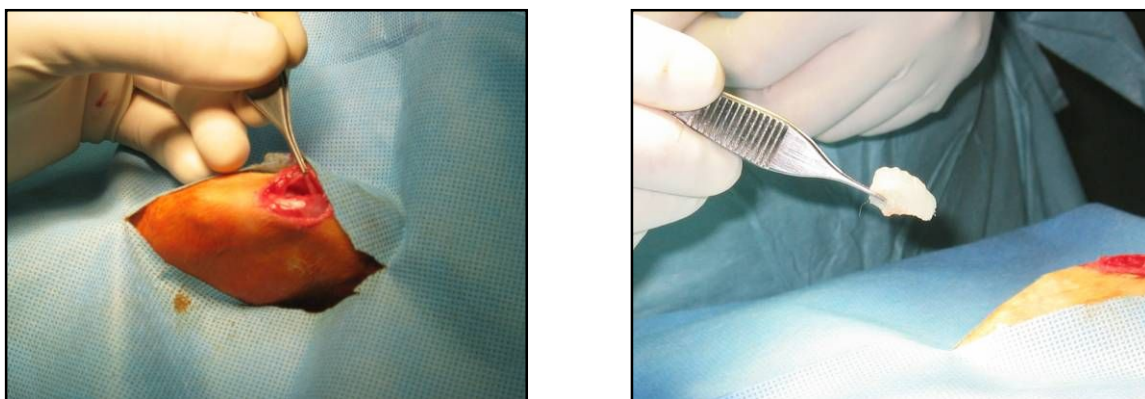


**Figure 2.14: Pictures from Surgical Implantation of FRMS Wedge into Surgically Created Pocket in Rabbit Knee Joint.** (a) A parapatellar incision was made to create a pocket which allows for exposure to the synovial fluid, (b) the implant is placed in the pocket and secured with a suture.

#### 2.5.4. Analysis

After four or eight weeks, the rabbits were euthanized and its knee joints dissected. The suprapatellar region of the synovium was inspected for any signs of infection or inflammation. The scaffold section along with 2-3 mm of the surrounding tissue was excised from the synovium and fixed in Carson's Buffered Formalin. Each section was then processed histologically and stained with either haematoxylin and eosin (H&E) or Masson's Trichrome. Ten sections were cut from each specimen at equal spacing - five for H&E staining and five for Masson's Trichrome staining. Haematoxylin is a basic dye which stains basophilic structures (e.g. cell nuclei) blue, while eosin, an acidic dye, stains eosinophilic structures (e.g. collagen) pink. Masson's Trichrome stains collagen blue, cytoplasm pink/red, and cell nuclei black. These stains were used to qualitatively evaluate the biological response to the implant.

Slides were graded blindly by a pathologist (Parisa Javidian, M.D., Associate Professor, Pathology and Laboratory Medicine, UMDNJ) on two separate dates. Scores from each day were averaged and analyzed statistically with a two-way ANOVA. All pairwise comparisons were accomplished with the Student-Newman-Keuls method. The specific grading system used in this experiment was based on those by other investigators as well as recommendations by the pathologist and is summarized in Table 2.3 below<sup>121, 181, 182</sup>.

**Table 2.3. Grading System Used By Pathologist to Qualitatively Evaluate Biological Response to Meniscus Scaffold Wedges Implanted Intraarticularly**

<b>Presence of Inflammatory Cells</b>	
<b>Lymphocytes</b>	<b>1: low → 4: high</b>
<b>Eosinophils</b>	<b>1: low → 4: high</b>
<b>Multi-Nucleated Giant Cells</b>	<b>1: low → 4: high</b>
<b>Cellular Infiltration</b>	<b>1: low → 4: high</b>
<b>Tissue Infiltration</b>	<b>1: low → 4: high</b>
<b>Neo-Tissue Matrix Organization</b>	<b>1: disorganized → 4: organized</b>
<b>Presence of Vascular Tissue and Blood Vessels</b>	<b>1: low → 4: high</b>
<b>Scaffold Degradation - Collagen</b>	<b>1: none observed → 4: high</b>

## 2.6 Functional *In Vivo* Evaluation of FRMS in Ovine Model

Based on the results from all previous experiments outlined in this project, an 'optimal' meniscus scaffold design was chosen for short term, functional *in vivo* evaluation in an ovine model. The purpose of this experiment was to determine if a fiber reinforced scaffold which mimics the geometry and structural organization of the normal meniscus would promote neo-fibrocartilaginous growth and deposition while preventing or delaying the onset of degenerative changes in the underlying cartilage. To quantify the short-term performance of this scaffold design, a series of biomechanical and histological analyses were accomplished. Due to the size constraints of the scaffold and its surgical implantation, as well as human anatomical approximation, a sheep model was chosen for this evaluation. All surgeries were performed at the Robert Wood Johnson Medical School Vivarium using an IACUC approved protocol.

### 2.6.1 Overview of Experimental Design

Medial meniscectomies were performed on 14 sheep for evaluation at two time points, 8 and 16 weeks. A summary of the experimental design is found below:

- Group I: 8 week meniscus scaffold (n=6)
  - Biomechanical Analysis (n=3)
  - Histological, Immunofluorescence staining (n=3)
- Group II: 16 week meniscus scaffold (n=6)
  - Biomechanical Analysis (n=3)
  - Histological, Immunofluorescence staining (n=3)
- Group III: 8 week control, meniscectomy only, histology (n=1)
- Group IV: 16 week control, meniscectomy only, histology (n=1)

### 2.6.2 Surgical Implantation Procedure

Twenty-four hours prior to surgery, animals were fasted and a Fentanyl patch (100 µg/hr) (Henry Schein, Melville, NY) was applied to a shaved patch of skin on its back for pain management. On surgery day, sheep were transported to the RWJMS Vivarium surgical prep area for anesthetic induction with Sodium Pentothal (15-20 mg/kg). Animals were then intubated for anesthetic maintenance with Isoforane (1.5-3%) in O<sub>2</sub>/N<sub>2</sub>O (50/50). To prevent a pH imbalance, a rumen tube was inserted into its stomach for drainage. Marcaine was administered subcutaneously on the medial aspect of the joint about 15 minutes prior to surgery. Antibiotics were administered pre-op (IV) and then again post-op (IM) to prevent infection.

Approximately 20 minutes prior to implantation, the meniscus scaffold was soaked in sterile saline (Figure 2.15a). The animal's right leg was shaved, scrubbed with betadine, and draped to create a sterile surgical field. The surgeon first made a mid-line incision over the right knee joint, followed by sharp dissection down through the subcutaneous tissue to the extensor mechanism creating a medial parapatellar arthrotomy (Figure 2.15b). The tibia was externally rotated to provide the surgeon more room to work and a total medial meniscectomy was performed using a size 11 scalpel blade. Two bone tunnels (Φ: 6 mm) were drilled from the medial aspect of the tibial shaft to the anterior and posterior insertion sites of the excised medial meniscus (Figure 2.15c). The sutured horn attachments of the meniscus were fed into the bone tunnels from the tibial plateau and pulled through so that approximately 8-10 mm of the scaffold entered the bone tunnel (Figure 2.15d). Suture ends were pulled completely through the bone tunnels and secured with a polypropylene button (Figure 2.15e). A stitch was added between the periphery of the implant and the surrounding synovial tissue to aid in scaffold fixation (done only for last half of the animals due to early results) (Figure 2.15f).

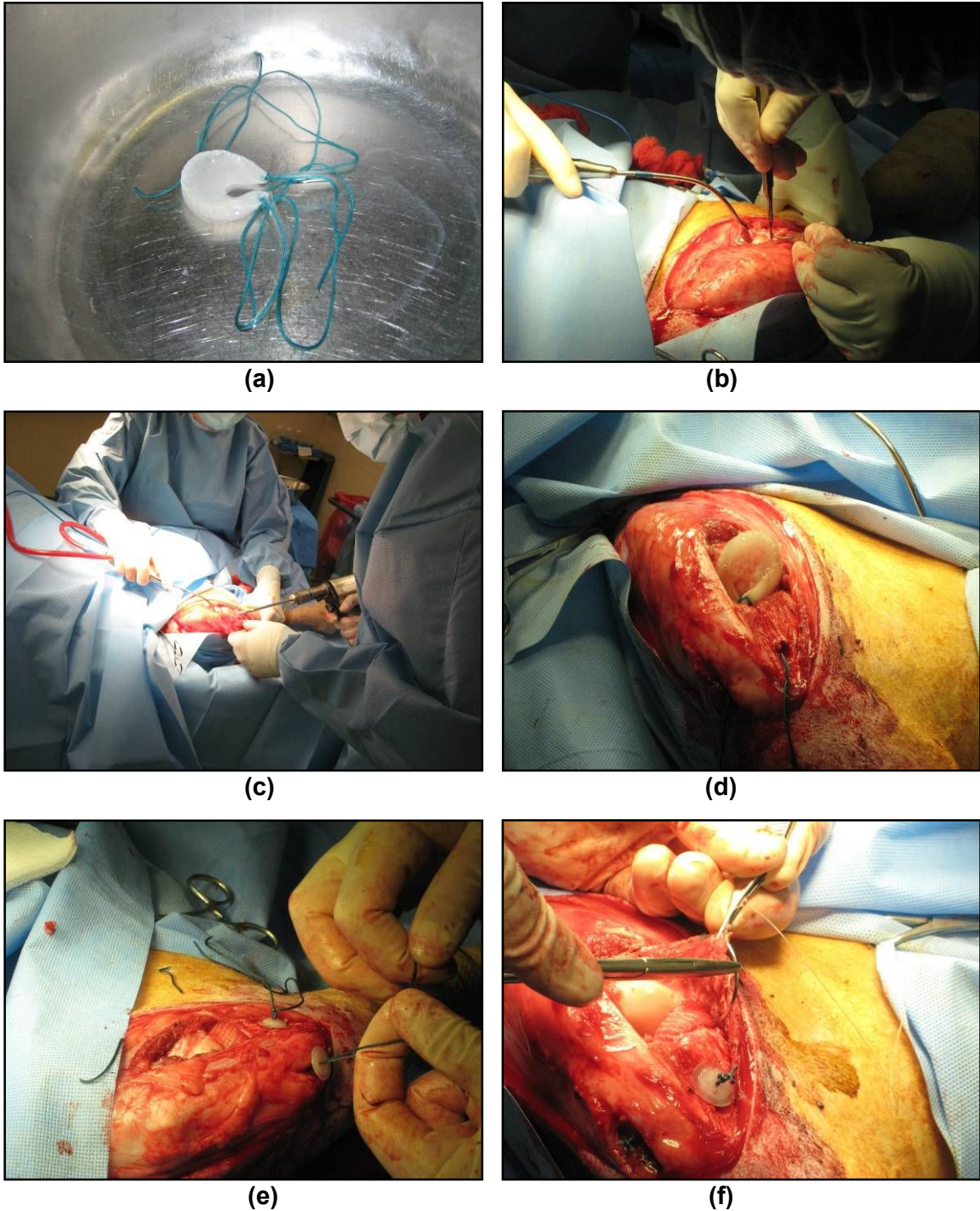


**Figure 2.15: Overview of Surgical Implantation Protocol.** (a) Scaffolds are soaked in sterile saline at least 20 minutes prior to implantation. (b) The surgeon creates a medial parapatellar arthrotomy. (c) Bone tunnels are drilled through the tibial plateau. (d) Sutures from the scaffold horn attachments are fed through the bone tunnels and pulled through. (e) Horn attachments are fed through the tunnels and then secured with a button on the lateral aspect of the tibia. (f) The scaffold is secured to the peripheral tissue by resorbable suture.

The arthrotomy was closed with interrupted 2-0 Vicryl sutures, the subcutaneous tissue re-approximated with interrupted 2-0 Vicryl sutures, and the dermis layer closed with a running (uninterrupted) subcuticular 4-0 Monocryl stitch. The animals were then returned to their cages and allowed unlimited movement.

Sheep were treated post-operatively with antibiotics for three days (500 mg Cefazolin, every 12 hours – Henry Schein, Melville, NY). The transdermal Fentanyl patch (100 µg/hr) treatment was continued for 3-6 days post-operatively as an analgesic. In addition, anti-inflammatory medication, Rimadyl (Henry Schein, Melville, NY) (1-2 mg/kg), was given every 12 hours for 3-7 days or until no species specific signs of pain were observed. Once the animals had achieved normal gait movement with no signs of infection (typically 2-4 weeks post-op), they were transferred to Perry farms for unrestricted movement and exercise.

As controls, two animals underwent a total medial meniscectomy only. No bone tunnels were drilled and no treatment was performed. Post-operative treatment for these animals was the same as the two experimental groups. One animal was scheduled for sacrifice at 8 weeks post-op, the other at 16 weeks.

### **2.6.3 Gross Evaluation**

At either 8 or 16 weeks, animals were sacrificed by an overdose of Sodium Pentothal. Both joints were dissected and gross observations noted. Specifically, observations were recorded concerning any visible damage to the articular cartilage and/or surrounding structures; the presence of fluid in the joint; irregularities on the articular surface; the presence of neo-tissue formation; as well as the size and condition of the scaffold.

## **2.6.4 Biomechanical Analysis**

Scaffold and native meniscus tissue samples were collected for tensile and compression testing. All tensile testing was performed on an Instron Model #5569 using cryogenic freeze clamps (Enduratec, Bose, Eden Prairie, MN). Unconfined compression testing was also completed on an Instron #5569 with standard compression plates.

### **2.6.4.1 Tensile Testing**

Three 8 week meniscus scaffold samples and three 16 week scaffolds were tested in tension. In addition, the lateral (n=9) and medial (n=9) menisci of the control legs were tested. For this tissue, results from each group were pooled to get a baseline structural property profile. It was assumed there would be no difference between control menisci from 8 and 16 week animals.

Prior to loading the native meniscal tissue into the cryoclamps, 1-2 mm of the inner margin was dissected out to prevent failure of the tissue by crack propagation. This was done based on results from preliminary testing completed on ovine menisci (data not reported). All samples were then loaded into the clamps at an initial gauge length of 8-10 mm and the samples' ends were allowed to freeze. Samples were pretensioned to 2 N and then pulled to failure at a crosshead speed of 10 mm/min. This procedure is similar to that used by Newman et al. in determination of the mechanical properties of canine menisci<sup>183</sup>. Time, deformation, and load were recorded. Yield load, ultimate load, and stiffness were calculated from this raw data. A one-way ANOVA was used to analyze the data and pairwise comparisons were made using the Student-Newman-Keuls Method.

#### **2.6.4.2 Unconfined Compression Testing**

When possible, biopsy plugs were harvested from excised scaffolds prior to tensile testing. Samples were taken from either the anterior or posterior horn sections.

Biopsy punches ( $\Phi$ : 5mm) were taken from samples and trimmed to have a height of 2-3 mm. Samples were placed on the bottom plate and compressed at a crosshead speed of 1 mm/min until a load of 1000N was reached. Time, deformation, and load were recorded. The compressive modulus was calculated from the first linear region. A one-way ANOVA was used to analyze the data and pairwise comparisons were made using the Student-Newman-Keuls Method.

#### **2.6.5 Standard Histological Analysis**

After compression testing, three samples were fixed in Carson's Buffered Formalin for histological processing. They were taken from the anterior, posterior, and middle third of the scaffold/tissue. Samples were oriented so that cuts were made through the cross-section or taken longitudinally (circumferentially). Five micron thick slices were taken from four equidistant levels of the tissue. For each level, two slides were prepared with multiple cuts on each. Samples from the first slide were stained with H&E and samples from the second with Masson's Trichrome.

Slides were analyzed by a UMDNJ pathologist in a blinded fashion. Each was judged qualitatively using the grading scheme used in the previous *in vivo* experiment (Table 2.3).

#### **2.6.6 Immunofluorescence Staining**

Immunofluorescence staining was used to identify collagen types I, II, III, and XII expression in the scaffold. Collagen types I and II are fibrillar proteins commonly found in the meniscus, with type I being the predominant <sup>32</sup>. Type III collagen is typically

associated with type I collagen, and is involved in its fibrillogenesis<sup>184</sup>. Type XII collagen is also found with type I collagen – and has been shown to be upregulated in collagenous structures undergoing high tensile stresses<sup>185</sup>. The purpose of this experiment was to characterize and identify the tissue forming around and into the scaffold, and compare that to the tissue found in a normal meniscus.

The following procedure was provided and conducted by Dr. Marion Gordon's laboratory (Department of Pharmacology and Toxicology, Rutgers University, Piscataway, NJ).

At sacrifice, sections of the FRMS and contralateral medial meniscus were harvested, embedded in OCT freezing compound (Tissue-Tek Sakura, Torrance, CA), and quickly frozen in liquid Nitrogen. Sections (8-10  $\mu\text{m}$  thick) were cut on a cryostat (Microm International, Walldorf, Germany; now owned by Thermo Fisher Scientific, Waltham, MA), and then placed on standard histological slides. They were allowed to air dry, and then stored at  $-80^{\circ}\text{C}$ . For experiments, sections were fixed in 100% methanol at  $-20^{\circ}\text{C}$  for 3 minutes, rinsed in PBS, and blocked with 5% normal goat sera in PBS and 0.05% Tween-20 (PBS/Tween) for 1 hour at room temperature. All primary and secondary antibodies were diluted with 1% normal goat sera in PBS/Tween. Sections were incubated with primary antibodies for one hour at room temperature then rinsed with three 5 minute changes of PBS/Tween. Sections were then incubated against appropriate secondary antibodies for one hour at room temperature, followed by three 5 minute changes of PBS/Tween. Nuclear staining was achieved by incubating sections with DAPI (Invitrogen, Carlsbad, CA) ( $5\mu\text{g/ml}$ PBS) for 10 minutes, then washing 3 times for 5 minutes with PBS. Slides were mounted with Prolong Gold Antifade Reagent (Invitrogen, Carlsbad, CA). Micrographs were taken on a Leica microscope using a ProgRes camera and ProgRes CapturePro imaging software

(Jenoptik Laser, Jena Germany). As a control, this procedure was also performed on pre-implanted scaffolds at a later date.

All primary antibodies used in this experiment are polyclonals.

- Type I Collagen Primary Antibody (Millipore, Billerica, MA) (AB745)
  - Diluted 1:30
  - Host: rabbit
  - Reacts with: bovine, canine, human, pig, sheep
- Type II Collagen Antibody (Abcam Inc., Cambridge, MA) (Ab34712)
  - Diluted 1:200
  - Host: rabbit
  - Reacts with: human, bovine, mammal
- Type III Collagen Antibody (Acris, Herford, Germany) (BP8012)
  - Diluted 1:40
  - Host: rabbit
  - Reacts with: bovine, sheep
- Type XII Collagen Antibody (Acrisgift from Dr. Marion Gordon and Dr. Don Gerecke)
  - Diluted 1:100
  - Host: rabbit

For types I, III, and XII collagen staining, the secondary antibody used was Invitrogen's (Carlsbad, CA) goat anti-rabbit AlexaFluor 488 ®, diluted 1:1000, which stains green. For type II collagen, Invitrogen's (Carlsbad, CA) goat anti-rabbit AlexaFluor 594 ®, diluted 1:1000 (stains red), was used.

Dr. Gordon's laboratory has extensive experience with collagen staining through immunohistochemistry<sup>181</sup>.

### 3. RESULTS

#### Phase I: Preliminary Development of Fiber Reinforced Meniscus Scaffolds

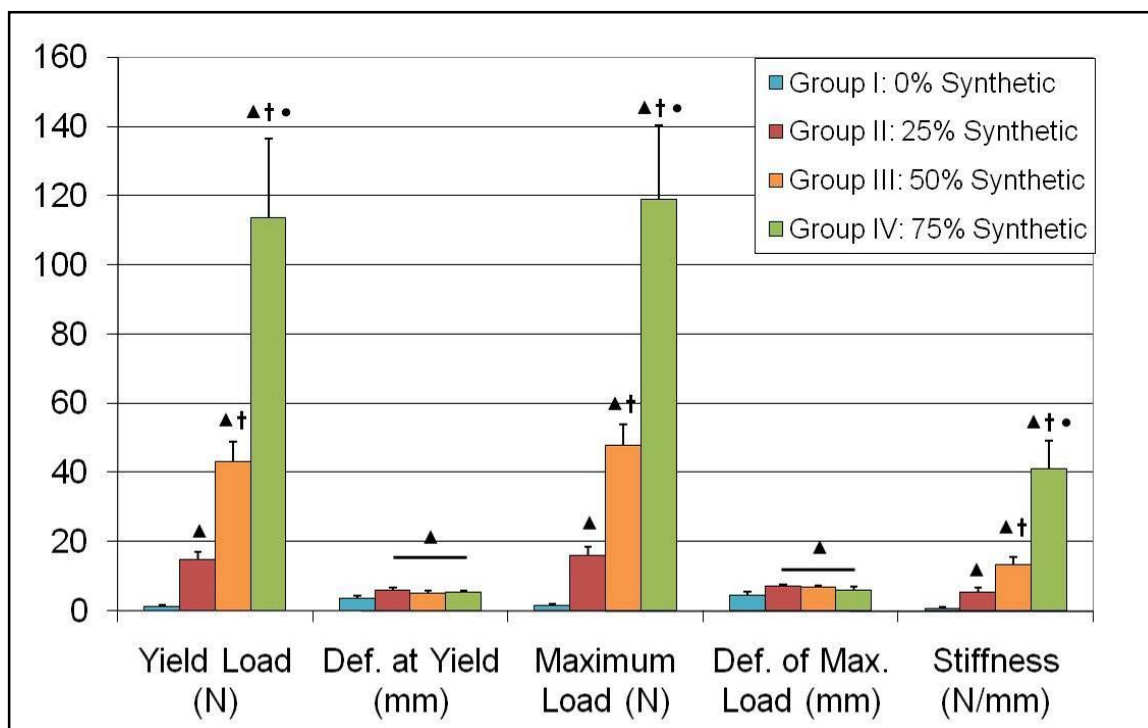
##### 3.1. Mechanical Characterization of First Generation FRMSs

Figure 3.1 shows the structural properties (yield load, deformation at yield, ultimate load, deformation at ultimate load, and stiffness) of first generation scaffolds tested mechanically in tension. For the following data sets, the normality test failed. Therefore, a Kruskal-Wallis one-way ANOVA on Ranks statistical analysis was performed. Increasing the amount of fiber reinforcing fiber was found to significantly increase the tensile yield load, maximum load, and stiffness of FRMSs ( $p < 0.05$ ). No significant differences were found in the deformation at yield or maximum load for fiber reinforced scaffolds. However, the deformations for fiber reinforced scaffolds were significantly increased with respect to a 100% collagen scaffold.

Comparison of these results with published mechanical data revealed that even the 75% synthetic FRMS had a tensile strength far below that of normal meniscal tissue <sup>3, 28, 90, 183, 186</sup>. Table 3.1 shows the yield load and stiffness of first generation scaffolds and the respective published values. These values were calculated from the material properties presented by the authors, assuming a cross-sectional area of 22 mm<sup>2</sup> (same area as typical ovine meniscus) and initial gauge length of 10 mm (same length used during all mechanical testing of meniscal tissue in this study). Conversion equations are found below:

$$\text{Calculated Yield Load [N]} = \text{Published Yield Stress [N/m}^2\text{]} * \text{Assumed Cross-sectional Area [m}^2\text{]}$$

$$\text{Calculated Stiffness [N/m]} = \frac{\text{Published Elastic Modulus [N/m}^2\text{]} * \text{Assumed Cross-sectional Area [m}^2\text{]}}{\text{Assumed Gauge Length [m]}}$$



**Figure 3.1: Structural Properties of First Generation FRMSs Mechanically Tested in Tension.** The presence of reinforcing polymer fibers resulted in significant increases in the yield load, maximum load, and stiffness of scaffolds. No differences were noted in deformation at load and maximum load between all fiber reinforced groups. All fiber reinforced groups had higher deformations at yield and maximum load with respect to non-reinforced scaffolds. ▲ indicates significant difference ( $p < 0.05$ ) with respect to Group I scaffolds. † indicates significant difference ( $p < 0.05$ ) with respect to Group II scaffolds. • indicates significant difference ( $p < 0.05$ ) with respect to Group III scaffolds.

**Table 3.1. Yield Load and Stiffness of First Generation FRMSs Compared to Respective Calculated Values from Published Data**

		Yield Load [N]	Stiffness [N/m]
<b>Fiber Reinforced Meniscus Scaffolds</b>	0% Synthetic	1.27 +/- 0.53	0.69 +/- 0.38
	25% Synthetic	14.81 +/- 2.31	5.30 +/- 1.42
	50% Synthetic	43.05 +/- 5.90	13.14 +/- 2.56
	75% Synthetic	113.76 +/- 22.75	40.96 +/- 8.17
<b>Calculated Values from Published Data</b>	Human, from Fithian et al <sup>3</sup>	n/a	204.99 +/- 115.28
	Human, from Tissakht et al <sup>186</sup>	332.20 +/- 65.56	160.27 +/- 50.40
	Canine, from Arnoczky et al <sup>90</sup>	688.82 +/- 186.12	347.58 +/- 117.26
	Canine, from Newman et al <sup>183</sup>	1518 +/- 484	167.2 +/- 85.8
	Bovine, from Proctor et al <sup>28</sup>	n/a	436.48 +/- 192.5

## 3.2. Second Generation FRMS

### 3.2.1. Projected Structural Properties

Based on this, designing of a fiber reinforced scaffold based on synthetic polymer-to-collagen mass ratio was abandoned. Further design efforts focused on the number of fibers intersecting any radially oriented cross-sectional area. The maximum number of intersecting fibers per scaffold was found to be approximately 1,000. This was based on the diameter of individual fibers as well as hands-on scaffold fabrication experience. However, concerns over inhibition of cellular and tissue ingrowth due to a substantial fiber density increase led to the consideration of another scaffold design which possessed half the maximum fiber density.

Single fiber testing was performed on five samples from six batches of p(DTD DD) values. From these values, the theoretical strength of second generation scaffolds was calculated. Table 3.2 shows the single fiber data and the calculated scaffold structural yield and ultimate load.

**Table 3.2. Measured Yield and Ultimate Load of p(DTD DD) Single Fibers and Projected Yield and Ultimate Loads of MS500 and MS1000 FRMSs.**

		Yield Load (N)	Ultimate Load (N)
<b>Single Fiber, Measured Values (n=30)</b>		1.17 +/- 0.40	1.38 +/- 0.52
<b>MS500 Scaffolds, Projected Values</b>	<b>at 0° radial plane</b>	579.57 +/- 232.79	682.92 +/- 356.59
	<b>at 45° radial plane</b>	581.89 +/- 233.73	685.65 +/- 358.02
	<b>at 90° radial plane</b>	591.06 +/- 237.41	696.46 +/- 363.66
<b>MS1000 Scaffolds, Projected Values</b>	<b>at 0° radial plane</b>	1109.91 +/- 445.82	1307.84 +/- 682.89
	<b>at 45° radial plane</b>	1114.55 +/- 447.68	1313.31 +/- 685.75
	<b>at 90° radial plane</b>	1134.15 +/- 455.56	1336.40 +/- 697.81

## **PHASE II: *In Vitro* Characterization of FRMS**

Since the projected tensile yield and ultimate load of both MS500 and MS1000 FRMSs fell within the range of calculated values from published data, both designs continued forward to the *in vitro* characterization phase of this research.

### **3.3. Mechanical Characterization of Second Generation FRMSs**

The purpose of this mechanical evaluation was to determine the extent to which a fiber reinforced collagen sponge could structurally function as a meniscus analog. From gross observation, the 1000 fiber scaffolds were more stable and able to maintain their shape better than the 500 fiber scaffold during all mechanical testing. They exhibited superior handleability and were easier to mount in the customized Instron mechanical testing system.

#### **3.3.1. Axial Compressive Loads Converted to Circumferential Tensile Loads**

A direct correlation was observed between the compressive load applied to scaffolds and the resultant tensile load measured at the anterior and posterior anchor attachments. Figure 3.2 (a-f) shows typical results for each of the scaffold designs under 10N-100N and 10N-250N cyclic loading as well as loading in the presence of no scaffold. On the first cycle, measured tensile values increased from the pre-tension value of ~2N to a certain maximum value. Subsequent increases and decreases in the applied compressive load were reflected by similar changes in the measured tensile loads. However, the measured minimum and maximum tensile loads within the body of the cyclic run always remained above the initial pre-tension value. On the final cycle of the 100N and 250N runs, the compressive load was increased to 150N and 260N, respectively, and then completely removed from the tibial jig. After removal, the measured tensile load on the anterior and posterior anchor attachments returned to the

pre-tension value. Cyclic loading in the presence of no scaffold revealed a relatively minor contribution to the measured tensile load from deformation of the tibial jig. 100% collagen scaffolds fell apart during anchoring to the tibial plateau and were considered untestable. No data for these scaffolds is reported for this experiment.

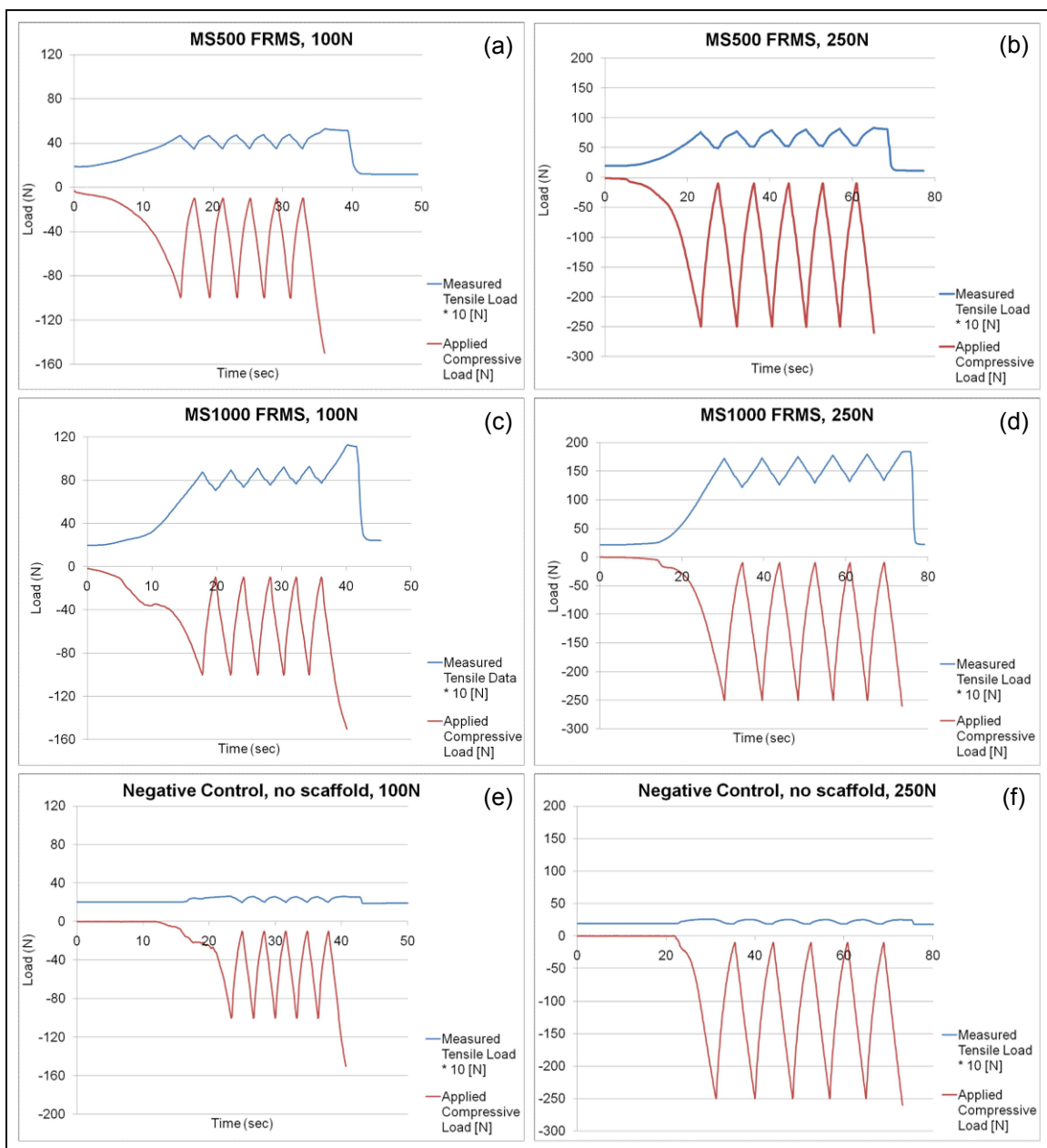


**Figure 3.2: Applied compressive load (bottom line) as compared to 10x the measured tensile load (top line) for each scaffold under each cyclic loading condition.** Results are typical for each scaffold evaluated. For each scaffold, there is a correlation between the applied compressive load and measured tensile load.

The minimum, maximum, and range of measured tensile loads for each run varied depending on the scaffold type and loading condition. Table 3.3 shows these values for each loading cycle. For both scaffold types, the range of loads significantly increased between the 100N and 250N loading cycles ( $p < 0.05$ ). Additionally, for both loading cycles, the range of loads for MS1000 FRMSs was significantly greater than that of the MS500 FRMSs ( $p < 0.05$ ).

**Table 3.3. Minimum, Maximum, and Range of Tensile Loads Measured at the Anterior and Posterior Anchor Attachments of FRMSs.**

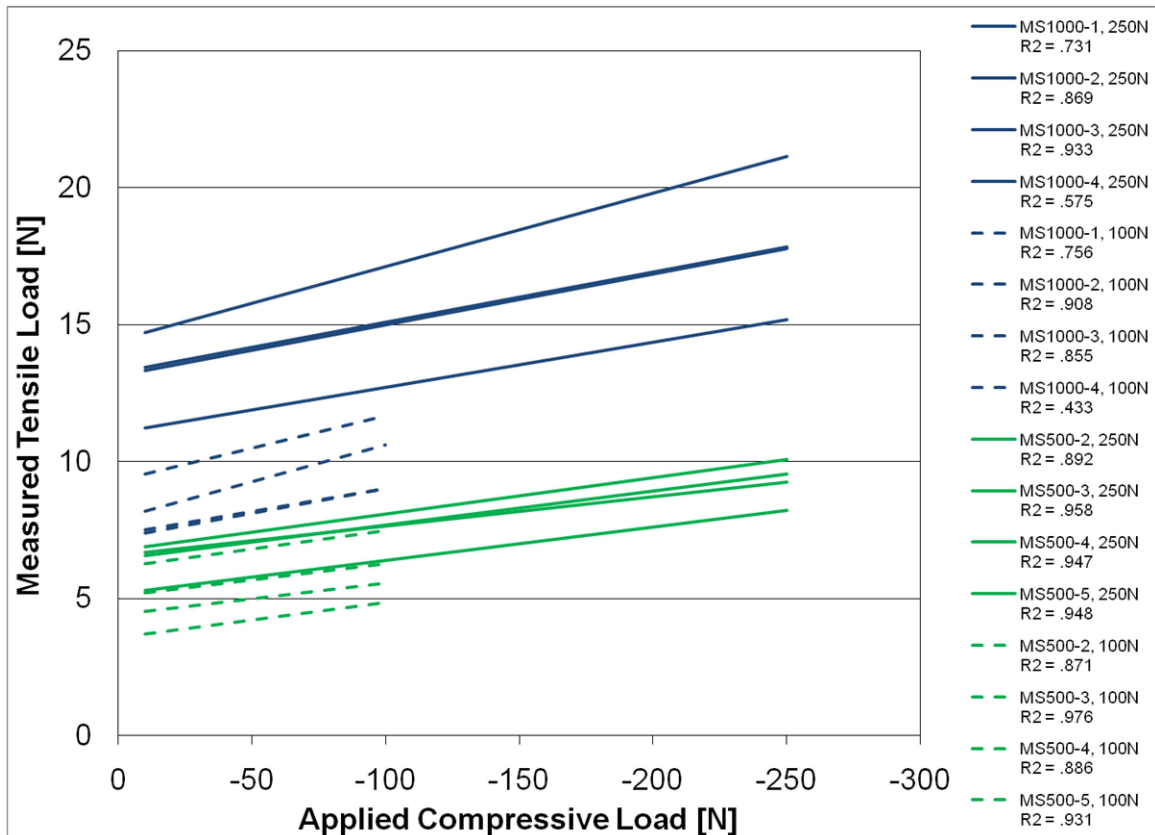
	10 N - 100 N Loading Cycle		
	Average Tensile Load Measured at 10 N Compressive Load [N]	Average Tensile Load Measured at 100 N Compressive Load [N]	Load Range [N]
MS500 FRMSs (n=4)	4.575 +/- 0.969	5.971 +/- 1.025	1.214 +/- 0.121
MS1000 FRMSs (n=4)	8.006 +/- 1.069	10.119 +/- 1.219	2.113 +/- 0.712

	10 N - 250 N Loading Cycle		
	Average Tensile Load Measured at 10 N Compressive Load [N]	Average Tensile Load Measured at 250 N Compressive Load [N]	Load Range [N]
MS500 FRMSs (n=4)	6.123 +/- 0.585	9.054 +/- 0.739	2.931 +/- 0.308
MS1000 FRMSs (n=4)	12.428 +/- 1.332	17.772 +/- 2.361	5.344 +/- 1.756

The applied compressive load was plotted against the measured tensile load for each cyclic run. For the 100N cyclic run, only tensile values corresponding with the compressive loads between 10N and 100N were included. Likewise, for the 250N cyclic run, only tensile values corresponding with the compressive loads between 10N and 250N were included. The linear relationship was calculated for each and the corresponding trendline was plotted in Figure 3.3. Corresponding  $R^2$  values for each evaluation are included in the legend.

Within the MS1000 scaffold group, two distinct linear relationships between the compressive and tensile loads were observed for the 100N and 250N cyclic load runs with no overlap between them. For the MS500 scaffold group, data from the 100N cycle run overlapped corresponding data from the 250N cycle run.



**Figure 3.3: Relationship Between the Applied Compressive Load and the Measured Tensile Load.** Data is from MS500 and MS1000 FRMSs at cyclic load evaluations between 10N and 100N, and 10N and 250N. Trendlines for each cyclic load run are included in this figure, with corresponding R<sup>2</sup> values in the legend. There is no overlap between the 100N and 250N cyclic runs for MS1000 scaffolds. However, there is overlap between the two cyclic runs for the MS500 scaffolds.

Table 3.4 summarizes the percentage of applied compressive load converted to a circumferential tensile load for incremental load ranges. For lower load ranges, MS500 and MS1000 scaffolds were found to convert a higher percentage ( $p < 0.05$ ) of

the applied load to a tensile load. As the applied load increased to more physiologically relevant values, the percentage converted significantly decreased ( $p < 0.05$ ). For all load ranges, MS1000 scaffolds were found to convert a statistically significantly higher percentage ( $p < 0.05$ ) than MS500 scaffolds. For both scaffold designs, there was also found to be a statistical difference ( $p < 0.05$ ) in converted load between the 100N and 250N runs within a given load range.

**Table 3.4. Calculated Percentage of Axial Compressive Load Converted to Circumferential Tensile Load for Select Load Ranges.**

Cyclic Loading Group	Compressive Load Range, CL [N]	MS500 (%)	MS1000 (%)
100 N	$75 \leq CL \leq 100$	6.23 +/- 0.58	11.07 +/- 0.94
	$50 \leq CL < 75$	9.14 +/- 0.93	15.21 +/- 1.81
	$25 \leq CL < 50$	14.80 +/- 2.73	24.50 +/- 4.75
	$0 \leq CL < 25$	32.36 +/- 9.37	53.82 +/- 15.31
250 N	$200 \leq CL \leq 250$	3.91 +/- 0.23	7.67 +/- 0.50
	$150 \leq CL < 200$	4.83 +/- 0.34	9.47 +/- 0.82
	$100 \leq CL < 150$	6.41 +/- 0.67	12.73 +/- 1.53
	$75 \leq CL < 100$	8.62 +/- 0.63	17.31 +/- 1.69
	$50 \leq CL < 75$	11.50 +/- 1.21	23.66 +/- 2.98
	$25 \leq CL < 50$	18.36 +/- 3.36	38.24 +/- 7.26
	$0 \leq CL < 25$	40.88 +/- 12.13	80.99 +/- 23.45

### 3.3.2. Evaluation of Load Distribution on Tibial Plateau

The purpose of this evaluation was to determine the extent to which FRMSs would facilitate the distribution of compressive loads on the tibial plateau. Figure 3.4 (left column) shows representative raw images of the pressure sensitive film from each scaffold group under 100N and 250N compressive loading.

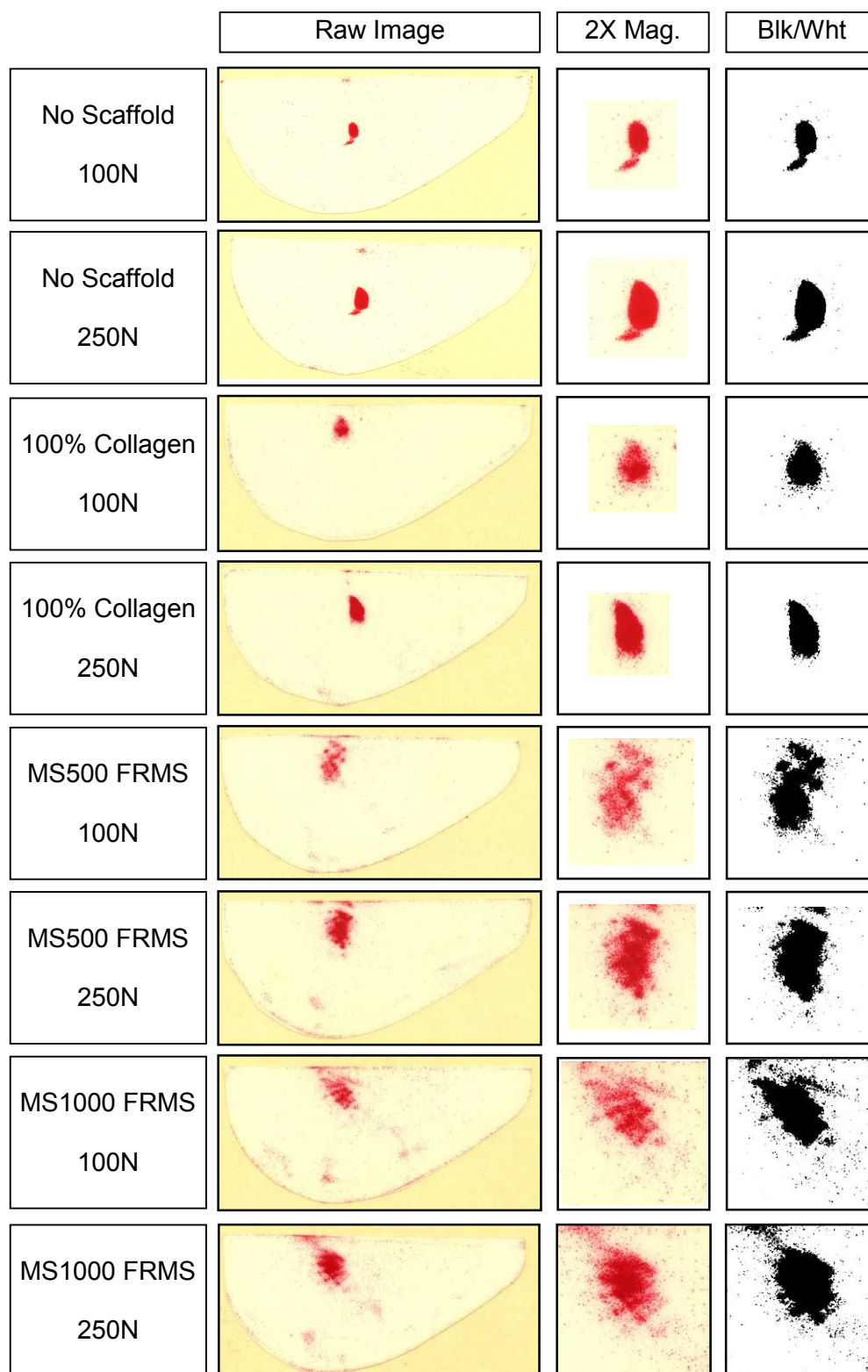


**Figure 3.4: Images of Pressure Sensitive Film After Compressive Loading.** The left column shows the raw image. The middle column shows the raw image cropped to remove artifact readings and magnified 2X. The right column shows the image converted to black and white for contact area analysis.

Raw images were analyzed with the Topaq® image analysis software to obtain a quantitative pressure profile on the tibial plateau. Figure 3.5 shows a representative pressure distribution with corresponding histogram for each scaffold group after compressive loading. Due to the sensitivity of the film as well as the irregular surface of the tibial plateau, artifact data was present for all samples. Images were cropped (Figure 3.4, middle column) and converted to black and white images (Figure 3.4 right column) to calculate the total contact area on the tibial plateau (Figure 3.6).

From Figure 3.6, little difference was found between the 'No Scaffold' and 'MSCOLL' groups. The total contact areas for both these groups were not statistically different ( $p > 0.05$ ). Furthermore, both had high pressure areas ( $>1000$  psi) which were indistinguishable from each other. The addition of anchored, circumferentially arranged fibers in scaffolds was found to significantly increase the contact area for both loading conditions. For the 100N loading condition, the total area under high pressure decreased with the addition of reinforcing fibers. No difference was seen between the MS500 and MS1000 scaffold groups ( $p > 0.05$ ). The total high pressure area did not significantly change between any of the scaffold groups for the 250N runs.

From the pressure histograms in Figure 3.5, the percentage of the contact area under relatively high stress decreased for fiber-reinforced scaffolds at both loading conditions. No differences were observed between the No Scaffold and MSCOLL groups for either load. Furthermore, no differences were found between the MS500 and MS1000 groups for the 100N load. A decrease in the total percentage of the area under high stress was observed between MS500 and MS1000 groups for the 250N load.

The peripheral height of hydrated scaffolds was measured before and after compressive loading to determine if (or to what extent) scaffolds would rebound to their original shape (Table 3.5). Each scaffold was initially fabricated to have a height of 1 cm. After processing (crosslinking, freeze-drying, and sterilization), MS500 scaffolds

had an average peripheral height of 6.832 +/- 0.301 mm, a 31.7% decrease from the fabricated height. Likewise, MS1000 scaffolds had an average height of 8.700 +/- 0.895 mm after processing, a 13.0% decrease from the fabricated height. After compressive loading, MS500 and MS1000 scaffolds averaged a decrease in height of 4.41% and 4.27%, respectively.

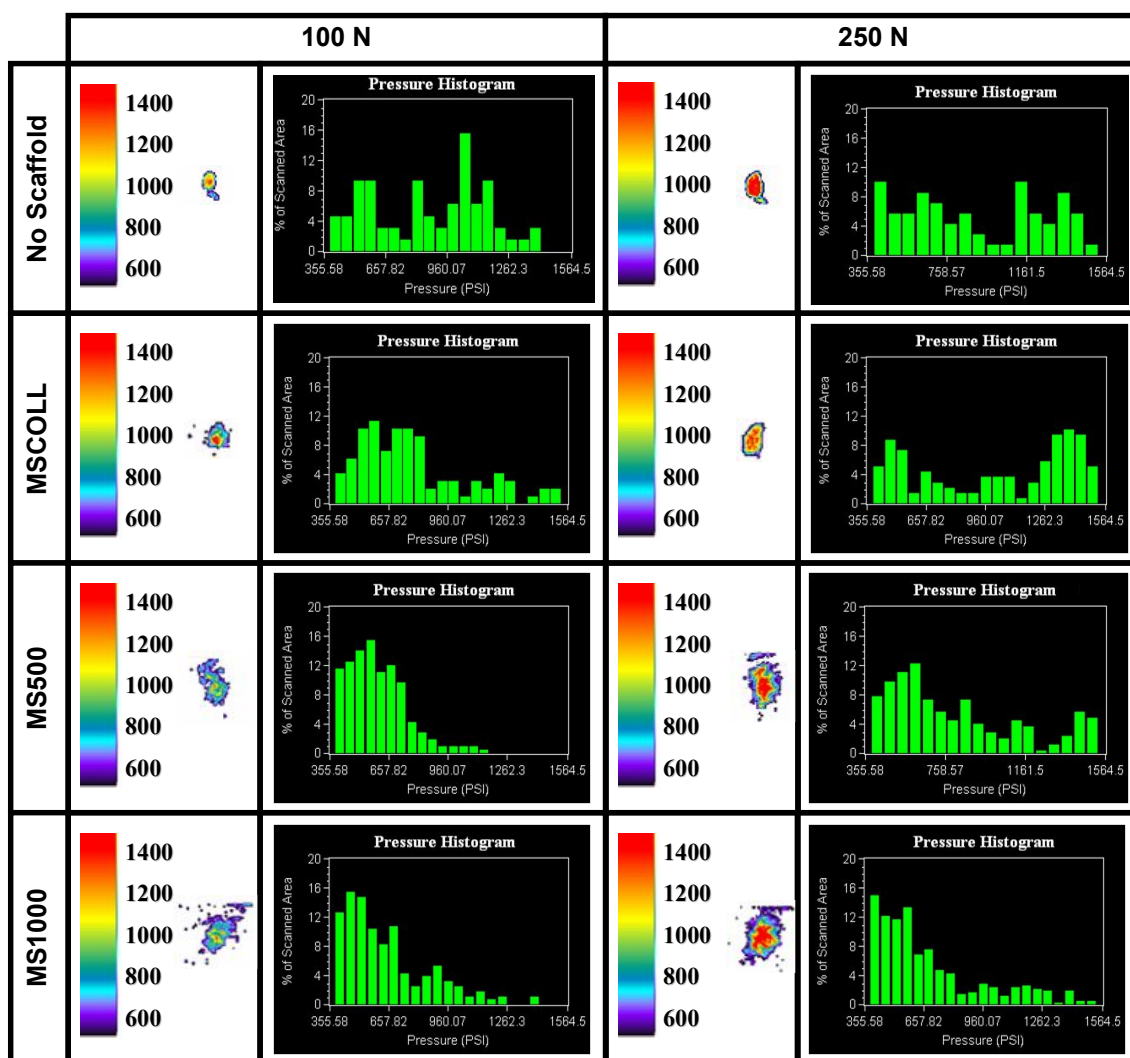


**Figure 3.5: Representative Pressure Distribution Profile on Tibial Plateau After Compressive Loading of Either 100N or 250N.** Three scaffold groups were evaluated: 100% collagen scaffolds, MSCOLL; MS500 FRMs; and MS1000 FRMs. As a control, the tibial plateau was also loaded in the presence of no scaffold.

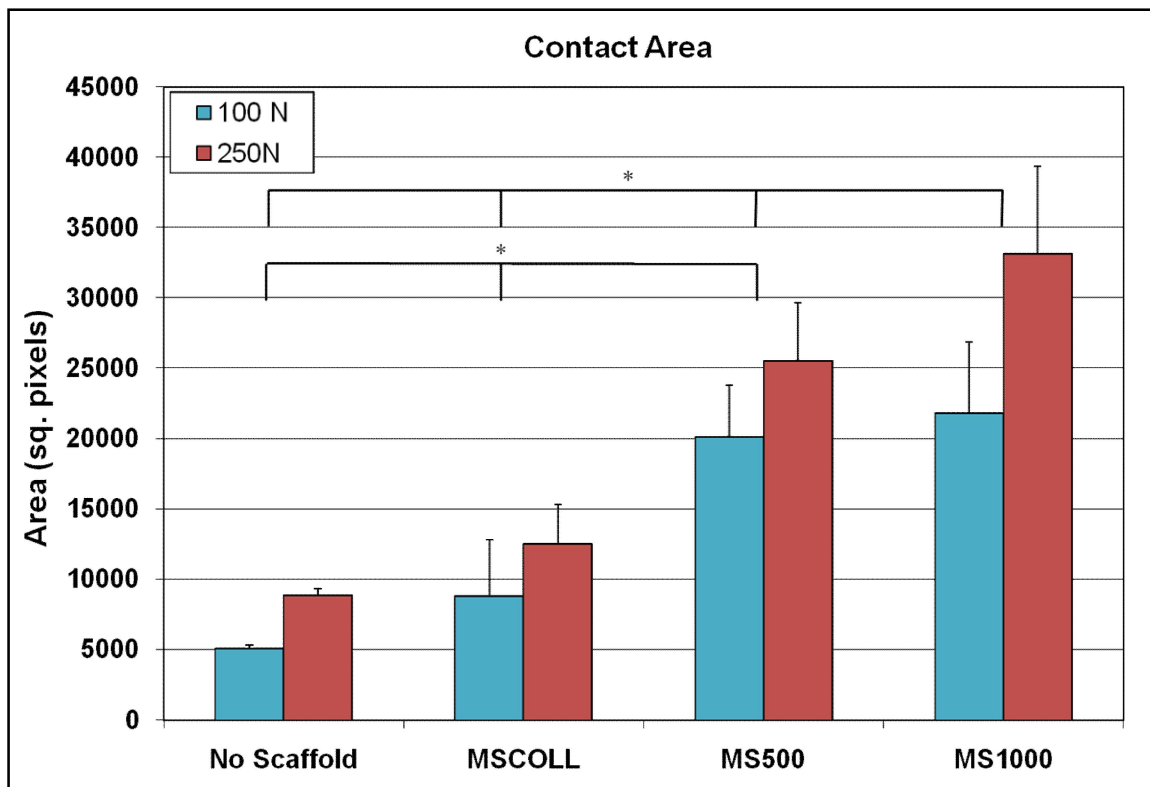


**Figure 3.6: Contact Area on Tibial Plateau After Compressive Loading.** Three scaffold groups were evaluated: 100% collagen scaffolds, MSCOLL; MS500 FRMSs; and MS1000 FRMSs. As a control, the tibial plateau was also loaded in the presence of no scaffold. Pressure profiles were converted to black/white images and the total number of black pixels per picture was found. Significant differences were found between the MS1000 FRMSs and all other scaffold groups, and between MS500 FRMSs and all other scaffold groups ( $p < 0.05$ ). No difference was found between the 100% collagen scaffold and the no scaffold groups. There was a significant difference between the 100N and 250N load conditions.

**Table 3.5. Average Peripheral Height of Scaffolds Before and After Compressive Loading.**

Scaffold	Sample Size	Initial Height (mm)	Final Height (mm)	Percent decrease (%)
MS500	n = 5	6.832 +/- 0.301	6.524 +/- 0.320	4.413 +/- 5.109
MS1000	n = 7	8.700 +/- 0.895	8.329 +/- 0.892	4.269 +/- 3.748

### 3.3.3. Circumferential Tensile Testing

In this experiment, the structural properties of FRMSs were evaluated and compared to those of the normal ovine meniscus. Figure 3.7 shows the tensile load at yield, tensile load at failure, and stiffness of FRMSs and ovine menisci. MS1000 scaffolds had a statistically higher yield load ( $p < 0.05$ ) than MS500 scaffolds and both lateral and medial ovine menisci. MS1000 scaffolds also had a significantly higher ( $p < 0.05$ ) load at failure than all other groups. Lateral menisci had a statistically higher ( $p < 0.05$ ) failure load than MS500 scaffolds and a higher stiffness ( $p < 0.05$ ) than that of all other groups. The stiffness of the medial meniscus was also found to be higher than that of the MS500 scaffolds ( $p < 0.05$ ). No other statistical differences were found.

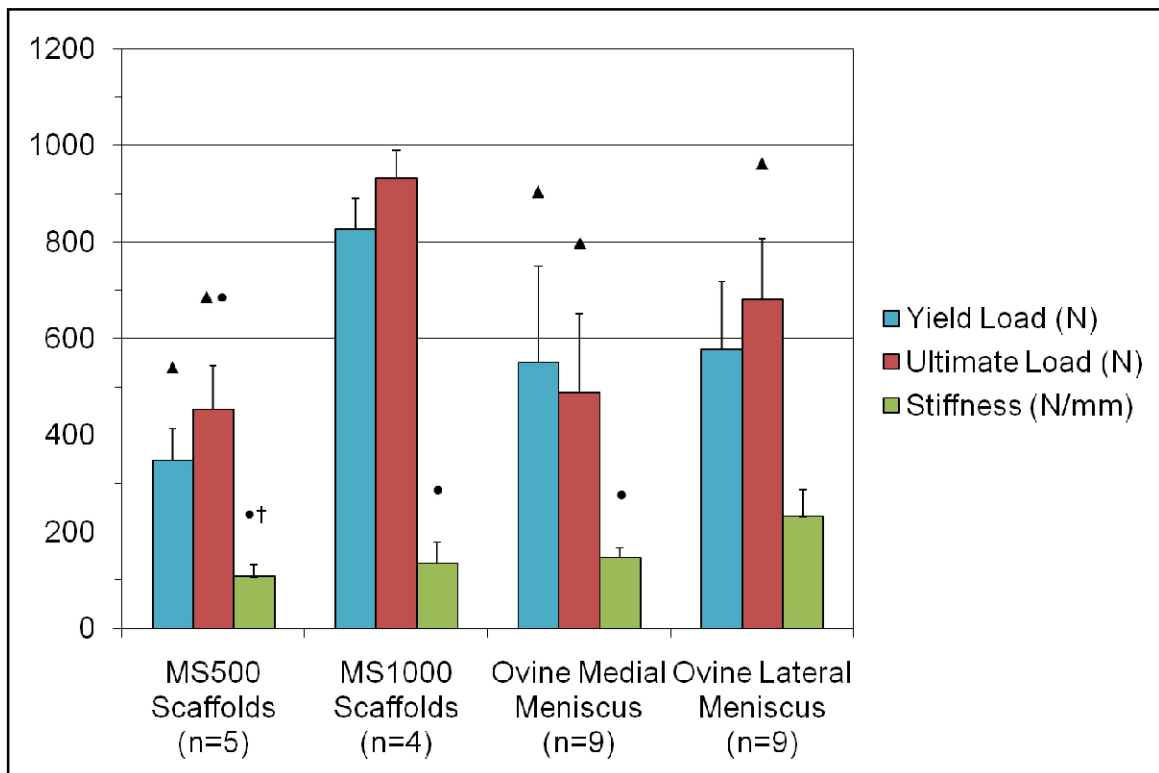


**Figure 3.7: Structural Properties of FRMSs and Native Ovine Meniscal Tissue Tested in Tension to Failure.** A one-way ANOVA was performed on this data set and pairwise comparisons made with the Student-Newman-Keuls Method. Significant differences ( $p < 0.05$ ) in relation to the MS1000 Scaffolds are noted by ▲. Significant differences ( $p < 0.05$ ) in relation to the Lateral Menisci are noted by ●. Significant differences ( $p < 0.05$ ) in relation to the Medial Menisci are noted by †.

### 3.4. *In Vitro* Cell Compatibility of FRMS

#### 3.4.1. Cell Line Harvest and Culture

Cells were harvested from the inner and outer portions of the rabbit menisci. Two basic phenotypes were observed in culture: (1) fusiform shaped cells resembling fibroblasts (Figure 3.8a), and (2) ovoid cells resembling chondrocytes (Figure 3.8b). Cells of the same phenotype could be found growing together (Figure 3.8 a-b), or in mixed colonies (Figure 3.8 c). Based on this, each scaffold was seeded with a mixture of fibroblast-like cells and chondrocytes-like cells.

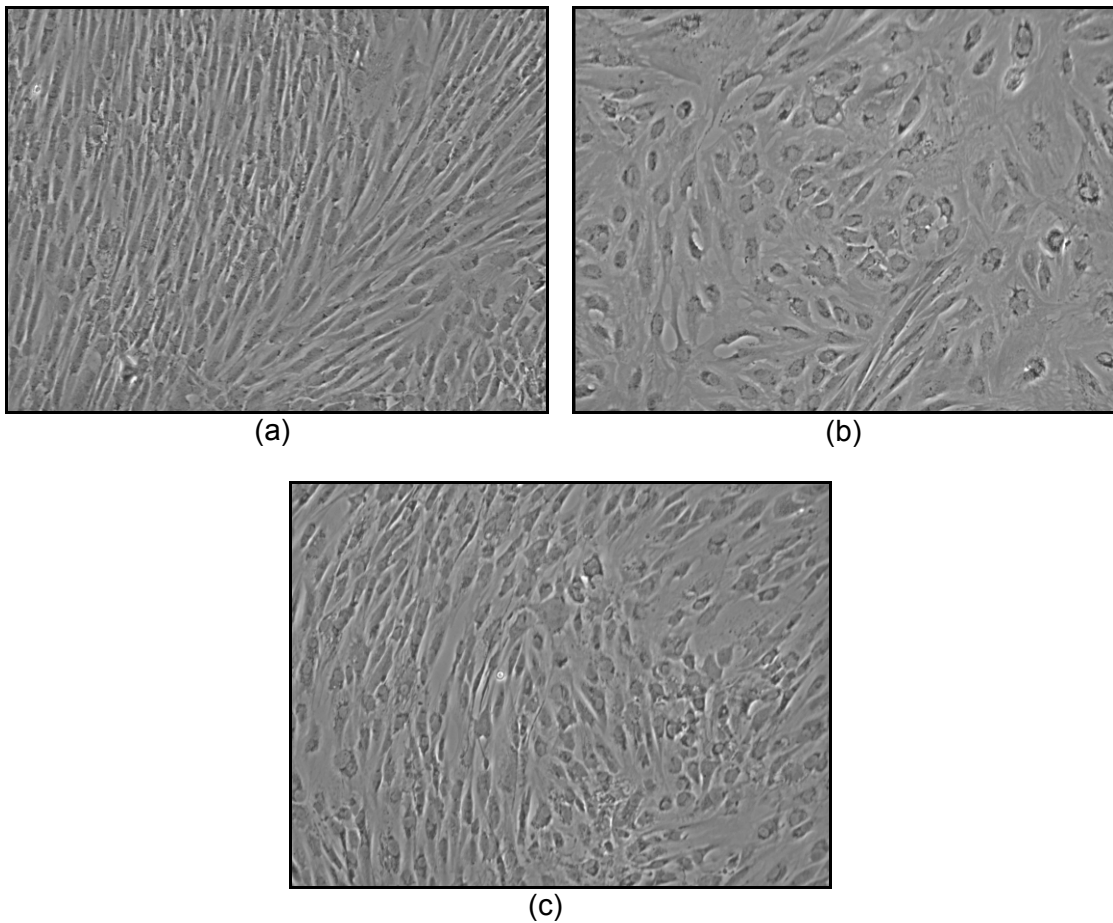


**Figure 3.8: Fibrochondrocytes from Rabbit Meniscus Growing in Culture.** Two basic cell phenotypes were observed in culture: (a) fibroblast-like cells, and (b) chondrocyte-like cells. Cells of the same phenotype were found growing together in groups (a) and (b), or mixed together (c).

### 3.4.2. Cell Viability Biochemical Analysis

For each time period and each type of scaffold, an MTS biochemical assay was used to determine the number of viable cells on scaffolds at four time points. A normal growth curve of fibrochondrocytes on the meniscal scaffold was observed (Figure 3.9). A two-way ANOVA was performed, with factor 1 being the time and factor 2 being the scaffold design. There was a statistically significant difference ( $p < 0.05$ ) between all time points as well as a between time points within both scaffold designs. There was no difference ( $p > 0.05$ ) between any scaffold design within a given time point. Furthermore, no differences were seen between scaffold body sections and scaffold horn sections.

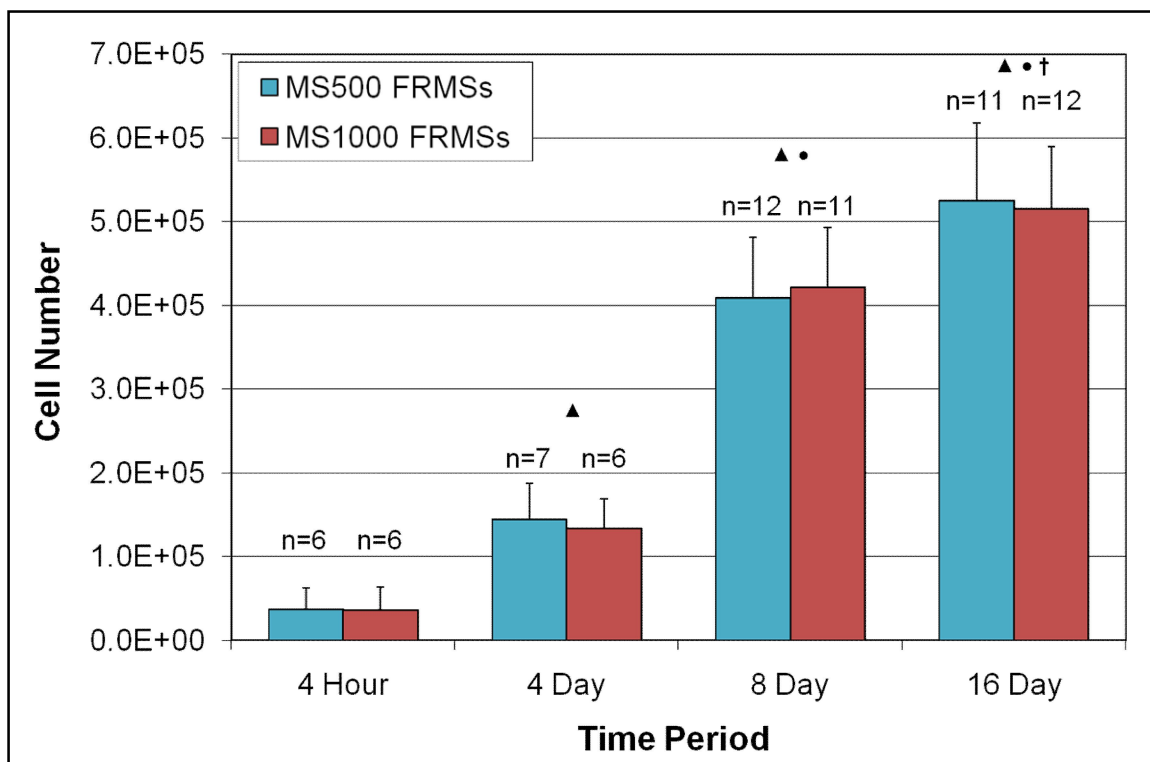
The dimensions of hydrated scaffold wedges were recorded prior to cell-seeding and at their respective time point. For both the main body scaffold sections as well as the horn scaffold sections, no significant differences were found in the dimensions for any time points.

### 3.4.3 Histological Analysis

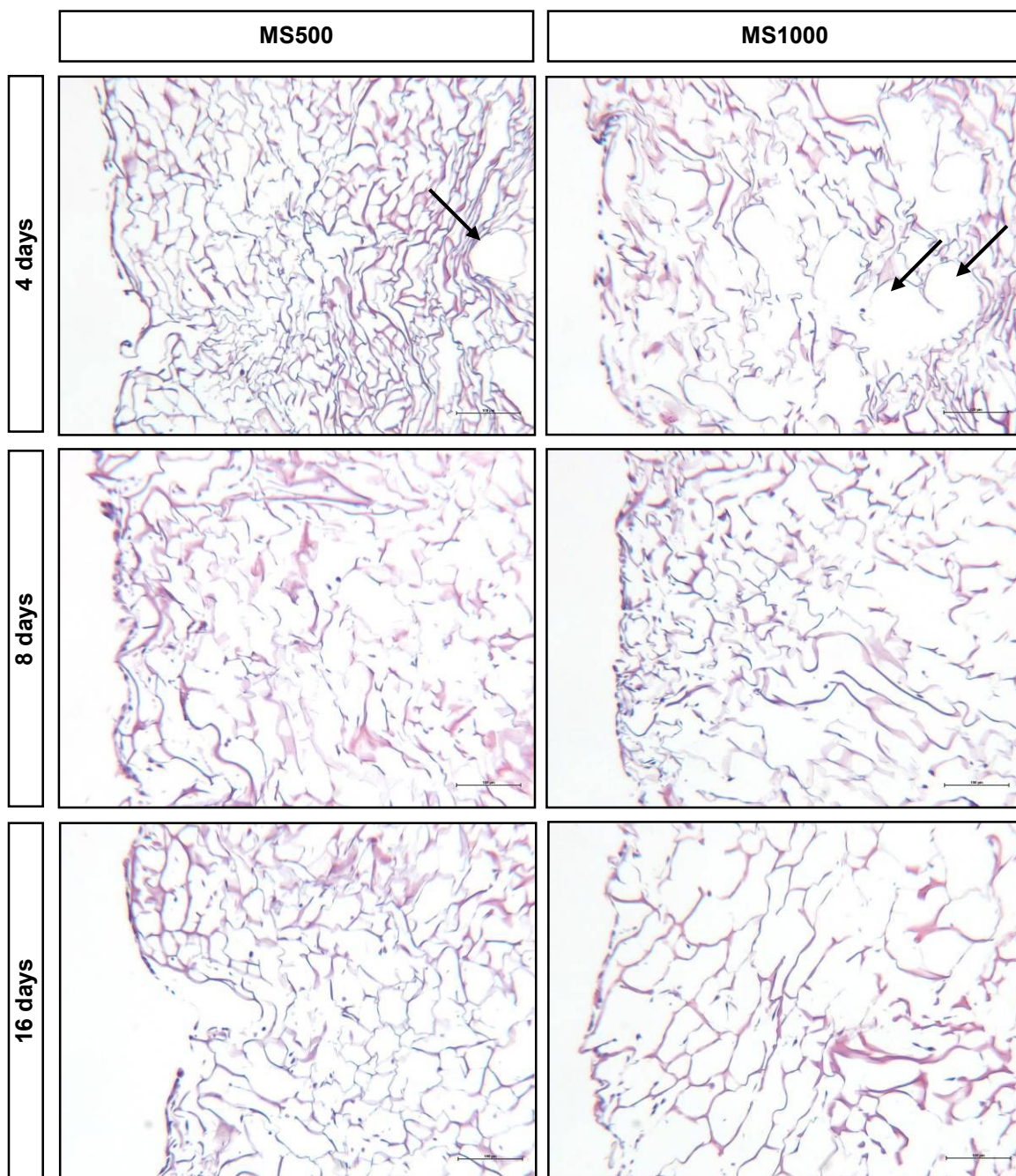
One scaffold from each time point was fixed in formalin and processed histologically with H&E stain. From a subjective, visual inspection, little difference was seen in cell attachment between MS500 and MS1000 scaffolds at each time point. The only difference noted was that the collagen matrix in the MS500 scaffold appears denser than that of the MS1000 scaffolds.

Figure 3.10 shows each scaffold at the 4, 8 and 16 day time points. By 4 days, cells are observed intermittently along the periphery of the scaffold (left edge of figure). By 8 and 16 days, a cell layer 1-2 cells thick can be seen at more regular intervals along the periphery of the scaffold. Furthermore, at these time points cellular infiltration was observed as deep as 200  $\mu\text{m}$  into the scaffold. The large ellipse shaped voids found

deeper in the scaffold represent the location of the reinforcing polymer (indicated by arrows in the figure). Because the polymers were found deeper in the scaffold than 200  $\mu\text{m}$ , fibrochondrocytes were found to primarily attach to the collagen portion of the scaffold.



**Figure 3.9: Number of Viable Fibrochondrocytes Cultured on FRMSs.** A two-way ANOVA was performed on this data set and pairwise comparisons made with the Student-Newman-Keuls Method. Significant differences ( $p < 0.05$ ) in relation to the '4 Hour' time point are noted by ▲. Significant differences ( $p < 0.05$ ) in relation to the '4 Day' time point are noted by ●. Significant differences ( $p < 0.05$ ) in relation to the '8 Day' time point are noted by †.



**Figure 3.10: Micrographs of Fibrochondrocyte-Seeded FRMSs After 4, 8, and 16 Days Culture.** Fibrochondrocytes can be seen along the periphery of the scaffold (left edge). All samples are stained with H&E. Magnification at 100x. Arrows indicate where reinforcing polymer fibers are located within the scaffold. The actual polymer is washed away by organic solvents during histological processing.

## Phase III: *In Vivo* Evaluation of FRMS

### 3.5. Preliminary *In Vivo* Evaluation in Rabbit Model

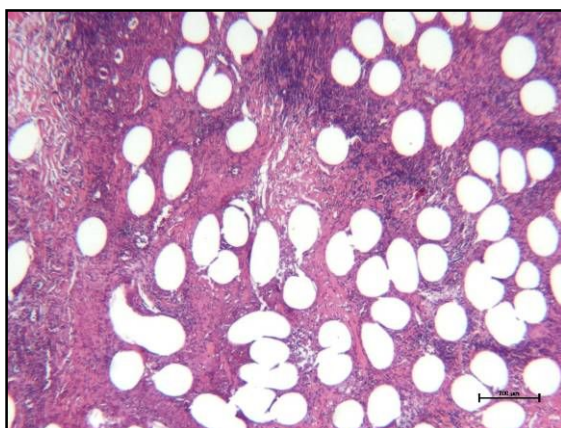
In this experiment, scaffold wedges were implanted into surgically created synovial pockets in both knees of a NZW rabbit. Samples were retrieved 4 or 8 weeks later and analyzed histologically to determine the biological response to implanted scaffolds in a synovial environment. Figures 3.11, 3.12, 3.13, and 3.14 show representative micrographs of MS500 and MS1000 scaffolds at 4 and 8 weeks post-implantation. Slides were stained with either Haematoxylin and Eosin (H&E) or Masson's Trichrome (MT). Empty white voids represent the location of the reinforcing polymer fibers which were washed away by organic solvents during histological processing. White voids containing erythrocytes are blood vessels. The collagen matrix portion of the scaffold had a distinct 'sponge-like' structure and was stained pink by H&E and dark blue by Trichrome. Newly synthesized collagen was morphologically distinct from the collagen scaffold matrix and tended to be a lighter blue under MT staining.

For both scaffold designs at both time periods, cells and vascular tissue were found to completely infiltrate the sections. Parts (A) and (B) of Figures 3.11, 3.12, 3.13, and 3.14 show H&E and Trichrome micrographs of sections at 40X magnification. A significant inflammatory response was observed consisting of plasma cells, eosinophils, histiocytes, and multi-nucleated giant cells (MNGCs). H&E slides show inflammation as the highly cellularized sections typically stained a dark purple, while MT slides show inflammation as highly cellularized sections stained red. Inflammation due to plasma cells (cells with round nuclei stained dark purple by H&E) was found predominantly around the collagen matrix portion of the scaffold (Figures 3.11C/D, 3.12 C/D, 3.13 C/D, and 3.14 C/D). The cytoplasm of eosinophils stains pink due in H&E to its eosinophilic cytoplasm. These cells (Figure 3.11F) were found sporadically among

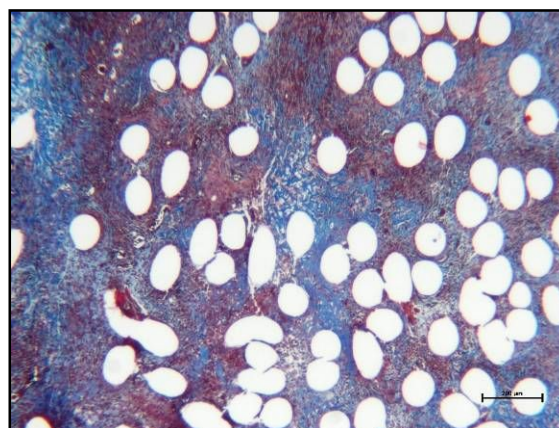
plasma cells and were also associated primarily with the collagen sponge. Histiocytes and MNGCs were predominantly found next to or around the reinforcing polymer fibers (Figure 3.11E, 3.12 E/F, 3.13 E/F, and 3.14 E/F). Under H&E staining, these cells appear as relatively large cells with pink cytoplasm and contain multiple dark-stained nuclei. Under MT staining, these cells are colored dark red.

A UMDNJ pathologist graded these slides in a blinded fashion for inflammation (type and amount), presence of vascular tissue, neo-tissue formation, organization of neo-tissue, and degradation of the collagen matrix portion of the scaffold. Figure 3.15 shows the results of this evaluation. There was a significant decrease ( $p < 0.05$ ) in the amount of plasma cell and eosinophil inflammation from 4 to 8 weeks post-implantation (Figure 3.15 A/B). This also held true between time points within each scaffold group. By 4 weeks, the level of histiocyte/MNGC inflammation was observed to be relatively high and did not significantly change by 8 weeks (Figure 3.15 C).

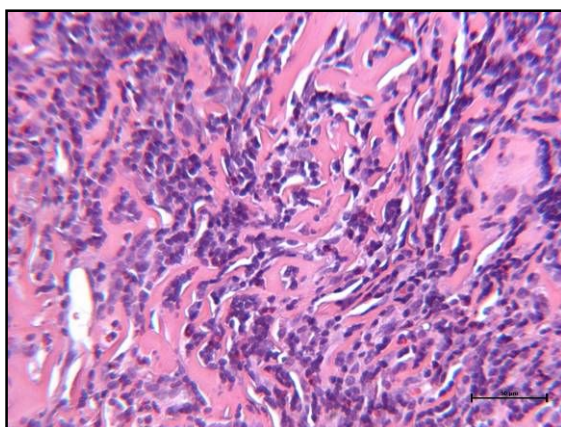
There was significantly less ( $p < 0.05$ ) of the collagen matrix portion of the scaffold after 8 weeks – which was also detected between 4 and 8 weeks within the MS1000 scaffold group (Figure 3.15 F). The amount of vascular tissue which infiltrated the implants increased ( $p < 0.05$ ) after 8 weeks (Figure 3.15 E). Again this was true between 4 and 8 weeks within both scaffold groups. No differences in the amount of tissue infiltration in the scaffolds were found (Figure 3.15 D).



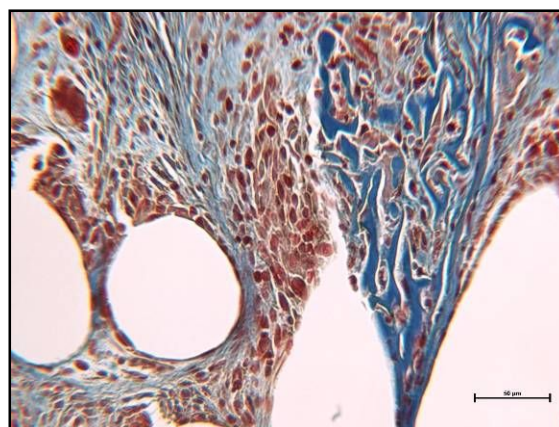
(A) MS500 FRMS, 40X magnification, H&E



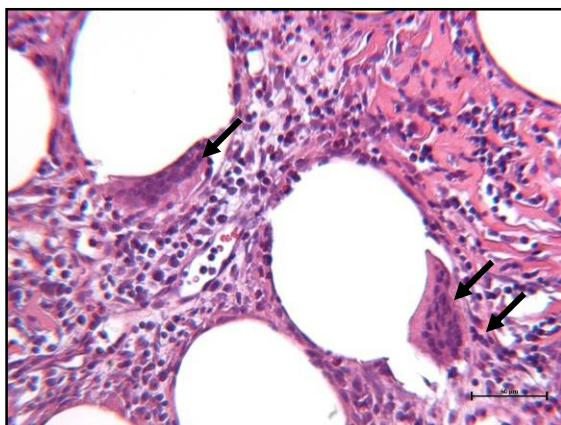
(B) MS500 FRMS, 40X magnification, MT



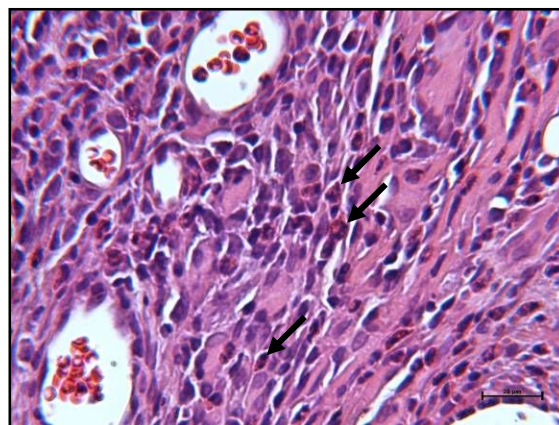
(C) MS500 FRMS, 200X magnification, H&E



(D) MS500 FRMS, 200X magnification, MT

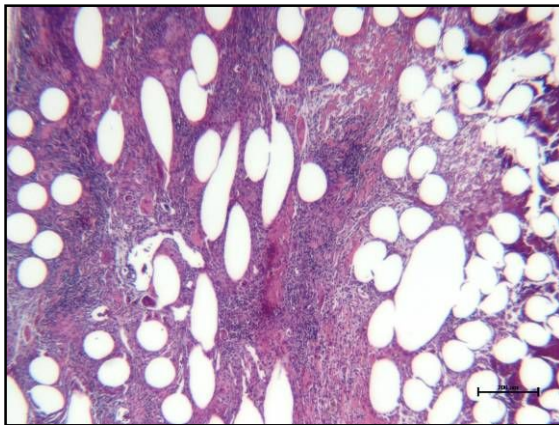


(E) MS500 FRMS, 200X magnification, H&E

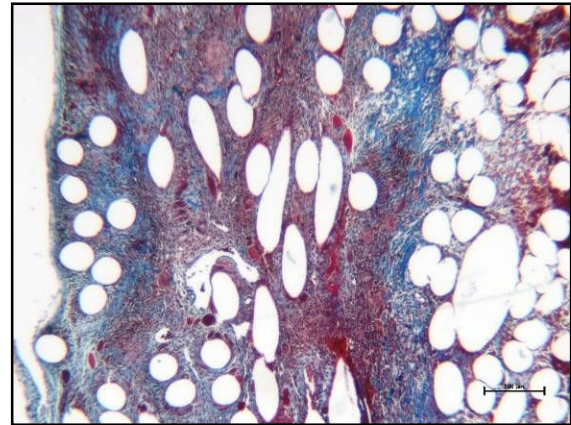


(F) MS500 FRMS, 400X magnification, MT

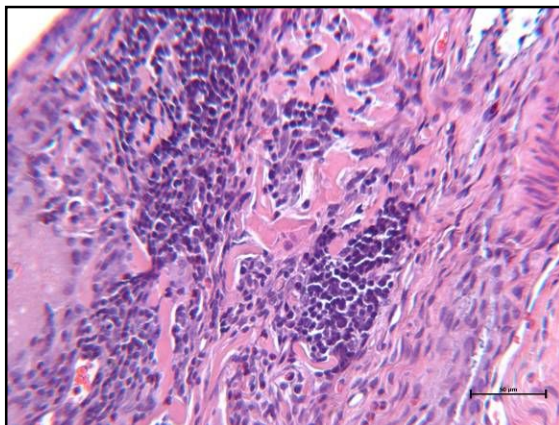
**Figure 3.11: Histological Sections of MS500 FRMSs at 4 weeks Post-Implantation.** (A) Representative H&E section at 40X. (B) Representative MT at 40X. (C) Collagen sponge (pink staining) infiltrated with plasma cells, 200X. (D) Collagen sponge (arrow, dark blue staining) next to new collagen (light blue). Inflammatory and matrix producing cells present in section, 200X. (E) Multi-nucleated Giant Cells (arrows) adjacent to polymer fibers, 200X. (F) Eosinophils (arrows) among plasma cells, 400X.



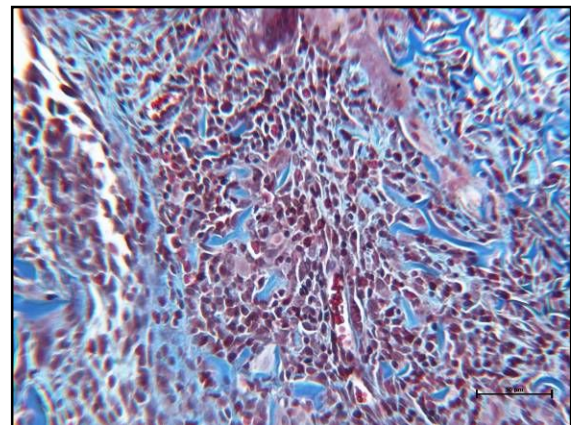
(A) MS1000 FRMS, 40X magnification, H&E



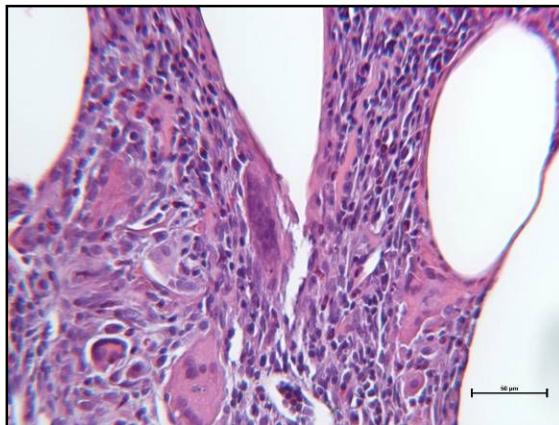
(B) MS1000 FRMS, 40X magnification, MT



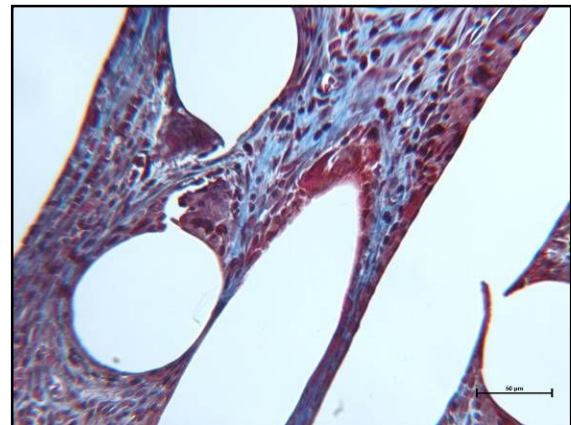
(C) MS1000 FRMS, 200X magnification, H&E



(D) MS1000 FRMS, 200X magnification, MT

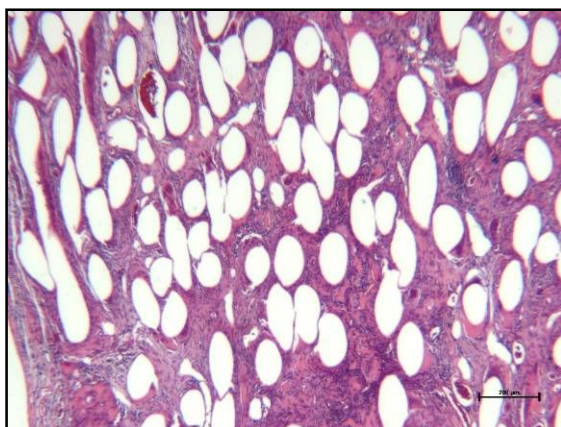


(E) MS1000 FRMS, 200X magnification, H&E

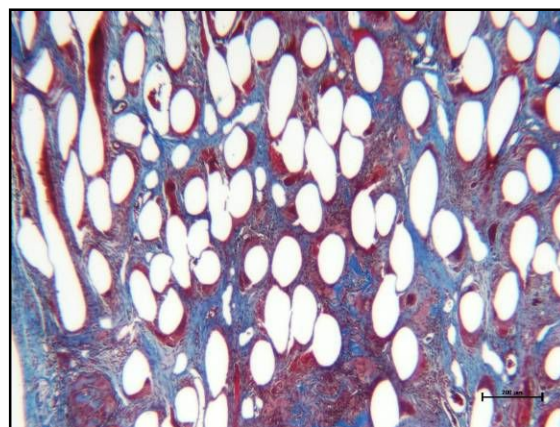


(F) MS1000 FRMS, 200X magnification, MT

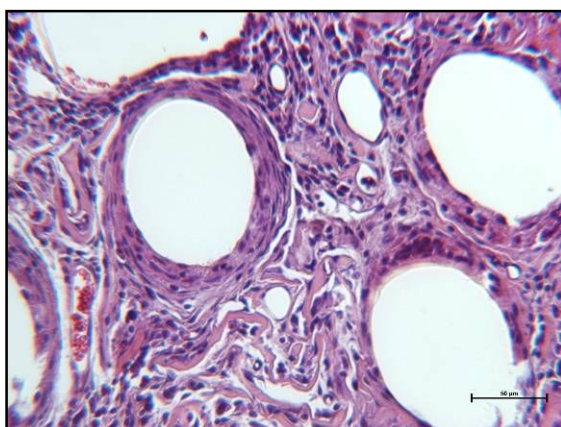
**Figure 3.12: Histological Sections of MS1000 FRMSs at 4 weeks Post-Implantation.** (A) Representative H&E section at 40X. (B) Representative MT at 40X. (C) Collagen sponge (pink staining) infiltrated with plasma cells, 200X. (D) Collagen sponge (arrow, dark blue staining) next to new collagen (light blue). Inflammatory and matrix producing cells present in section, 200X. (E) MNGCs (arrows) adjacent to polymer fibers, H&E, 200X. (F) MNGCs (arrows) adjacent to fibers, MT, 200X.



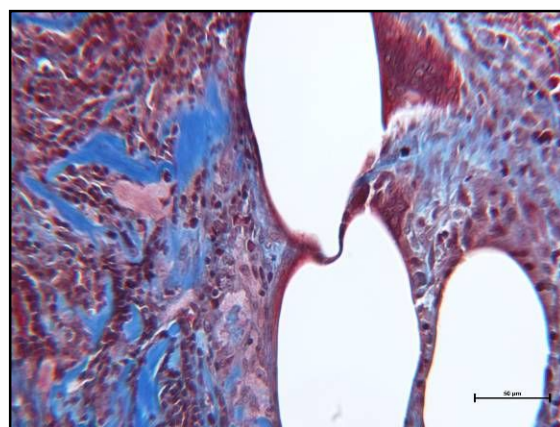
(A) MS500 FRMS, 40X magnification, H&E



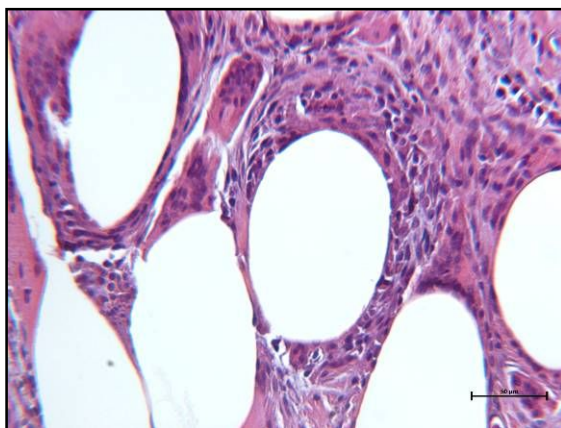
(B) MS500 FRMS, 40X magnification, MT



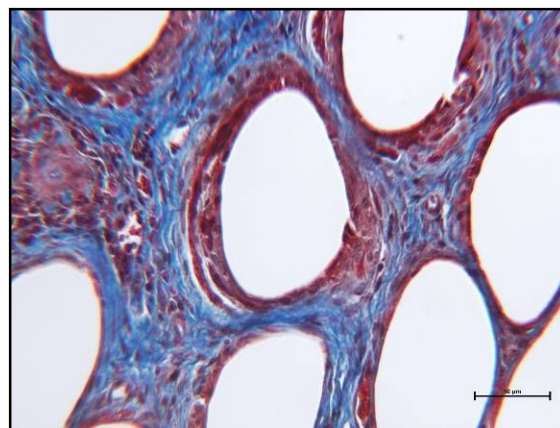
(C) MS500 FRMS, 200X magnification, H&E



(D) MS500 FRMS, 200X magnification, MT

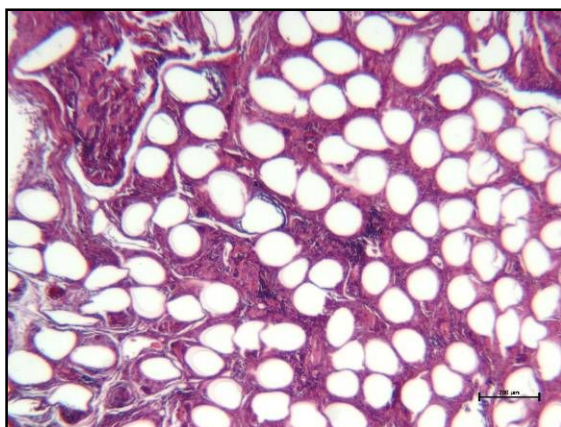


(E) MS500 FRMS, 200X magnification, H&E

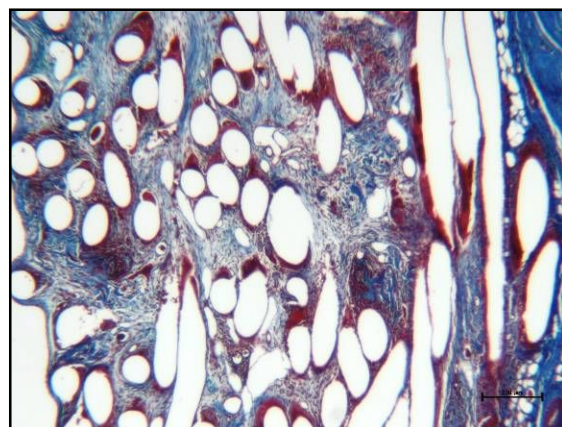


(F) MS500 FRMS, 200X magnification, H&E

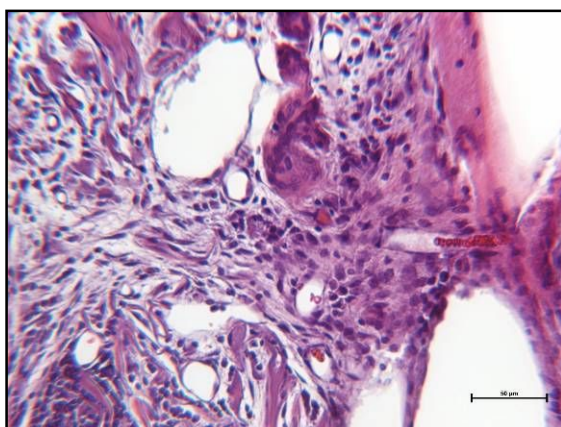
**Figure 3.13: Histological Sections of MS500 FRMSs at 8 weeks Post-Implantation.** (A) Representative H&E section at 40X. (B) Representative MT at 40X. (C) Collagen sponge (pink staining) infiltrated with plasma cells and MNGCs around polymer fibers, H&E, 200X. (D) Collagen sponge (dark blue) infiltrated with plasma cells with newly synthesized collagen (light blue). MNGCs located around polymer fibers, MT, 200X. (E) MNGCs around polymer fibers, H&E, 200X. (F) MNGCs around fibers. MT. 200X.



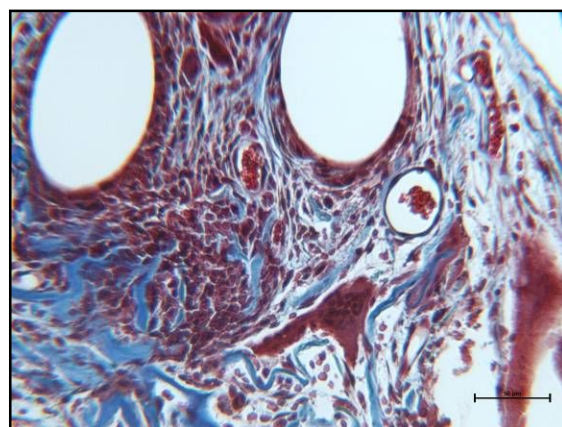
(A) MS1000 FRMS, 40X magnification, H&E



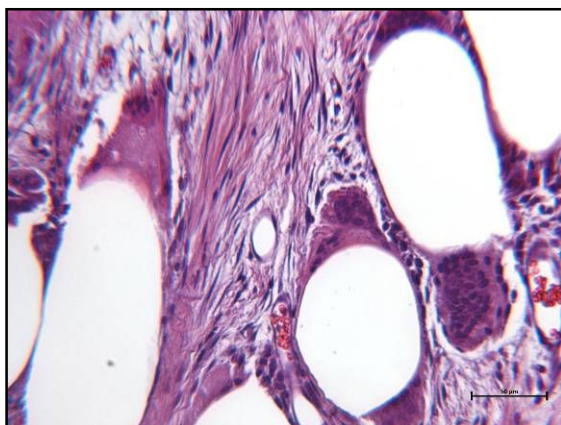
(B) MS1000 FRMS, 40X magnification, MT



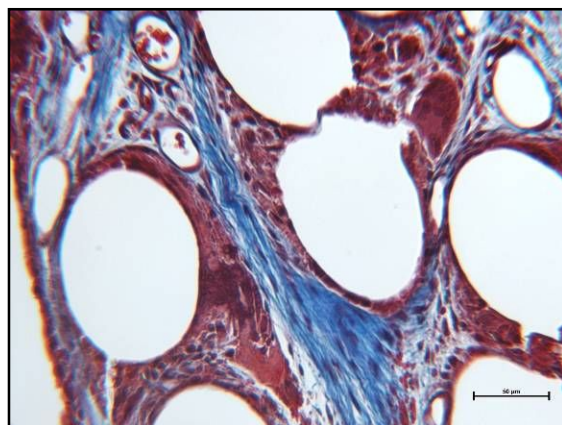
(C) MS1000 FRMS, 200X magnification, H&E



(D) MS1000 FRMS, 200X magnification, MT



(E) MS1000 FRMS, 200X magnification, H&E



(F) MS1000 FRMS, 200X magnification, MT

**Figure 3.14: Histological sections of MS1000 FRMSs at 8 weeks post-implantation.** (A) Representative H&E section at 40X. (B) Representative MT at 40X. (C) Collagen sponge infiltrated with plasma cells and MNGCs around polymer fibers, H&E, 200X. (D) Collagen sponge (dark blue) infiltrated with plasma cells with newly synthesized collagen (light blue). MNGCs located around polymer fibers, MT, 200X. (E) MNGCs around polymer fibers, H&E, 200X. (F) MNGCs around fibers, MT, 200X.

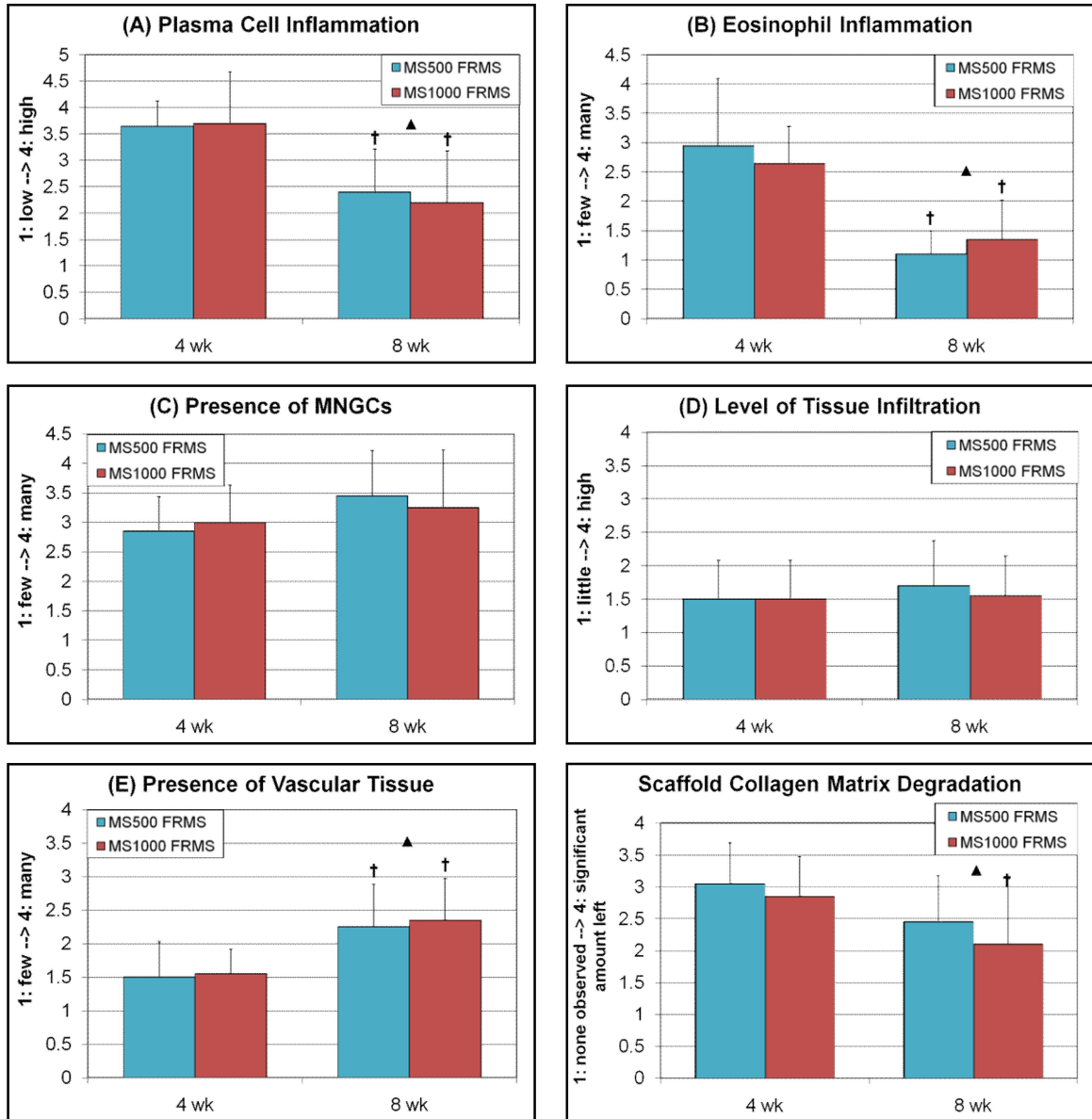


**Figure 3.15: Comparison of Graded Histological Samples.** (A) Presence of Plasma Cells. (B) Presence of Eosinophils. (C) Presence of MNGCs. (D) Level of Tissue Infiltration into Scaffold. (E) Presence of Vascular Tissue. (F) Level of Collagen Matrix Degradation. A two-way ANOVA was performed with pairwise multiple comparisons made using the Student-Newman-Keuls Method. Significant differences ( $p < 0.05$ ) as compared to the 4 week time point are denoted by ▲. Significant differences ( $p < 0.05$ ) within a scaffold group as compared to the 4 week time point are denoted by †.

### **3.6. Functional *In Vivo* Evaluation in Ovine Model**

MS1000 fiber reinforced meniscus scaffolds were evaluated as a replacement for the medial meniscus in an ovine model at 8 and 16 weeks. Gross observation, biomechanical analysis, histology, and immunofluorescence staining were used to measure the overall performance of the device with regards to the neo-tissue formation and protection of the underlying articular surfaces.

No complications were noted by the surgeon or support staff during the implantation procedure. Furthermore, no serious post-operative complications were found for any animals. Generally, for the first week after surgery, animals bore little-to-no weight on the surgical leg. From then on, weight-bearing increased daily at a slow rate, and typically by the third week, animals had regained most of the original function of the leg. Between 3 and 4 weeks post-surgery, they were then transferred to an IACUC approved sheep farm for the remainder of their post-operative care where they were observed to ambulate with minimal or no discernable limp. The post-operative timeline of each individual animal is found in Table 3.6.

#### **3.6.1. Gross Evaluation**

At sacrifice, gross observations of the scaffold, synovial tissue, and cartilage were recorded. Observations of the scaffold for each animal are found in Table 3.7. At 8 weeks post-implantation, 3 of 6 implants were found to be intact with structurally sound anchor attachments. Two more were intact, but the posterior had partially slipped out of the posterior tunnel and one had failed at the posterior horn. At 16 weeks post-implantation, 1 of 6 implants was observed to be intact with structurally sound anchor attachments. Two others were intact, but again, slippage from the posterior tunnel was observed. Three had pulled out of the posterior horn bone tunnel.

**Table 3.6. Post-Operative Timeline of Sheep After Implantation of FRMS.** GS-MS-# sheep were treated with the implantation of a MS1000 meniscal scaffold after a full medial meniscectomy. GS-C-# animals received no treatment after a medial meniscectomy.

Sheep ID	Surgery Date	Time Point	Time (weeks)															
			1	2	3	4	5	6	7	8	9	10	11	12	13	14	15	16
GS-MS-2	7/24/2008	8 wks	Red	Red	Yellow	Green												
GS-MS-3	7/31/2008	8 wks	Red	Red	Yellow	Green												
GS-MS-7	8/28/2008	8 wks	Red	Red	Yellow	Green												
GS-MS-9	9/11/2008	8 wks	Red	Red	Yellow	Green												
GS-MS-13	10/23/2008	8 wks	Red	Red	Yellow	Green												
GS-MS-14	1/29/2009	8 wks	Red	Red	Yellow	Green												
GS-C-12	9/18/2008	8 wks	Green	Green	Green	Green	Green	Green	Green	Green	Green	Green	Green	Green	Green	Green	Green	Green
GS-MS-1	7/24/2008	16 wks	Red	Red	Yellow	Green												
GS-MS-4	7/31/2008	16 wks	Red	Red	Yellow	Green												
GS-MS-5	8/14/2008	16 wks	Red	Red	Yellow	Green												
GS-MS-6	8/14/2008	16 wks	Red	Red	Yellow	Green												
GS-MS-8	8/28/2008	16 wks	Red	Red	Yellow	Green												
GS-MS-10	9/11/2008	16 wks	Red	Red	Yellow	Green												
GS-C-11	9/18/2008	16 wks	Green	Green	Green	Green	Green	Green	Green	Green	Green	Green	Green	Green	Green	Green	Green	Green

Legend:	
Red	No significant weight-bearing on surgical leg
Orange	Minimal weight-bearing on surgical leg, significant limp
Yellow	Moderate weight-bearing on surgical leg, moderate/slight limp
Green	Sound on surgical leg, minimal or no limp
Δ	Transferred to Perry Sheep Farm
Ω	Sacrifice

**Table 3.7. Observations of Meniscal Scaffold Made at Sacrifice.**

Sheep ID	Time Point	Observations of Scaffold at Sacrifice
GS-MS-2	8 wks	Ruptured at posterior horn attachment
GS-MS-3	8 wks	Intact; posterior horn slightly pulled from tunnel
GS-MS-7	8 wks	Intact; attachments structurally sound
GS-MS-9	8 wks	Intact; posterior horn pulled from tunnel; scaffold shifted 90°; main body of scaffold positioned at anterior aspect of tibial plateau
GS-MS-13	8 wks	Intact; attachments structurally sound
GS-MS-14	8 wks	Intact; attachments structurally sound
GS-C-12	8 wks	N/A
GS-MS-1	16 wks	Intact; anterior aspect of implant extruded out of joint and caught on lateral aspect of tibia; posterior horn of scaffold loosely attached
GS-MS-4	16 wks	Ruptured/pulled out at posterior horn attachment
GS-MS-5	16 wks	Ruptured/pulled out at posterior horn attachment
GS-MS-6	16 wks	Intact; loose attachments
GS-MS-8	16 wks	Pulled out of posterior tunnel; bunched up at anterior aspect of joint
GS-MS-10	16 wks	Intact; attachments structurally sound
GS-C-11	16 wks	N/A

Scaffolds typically had a pinkish color, suggesting vascularization. Tissue infiltration into the scaffold was observed for all GS-MS sheep, and was not found to depend on whether or not the scaffold was intact. Furthermore, all scaffolds were firmly adhered to the peripheral soft tissue, and in most cases the boundary between the scaffold and synovium was indistinct. Neo-tissue appeared to have fully infiltrated into the scaffold and provided some structural integrity which allowed for handling without permanent deformation. However, the scaffolds did not possess the overt stiffness and resilience of the normal meniscus. No neo-tissue was observed at the site of the meniscectomy in the two control animals.

The reinforcing polymer fibers were more visible in the 8 week group than in the 16 week group. For both groups, fibers had lost their original angled orientation and were all arranged circumferentially. For scaffolds that were observed to have loose attachments, a portion of each scaffold was found to be caught behind the edge of the medial aspect of the tibial plateau. For scaffolds that were observed to have ruptured or pulled out of the posterior bone tunnel, the remainder of it tended to bunch up near its anterior attachment. Pictures of scaffolds at 8 and 16 weeks post-implantation are found in Figures 3.16 and 3.17, respectively. Figure 3.18 shows excised scaffolds at 8 and 16 weeks prior to mechanical evaluation.

Moderate degeneration and wear on the medial condyle of the surgical leg was observed for all animals. No discernible difference was grossly observed between either time point, nor between experimental or control groups.

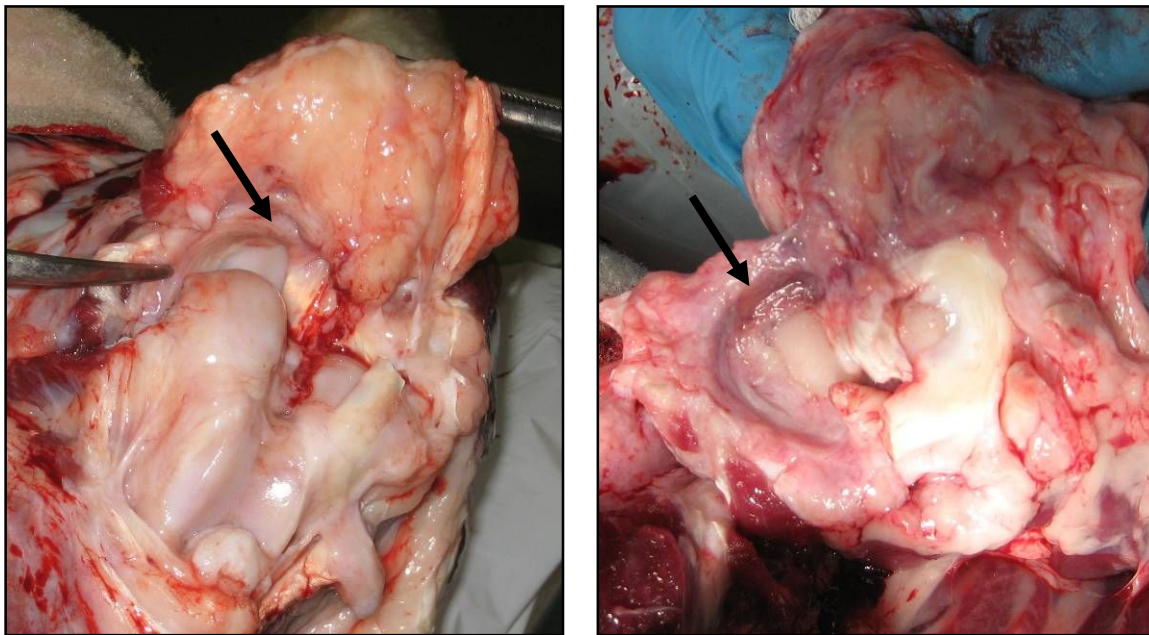


**Figure 3.16: Meniscal Scaffolds at 8 Weeks Post-Implantation.** Scaffolds are indicated by arrows. (Left) GS-MS-9: The implant was intact; however the posterior horn attachment of the scaffold had pulled out of the posterior bone tunnel. (Right) GS-MS-14: The scaffold was intact with structurally sound attachments. Tissue infiltration and adherence to the peripheral tissue can easily be seen.

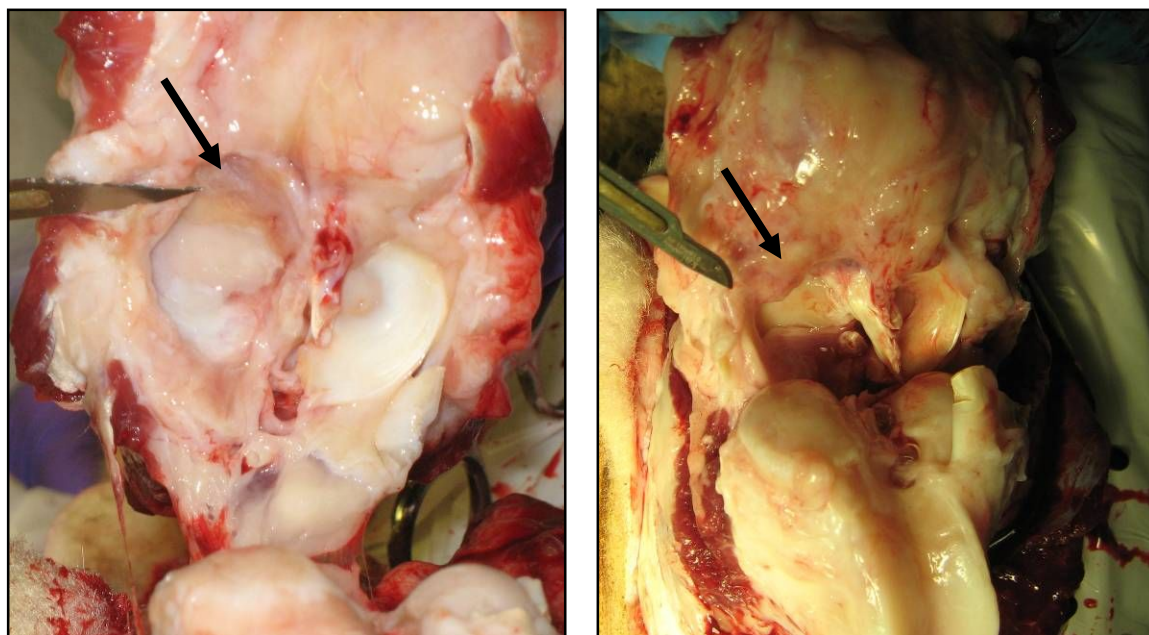


**Figure 3.17: Meniscal Scaffolds at 16 Weeks Post-Implantation.** Scaffolds are indicated by arrows. (Left) GS-MS-8: The posterior horn attachment of the implant had pulled completely out of the bone tunnel. The scaffold was found localized in anterior portion of the joint. (Right) GS-MS-6: The scaffold was intact with loose horn attachments. Tissue infiltration into the scaffold and adherence to the surrounding synovium were observed.



**Figure 3.18: Excised Meniscal Scaffolds and Ovine Lateral Meniscus.** (Left) Excised scaffold at 8 Weeks Post-Implantation. (Middle) Excised scaffold at 16 Weeks Post-Implantation. (Right) Excised Native Ovine Lateral Meniscus.

### 3.6.2. Biomechanical Analysis

#### 3.6.2.1. Tensile Testing

Three scaffolds from each time point were tested mechanically in tension until failure. The yield load, ultimate load, and stiffness were calculated and compared against those of the normal ovine medial meniscus as well as pre-implanted meniscal implants (Figure 3.19). The yield and ultimate loads of pre-implanted scaffolds were found to be significantly higher ( $p < 0.05$ ) than those of the normal ovine menisci, as well as meniscus scaffolds after 8 and 16 weeks implantation. The ovine medial meniscus had significantly higher ( $p < 0.05$ ) yield and ultimate loads than implanted scaffolds. The stiffness of pre-implanted scaffolds and the ovine menisci were not statistically different from each other, but were both statistically higher ( $p < 0.05$ ) than the implanted scaffolds. No significant differences were found for any of the structural properties between scaffolds implanted at 8 and 16 weeks.

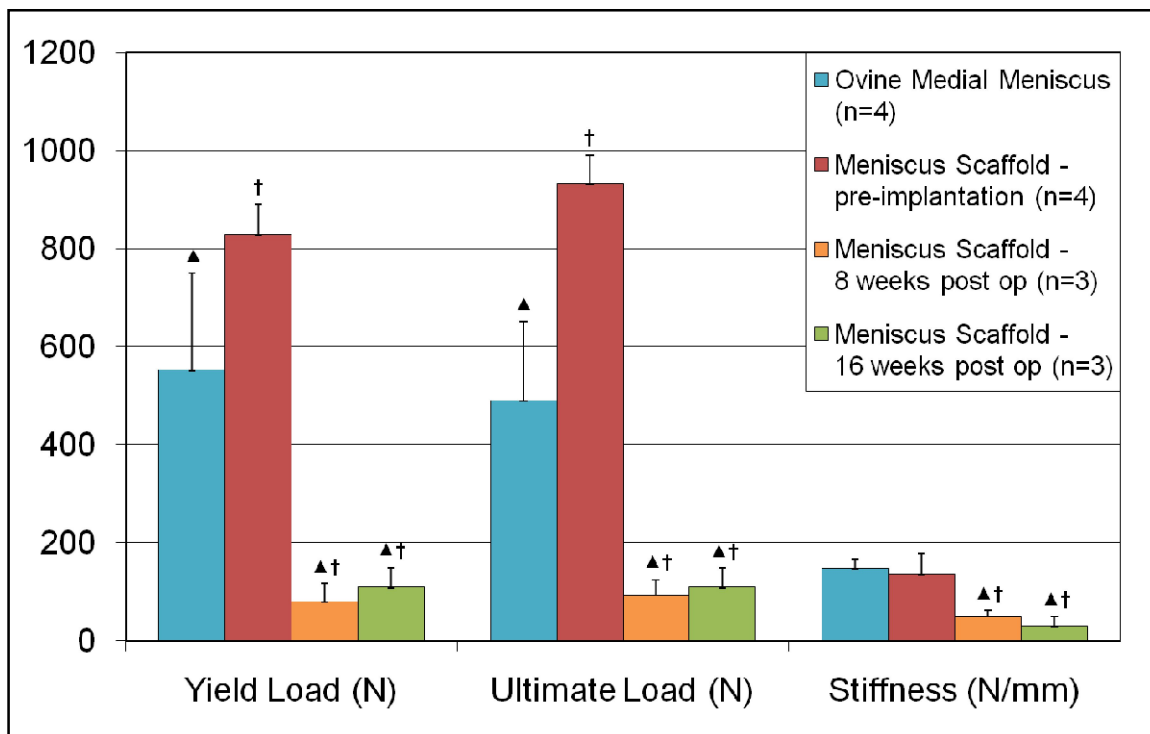


**Figure 3.19: Structural Tensile Properties of Meniscus Scaffolds Pre-Implantation, 8 Weeks Post-Implantation, and 16 Weeks Post-Implantation as Compared to the Native Ovine Medial Meniscus.** Significant differences ( $p < 0.05$ ) as compared to the pre-implanted meniscus scaffold are denoted by ▲. Significant differences ( $p < 0.05$ ) as compared to the normal ovine meniscus are denoted by †.

### 3.6.2.2. Unconfined Compression Testing

When possible, cylindrical plugs (5 mm diameter, 1-2 mm height) were taken from excised scaffolds and tested in unconfined compression. The compressive modulus of scaffolds at 8 and 16 weeks was measured and compared against measured values of the normal medial meniscus (Figure 3.20). Only one sample for compression was able to be collected from the 8 week group. Six samples were collected from the 16 week group from 2 sheep (4 from one meniscus, 2 from another). The ovine menisci had a significantly higher compressive modulus than either the 8 or 16 week scaffold samples. Due to the small sample size, statistical analysis was not performed.

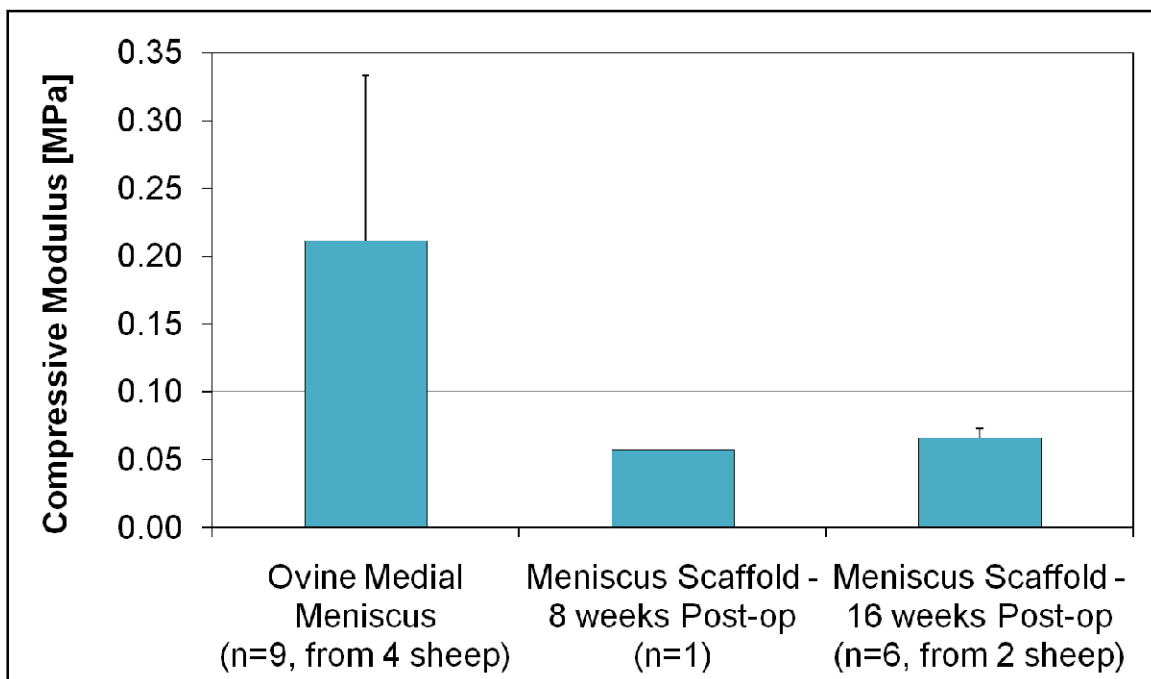


**Figure 3.20: Compressive Modulus of Meniscus Scaffolds.** The unconfined compressive modulus of meniscus scaffolds after 8 and 16 weeks post-implantation as compared to that of the native ovine medial meniscus.

### 3.6.3. Standard Histological Analysis

Three scaffolds per time point were harvested at sacrifice, fixed in formalin, and then processed histologically with H&E or Masson's Trichrome. Slides were subjectively analyzed by a university pathologist on two separate dates. Figures 3.21 – 3.26 show representative slides from the scaffold, bone tunnels, and articular cartilage for each time group.

By 8 weeks post-implantation, cellular and tissue infiltration into the scaffolds was complete (Figure 3.21). A moderate chronic inflammatory response was observed throughout the implants, consisting primarily of lymphocytes, histiocytes, and giant cells. There was a minor eosinophil presence noted in them as well. Giant cells and histiocytes were associated primarily with the polymer fiber portion of the scaffold. Lymphocytes and scattered eosinophils were found between these areas. A high

degree of vascularization was observed throughout the body of scaffolds. Trichrome stained slides show the presence of new collagen – which was distinct from the collagen portion of the scaffold. Very little of the original collagen scaffold was observed in any of the samples at 8 weeks. Viewing H&E slides under polarized light revealed areas of organized collagen which fluoresced. Fluorescence was observed randomly throughout the neo-tissue and did not correspond to the orientation of the fibers.

Figure 3.22 shows a representative micrograph of the bone tunnels with (Figure 3.22A) and without (Figure 3.22B) the presence of the scaffold polymer fibers after 8 weeks implantation. At the proximal end of the tunnel, the polymer fibers were packed closely together and little tissue or cellular infiltrate was found between them. Furthermore, the diameter of the bone tunnel did not decrease appreciably near the fibrous sections. At the distal end of the tunnel, only the non-resorbable sutures persisted. The diameter of the bone tunnel had decreased significantly as new bone grew into it.

Figure 3.23 shows micrographs of H&E stained cartilage sections from the medial femoral condyles of control and experimental knees from the 8 week group. In the control legs, the surface of the cartilage was relatively smooth and continuous. Some hypercellularization was noted in a few specimens, a possible indicator of degenerative changes in the tissue. In the experimental legs, areas of moderate degeneration (Figure 3.23D) were found along with areas of mild or no degeneration (Figure 23C). This observation corresponds with gross observations in which only a small area of the articulating surface showed signs of wear.

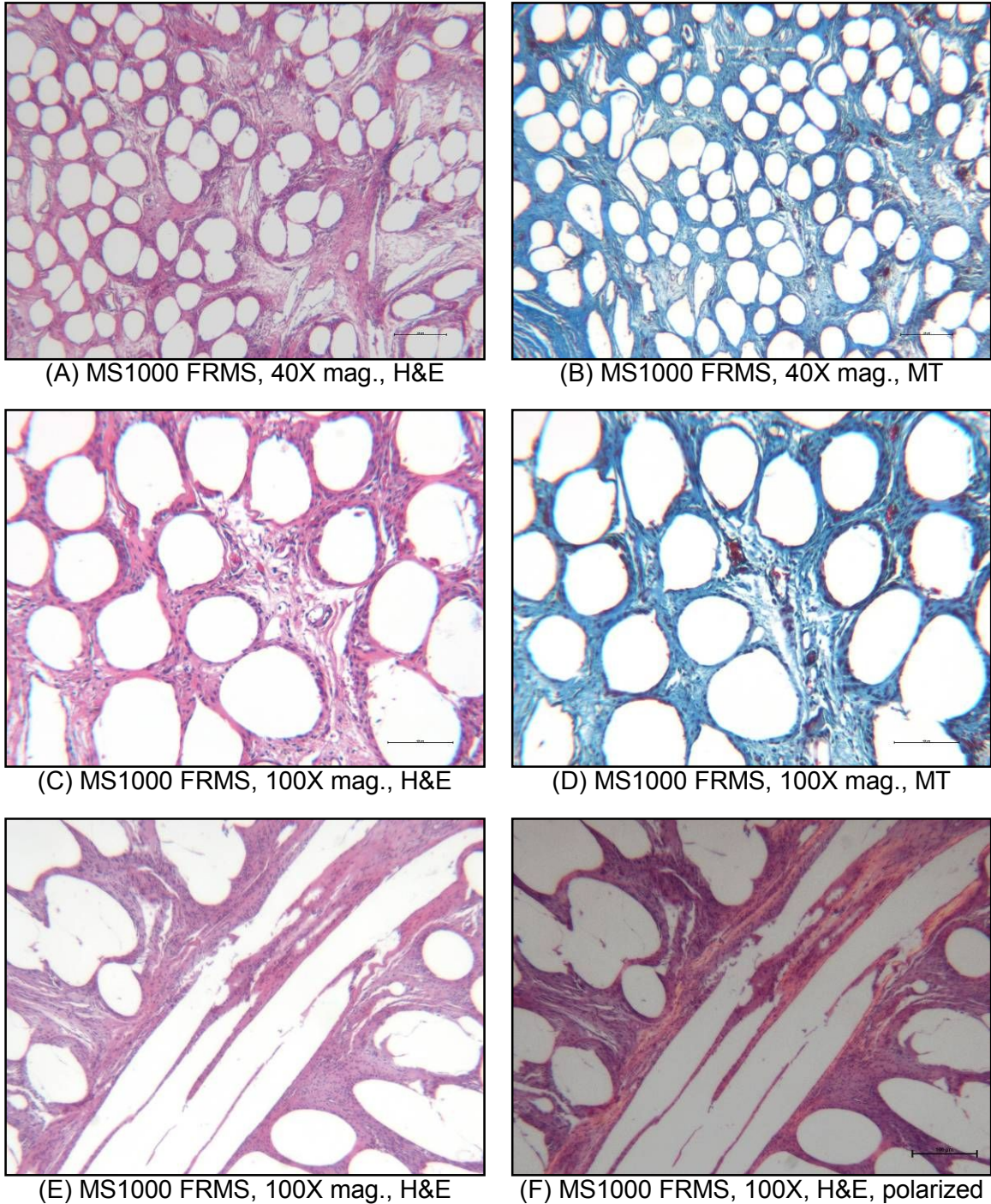
At 16 weeks, the inflammatory response to the scaffold had decreased from the 8 week scaffolds, but was still considered moderate (Figure 3.24). Identification of inflammatory cells was not possible due to an error during histological processing in which scaffolds underwent a decalcification process. From H&E and Trichrome stained

slides, giant cells were again observed around the polymer fibers. Lymphocyte-like cells were observed between these areas – similar to what was seen in 8 week samples. Scaffolds were well vascularized and little difference was seen between 8 and 16 week timepoints.

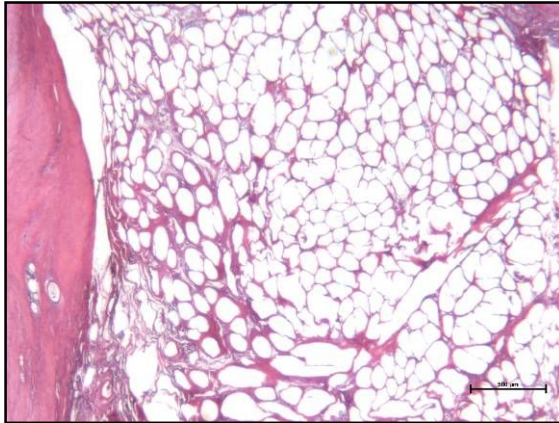
Slightly more tissue was observed around fibers in the 16 week group, as indicated by the Trichrome slides. H&E slides viewed under polarized light again revealed the presence of organized collagen within the scaffold. The presence of organized tissue was not specific to the orientation of the polymer fibers. There was no difference in the amount of fluoresced tissue between 8 and 16 week groups.

Figure 3.25 shows three micrographs from the bone tunnels of the tibia after 16 weeks implantation. There was slightly more tissue between the polymer fibers in the proximal portion of the tunnel at 16 weeks as compared to 8 weeks post-implantation (Figure 3.25A). As with the 8 week group, the diameter of the tunnel did not appreciably change when closely packed fibers filled it. The diameter of the distal end of the tunnel did decrease significantly between 8 and 16 weeks, with new bone forming around the non-resorbable sutures. In two tunnels (from two separate sheep), an area of new bone formation was observed adjacent to areas of some polymer fibers (Figure 3.25C). However, the lack of high fiber density may be indicative of implant failure due to attachment pullout.

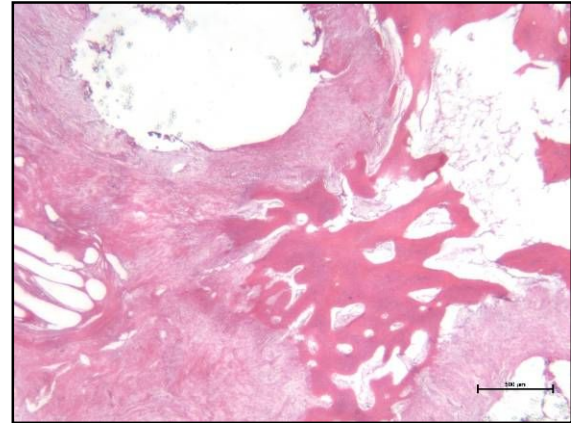
Figure 3.26 shows micrographs of H&E stained sections of the medial femoral condyle from the control and experimental knees at 16 weeks post-implantation. Control sections showed a smooth surface with some area hypercellularity (Figure 3.26A). Areas of mild degeneration (Figure 3.26C) were observed along with areas of moderate/severe degeneration (Figure 3.26D). Again, these findings reflect the gross observations in which small areas of degeneration were found adjacent to normal areas.



**Figure 3.21: MS1000 FRMSs After 8 Weeks Implantation in an Ovine Knee.** (A) Representative H&E slide at 40X magnification. (B) Representative MT slide at 40X. (C) Representative H&E slide at 100X. (D) Representative MT slide at 100X. (E) H&E slide with fibers running in circumferential (longitudinal cross-section) and radial (lateral cross-section) directions. (F) Same section from (E) under polarized light. Areas of tissue that fluoresce represent organized extra-cellular matrix.

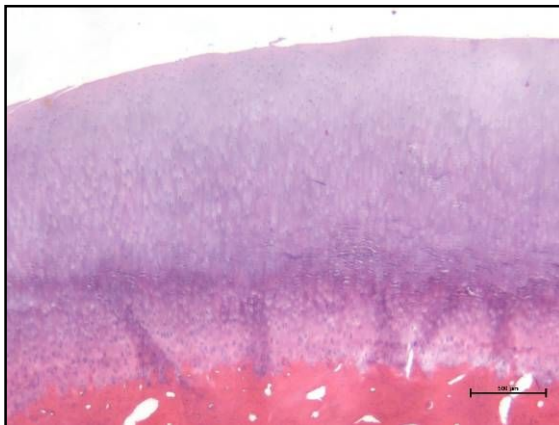


(A) Proximal Bone Tunnel, 40X mag.

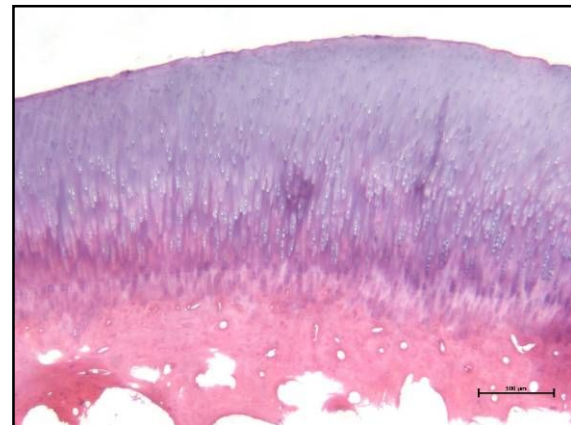


(B) Distal Bone Tunnel, 40X mag.

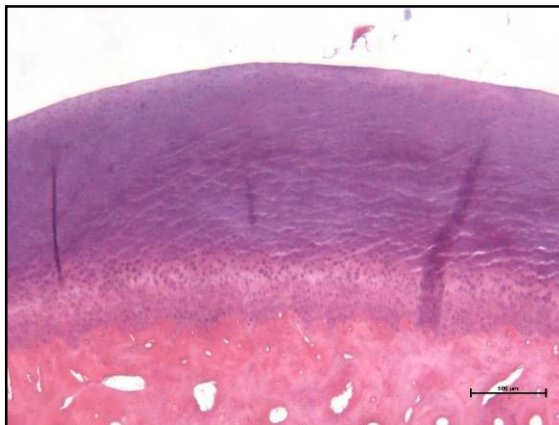
**Figure 3.22: MS1000 FRMSs in the Bone Tunnel After 8 Weeks Implantation in an Ovine Knee.** (A) Section from bone tunnel 2-3 mm from tibial plateau; H&E, 40X. (B) Section from bone tunnel 5-9 mm from tibial plateau; H&E, 40X.



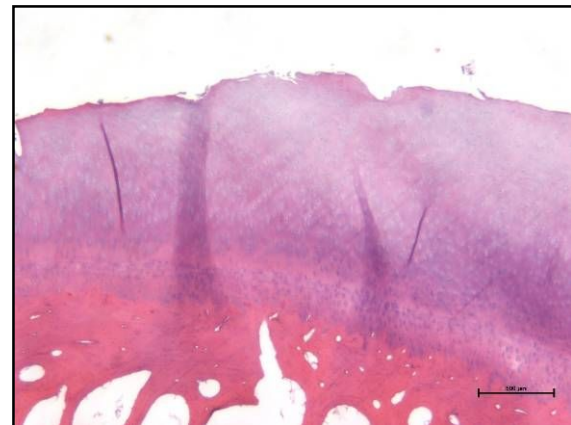
(A) Con Leg., Med. Femoral Condyle, 20X



(B) Con Leg., Med. Femoral Condyle, 20X



(C) Exp Leg., Med. Femoral Condyle, 20X



(D) Exp Leg., Med. Femoral Condyle, 20X

**Figure 3.23: Medial Femoral Condyles from Control and Experimental Knees After 8 Weeks Implantation.** (A) MFC from control leg; H&E 20X. (B) FC from control leg; H&E 20X. (C) MFC from exp. leg; H&E, 20X. (D) MFC from exp. leg; H&E, 20X.

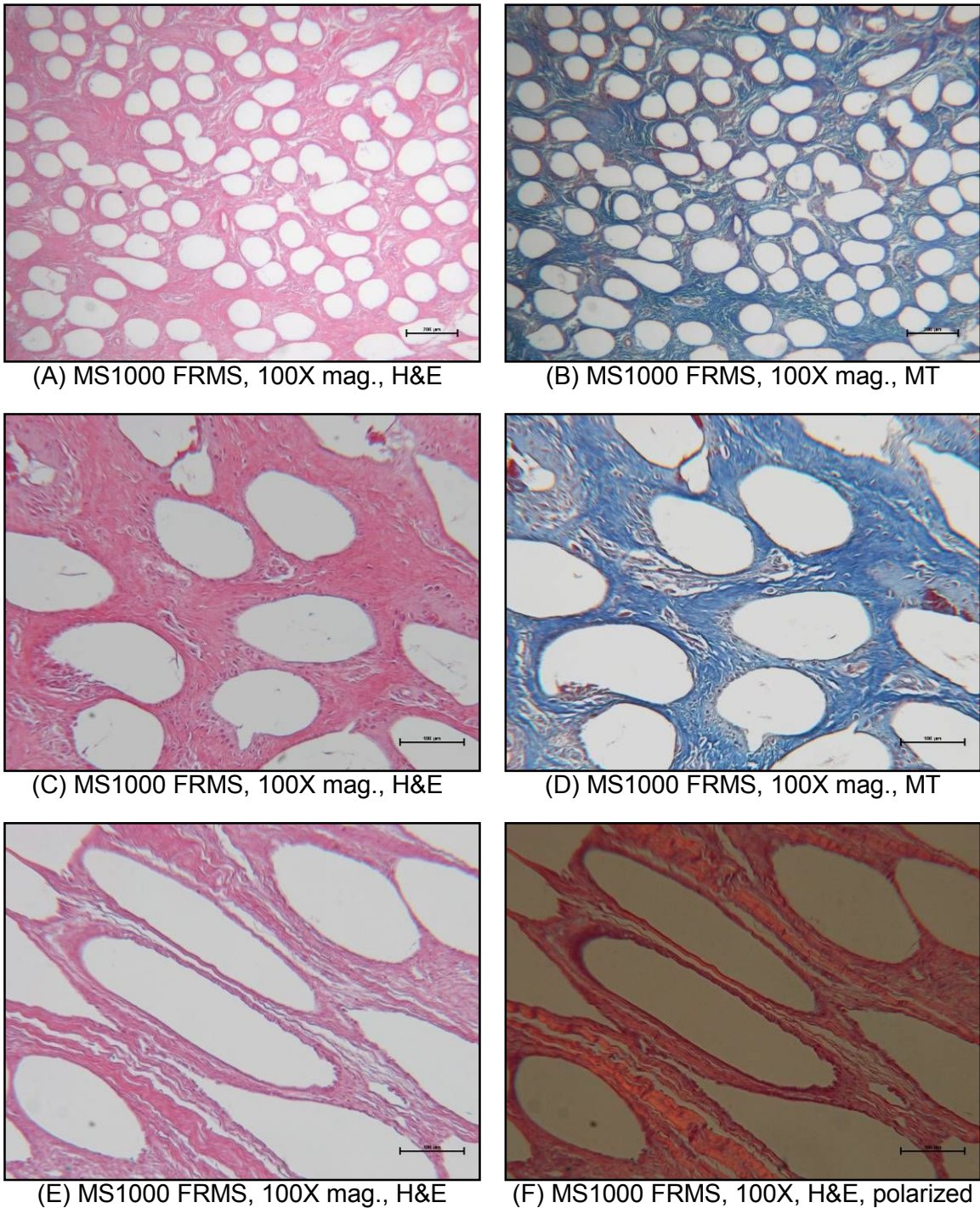
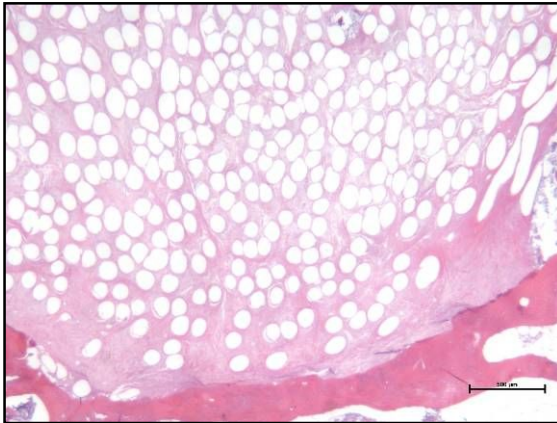


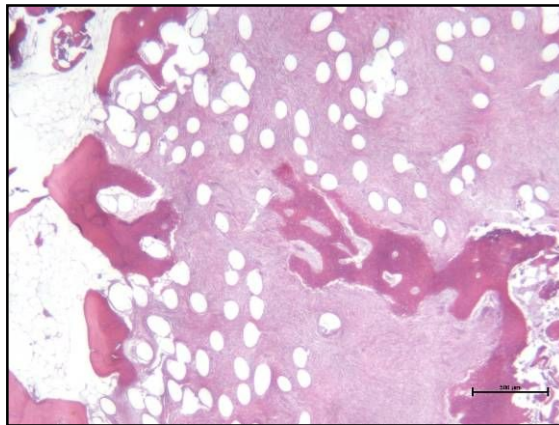
**Figure 3.24: MS1000 FRMSs After 16 Weeks Implantation in an Ovine Knee.** (A) Representative H&E slide at 40X magnification. (B) Representative MT slide at 40X. (C) Representative H&E slide at 100X. (D) Representative MT slide at 100X. (E) H&E slide with fibers running in semi-circumferential (longitudinal cross-section (F) Same section from (E) under polarized light. Areas of tissue that fluoresce represent organized extra-cellular matrix.



(A) Proximal Bone Tunnel, 40X mag.

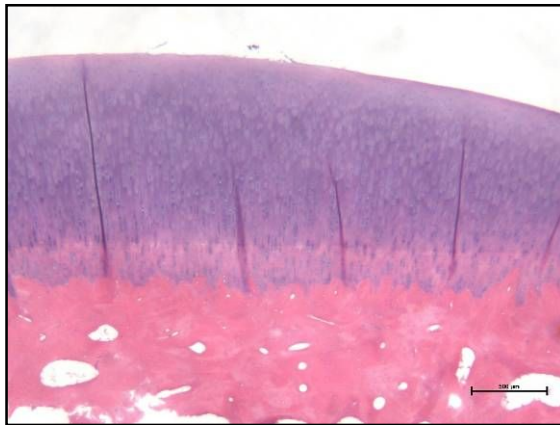


(B) Distal Bone Tunnel, 40X mag.

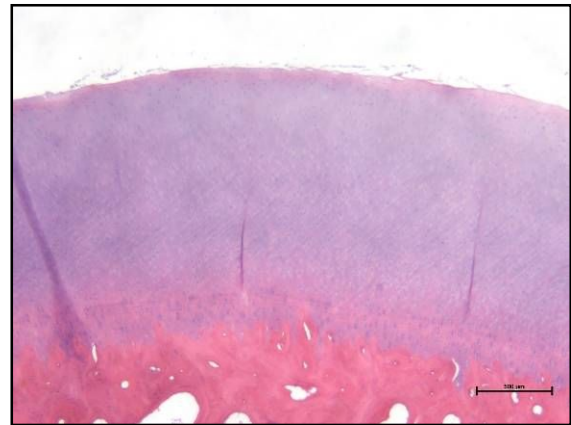


(C) Proximal Bone Tunnel, 40X mag.

**Figure 3.25: MS1000 FRMSs in the Bone Tunnel After 16 Weeks Implantation in an Ovine Knee.** (A) Section from bone tunnel 2-3 mm from tibial plateau; H&E, 40X. (B) Section from bone tunnel 5-9 mm from tibial plateau; H&E, 40X. (C) Section of bone tunnel from proximal end of tunnel which shows integration of new bone adjacent to polymer fibers.



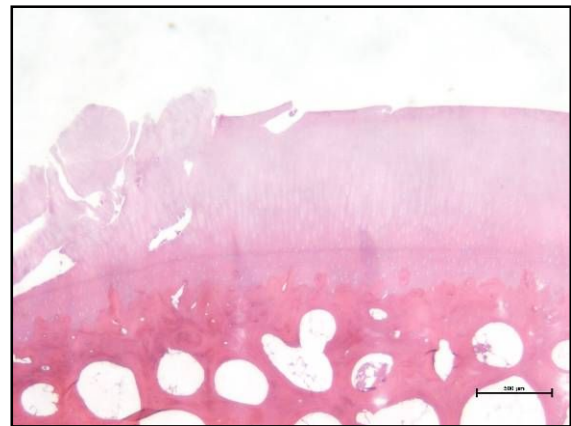
(A) Con Leg., Med. Femoral Condyle, 20X



(B) Con Leg., Med. Femoral Condyle, 20X



(C) Exp Leg., Med. Femoral Condyle, 20X



(D) Exp Leg., Med. Femoral Condyle, 20X

**Figure 3.26: Medial Femoral Condyles from Control and Experimental Knees After 16 Weeks Implantation.** (A) MFC from control leg; H&E 20X. (B) FC from control leg; H&E 20X. (C) MFC from exp. leg; H&E, 20X. (D) MFC from exp. leg; H&E, 20X.

Histological trends with regards to lymphocyte inflammation, giant cell inflammation, collagen scaffold degradation, cellular infiltration, vascularization, and neo-tissue organization are found in Figures 3.27. Due to the small sample size, statistical comparison was not performed as it was deemed impractical. Trends were reported for histological sections taken from the body of the scaffold (Figure 3.27 A/B) and the portion of scaffold within the tibial bone tunnel (Figure 3.27 C/D), approximately 2-4 mm from the articular surface. General observations from the pathologist are reflected in this figure:

1. There was a marked decrease in lymphocyte inflammation from 8 to 16 weeks. Trends were similar for sections taken at the body of the scaffold as well as the horn attachment sections located in the bone tunnel.
2. Giant cells comprised the majority of the inflammatory response. There was a slight decrease between 8 and 16 weeks. Again, trends were similar for both section locations.
3. Very little of the collagen portion of the scaffold was observed in the body of the scaffold at 8 weeks. At 16 weeks, a very small amount of the collagen was observed in one animal, while none was found in the other two. Degradation of the sponge was slower within the bone tunnel, but still decreased between 8 and 16 weeks.
4. There was an increase in the number and density of connective tissue-like cells between 8 and 16 weeks.
5. For both scaffold locations, robust vascularization within the scaffold was observed by 8 weeks, which increased slightly at 16 weeks.
6. For both locations, there was a marked increase in organization of the neo-tissue between 8 and 16 weeks.

Overall, from 8 to 16 weeks, there was less inflammation, more new tissue, and increased tissue organization. Bone growth within the tunnels seemed to be impeded by the presence of polymer fibers, and significant growth was only seen distal to the horn attachment.

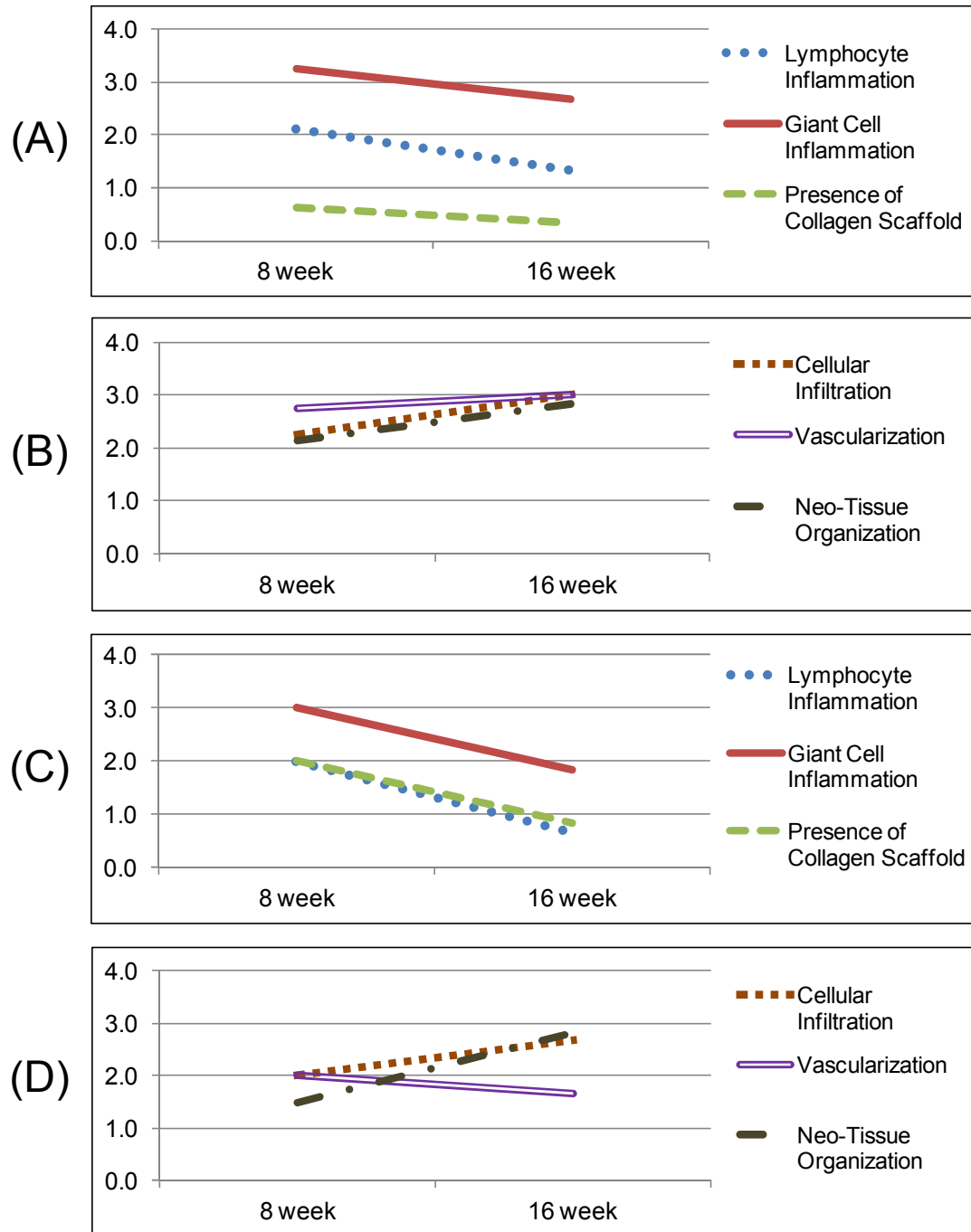


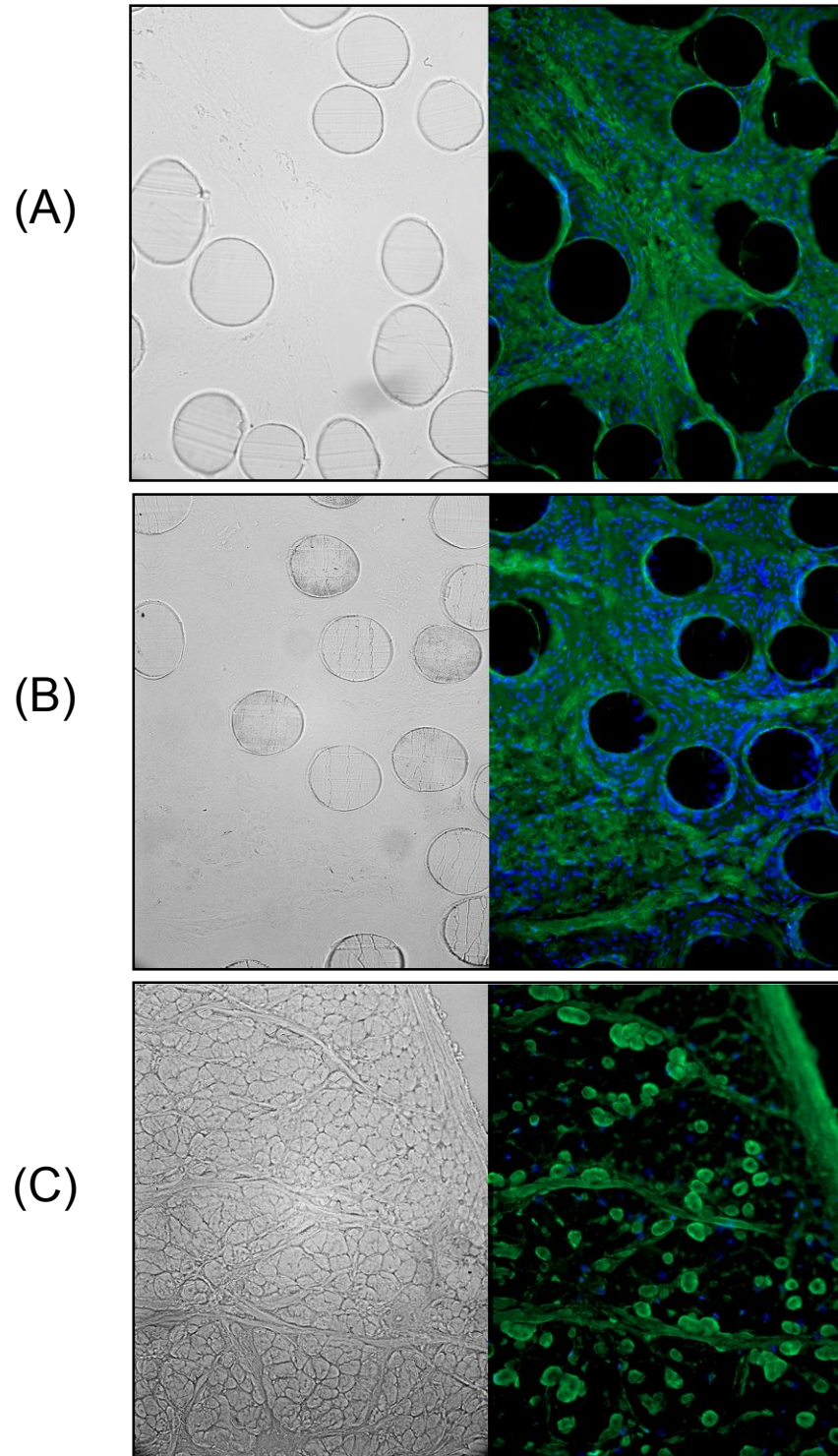
**Figure 3.27: Histological Trends of Biological Response to MS1000 Scaffolds.** 'Lymphocyte Inflammation' and 'Giant Cell Inflammation' refers to the overall number and density of these cells. 'Presence of Collagen Scaffold' is to how much of the original scaffold material is observed. 'Cellular Infiltration' refers to the number and density of matrix producing cells observed. 'Vascularization' refers to the amount of blood vessels seen. 'Neo-Tissue Organization' refers to the level of reorganization of the deposited granulation tissue. (A) & (B) are ranks of samples from the body of the scaffold. (C) & (D) are ranks from samples of scaffold in the bone tunnel, located approximately 2-4 mm from the tibial plateau.

### 3.6.4 Immunofluorescence Staining

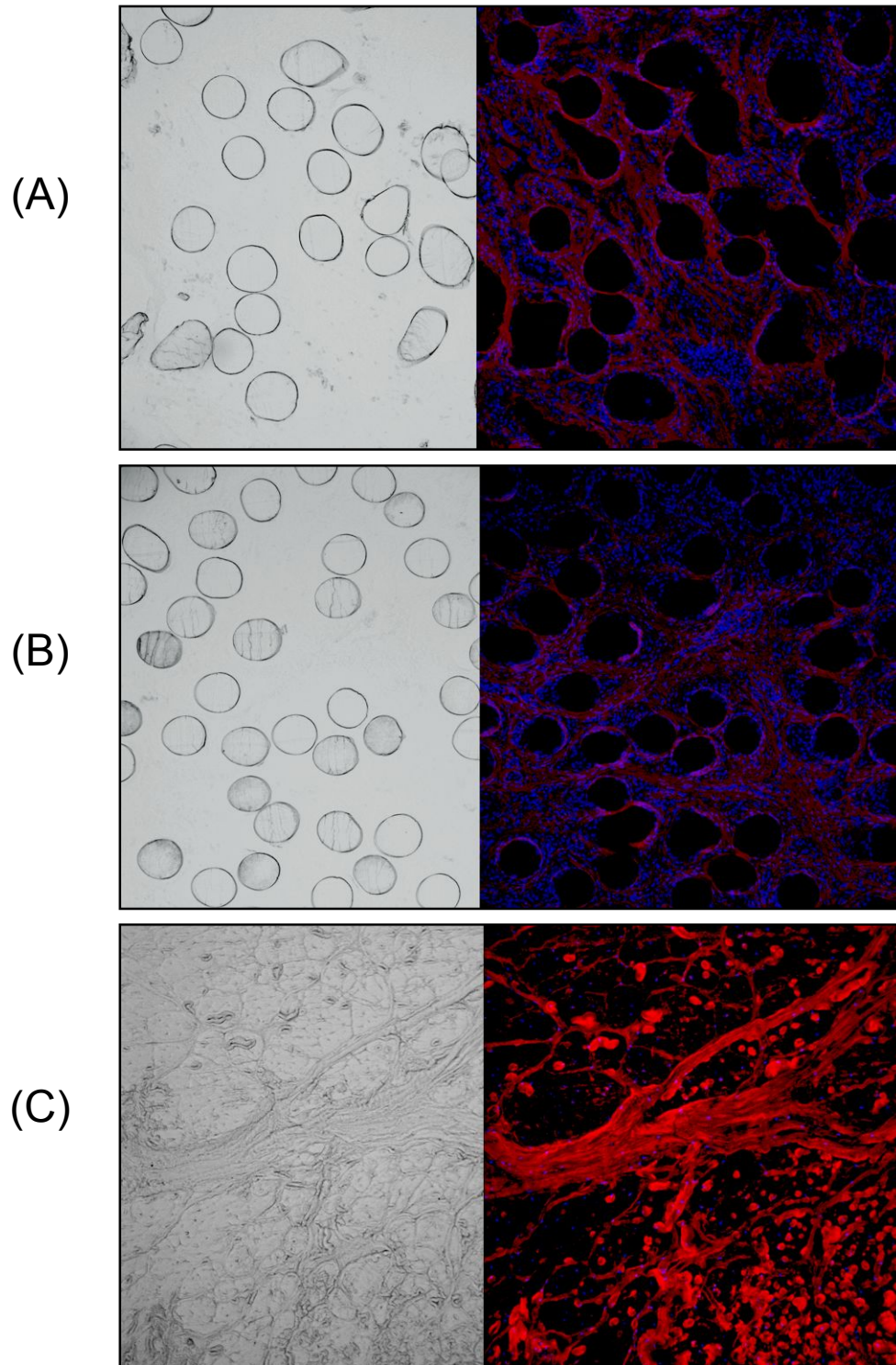
Immunofluorescence staining techniques were employed to determine the make-up of the infiltrating tissue into the scaffold. It was found that scaffolds harvested at 8 and 16 weeks reacted with antibodies of type I, II, III, and XII collagen. For all samples, it was observed that infiltrating tissue lacked the high organization present in the native meniscal tissue.

Figure 3.28 shows comparative micrographs of type I collagen staining between scaffolds and the native meniscus. High levels of type I collagen staining were present throughout the scaffold. Subjectively, little difference can be seen in the amount or organization of this neo-tissue. Figure 3.29 shows similar micrographs of tissue stained for type II collagen. Moderate levels of type II collagen were found in some areas of the sample. Unlike type I collagen, this tissue was not found throughout the sample. No subjective difference was found between time points. However, the native meniscus stained darker red than the neo-tissue within the scaffold. Figure 3.30 shows comparative micrographs for type III collagen. High levels of staining were found throughout the sample, with some slight increase in expression between 8 and 16 weeks. Figure 3.31 shows micrographs for type XII collagen. High levels of staining were observed throughout the sample, with no discernible difference between 8 and 16 weeks.

Figure 3.32 shows control micrographs for each antibody on the pre-implanted scaffold. Type I and III collagen both had moderate staining, while type II had minimal, and type XII had none.



**Figure 3.28: Immunofluorescence Staining of Type I Collagen.** (A) FRMS at 8 weeks post-implantation. (B) FRMS at 16 weeks post-implantation. (C) Ovine medial meniscus. The primary antibody is a rabbit polyclonal diluted 1:30. The secondary antibody is goat anti-rabbit Alexa Fluor® 488 (Invitrogen, Carlsbad, CA) diluted 1:1000, which stains the collagen green. Nuclear staining was accomplished with DAPI, which stains cell nuclei blue. Magnification 200X.



**Figure 3.29: Immunofluorescence Staining of Type II Collagen.** (A) FRMS at 8 weeks post-implantation. (B) FRMS at 16 weeks post-implantation. (C) Ovine medial meniscus. The primary antibody is a rabbit polyclonal diluted 1:200. The secondary antibody is goat anti-rabbit Alexa Fluor® 594 (Invitrogen, Carlsbad, CA) diluted 1:1000, which stains the collagen red. Nuclear staining was accomplished with DAPI, which stains cell nuclei blue. Magnification 200X.

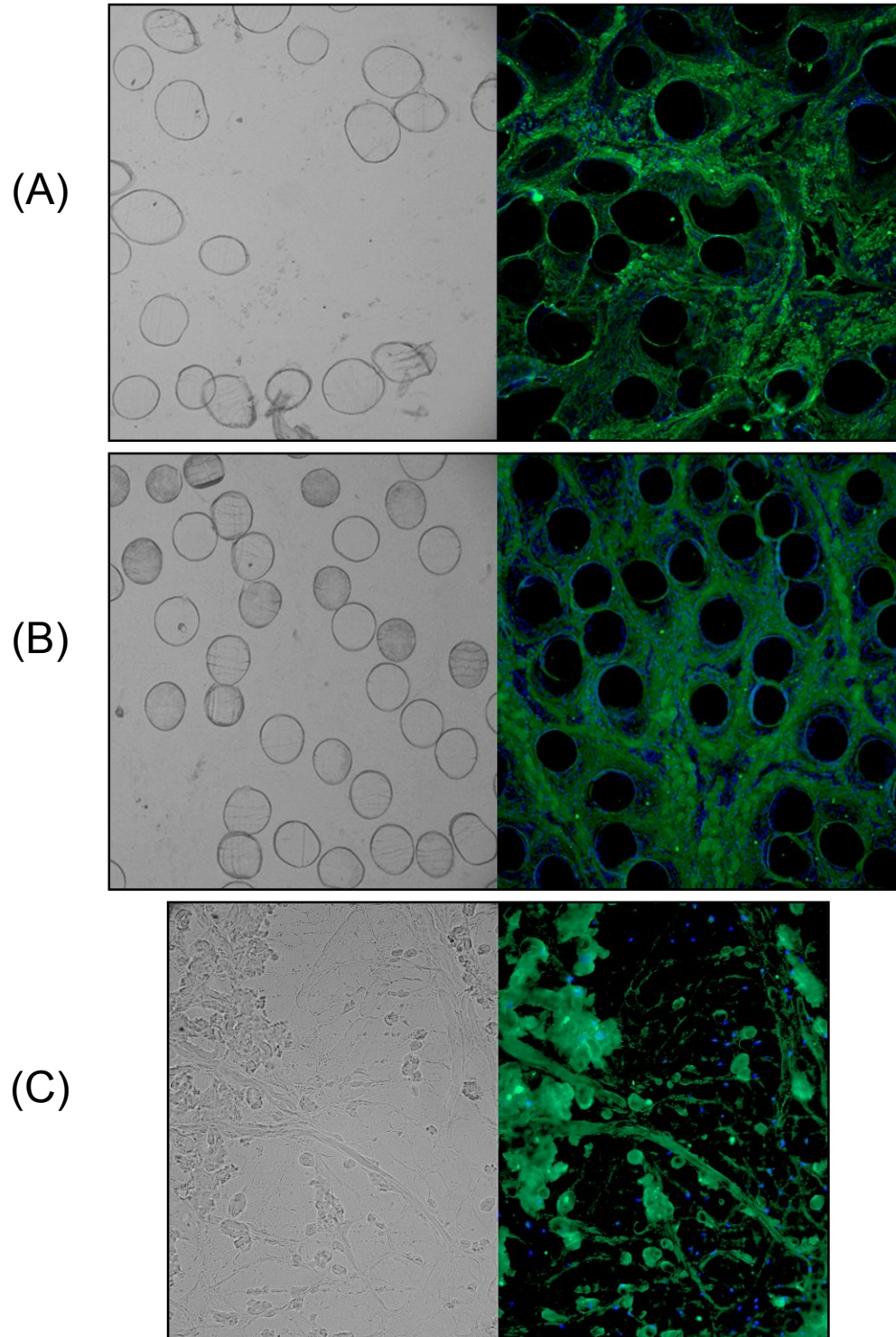


**Figure 3.30: Immunofluorescence Staining of Type III Collagen.** (A) FRMS at 8 weeks post-implantation. (B) FRMS at 16 weeks post-implantation. (C) Ovine medial meniscus. The primary antibody is a rabbit polyclonal diluted 1:40. The secondary antibody is goat anti-rabbit Alexa Fluor® 488 (Invitrogen, Carlsbad, CA) diluted 1:1000, which stains the collagen green. Nuclear staining was accomplished with DAPI, which stains cell nuclei blue. Magnification 200X.

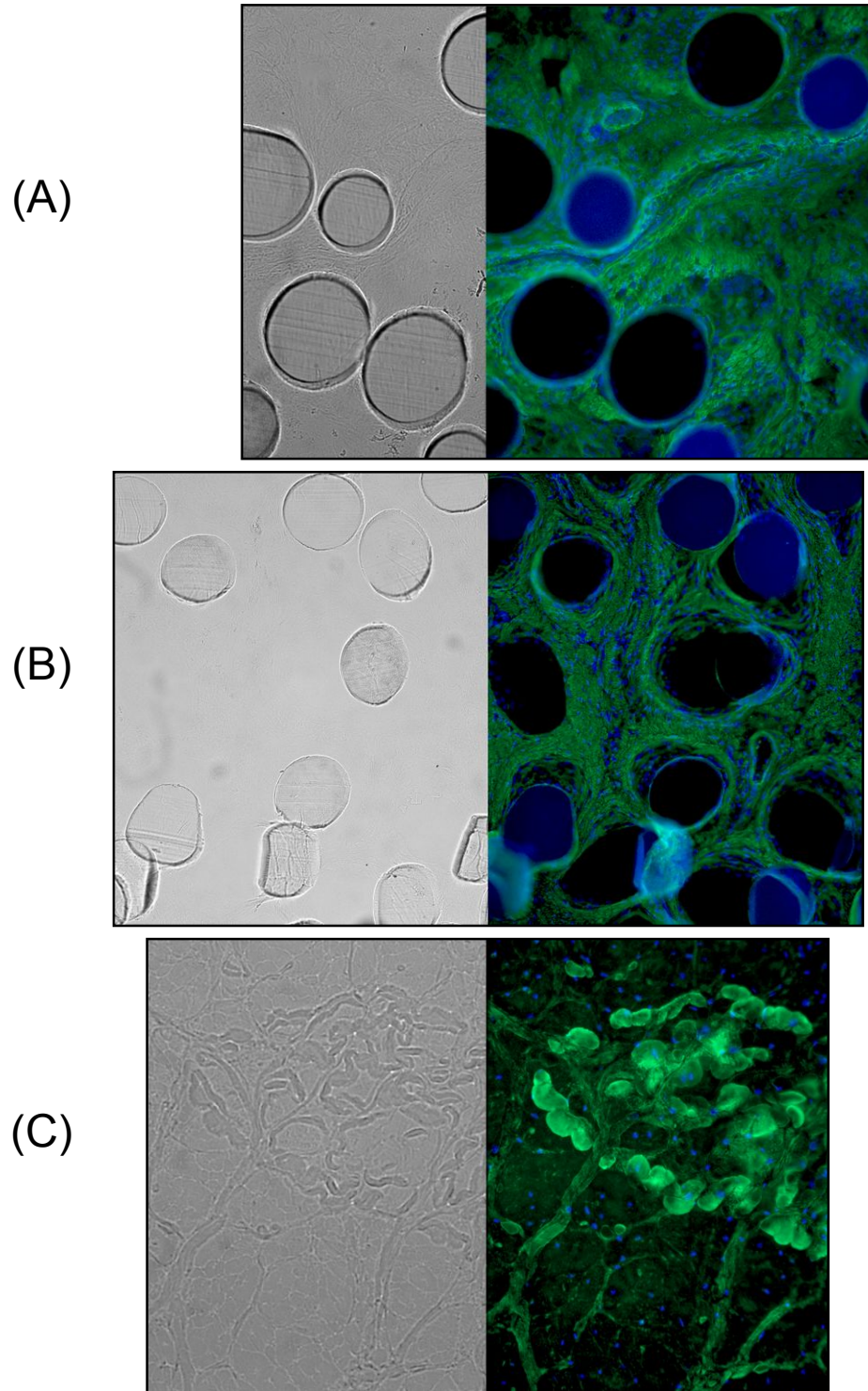


**Figure 3.31: Immunofluorescence Staining of Type XII Collagen.** (A) FRMS at 8 weeks post-implantation. (B) FRMS at 16 weeks post-implantation. (C) Ovine medial meniscus. The primary antibody is a rabbit polyclonal diluted 1:100. The secondary antibody is goat anti-rabbit Alexa Fluor® 488 (Invitrogen, Carlsbad, CA) diluted 1:1000, which stains the collagen green. Nuclear staining was accomplished with DAPI, which stains cell nuclei blue. Magnification 200X.

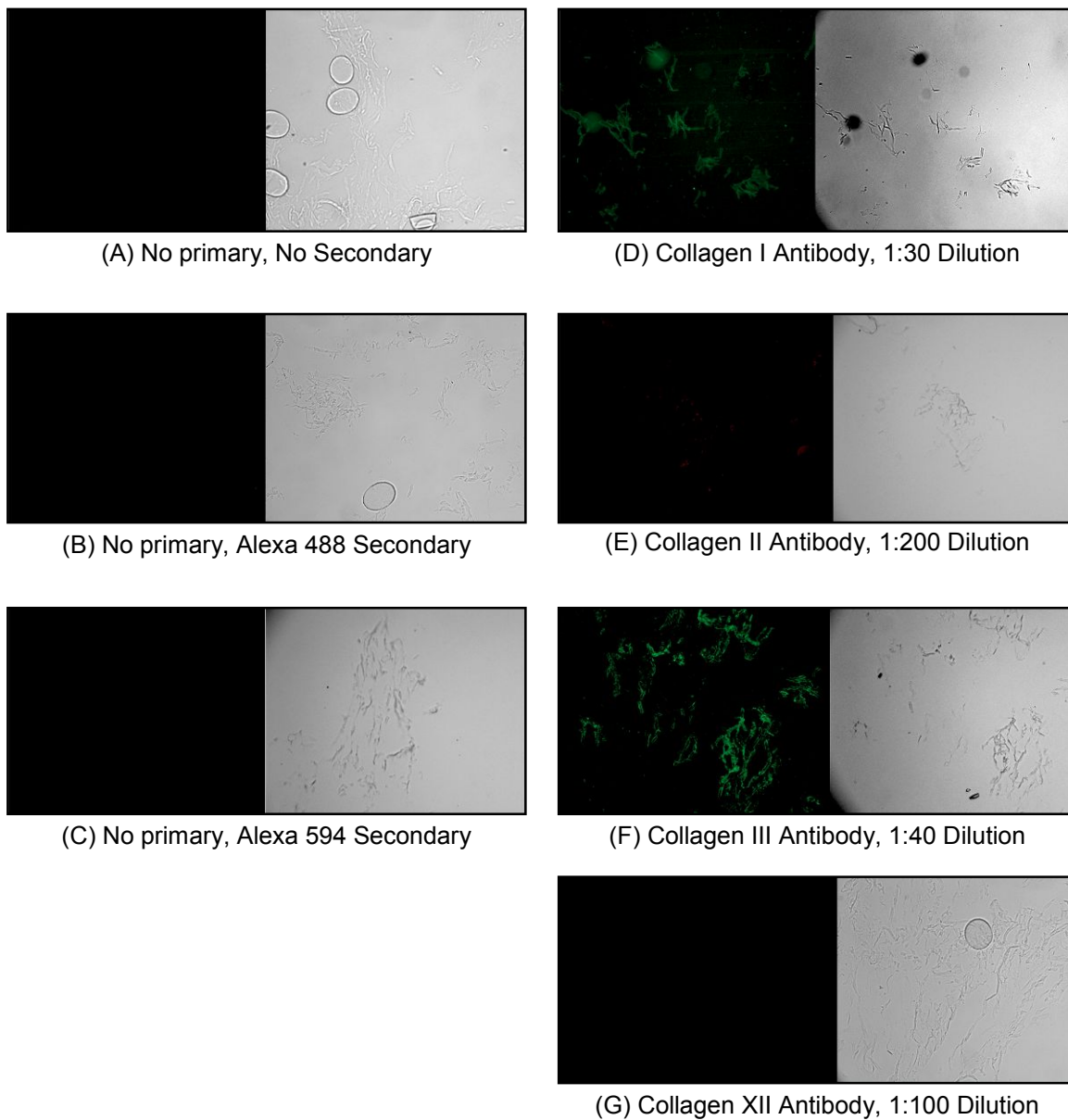


**Figure 3.32: Individual Reactivities of Antibodies with FRMS.** The collagen portion of the scaffold had moderate staining for Type I and III collagen, and minimal staining for type II. No staining was observed for type XII collagen. Magnification 200X.

## 4. DISCUSSION

The meniscus is a tissue which experiences complex loading under normal daily activities, and is vulnerable to permanent, debilitating injury due to its limited healing potential. The field of Functional Tissue Engineering (FTE) offers the potential to replace severely damaged tissues such as these with an implant that will perform the mechanical function of the native tissue, while promoting the degradation of the implant at a rate which corresponds to the growth of a fully functional neo-tissue<sup>60, 61</sup>. In this dissertation, the design, development, and analysis of a tissue engineered meniscus scaffold was described. The implant possessed the necessary initial structural properties to function as a load-bearing device in the knee, and provided a biocompatible substrate for cells to infiltrate and proliferate into. Results from the functional, *in vivo* evaluation of the scaffold provided promising short-term data and identified several key factors necessary for its advancement.

### **PHASE I: Preliminary Development of Fiber Reinforced Meniscus Scaffolds**

Several fundamental Functional Tissue Engineering principles described by Butler et al were applied during the development of this meniscus scaffold<sup>60, 61</sup>. The biomechanical properties typically experienced by meniscal tissue during normal daily activities were identified and prioritized. With regards to mechanics, the meniscus can be considered one of the most complex soft tissues in the body. It undergoes a myriad of stresses and strains which dictate its microstructure and function<sup>46, 130, 187-193</sup>, as well as the overall health of the surrounding structures. At its periphery, the primary mode of loading is tension, while at its inner margin, the primary mode is compression. Several investigators have experimented with polymer sponges for meniscal replacement –

concentrating primarily on the compression mode of loading<sup>122-125, 131-135</sup>. Of the investigators who have considered fibrous scaffolds, few have reported the tensile properties either before or after implantation<sup>98, 126, 127</sup>. In this study, tension was the primary mode of loading considered during the development of a meniscus scaffold – specifically the generation of tensile forces in response to compressive loads. To this end, circumferential fiber-reinforcement of a device was considered. By providing a biocompatible scaffold which offers an appropriate mechanical environment, matrix producing cells may be encouraged to synthesize and organize an extracellular matrix which resembles and functions as fibrocartilage.

#### **4.1. First Generation Meniscus Scaffolds**

The design for first generation meniscus scaffolds was based solely on the concept of a fiber-reinforced, biocompatible substrate. Few investigators have explored the use of fibrous structures for replacing damaged meniscal tissue. In the early 80's, Veth et al. experimented with the use of carbon-fiber reinforced polymers as permanent meniscal prostheses<sup>110, 111</sup>. As with most permanent devices for meniscal applications, they fell to the wayside as the field of tissue engineering developed and offered more promising alternatives. Resorbable polymer mesh scaffolds have also been used by several investigators as meniscus replacements<sup>98, 129, 130</sup>. However, data on these devices is limited to *in vitro* cytocompatibility<sup>129, 130</sup> and small animal testing<sup>98</sup>. While compressive mechanical properties of scaffolds were reported by Kang and Baker, tensile properties were not reported by any investigators. As with the sponge-based meniscus scaffold studies, the primary concern in these studies did not appear to be the development of an implant which would function in tension. Chari et al. and Kon et al. did consider circumferential reinforcement in the development of their meniscal scaffolds<sup>126, 127</sup>. However, the fiber reinforcement was limited and used primarily for attachment of

the scaffold to the stumps of the resected meniscus. No mechanical properties were reported in these studies; only gross and histological data.

For this study, a more robust fiber-reinforcement was considered. After rejecting three fiber reinforcement patterns due to either complexity, reproducibility, or fixation, the quasi-circumferential pattern was chosen. Using this pattern, several designs were chosen varying in collagen sponge dispersion concentration and collagen-to-polymer fiber weight ratio. For ease of initial mechanical evaluation, a 'donut-shaped' scaffold was employed. After initial tensile testing, none of these designs were found to possess the strength necessary to function as a meniscal replacement. Furthermore, the geometry of these scaffolds – while conducive to simple tensile evaluation – was not practical for a device required to function as a meniscus. And finally, the 'donut-shape' provided no strong attachment sites which were continuous with the fiber reinforcement of the main body. Through careful study of how the meniscus functions and from the mechanical data collected during this initial evaluation, a second generation scaffold design was pursued.

## **4.2. Second Generation Meniscus Scaffolds**

### **4.2.1. Design Considerations**

Because the structural behavior of the meniscus is highly dependent on its geometry, the overall shape and dimensions of the meniscus scaffold were first altered to mimic those of the normal tissue. A wedge-shaped cross-section was obtained by creating a non-uniform fiber distribution pattern, in which specific low radius weaves were employed near the base of the device, and high radius weaves were used at its apex. A gradient of weaves was used between these two extremes to create a uniform fiber density within the body of the implant (see Methods Section for fiber weaving pattern and Appendix 1 for specific pattern order).

The shape of the scaffold was then modified to the semi-lunar shape of the normal meniscus. The ends of the scaffolds were extended to form high strength, fibrous tissue anchors which were continuous with the fiber reinforcement within the main body of the device. These anchor attachments, coupled with the proper scaffold geometry, were critical to designing a device which could replicate – to some degree – the creation of tensile hoop stresses during normal compressive loading of the knee. By providing a substrate which allows for matrix producing cells to experience the same complex biomechanical loads they would in a normal meniscus, the development of a neo-fibrocartilaginous tissue can be promoted.

Using published mechanical properties<sup>3, 28, 90, 183, 186</sup> of the meniscus, the amount of fiber reinforcement required for a meniscus scaffold was extrapolated from first generation scaffold mechanical evaluation. It was found that scaffolds containing approximately 500 cross-sectional fibers (MS500) would possess tensile properties within the range of published values, but approximately 30% less than the average<sup>3, 28, 90, 183, 186</sup>. Research from our lab has consistently demonstrated a dramatic decrease<sup>145, 146, 148, 149, 194-196</sup> in mechanical function as soon as 1 week post-implantation – an effect compounded when implanted in a synovial environment. Therefore, a 1,000 cross-sectional fiber scaffold (MS1000) was also considered for further evaluation. This scaffold design also possessed tensile values within range of the published values, but exceeded the average by approximately 50%.

MS1000 scaffolds represented the highest fiber density attainable for a scaffold reinforced with this pattern and constrained by the dimensions of an ovine meniscus. One potential concern with this design was that high fiber density would impede cellular and tissue ingrowth within the scaffold, thus delaying its incorporation and promoting an encapsulation response. While MS500 scaffolds possessed significantly lower tensile properties than MS1000 scaffolds, they had a lower fiber density, which may have

allowed for increased proliferation into the implant, thus improving the overall biological response to the device. This 'mechanical strength versus biological incorporation' trade-off was the focus of the experiments discussed in the first and second phases of this project.

## **PHASE II: *In Vitro* Characterization of FRMS**

### **4.3. Mechanical Characterization of Meniscus Scaffolds**

The meniscus is a soft tissue which undergoes complex biomechanical loading under normal daily activities. The purpose of this biomechanical evaluation was to determine how a fiber reinforced meniscus analog with the above-described geometry and tissue attachments would perform when implanted as a meniscus replacement. Based on FTE prioritization<sup>60, 61</sup>, three areas of meniscal biomechanics were considered for these experiments: (1) the conversion of axial compressive loads to circumferential hoop stresses, (2) the extent to which the scaffold would distribute loads on the tibial plateau, and (3) the overall circumferential tensile strength of the scaffold. The experiments performed were used to test the following three hypotheses:

- (II-1) Fiber-reinforced meniscus scaffolds will convert a portion of an axial compressive load to a circumferential tensile load,
- (II-2) Fiber-reinforced meniscus scaffolds will cause an increase in contact area and overall pressure distribution on the tibial plateau after compressive loading,
- (II-3) Fiber-reinforced meniscus scaffolds will possess tensile properties on par with those of the normal ovine meniscus,

(II-4) Fiber-reinforced meniscus scaffolds containing a higher fiber content will outperform lower fiber scaffolds with regards to compression-to-tensile load conversion, contact area and pressure distribution, and overall tensile strength.

#### **4.3.1. Axial Compressive Loads Converted to Circumferential Tensile Loads**

In the normal meniscus, axial compressive forces experienced during loading of the knee joint are dissipated by the generation of tensile forces in the circumferential direction. This experiment sought to quantify the extent to which – if at all – a fiber reinforced meniscus scaffold could replicate this behavior.

A five cycle repetition was chosen to simulate repetitive loading in the hind-limb of a quadruped weighing 40-60 kg. The 100N cycle represented relatively low stress loading (such as simple weight-bearing), while the 250N cycle represented a higher stress loading situation (such as walking). In order to isolate the response of the scaffold to compressive loading, no other tissue attachments in the knee joint were simulated. Previous evaluation of meniscal biomechanics employed the use of a DVRT strain gauge to measure the circumferential deformation of the tissue under compressive loads<sup>173, 197, 198</sup>. However, for this type of scaffold, a strain gauge was found to be impractical and a direct measurement method of tensile loads was used instead.

Both scaffold designs were able to withstand repetitive loading without significant, permanent deformation. They maintained their semi-lunar shape and wedge cross-section throughout the evaluation. Furthermore, the collagen matrix around the fibers did not degenerate or wear away appreciably after repetitive loading, suggesting that EDC crosslinking was appropriate for this application. From gross observations during and after testing, it was found that MS1000 scaffolds were denser and easier to manipulate than MS500 scaffolds.

Results from this experiment support hypothesis II-1 by showing that fiber-reinforced meniscus scaffolds loaded axially in compression could convert a portion of the load to a circumferentially oriented tensile load measured directly at the anterior and posterior scaffold horn attachments. The percentage converted approximately doubled between MS500 and MS1000 scaffolds. This was likely due to the increased fiber density of MS1000 scaffolds, which also increased their overall handleability as compared to MS500 scaffolds. At physiologically relevant loads, MS500 scaffolds converted about 4-9% of the compressive load, while MS1000 scaffolds converted approximately 8-17%. Interestingly, the average values for the 100N cycle runs did not match up with the average values of the first 100N of the 250N cycle runs (Figure 3.3 – dotted lines vs solid lines). Instead, distinct trendlines for each run were observed, especially for the MS1000 scaffolds. During the initial application of the load during the first cycle of loading, measured tensile loads did match up for the 100N and 250N runs. However, after the first peak value was reached, each run responded differently to continued, repetitive loading. This is likely an indicator that scaffolds do not have the high level of resilience normal meniscal tissue does. After the application of a relatively high load (250N) and its subsequent removal, scaffolds were not able to recover to their original shape quickly enough to prepare for the next loading cycle. As a result, scaffolds remained at a higher stress state until the cycle was complete.

To our knowledge, no other group has directly measured the tensile loads generated in a meniscus (or meniscus analog) as a result of axial loading. Studies have instead focused primarily on the measurement of hoop strains through the use of a strain gauge<sup>173, 197-200</sup>. It is difficult to make an accurate comparison between these studies and the results from this project due to obvious experimental differences. First, the DVRT evaluation was completed on a knee joint with robust soft tissue support. The periphery of the meniscus was still intact and attached, and the cruciate and collateral

ligaments provided overall structural integrity to the joint. In the scaffold evaluation, there was no soft tissue stabilization between the femur and tibia. Radin et al demonstrated that any abnormality in the knee joint (i.e. missing of any tissues) would result in irregular loading conditions<sup>201</sup>. Therefore, while the DVRT evaluations provided physiologically relevant mechanical data for intact knees, the scaffold evaluations did not. Instead, these experiments showed only that the implants had the potential to convert compressive loads.

There were several other limitations to this experiment. First, acquiring accurate measurements was found to be highly dependent on the positioning and pre-tensioning of the scaffold. Experimental runs in which scaffolds were improperly placed on the tibial plateau, not pre-tensioned, or pre-tensioned too much yielded results in which little or no circumferential load transfer occurred. Second, because tensile loads were measured directly through the bone tunnels, there was an inherent force-loss due to friction between the scaffold and bone tunnel wall. Third, there was no peripheral attachment of the scaffolds to the tibial plateau as with the normal meniscus. This attachment is important in maintaining the overall position of the scaffold during repetitive loading. These limitations make direct comparison with published literature difficult. The key implication in this experiment is that fiber reinforced scaffolds do have the ability to convert axial compressive loads to circumferential tensile loads. This data is valid only for pre-implanted scaffolds and gives no indication on whether or not this behavior would persist after short- or long-term implantation in a synovial environment.

#### **4.3.2. Pressure Distribution on Tibial Plateau**

The meniscus provides protection the tibial and femoral articular cartilage by distributing axial loads along the surface. The purpose of this evaluation was to

determine if, and to what extent, fiber reinforced meniscus scaffolds would mimic this behavior.

Prior to, and immediately after each compressive run, the height of each scaffold was measured. These values were compared to determine the extent to which scaffolds would rebound to their original shape after loading. Both scaffolds decreased in height by approximately 4% immediately after loading. Rehydration of scaffolds with saline caused them to return to their original height. Because no hydrophilic molecules were used in the design of this scaffold, the decrease in height after loading was an anticipated result. The scaffold exhibited a passive water absorbing behavior similar to that of a sponge, instead of the active increase in osmotic pressure as seen in highly hydrophilic tissues such as the meniscus. This may have a negative effect on the durability of the scaffold, as well as the delivery and removal of cellular waste through the synovial fluid.

From the raw images of the pressure sensitive film (Figure 3.4), it can be seen that hypothesis II-2 is supported in that the presence of fiber reinforcement significantly increased the overall contact area on the tibial plateau after compressive loading as compared to loading in the presence of no scaffold or a 100% collagen scaffold. The pressure distribution profile reveals a reduction in high peak stresses for fiber reinforced scaffolds at 100N compressive loading (Figure 3.5). However, this was not seen at 250N compressive loading. No significant differences were observed between MS500 and MS1000 scaffolds with regards to total contact area or high stress area for either loading conditions. Scaffolds are initially unable to adequately dissipate high loads harmful to cartilage evenly on the tibial plateau. This supports the need for a rehabilitation period consisting of a non-weight-bearing and range of motion exercises.

Other investigators have also used pressure sensitive film to characterize the effect of the meniscus on the femur-tibia interaction <sup>9, 197-199</sup>. As with the DVRT studies

mentioned in the previous section, these experiments were performed at higher loads on human knees with intact supporting tissues – to include the cruciate ligaments, collateral ligaments, lateral meniscus, and surrounding peripheral synovial tissue. As a result, direct comparison of these results with experimental scaffold results is difficult.

Under all scaffold and loading conditions, higher peak stresses were observed as compared to the human studies<sup>9, 197-199</sup>. Simple anatomical differences between human and sheep knee joints may also contribute to these differences. The human tibial plateau is flatter than the convex sheep plateau, making distribution of axial compressive loads – even in the absence of a viable meniscus – more liable in humans. Radin et al found that irregularities in the meniscus – to include mismatched mating surfaces – would result in increased pressures on the articular surfaces<sup>201</sup>. All scaffolds were fabricated with the same dimensions and did not conform to the femoral and tibial surfaces of the jig as closely as that of normal meniscal tissue. As a result, stress distribution was not likely to be optimal. Furthermore, Radin et al found that removal of one meniscus (lateral or medial) would lead to increased stress on the opposite side<sup>201</sup>. Scaffolds were evaluated without any other soft tissue support – to include a lateral meniscus or its analog. This may have also led to increased peak stresses on the tibial plateau during loading.

Comparison of fiber reinforced meniscus scaffolds with 100% collagen scaffolds reveals a distinct difference in load distribution and contact area. The 100% collagen scaffolds are comparable to the Collagen Meniscus Implant (CMI) currently undergoing clinical trials in Europe<sup>133, 137, 140</sup>. No significant differences in pressure distribution or contact area were found between runs with the 100% collagen scaffold and runs in the presence of no scaffold. This suggests that non-fiber reinforced collagen implants may not have the necessary biomechanical properties to provide a protective effect to the underlying articular cartilage.

With regards to contact area, investigators have consistently shown with pressure sensitive film that the absence of a meniscus decreases the contact area between the femur and tibia by 50-70%<sup>9, 183, 197-199</sup>. This trend was also observed for the fiber reinforced meniscus scaffolds in this evaluation. However, the contact area increased by 200-300% as compared to the 100% collagen scaffold and no scaffold runs. This dramatic difference in percentages may be accounted for again by simple anatomical differences between human and sheep knees. The flat tibial plateau of the human joint promotes a greater degree of contact between the bone surfaces under loading.

The main implication of the results from this experiment is that the presence of a fiber reinforced scaffold will increase the contact area on the tibial plateau and – under moderate loads – decrease the areas of high stress on the cartilaginous surface. Again, these results do not predict what will happen after short- or long-term implantation in a synovial environment.

#### **4.3.3. Circumferential Tensile Testing**

The meniscus is an anisotropic material which exhibits a high degree of tensile strength in the circumferential direction. The purpose of this evaluation was to determine the initial tensile strength of fiber reinforced meniscal scaffolds for comparison to normal meniscal tissue. Results from this experiment supported hypothesis II-3.

The material properties of the meniscus are typically reported in publications<sup>3, 28, 90, 183, 186</sup>. Typically, small, dog-bone shaped sections are harvested from the tissue and tested in tension until failure. This method was not a viable option for testing meniscus scaffolds because preparation of the samples would require severing the fiber reinforcement, thus negating the entire purpose of the scaffold. Therefore, scaffolds

were tested whole to obtain their structural properties. This method is similar to that used by Newman et al., who tested whole menisci in tension after trimming away the inner margin and outer periphery<sup>183</sup>.

Structural properties were extrapolated from published data using dimensions similar to those of the meniscus scaffold<sup>3, 28, 90, 183, 186</sup>. This introduces a high degree of error since these calculations assume radial uniformity in the circumferential orientation – which is found to not be true as the inner margin of the tissue lacks the tangential strength of its periphery. However, because these calculations assume the highest tensile strength for the entire tissue, the results are overestimates of actual structural property values. This puts MS500 scaffolds on par with the normal meniscus, and MS1000 scaffolds approximately twice as strong.

There are several limitations to this experiment. First, comparison of this data with published data is difficult due to the nature of the scaffold. Conversion of published material property data to structural property data yielded values which erred on the high side. Therefore, comparing experimental values against these converted values was not considered a major obstacle. Another potential source of error is the low length-to-width ratio of the test samples. Due to the size and shape of these scaffolds, a 1:1 ratio was the best that could be achieved during testing. Additionally, there was a high degree of variability in the material properties of the reinforcing fibers. These two conditions may be the reason that measured structural properties (Figure 3.6) were slightly less than calculated values (Table 3.2). Despite these limitations, fiber reinforced scaffolds were shown to possess initial tensile properties within the load range of the normal meniscus.

The biomechanical evaluation of fiber reinforced scaffolds demonstrates that a properly positioned, anchored, and pre-tensioned scaffold will convert a percentage of

an applied axial compressive load to a circumferentially oriented tensile load, increase the contact area between the femur and tibia under moderate/high loads, and decrease the level of peak stresses under moderate loads. Therefore, hypotheses II-1, II-2, and II-3 were supported by this data. And while MS1000 scaffolds did outperform MS500 scaffolds with regard to compression-to-tensile load conversion, overall tensile strength, and total contact area under high loading conditions, no significant difference was observed between the two designs with regard to pressure distribution on the tibial plateau.

MS500 scaffolds did function within the range of the normal meniscus. However, based on previous data from our lab<sup>147-149, 196</sup>, it is anticipated that there would be a dramatic reduction in mechanical properties after implantation in the synovial environment. Therefore, from a biomechanical perspective, it is logical to pursue development of an implant with an added safety factor. MS1000 scaffolds possess an initial tensile strength significantly higher than, but still in range of, that of the normal meniscus. This reduced the concern of implanting a device which may cause stress shielding due to its high strength.

From a biomechanical perspective, MS1000 scaffolds possess superior properties and should be considered for further evaluation. The cytocompatibility of both scaffolds will be explored in the next section.

#### **4.4. *In Vitro* Cell Compatibility of Meniscus Scaffolds**

For a potential meniscal scaffold to be considered for further development, it must exhibit cytocompatibility, supporting the growth and proliferation of fibrochondrocytes. In this experiment, rabbit meniscal cells were harvested, grown in culture, and then seeded onto fiber reinforced meniscus scaffolds for either 4 hours, 4

days, 8 days, or 16 days. The following two hypotheses were tested in this portion of Phase II:

- (II-4) Fibrochondrocytes seeded onto fiber-reinforced meniscus scaffolds would exhibit a normal growth curve and
- (II-5) Fibrochondrocytes seeded onto MS500 fiber-reinforced meniscus scaffolds would infiltrate further than into MS1000 scaffolds after 16 days.

Meniscus cells, or fibrochondrocytes, differ in morphology depending on their location in the tissue. Cells near the periphery tend to be more elongated and fibroblast-like while cells near the inner margin tend to be more ovoid and chondrocytes-like<sup>39</sup>. Because of this, standard fibroblast or chondrocyte culture techniques were deemed inappropriate as one method would favor one cell type over the other. In this experiment, a cell culture protocol which promoted the proliferation of both cell subpopulations was employed<sup>176, 177, 202, 203</sup>. Micrographs of plated cells during the first or second passage showed a mixture of elongated fibroblast-like cells mixed with ovoid chondrocytes-like cells (Figure 3.7). As this represents the normal cell population of the meniscus, this cell line was deemed appropriate for this experiment.

Quantitatively, a normal growth curve was observed, with no significant difference in cell number between scaffold designs. Qualitatively, no differences were seen histologically with regards to cell distribution on and penetration into the scaffold. Fibrochondrocytes tended to adhere to the collagen sponge portion of scaffolds as opposed to the synthetic fiber portion. This likely occurred because polymer fibers were located too deep in the scaffolds to be reached by migrating cells by 16 days. Blassingame demonstrated through *in vitro* analysis of p(DTD DD) and collagen fibers that fibroblasts will attach to, and proliferate on the polymer fibers as well as the collagen (data not reported). Short-term *in vivo* studies performed by Blassingame also

demonstrated that polymer fibers did not elicit an excessive inflammatory response when implanted subcutaneously.

Mueller et al performed a similar *in vitro* evaluation on collagen sponge matrices<sup>177</sup>. In this study, a more robust cellular layer was observed along the periphery of the sponges as compared to what was observed here. While there were slight differences in matrix composition, this discrepancy was more likely due to the fact that this group initially seeded approximately 9X the number of fibrochondrocytes than we did on a scaffold roughly half the size.

Since fiber-reinforced meniscus scaffolds support the proliferation of fibrochondrocytes, the potential exists to use them as bioreactors for the synthesis of an implant which biologically resembles the normal meniscus closer than a purely synthetic analog. Numerous investigators have explored the effect of growth factors<sup>189, 191, 192, 204-206</sup> and/or mechanical stimulus<sup>188-192</sup> on meniscal cells seeded onto natural or synthetic scaffolds. Future versions of the fiber-reinforced meniscus scaffold may benefit from the addition of these factors to jumpstart the incorporation process and restore joint function.

The results from this experiment suggest that both scaffold designs have the potential to elicit an appropriate biological response *in vivo*. This data supports hypothesis II-5 since fibrochondrocytes exhibited a normal growth curve on both scaffold types. However, hypothesis II-6 was not supported as minimal infiltration into scaffolds was observed for both designs. The data presented does not resolve the issue of whether or not MS1000 scaffolds may be too dense to allow for complete, timely cellular infiltration. Both scaffold designs were therefore advanced to the non-functional *in vivo* evaluation portion of this study.

#### 4.5. Preliminary *In Vivo* Evaluation in Rabbit Model

To determine the effect of polymer fiber density in meniscus scaffolds on the biological response, a non-functional *in vivo* evaluation was performed in a rabbit model.

The following three hypotheses were tested in this portion of Phase III experimentation:

- (III-1) Fiber-reinforced meniscus scaffolds would promote cellular and tissue infiltration into the scaffold,
- (III-2) The collagen and fiber portions of the scaffold would exhibit significant degradation between 4 and 8 weeks post-implantation, and
- (III-3) Fiber-reinforced meniscus scaffolds with a higher fiber content would impeded cellular and tissue ingrowth within the scaffolds, exhibit slower incorporation, and degrade slower than lower fiber content scaffolds.

Because this device is meant to function in the joint, a simple subcutaneous model was deemed inappropriate for this evaluation. Instead, scaffolds were implanted into a surgically created synovial pocket in the knee, exposing them to the harsh enzymatic environment of the joint<sup>179, 180</sup>. In addition, this experimental protocol isolated the biological response from the mechanical stimulation. This caused minimal interference with joint function and as a result allowed the use of both knee joints of each animal in the experimental design.

Analysis of histological slides was completed by a university pathologist on two separate dates. No significant differences were found between MS500 and MS1000 scaffolds. A chronic inflammatory response was observed in all samples, which decreased between 4 to 8 weeks post-implantation. The overall response to the meniscus scaffold is consistent with what is understood about the body's reaction to implanted biomaterials. Briefly, there are six phases which characterize this response

- (1) The injury: This is inherent to the surgical implantation of any device which requires cutting of blood vessels and connective tissue.
- (2) Acute inflammation: This phase tends to last a few days to a week depending on the severity of the injury and involves the migration of leukocytes (typically neutrophils) to the wound site.
- (3) Chronic inflammation: This phase can last weeks to months depending on a series of local and systemic factors and is characterized by the presence of monocytes, macrophages, lymphocytes, as well as the proliferation of blood vessels and connective tissue.
- (4) Granulation Tissue: This phase involves the synthesis and deposition of unorganized connective tissue and, in the case of foreign materials, may also be characterized by the presence of granulomas, which are small collections of loose connective tissue surrounded by a rim of lymphocytes.
- (5) Foreign Body Reaction: This phase involves the presence multi-nucleated giant cells and granulation tissue which function to wall-off the foreign material from the rest of the body.
- (6) Fibrous Encapsulation: In this final phase, the biomaterial is completely separated from the body by a layer of connective tissue which will vary in thickness depending on the surface characteristics of the material.

In this experiment, two modes of biologic response were observed, each corresponding with a specific constituent of the scaffold. A resorption and deposition response was observed around the collagen sponge portion of the scaffold and was indicated primarily with the presence of lymphocytes and eosinophils. This is consistent with the chronic inflammation and granulation tissue phases of the body's reaction to biomaterials<sup>207</sup>. A

foreign-body reaction consisting of histiocytes and multi-nucleated giant cells (MNGCs) was observed in response to the presence of the slowly degrading polymer fibers – which is consistent with an encapsulation response. Both these reactions are similar to what was observed previously with experiments involving collagen and/or polymer-based scaffolds<sup>127, 144, 146, 194, 195, 208</sup>.

The collagen sponge portion of this scaffold is composed of fragmented type I collagen, which has shown to have chemotactic properties essential to the wound healing process<sup>150-154, 207</sup>. The process initiates with the adherence of platelets to cleaved collagen, which in turn release a variety of growth factors<sup>150, 207, 209</sup>. These growth factors facilitate the migration and proliferation of inflammatory cells to the site. Proteolytic enzymes are released, further breaking down the matrix and releasing more chemotactic degradation byproducts – thus continuing the inflammatory phase. In a normal wound, the inflammatory phase typically decreases substantially by the second week<sup>207</sup>. In this experiment, a chronic inflammatory response was still evident at 8 weeks. This may be accounted for by the surplus of fragmented collagen in the scaffold – which is also crosslinked and therefore more difficult to break down. By 8 weeks, there was significantly less collagen matrix observed, which correlated with a significant decrease in inflammation. Based on these results, it can be anticipated that this lymphocytic inflammatory response would continue to decrease as the collagen matrix portion of the scaffold was completely digested and removed.

Despite the chronic inflammation, there was evidence of collagen deposition (blue stained tissues in micrographs, Figures 3.10-3.13). There was no substantial change in neo-tissue formation between 4 and 8 weeks (Figure 3.14). Since the presence of cleaved collagen promotes the presence of collagenases at the wound site<sup>209</sup>, it is logical to assume that any appreciable synthesis and deposition of collagen would occur only after the inflammatory phase has been resolved further.

The other biological response observed in this experiment involved the p(DTD DD) synthetic fibers. In this experiment, there was no significant difference in fiber diameter observed between 4 and 8 weeks, indicating the slow degradation rate of the polymer. Other investigators have also observed the slow resorption rate of this polymer in *in vivo* applications<sup>194</sup>. This slow degradation rate has several implications. First, the polymer will persist for a longer period of time in the knee joint, where neo-tissue formation and organization typically take a long time. Second, the fibers are more likely to promote a foreign-body encapsulation response. This behavior was observed at 4 weeks with the presence of histiocytes and MNGCs which functioned to sequester the polymer from the rest of the body (Figures 3.10-3.13). No significant change was observed in the level of MNGCs between 4 and 8 weeks, suggesting that this foreign-body reaction initiated and stabilized within the first month.

This type of biological response was anticipated based on previous studies involving EDC-crosslinked collagen scaffolds and p(DTD DD) fibers<sup>146, 147, 194</sup>. EDC crosslinked collagen was found previously to be cytocompatible and degradable *in vivo*<sup>146, 147, 160-163</sup>. Furthermore, this class of polymer fiber – while possessing a degradation rate much slower than that of collagen – was also shown to be biocompatible<sup>194</sup>.

It should be noted that the results of this experiment are not necessarily indicative of what will be seen in the functional *in vivo* evaluation. The goal of this study was to determine if scaffolds implanted would elicit an appropriate biological response (i.e. incorporation as opposed to encapsulation). By isolating the scaffold wedge from any physical stimulation, matrix-producing cells may not experience the chemotactic mechanical signals necessary for robust neo-tissue synthesis and organization.

Hypothesis III-1 was supported by this experiment since heavy cellular and tissue infiltration were observed for both scaffold types. However, encapsulation of the individual polymer fibers was also observed. It is unclear how long this response would

have persisted. Hypothesis III-2 was also partially supported as the collagen portion of the scaffold did degrade more over time, while there was no visible evidence of polymer degradation between 4 and 8 weeks. Overall, no significant differences were observed between MS500 and MS1000 scaffolds, thus disproving hypothesis III-3. When initially fabricated, MS1000 were denser than MS500 scaffolds. However, during the implantation process, scaffolds were compressed into the synovial pocket – likely making their overall density comparable *in vivo*, and thus, their elicited reactions. From a biological response perspective, neither scaffold out-performed the other. Therefore, the decision as to which scaffold proceeded to the next phase of evaluation defaulted back to the biomechanical evaluation. Because MS1000 scaffolds possessed a higher strength and stiffness, they were chosen to proceed to the functional *in vivo* evaluation in a sheep model.

#### **4.6. Functional *In Vivo* Evaluation in Ovine Model**

The fiber-reinforced meniscus scaffold was designed for use as a fully functional analog for the tissue after its complete removal. The preceding experiments demonstrate that the device has initial biomechanical properties necessary for function as a load-bearing device in the knee. Its structure and geometry allow for the conversion of axial compressive loads to circumferential tensile loads, as well as distribution of loads on the articular surfaces. Furthermore, the initial tensile strength of MS1000 exceeds that of the normal tissue. *In vitro* and *in vivo* biocompatibility testing demonstrated this device to be safe for implantation and promotes cellular and tissue infiltration. Additionally, in both experiments, no differences were observed in the biological response to MS500 and MS1000 scaffolds. It was therefore decided to pursue the development of the stronger scaffold, MS1000 FRMS, in a large animal model for functional evaluation. The following hypotheses were tested in this experiment:

- (III-5) Fiber-reinforced meniscus scaffolds would promote the cellular and tissue infiltration into the scaffold,
- (III-6) The collagen and fiber portions of the scaffold would exhibit significant degradation between 8 and 16 weeks post-implantation, and
- (III-7) The replacement of a surgically removed medial meniscus with a fiber-reinforced meniscus scaffolds would prevent or delay the onset of degenerative changes in the articular surfaces.

To my knowledge, this is the first study which looks at the development of a meniscus scaffold with substantial fiber-reinforcement which is continuous with the anchor attachments. Several investigators have looked at augmenting amorphous polymer sponges with 1-4 non-resorbable sutures which were extended to make anchor attachments<sup>98, 115-117, 123, 124, 208</sup>. Chiari et al. and Kon et al. embedded a relatively small amount of PLA fibers in their polymer scaffolds and extended them out at the anterior and posterior horns for attachment to the tibia<sup>126, 127</sup>. No tensile mechanical data was presented for any of these studies, suggesting that this was not a priority in the design of these devices. The fiber-reinforced meniscus scaffold in this project separates itself from these scaffolds by providing a robust, circumferential support structure which mimics that of the normal meniscus.

#### **4.6.1. Gross Evaluation**

From a macroscopic perspective, scaffolds had a moderate success rate. At 8 weeks post-implantation, 3 out of 6 implants were intact and structurally sound, 2 were intact with loose posterior horn attachments, and 1 had ruptured at the posterior horn. At 16 weeks only 1 out of 6 of the scaffolds were intact and structurally sound while 2 were intact with loose peripheral attachments, and 3 had ruptured or pulled-out of the

posterior bone tunnel. From gross inspection, all scaffolds were completely infiltrated with tissue and adhered to the synovium. Sheep were typically able to ambulate normally by 1 week post-op, and showed no signs of joint lameness by 16 weeks. While no synovitis was observed in any of the soft tissues, some level of moderate articular cartilage degeneration was observed for most joints.

#### **4.6.2. Surgical Implantation**

The number of failures observed here can be attributed to several factors. First, due to anatomical differences between sheep and human knees, surgical implantation of full meniscal scaffolds was difficult and could not be accomplished arthroscopically. The two main differences between the joint anatomy that affected this experiment the most were: (1) sheep knee joints are much tighter than humans, making the overall surgical implantation of scaffolds difficult, and (2) the ridge of the tibial plateau is much sharper in sheep than humans, increasing the probability of the scaffold getting caught on the outer edge of the tibia during loading. At sacrifice, incorrect placement of the posterior horn bone tunnel was observed for many of the sheep which were operated on early in the study. This is a direct consequence of the surgeon having little room for completing the surgery. Furthermore, the first half of the sheep operated on did not have the periphery of the implant sutured to the synovium – this step was added midway through the study after initial results came back. The sharp ridge of the tibial plateau was thought to be a contributing factor in several instances where loosening of the graft was observed. One possible mechanism for this would be during weight-bearing of the leg in which the scaffold is extruded out of the joint – especially after significant reduction in mechanical strength due to prolonged implantation. The scaffold could have gotten caught on the outside ridge of the tibia and unable to move back into its proper position. A scaffold

which does not rebound back to its normal position can offer little protection to the underlying cartilage.

The surgical procedure used in this experiment was similar to that used by several other researchers studying the use of allografts<sup>43, 69-90</sup>, resorbable, synthetic scaffolds<sup>113-130</sup>, resorbable, collagen-based scaffolds<sup>131-143</sup>, and permanent prostheses<sup>100-111</sup> as meniscal replacements. In these experiments, a non-resorbable suture was attached to the 'horns' of the device and passed through tibial bone tunnels originating at the sites of the anterior and posterior horns of the native meniscus and exiting out the side of the tibia. A peripheral stitch was also incorporated to fix the implant to the peripheral synovium – the most likely source for cells to infiltrate from. Kang et al performed a study in rabbits in which a single suture was passed through the anterior horn of a synthetic scaffold, then through the periphery, and out through the posterior horn to form a continuous fiber reinforcement which anchors at the appropriate sites<sup>98</sup>. This group reported complete regeneration of a meniscus-like tissue after 36 weeks using a cell-seeded PLGA sponge, but failed to report the condition of the underlying cartilage. Using a polyurethane polymer, Klompmaker et al and Tienen et al implanted a porous scaffold in a canine knee. Each scaffold had two sutures passing through the body of the scaffold in the circumferential direction which were extended at the anchor points and used for fixation to the tibial plateau<sup>114-116, 122, 123, 208</sup>. While some success was seen with the regrowth of neo-fibrocartilaginous tissue, by two years significant cartilage degeneration was observed and found to be highly variable between subject<sup>114-116, 122, 123, 208</sup>. Using an ovine model, Chiari et al investigated the use of polycaprolactone as a biomaterial in a full meniscal replacement<sup>126</sup>. These scaffolds were augmented by four PLA fibers which were oriented circumferentially in the body of the implant, and extended out at the horn ends for attachment to the tibial. This group also found degenerative changes in the knee after only 6 weeks implantation.

These three groups come closest to fully addressing the importance of the circumferential support structure necessary for a proper biomechanics of a meniscal replacement. However, in designing their surgical protocol, they provided minimal circumferential reinforcement, instead focusing on the compressive biomechanics of the tissue. And two groups used a non-resorbable suture, which will only be encapsulated in the long term – essentially taking up space which could be used for functioning tissue.

Another tibial bone tunnel surgical method used by other investigators involved simply passing suture through the horns of the device for passage through the tunnel<sup>98, 126, 127</sup>. This surgical protocol may present problems during repetitive compressive loading which will extrude the implant from the joint. While the sutured horns may provide some resistance to this compression, it is likely the sponge structure will eventually tear through the suture after persistent loading. Some successes were found, but in general, degenerative changes could not be completely prevented.

Some investigators simply sutured the horn of the implant to the leftover anterior and posterior horn stumps, and then to the peripheral synovium<sup>43, 72, 76, 78, 210</sup>. This type of implantation procedure is likely to work best for allografts or autografts, where the tissue is typically denser and more resilient than porous sponges.

One significant issue which we encountered – which was also experienced by most other investigators studying full meniscal replacements – was the challenge of preventing immediate weight-bearing of the animal after surgery. During this time, animals were highly medicated, and likely able to take a relatively high level of pain. Coupled with a confusing, stressful environment, erratic and aggressive movements were not uncommon. It is likely that many of the observed failures occurred within the first few days of implantation. For large animals such as dogs or sheep, a cast was simply not a feasible option. Inhibiting movement of the leg by wrapping it was also out of the question since animals tend to chew it off. Kohn et al., Burns et al., and Martinek

et al. presented a possible solution during their respective meniscal replacement studies<sup>142, 210, 211</sup>. After implantation of their device (allograft or collagen meniscus implant), the Achilles tendon of each animal was partially cut. This prevented weight-bearing of the leg for 4-6 weeks. After this time period, animals regained full movement of their legs. This approach may be a viable option for consideration during future evaluations of fiber-reinforced meniscus scaffolds.

#### **4.6.3. Posterior Horn Attachment**

The primary mode of failure in this experiment was pull-out at the peripheral horn attachment. It is likely that moderate-to-high axial loads led to comparable extrusion in the scaffold which concentrated at the posterior side of the tibial plateau. In addition, since the coefficient of friction between the scaffold and articular cartilage is higher than between the normal meniscus and cartilage, high shear forces may have also contributed to pullout. Posterior horn failure was also observed by other investigators during similar evaluations of allografts, synthetic scaffolds, and the CMI<sup>76, 126, 127, 142</sup>. In the evaluation of cryopreserved allografts, two out of three animals had grafts which failed at the posterior horn at 1 month, while one of three failed at 3 months<sup>76</sup>. Chiari et al conducted a study on a synthetic scaffold augmented with PLA fibers in an ovine model and observed that two out of three of the scaffolds have pulled out of the posterior bone tunnel at 6 weeks post-implantation<sup>126</sup>. Kon et al performed another evaluation of a synthetic scaffold in a sheep model and had a failure rate of 5 out of 12 after 16 weeks<sup>127</sup>. It is likely that the implantation procedure used in these studies, as well as ours, placed abnormal stress on the posterior horn of the scaffold. Evaluation of the CMI in an ovine model found abnormal wrinkling of the scaffold at the posterior horn after 3 months<sup>142</sup>. Kelly et al. sought to rectify this issue by attaching the posterior horn of a permanent hydrogel scaffold with the knee flexed, and its anterior horn with the knee in extension

<sup>212</sup>. However, after 1 year post-implantation, all implants had failed with a radial split located in the posterior half of the prosthesis.

Observations from the surgeon in this project found that many of the failed grafts had posterior bone tunnels which were slightly off the attachment site of the native meniscus posterior horn. It may be that exact positioning of tibial bone tunnels – which is difficult in the tight knee joint of the sheep – is critical for the long-term success of the scaffolds.

#### **4.6.4. Scaffold Shrinkage**

No significant shrinkage of was observed in this evaluation, or the previous non-functional *in vivo* in a rabbit. This contrasts with observations from some studies using allograft tissue and the CMI <sup>72, 138, 142, 213, 214</sup>. The common factor in all these experiments is the collagen matrix. In allografts, the tissue may be processed prior to implantation (i.e. frozen, crosslinked, sterilized), leading to general breakdown of the extracellular matrix. The CMI is a highly porous matrix with relatively low structural integrity. The cellular affinity of collagen opens these types of implants up to relatively quick proteolytic degradation. As granulation tissue is deposited, the matrix producing cells may provide a tensioning function, similar to that seen in scar formation on the skin <sup>207</sup>.

The presence of a synthetic material – such as the polymer in the FRMS or the sponge in the numerous synthetic scaffolds – may help mitigate early structural loss. Furthermore, the superior mechanical strength of these polymers may provide some resistance to cellular stresses generated during the wound healing response.

#### **4.6.5. Biomechanics**

Three scaffolds from each time point were evaluated mechanically to determine the tensile properties of neo-tissue for comparison to normal meniscal tissue. Pre-

implanted scaffolds were found to have tensile properties significantly higher than those of the ovine medial meniscus. However, after 8 and 16 weeks post-implantation, a marked decrease was observed. Even considering the wide range of published tensile properties of meniscal tissue, these implants possessed properties significantly lower. And due to the failure of the grafts at the posterior horn, it is unlikely that these properties would have increased appreciably at longer time points.

Few investigators have looked at the tensile strength of their meniscal replacements before or after implantation. In the investigation of autograft tissue from the patellar tendon and perichondrium, Kohn et al. and Bruns et al. measured the tensile properties of the tissue pre- and post-implantation<sup>210, 211</sup>. Both investigators observed a similar sharp decrease in tensile mechanical strength at 3, 6, and 12 months post—implantation. In these time periods, Bruns et al. found no increase in mechanical strength<sup>210</sup>, while Kohn et al. observed a mild increase in strength at 12 months<sup>211</sup>. Kohn et al. used a bone tunnel implantation method similar to that used by us<sup>211</sup>, while Bruns et al. only sutured the tissue to the synovium and meniscal horn stumps<sup>210</sup>. Despite this difference, both observed new, fibrocartilaginous-like tissue growth after 12 months. Unfortunately, both investigators also observed degenerative changes in the underlying articular cartilage by 12 months, although they were less than that of control sheep which had undergone a total meniscectomy without further treatment.

#### **4.6.6. Tissue Incorporation**

Tissue adherence and incorporation was observed grossly and histologically by 8 weeks post-implantation. By 16 weeks post-implantation, a marked increase in the amount of tissue and its organization was found. This corresponded with an overall decrease in lymphocyte inflammation and giant-cell inflammation. However at 16 weeks, multi-nucleated giant cells and histiocytes were the predominant type of

inflammatory cells observed, and were associated primarily with the polymer fiber portion of the scaffold. This inflammatory response is likely dictated by the degradation profiles of the constituents of the scaffold. Lymphocytes were mostly found within the areas formerly occupied by the collagen scaffold. As the collagen portion of the device degrades and is resorbed, logically, the number of lymphocytes would also decrease. The polymer fiber is found to persist in the body, with little resorption observed – as seen by the lack of fiber diameter change between 8 and 16 weeks. This would likely promote a foreign body response, resulting in encapsulation of the polymer<sup>207</sup>. The activity of the encapsulating cells will dictate the extent to which the polymer will continue to degrade.

Comparison of these 8 week results with those from the previous non-functional *in vivo* evaluation reveal a marked increase in the amount of new collagen deposited within the scaffold. Several potential explanations exist for this. First, it is possible that infiltrating cells were synthesizing more collagen in response to the additional mechanical stimulation experienced in a functional evaluation.

It is also likely that the surgical implantation and location of the scaffolds played a key role in the biological response. In the rabbit model, scaffold wedges were placed in a pocket between the muscle and the synovium. This exposed the implant to the synovial fluid, but substantially less severed connective tissue as compared to the sheep model, where the peripheral vascular bed of the entire meniscus was cut during meniscal resection. The increase in collagen deposition in the sheep may simply be a result of there being a larger wound healing response initiated in this experiment.

Due to the complexity of the problem, published results of tissue engineered solutions to meniscal damage tend to be somewhat inconsistent. For example, remodeling of the allografts/autografts into a fibrocartilaginous-like tissue was observed by some investigators<sup>70, 76, 77, 210, 211, 213, 215</sup>, while others found abnormal remodeling<sup>69, 75, 213</sup>. And even in the experiments that were considered a success, alterations in the

biochemistry of the tissue<sup>89</sup> and changes in cellularity were observed<sup>71, 90, 211</sup>. Many of the observed discrepancies may be attributed to differences in experimental design, surgical procedure, model used, tissue storage, tissue processing, rehabilitation, or the analysis of the results.

In the evaluation of their resorbable synthetic scaffolds, Chiari et al. and Kon et al. found that vascularization of the scaffold was only 2/3 complete by 6 weeks in an ovine model<sup>126, 127</sup>. Furthermore, the primary inflammatory cells by 6 weeks observed were giant cells; very few lymphocytes were observed. Tienen et al. observed a similar response to their synthetic scaffold in a canine model<sup>123, 208</sup>. Scattered lymphocytes were observed, but the majority of inflammation as due to a foreign body reaction involving giant cells. The number of giant cells continued to increase from 3 to 6 months post-implantation.

Investigation of collagen-based scaffolds generally showed biological incorporation into the synovial tissues. Cook et al. and Fox et al. demonstrated this with subintestinal submucosa implants for use in a partial meniscectomy model<sup>181, 214</sup>. Results from the evaluation of the Collagen Meniscus Implant, or CMI, are somewhat limited. Most publications are written by the inventors of the device<sup>131, 133-135, 137</sup>, and present positive results for the implant. This raises concerns of bias, which were supported by a recent article in the Wall Street Journal which outlines the unethical methods used by the company backing this device in getting FDA approval<sup>216</sup>. Fortunately, there are several independent groups which have evaluated the CMI and presented what appear to be non-biased results. Martinek et al. studied the effect of cell seeding on the performance of the CMI in an ovine model<sup>142</sup>. Cell seeding was found to have no impact on the outcome. In addition, after three months, resorption of the collagen scaffold was not complete. Reguzzini et al. found that the collagen scaffold persisted at 6 months<sup>136</sup>, and Genovese et al. concluded that by two years post-

implantation, tissue maturation was not complete<sup>138</sup>. One possible reason for this is the use of glutaraldehyde crosslinking. The resistance to enzymatic degradation afforded the implant by this may not be conducive to neo-tissue growth or remodeling into a fibrocartilaginous tissue.

*In vivo* evaluation of the FRMS demonstrated complete vascularization of the tissue by 4 weeks in a rabbit model, and 8 weeks in an ovine model. Furthermore, while giant cells were the primary mode of inflammation observed, there were a significant amount of lymphocytes also observed throughout the device. Both these differences can be attributed to the collagen portion of the scaffold, which likely promotes a more robust biological response than purely synthetic materials. The collagen in the FRMS differs from that which comprises the CMI in crosslinking. In the short-term, the collagen portion of the FRMS scaffold functions as a chemotactic agent which promotes the initial wound healing response. Cells infiltrate the scaffold and quickly degrade the collagenous portion. This may be beneficial in allowing cells to attach to the load-bearing fibers of the scaffold, thus promoting mechanochemical transduction pathways towards the synthesis and organization of an ECM which resembles normal meniscal tissue. The persistence of the collagen in the CMI is likely to cause a prolonged period of inflammation. And due to its lack of structural integrity, it is unlikely this device would offer the same mechanical environment conducive to proper remodeling.

#### **4.6.7. Immunofluorescence Staining**

Immunofluorescence staining revealed several types of collagen present in the infiltrating neo-tissue. The most prevalent were types I, III, and XII. Type III collagen is a molecule which is important in the fibrillogenesis of Type I collagen<sup>184</sup>, and is a common protein found in granulation tissue<sup>207</sup>. Its presence in the neo-tissue is anticipated, especially at these relatively early time points in the wound healing process.

A significant amount of type XII collagen was also detected in this experiment. This production of this type of collagen has been shown to be upregulated in collagenous tissues which undergo high tensile loads<sup>185, 217</sup>. The presence of this protein may be indicative that this scaffold is experiencing some tensile loads *in vivo*. However, inadequate controls were available to make a definitive claim to this.

The presence of type I and II collagen in newly synthesized tissue grown into a synthetic meniscal scaffold has also been observed by Kang et al. and Klompmaker et al.<sup>98, 115, 117</sup>. As these are the two predominant types of collagen matrix within the normal meniscus, this is an anticipated, and encouraging, result. In these long-term evaluations, both investigators observed tissue which was highly organized, resembling that of normal fibrocartilage. Based on this, it is plausible that – in the long term – neo-tissue within the scaffold may be organized into tissue with similar properties of the normal meniscus.

#### **4.6.8. Cartilage Degeneration**

Ultimately, the goal of any tissue engineered solution for meniscal replacement is to provide protection to the underlying articular cartilage of the knee. In this study, mild to moderate cartilage degeneration was found for all subjects. Little difference was observed between the control animals and the experimental animals. This is likely due to the loss of structural integrity of the scaffolds from loosening at the attachments. Furthermore, the time points looked at in this study may be too short to adequately demonstrate any chondroprotective effect.

Proving the effectiveness of a meniscal replacement has been an ongoing challenge which other investigators also contend with. Despite positive results found with regards to cellular infiltration and tissue incorporation and remodeling, many experiments have shown that in the short- and long-term, allografts do not fully protect

underlying cartilage from degenerative changes<sup>43, 69, 71, 78, 89, 94, 211, 213</sup>. In addition, evaluations of synthetic scaffolds have yielded similar negative results<sup>79, 123, 126, 127, 208</sup>. Tienen et al. commented in their evaluation of a polymer sponge scaffold that throughout the study, the health of the cartilage was highly variable between animals, and that by 2 years, no chondroprotective effect was found<sup>123, 208</sup>. And currently, there is inconclusive evidence one way or the other as to the efficacy of the CMI in providing a chondroprotective effect<sup>143</sup>.

Several possible reasons exist for the observed cartilage degeneration in this study, as well as others. First, replicating the precise mechanical, structural, and biochemical properties of the normal meniscus is impractical with a resorbable device. This lends credence to incorporating a period of non-weight bearing immediately after implantation, followed by a period of low weight bearing and range-of-motion exercises. Results from this study also illustrated the necessity of precise and accurate placement and fixation of the device within the knee. Even small deviations may result in abnormal stresses in the knee, which in turn could lead to degenerative changes. Also, scaffold movement, shrinkage, or deformation may result in excessive exposure of the articular cartilage, leading to increased contact stresses and eventual degenerative changes.

Another possible mode of cartilage degeneration may be a result of the surgical intervention involved in repairing or replacing the tissue – or even by the injury itself. Exposure of cartilage to blood has been shown to have a deleterious effect on the tissue<sup>218-221</sup>. As seen in the surgery pictures, FRMSs are soaked in blood during the implantation process. As a sponge, the collagen portion of the scaffold may retain it for a relatively extended period of time, thus promoting its degenerative effect on the articular surfaces.

Overall, the data in this *in vivo* experiment did support Hypothesis III-5. As with the rabbit experiment, Hypothesis III-6 was only partially supported since the collagen portion of the scaffold exhibited significant degradation by 8 and 16 weeks, while there was no visible degradation with the polymer fibers at these timepoints. Due to the lack of a large control group, and the high variation of results seen in the experimental group, hypothesis III-7 could not be proven or disproven.

#### **4.6.9. Limitations**

Several limitations were present in this evaluation. First, anatomical differences between human and sheep knees played a key role in several observed failures. Sheep knees were found to be smaller and tighter than human knees, which made arthroscopic implantation impractical. Despite the open arthrotomy procedure used, it was observed that accurate placement of the posterior horn was difficult to achieve. Misplaced posterior attachments led to abnormal stresses on the implant and its eventual failure.

Post-surgical rehabilitation was difficult with sheep, as well. After surgery, animals were allowed unrestricted cage movement and began weight-bearing within a couple days. Past experience has repeatedly shown that sheep do not respond well to full or partial immobilization of the surgical leg.

Due to cost restraints, a large control group was unable to be used. Multiple control animals are necessary to determine the protective effect of FRMSs on the articular cartilage. Even within time groups, the condition of the cartilage was found to be highly variable. The use of one control animal at 8 and 16 weeks simply did not offer a basis of comparison to objectively grade cartilage degeneration.

#### 4.7. Future Directions

This scaffold did not place much emphasis on the compressive properties of the scaffold during design. Alterations to the collagen portion of the scaffold may be necessary to provide an adequate substrate. For example, the addition of glycosaminoglycans such as chondroitin sulfate, keratin sulfate, or hyaluronic acid (three molecules normally found in the meniscus) may provide viscoelastic resiliency to the scaffold. Furthermore, the addition of type II collagen may be considered due to its role in the normal meniscus. These methods have been explored by other investigators for applications in cartilage engineering<sup>222, 223</sup>.

Collagen and degradable polymers may also be used for the delivery of growth factors<sup>156-159, 167</sup>. This may help jumpstart the wound-healing process, especially the deposition of granular tissue. Ideally, a relatively significant amount of granulation tissue should be available when the patient begins range-of-motion rehabilitation exercise. The addition of low mechanical stimulation – which will slowly increase in intensity – would provide the cells with the necessary stimulation to remodel the ECM into a fibrocartilaginous tissue.

The addition of platelet-rich-plasma (PRP) may also be considered for future designs. This involves a relatively simple, non-invasive procedure which provides the patient with an autologous bolus of platelets, which in turn release growth factors and potentially speed up the wound-healing process<sup>224-226</sup>.

An alternative polymer may also be considered for future designs. P(DTD DD) did not exhibit the anticipated degradability at 16 weeks post-implantation. *In vitro* studies have demonstrated that in an aqueous environment, these polymer fibers will exhibit a significant decrease in strength retention and molecular weight in the short-term (data not reported). A polymer which has similar mechanical properties, but a more definable *in vivo* degradation profile may be beneficial.

From a fabrication standpoint, it may be beneficial to explore alternate methods of fiber reinforcement pattern, as well. Since fiber density was found to have minimal impact on the incorporation of the scaffold into the synovial tissue, the use of fiber bundles composed of varying lengths of fibers may be a viable option. These bundles could be dipped in a collagen dispersion and then molded into a semi-lunar shape such that longer fibers were at the periphery of the implant, and shorter fibers at the inner margin. A radial weave could be used to maintain the shape. Such a design, or variation thereof, may significantly decrease the fabrication time of each construct.

Further functional evaluations in a large animal may benefit with the addition of an immobilizing protocol, similar to that used by other investigators<sup>142, 210, 211</sup>. By inhibiting the weight-bearing of the animals for 4-6 weeks post-op, the scaffold is provided the opportunity to become fully infiltrated with matrix-producing cells and unorganized granulation tissue necessary for full wound healing.

More in-depth evaluation of the underlying cartilage is also required to adequately assess the performance of the scaffold. This would require a larger control group than used in this study. Gross comparison of the articular surfaces may also offer a better overview of the effect of FRMSs. The use of India Ink has been shown to be used in identifying areas of damaged or worn articular cartilage. This method may provide a way to identify and quantify the areas of the cartilage undergoing high stress.

## **5. CONCLUSION**

This dissertation described the development and evaluation of a novel polymer fiber-reinforced collagen scaffold for use as a meniscal replacement. To test the device's feasibility as a meniscus scaffold, this study was broken down into three phases: Phase I: Preliminary development of fiber reinforced meniscus scaffolds (FRMSs); Phase II: *In vitro* characterization of FRMSs; and Phase III: *In vivo* characterization of FRMSs. In Phase I, one type of scaffold design was isolated based on preliminary mechanical testing data as well as data on resorbable devices generated in our lab. Two variations of this design, MS500 and MS1000, were chosen for further evaluation in Phases II and III.

In Phase II of this study, MS500 and MS1000 scaffolds underwent a battery of mechanical evaluations to determine their ability to mimic the biomechanical function of the normal meniscus. Overall, MS1000 scaffolds exhibited superior handleability as compared to MS500 scaffolds. The first hypothesis tested in this phase was that both scaffolds would convert a portion of an applied axial compressive load to a circumferential tensile load. This was supported by the data presented in this study. For the compressive load ranges explored, the tensile load measured for MS1000 scaffolds was approximately twice that of the load measured for MS500 scaffolds. The second hypothesis tested was that fiber-reinforced meniscus scaffolds would cause an increase in contact area and overall pressure distribution on the tibial plateau after loading. This was also supported by the data. When compared against loading in the presence of no scaffold and a 100% collagen scaffold, fiber-reinforced scaffolds showed a significant increase in contact area and overall pressure distribution. No difference was found between designs for any loading condition. The third hypothesis was that scaffolds would possess circumferential tensile properties on par with those of the normal ovine

meniscus. Comparison of experimental results with published data showed that both scaffold designs possessed a strength and stiffness within the range of the normal meniscus, with MS500 scaffolds near the lower end of the published values, and MS1000 scaffolds near the upper. From a biomechanical perspective, MS1000 scaffolds were found to be the superior design.

An *in vitro* cytocompatibility evaluation was also performed in this phase of the study. Harvested rabbit fibrocondrocytes were seeded onto scaffolds and then cultured for time points up to 16 days. It was hypothesized that these cells would exhibit a normal growth curve and that cells would infiltrate further into MS500 scaffolds than MS1000. Data from this experiment showed that fibrochondrocytes did have a normal growth curve when seeded onto scaffolds. However, for both designs, minimal cellular infiltration was observed histologically. Cells were predominantly located at the surface of the scaffold where they then proliferated.

In Phase III of this experiment, the *in vivo* biological response to scaffolds was evaluated. In the first experiment, MS500 and MS1000 scaffolds were compared in a non-functional capacity in a rabbit model. It was first hypothesized that scaffolds would promote cellular and tissue infiltration into the scaffold. This was supported by histological observations as heavy cellular and tissue infiltration was observed after 4 and 8 weeks. It was also hypothesized that scaffolds would significantly degrade between 4 and 8 weeks post-implantation. This was partially supported by the data. For both scaffolds, significant degradation of the collagen sponge portion of the scaffold was observed by 4 weeks post-implantation, which increased by 8 weeks. However, for both designs, no significant degradation of the polymer fibers was observed histologically between 4 and 8 weeks post-implantation. It was also hypothesized that fiber-reinforced meniscus scaffolds with a higher fiber content would impede cellular and tissue ingrowth, exhibit slower incorporation, and degrade slower than lower fiber content scaffolds. This

was not supported by the data. No differences were observed histologically between the biological response to MS500 and MS1000 scaffolds.

Since there was no observed difference in the *in vitro* or *in vivo* biological response to MS500 or MS1000 scaffolds, the design choice for the further evaluation in a large animal model was made based on the mechanical data from Phase II experimentation. MS1000 scaffolds were chosen as they mechanically outperformed MS500. MS1000 scaffolds were evaluated in an ovine model to determine the potential utility of this device as a functional implant to replace a surgically resected meniscus. It was again hypothesized that scaffolds would promote cellular and tissue infiltration and exhibit significant degradation between 8 and 16 weeks. Gross observation and histological analysis showed the presence of heavy cellular and neo-tissue formation within the scaffold. Trichrome stained slides revealed significantly more neo-tissue formation than observed in the previous rabbit evaluation. As with the evaluation in the rabbit, little evidence of polymer fiber degradation was observed histologically, while significant degradation of the collagen portion of the scaffold was observed at 8 weeks. The last hypothesis tested was that replacement of a surgically resected medial meniscus with a MS1000 meniscus scaffold would prevent or delay the onset of degenerative changes in the articular surfaces. This hypothesis could not be fully supported or refuted. Varied levels of articular cartilage degeneration were observed in all animals, and did not appear to depend on the implantation time point. Additionally, the lack of a complete control group for each time point prevented the collection of comparative data. Further evaluation at longer time points, with a complete control group is necessary to fully address this hypothesis.

The long term goal of this research is to develop a resorbable scaffold which can be used after a subtotal or total meniscectomy to induce neo-fibrocartilaginous tissue growth while preventing or delaying the onset of degenerative changes of the articular

cartilage. Such a device would fill a large void in treatment alternatives for patients suffering from severe meniscal deficiency. The results of this dissertation demonstrate proof of principal for a fiber-reinforced meniscus scaffold. This device was found to be safe for implantation and incorporated well within the surrounding tissues. Furthermore, it maintained its shape, geometry, and a level of structural integrity necessary for continued function as a load-bearing device. As a prototype, it shows promise as a medical device which can alleviate the pain and damage associated with a total meniscectomy. However, further optimization of the design is required before it can be considered for clinical use.

## **6. References**

1. Arnoczky, S.P., *Gross and Vascular Anatomy of the Meniscus and Its Role in Meniscal Healing, Regeneration, and Remodeling*, in *Knee Meniscus: Basic and Clinical Foundations*, V.C. Mow, S.P. Arnoczky, and D.W. Jackson, Editors. 1992, Raven Press: New York. p. 1-14.
2. Mow, V., et al., *Structure and Function Relationships of the Menisci of the Knee*, in *Knee Meniscus: Basic and Clinical Foundations*, V. Mow, S. Arnoczky, and D. Jackson, Editors. 1992, Raven Press: New York. p. 37-57.
3. Fithian, D.C., M.A. Kelly, and V.C. Mow, *Material properties and structure-function relationships in the menisci*. Clin Orthop, 1990(252): p. 19-31.
4. Ahmed, A., *The load-bearing role of knee menisci*, in *Knee Meniscus: Basic and Clinical Foundations.*, V. Mow, S. Arnoczky, and D. Jackson, Editors. 1992, Raven: New York, NY. p. 59-73.
5. Bylski-Austrow, D., et al., *Knee joint contact pressure decreases after chronic meniscectomy relative to acutely meniscectomized joints: A mechanical study in the goat*. J of Ortho Res, 1993. **11**: p. 796-804.
6. Chatain, F., et al., *A comparative study of medial versus lateral arthroscopic partial meniscectomy on stable knees: 10-year minimum follow-up*. Arthroscopy, 2003. **19**(8): p. 842-9.
7. Cox, J.S., et al., *The degenerative effects of partial and total resection of the medial meniscus in dogs' knees*. Clin Orthop, 1975(109): p. 178-83.
8. Fairbank, T., *Knee joint changes after meniscectomy*. J Bone Joint Surg (Br), 1948. **30**: p. 664-70.
9. Fukubayashi, T. and H. Kurosawa, *The contact area and pressure distribution pattern of the knee. A study of normal and osteoarthrotic knee joints*. Acta Orthop Scand, 1980. **51**(6): p. 871-9.
10. Hoser, C., C. Brown, and J. Bartlett. *Ten year follow-up of arthroscopic partial lateral meniscectomy*. in *2nd World Congress on Sports Trauma/AOSSM 22nd Annual Meeting*. 1996. Lake Buena Vista, FL.
11. Jaureguito, J.W., et al., *The effects of arthroscopic partial lateral meniscectomy in an otherwise normal knee: a retrospective review of functional, clinical, and radiographic results*. Arthroscopy, 1995. **11**(1): p. 29-36.
12. King, D., *The function of semilunar cartilages*. J Bone Joint Surg, 1936. **18**: p. 1069-76.
13. Krause, W., et al., *Mechanical changes in the knee after meniscectomy*. J Bone Joint Surg, 1976. **58**(A): p. 599-604.
14. Kurosawa, H., T. Fukubayashi, and H. Nakajima, *Load-bearing mode of the knee joint: physical behavior of the knee joint with or without menisci*. Clin Orthop Relat Res, 1980(149): p. 283-90.
15. Renstrom, P. and R.J. Johnson, *Anatomy and biomechanics of the menisci*. Clin Sports Med, 1990. **9**(3): p. 523-38.
16. Rockborn, P. and K. Messner, *Long-term results of meniscus repair and meniscectomy: a 13-year functional and radiographic follow-up study*. Knee Surg Sports Traumatol Arthrosc, 2000. **8**(1): p. 2-10.
17. Rockborn, P. and J. Gillquist, *Outcome of arthroscopic meniscectomy. A 13-year physical and radiographic follow-up of 43 patients under 23 years of age*. Acta Orthop Scand, 1995. **66**(2): p. 113-7.
18. Shrive, N., J. O'Connor, and J. Goodfellow, *Load-bearing in the knee joint*. Clin Orthop Rel Res, 1978. **131**: p. 279-87.

19. Walker, P. and M. Erkman, *Role of the menisci in force transmission across the knee*. Clin Orthop, 1975. **109**: p. 184-92.
20. Shrive, N.G., J.J. O'Connor, and J.W. Goodfellow, *Load-bearing in the knee joint*. Clin Orthop Relat Res, 1978(131): p. 279-87.
21. Seedhom, B. and D. Hargreaves, *Transmission of the load in the knee joint with special reference to the role of menisci*. Eng med, 1979. **8**: p. 220-8.
22. Heller, L. and J. Langman, *The Menisco-Femoral Ligaments of the Human Knee*. J Bone Joint Surg Br, 1964. **46**: p. 307-13.
23. Kaplan, E.B., *The lateral meniscofemoral ligament of the knee joint*. Bull Hosp Joint Dis, 1956. **17**(2): p. 176-82.
24. Arnoczky, S.P. and R.F. Warren, *Microvasculature of the human meniscus*. Am J Sports Med, 1982. **10**(2): p. 90-5.
25. Arnoczky, S.P., R.F. Warren, and N. Kaplan, *Meniscal remodeling following partial meniscectomy--an experimental study in the dog*. Arthroscopy, 1985. **1**(4): p. 247-52.
26. Arnoczky, S.P. and R.F. Warren, *The microvasculature of the meniscus and its response to injury. An experimental study in the dog*. Am J Sports Med, 1983. **11**(3): p. 131-41.
27. King, D., *The healing of semilunar cartilages*. Clin Orthop Relat Res, 1936(252): p. 4-7.
28. Proctor, C.S., et al., *Material properties of the normal medial bovine meniscus*. J Orthop Res, 1989. **7**(6): p. 771-82.
29. Ingman, A.M., P. Ghosh, and T.K. Taylor, *Variation of collagenous and non-collagenous proteins of human knee joint menisci with age and degeneration*. Gerontologia, 1974. **20**(4): p. 212-23.
30. Eyre, D.R. and J.J. Wu, *Collagen of fibrocartilage: a distinctive molecular phenotype in bovine meniscus*. FEBS Lett, 1983. **158**(2): p. 265-70.
31. Adams, M.E. and Y.A. Ho, *Localization of glycosaminoglycans in human and canine menisci and their attachments*. Connect Tissue Res, 1987. **16**(3): p. 269-79.
32. Adams, M.E. and D.W.L. Hukins, *The Extracellular Matrix of the Meniscus*, in *Knee Meniscus: Basic and Clinical Foundations*, V.C. Mow, S.P. Arnoczky, and D.W. Jackson, Editors. 1992, Raven Press: New York. p. 15-28.
33. Adams, M.E. and H. Muir, *The glycosaminoglycans of canine menisci*. Biochem J, 1981. **197**(2): p. 385-9.
34. Skaggs, D.L., W.H. Warden, and V.C. Mow, *Radial tie fibers influence the tensile properties of the bovine medial meniscus*. J Orthop Res, 1994. **12**(2): p. 176-85.
35. McNicol, D. and P.J. Roughley, *Extraction and characterization of proteoglycan from human meniscus*. Biochem J, 1980. **185**(3): p. 705-13.
36. Hardingham, T., *Proteoglycans: their structure, interactions and molecular organization in cartilage*. Biochem Soc Trans, 1981. **9**(6): p. 489-97.
37. Hardingham, T.E., et al., *Viscoelastic properties of proteoglycan solutions with varying proportions present as aggregates*. J Orthop Res, 1987. **5**(1): p. 36-46.
38. Arnoczky, S.P., et al., *Meniscus*, in *Injury and Repair of Musculoskeletal Soft Tissue*, S.L. Woo and J.A. Buckwalter, Editors. 1988, American Academy of Orthopaedic Surgeons: Park Ridge. p. 485-537.
39. McDevitt, C.A., R.R. Miller, and K.P. Spindler, *The Cells and Cell Matrix Interactions of the Meniscus*, in *Knee Meniscus: Basic and Clinical Foundations*, V.C. Mow, S.P. Arnoczky, and D.W. Jackson, Editors. 1992, Raven Press: New York. p. 29-36.

40. Moon, M.S., J.M. Kim, and I.Y. Ok, *The normal and regenerated meniscus in rabbits. Morphologic and histologic studies.* Clin Orthop Relat Res, 1984(182): p. 264-9.
41. Davies, D., *The biology of joints*, in *Textbook of the Rheumatic Diseases*, C. WSC, Editor. 1969, London and Edinburgh: Livingston. p. 40-86.
42. Ghadially, F.N., et al., *Ultrastructure of rabbit semilunar cartilages.* J Anat, 1978. **125**(3): p. 499-517.
43. Szomor, Z.L., et al., *The protective effects of meniscal transplantation on cartilage. An experimental study in sheep.* J Bone Joint Surg Am, 2000. **82**(1): p. 80-8.
44. Gao, J., G. Oqvist, and K. Messner, *The attachments of the rabbit medial meniscus. A morphological investigation using image analysis and immunohistochemistry.* J Anat, 1994. **185 ( Pt 3)**: p. 663-7.
45. Johnson, D.L., et al., *Insertion-site anatomy of the human menisci: gross, arthroscopic, and topographical anatomy as a basis for meniscal transplantation.* Arthroscopy, 1995. **11**(4): p. 386-94.
46. Setton, L.A., et al., *Biomechanical factors in tissue engineered meniscal repair.* Clin Orthop, 1999(367 Suppl): p. S254-72.
47. McBride, I.D. and J.G. Reid, *Biomechanical considerations of the menisci of the knee.* Can J Sport Sci, 1988. **13**(4): p. 175-87.
48. Aspden, R.M., Y.E. Yarker, and D.W. Hukins, *Collagen orientations in the meniscus of the knee joint.* J Anat, 1985. **140 ( Pt 3)**: p. 371-80.
49. Bullough, P.G., et al., *The strength of the menisci of the knee as it relates to their fine structure.* J Bone Joint Surg Br, 1970. **52**(3): p. 564-7.
50. Kelly, M.A., et al., *Structure and function of the meniscus: basic and clinical implications*, in *Biomechanics of diarthrodial joints*, V.C. Mow, A. Ratcliffe, and S.L. Woo, Editors. 1990, Springer-Verlag: New York. p. 191-211.
51. Spilker, R.L. and P.S. Donzelli, *A Biphasic Finite Element Model of the Meniscus for Stress-Strain Analysis*, in *Knee Meniscus: Basic and Clinical Foundations*, V. Mow, S. Arnoczky, and D.W. Jackson, Editors. 1992, Raven Press: New York.
52. Spilker, R.L., P.S. Donzelli, and V.C. Mow, *A transversely isotropic biphasic finite element model of the meniscus.* J Biomech, 1992. **25**(9): p. 1027-45.
53. Zhu, W., K.Y. Chern, and V.C. Mow, *Anisotropic viscoelastic shear properties of bovine meniscus.* Clin Orthop Relat Res, 1994(306): p. 34-45.
54. DeHaven, K., *Meniscectomy Versus Repair: Clinical Experience*, in *Knee Meniscus: Basic and Clinical Foundations*, V.C. Mow, S.P. Arnoczky, and D.W. Jackson, Editors. 1992, Raven Press: New York. p. 131-139.
55. Baratz, M., F. Fu, and R. Mengato, *Meniscal tears: The effect of meniscectomy and of repair on intraarticular contact areas and stress in the human knee.* Am J Sports Med, 1986. **14**(270-5).
56. Andersson-Molina, H., H. Karlsson, and P. Rockborn, *Arthroscopic partial and total meniscectomy: A long-term follow-up study with matched controls.* Arthroscopy, 2002. **18**(2): p. 183-9.
57. Brown, T.D. and D.T. Shaw, *In vitro contact stress distribution on the femoral condyles.* J Orthop Res, 1984. **2**(2): p. 190-9.
58. Jorgensen, U., et al., *Long-term follow-up of meniscectomy in athletes. A prospective longitudinal study.* J Bone Joint Surg Br, 1987. **69**(1): p. 80-3.
59. McNicholas, M.J., et al., *Total meniscectomy in adolescence. A thirty-year follow-up.* J Bone Joint Surg Br, 2000. **82**(2): p. 217-21.

60. Butler, D.L., et al., *Functional tissue engineering parameters toward designing repair and replacement strategies*. Clin Orthop Relat Res, 2004(427 Suppl): p. S190-9.
61. Butler, D.L., S.A. Goldstein, and F. Guilak, *Functional tissue engineering: the role of biomechanics*. J Biomech Eng, 2000. **122**(6): p. 570-5.
62. Woo, S.L., et al., *Biomechanics of knee ligaments: injury, healing, and repair*. J Biomech, 2006. **39**(1): p. 1-20.
63. Huard, J., et al., *Gene therapy and tissue engineering for sports medicine*. J Gene Med, 2003. **5**(2): p. 93-108.
64. Cancedda, R., et al., *Tissue engineering and cell therapy of cartilage and bone*. Matrix Biol, 2003. **22**(1): p. 81-91.
65. Feng, Z., et al., *Investigation on the mechanical properties of contracted collagen gels as a scaffold for tissue engineering*. Artif Organs, 2003. **27**(1): p. 84-91.
66. Garvin, J., et al., *Novel system for engineering bioartificial tendons and application of mechanical load*. Tissue Eng, 2003. **9**(5): p. 967-79.
67. Lamberti, P.M. and F.H. Wezeman, *Biologic behavior of an in vitro hydrated collagen gel-human tenocyte tendon model*. Clin Orthop Relat Res, 2002(397): p. 414-23.
68. Noth, U., et al., *Anterior cruciate ligament constructs fabricated from human mesenchymal stem cells in a collagen type I hydrogel*. Cytotherapy, 2005. **7**(5): p. 447-55.
69. Mora, G., et al., *Articular cartilage degeneration after frozen meniscus and Achilles tendon allograft transplantation: experimental study in sheep*. Arthroscopy, 2003. **19**(8): p. 833-41.
70. Shibuya, S., *Meniscus transplantation using a cryopreserved allograft. Histological and ultrastructural study of the transplanted meniscus*. J Orthop Sci, 1999. **4**(2): p. 135-41.
71. Rath, E., et al., *Meniscal allograft transplantation. Two- to eight-year results*. Am J Sports Med, 2001. **29**(4): p. 410-4.
72. Wirth, C.J., et al., *Long-term results of meniscal allograft transplantation*. Am J Sports Med, 2002. **30**(2): p. 174-81.
73. Martinek, V., et al., *Genetic engineering of meniscal allografts*. Tissue Eng, 2002. **8**(1): p. 107-17.
74. Jackson, D.W., J. Whelan, and T.M. Simon, *Cell survival after transplantation of fresh meniscal allografts. DNA probe analysis in a goat model*. Am J Sports Med, 1993. **21**(4): p. 540-50.
75. de Boer, H.H. and J. Koudstaal, *Failed meniscus transplantation. A report of three cases*. Clin Orthop Relat Res, 1994(306): p. 155-62.
76. Arnoczky, S.P., R.F. Warren, and C.A. McDevitt, *Meniscal replacement using a cryopreserved allograft. An experimental study in the dog*. Clin Orthop Relat Res, 1990(252): p. 121-8.
77. Jackson, D.W., et al., *Meniscal transplantation using fresh and cryopreserved allografts. An experimental study in goats*. Am J Sports Med, 1992. **20**(6): p. 644-56.
78. Elliott, D.M., et al., *Joint degeneration following meniscal allograft transplantation in a canine model: mechanical properties and semiquantitative histology of articular cartilage*. Knee Surg Sports Traumatol Arthrosc, 2002. **10**(2): p. 109-18.
79. Rijk, P.C., *Meniscal allograft transplantation--part II: alternative treatments, effects on articular cartilage, and future directions*. Arthroscopy, 2004. **20**(8): p. 851-9.

80. Rijk, P.C., *Meniscal allograft transplantation--part I: background, results, graft selection and preservation, and surgical considerations*. *Arthroscopy*, 2004. **20**(7): p. 728-43.
81. Peters, G. and C.J. Wirth, *The current state of meniscal allograft transplantation and replacement*. *Knee*, 2003. **10**(1): p. 19-31.
82. Rodeo, S.A., *Meniscal allografts--where do we stand?* *Am J Sports Med*, 2001. **29**(2): p. 246-61.
83. Noyes, F.R., S.D. Barber-Westin, and M. Rankin, *Meniscal transplantation in symptomatic patients less than fifty years old*. *J Bone Joint Surg Am*, 2004. **86-A**(7): p. 1392-404.
84. Sgaglione, N.A., et al., *Current concepts in meniscus surgery: resection to replacement*. *Arthroscopy*, 2003. **19 Suppl 1**: p. 161-88.
85. Cameron, J.C. and S. Saha, *Meniscal allograft transplantation for unicompartmental arthritis of the knee*. *Clin Orthop Relat Res*, 1997(337): p. 164-71.
86. Chen, M.I., T.P. Branch, and W.C. Hutton, *Is it important to secure the horns during lateral meniscal transplantation? A cadaveric study*. *Arthroscopy*, 1996. **12**(2): p. 174-81.
87. van Arkel, E.R. and H.H. de Boer, *Human meniscal transplantation. Preliminary results at 2 to 5-year follow-up*. *J Bone Joint Surg Br*, 1995. **77**(4): p. 589-95.
88. Johnson, D.L. and D. Bealle, *Meniscal allograft transplantation*. *Clin Sports Med*, 1999. **18**(1): p. 93-108.
89. Fabbriani, C., et al., *Meniscal allografts: cryopreservation vs deep-frozen technique. An experimental study in goats*. *Knee Surg Sports Traumatol Arthrosc*, 1997. **5**(2): p. 124-34.
90. Arnoczky, S.P., et al., *The effect of cryopreservation on canine menisci: a biochemical, morphologic, and biomechanical evaluation*. *J Orthop Res*, 1988. **6**(1): p. 1-12.
91. Reckers, L.J., D.J. Fagundes, and M. Cohen, *The ineffectiveness of fibrin glue and cyanoacrylate on fixation of meniscus transplants in rabbits*. *Knee*, 2009.
92. Sohn, D.H. and A.P. Toth, *Meniscus transplantation: current concepts*. *J Knee Surg*, 2008. **21**(2): p. 163-72.
93. Lee, D.H., et al., *Evaluation of meniscus allograft transplantation with serial magnetic resonance imaging during the first postoperative year: focus on graft extrusion*. *Arthroscopy*, 2008. **24**(10): p. 1115-21.
94. Verdonk, P.C., et al., *Transplantation of viable meniscal allograft. Surgical technique*. *J Bone Joint Surg Am*, 2006. **88 Suppl 1 Pt 1**: p. 109-18.
95. Dienst, M., et al., *Effect of lateral meniscal allograft sizing on contact mechanics of the lateral tibial plateau: an experimental study in human cadaveric knee joints*. *Am J Sports Med*, 2007. **35**(1): p. 34-42.
96. Rodeo, S.A., et al., *Histological analysis of human meniscal allografts. A preliminary report*. *J Bone Joint Surg Am*, 2000. **82-A**(8): p. 1071-82.
97. Verdonk, P.C., et al., *Transplantation of viable meniscal allograft. Survivorship analysis and clinical outcome of one hundred cases*. *J Bone Joint Surg Am*, 2005. **87**(4): p. 715-24.
98. Kang, S.W., et al., *Regeneration of whole meniscus using meniscal cells and polymer scaffolds in a rabbit total meniscectomy model*. *J Biomed Mater Res A*, 2006. **78**(3): p. 659-71.
99. McDermott, I.D., et al., *The effects of lateral meniscal allograft transplantation techniques on tibio-femoral contact pressures*. *Knee Surg Sports Traumatol Arthrosc*, 2008. **16**(6): p. 553-60.

100. Toyonaga, T., N. Uezaki, and H. Chikama, *Substitute meniscus of Teflon-net for the knee joint of dogs*. Clin Orthop Relat Res, 1983(179): p. 291-7.
101. Messner, K. and J. Gillquist, *Prosthetic replacement of the rabbit medial meniscus*. J Biomed Mater Res, 1993. **27**(9): p. 1165-73.
102. Messner, K., *The concept of a permanent synthetic meniscus prosthesis: a critical discussion after 5 years of experimental investigations using Dacron and Teflon implants*. Biomaterials, 1994. **15**(4): p. 243-50.
103. Sommerlath, K. and J. Gillquist, *The effect of a meniscal prosthesis on knee biomechanics and cartilage. An experimental study in rabbits*. Am J Sports Med, 1992. **20**(1): p. 73-81.
104. Wood, D.J., R.J. Minns, and A. Strover, *Replacement of the rabbit medial meniscus with a polyester-carbon fibre bioprosthesis*. Biomaterials, 1990. **11**(1): p. 13-6.
105. Kobayashi, M., J. Toguchida, and M. Oka, *Preliminary study of polyvinyl alcohol-hydrogel (PVA-H) artificial meniscus*. Biomaterials, 2003. **24**(4): p. 639-47.
106. Kobayashi, M., *A study of polyvinyl alcohol-hydrogel (PVA-H) artificial meniscus in vivo*. Biomed Mater Eng, 2004. **14**(4): p. 505-15.
107. Kobayashi, M., Y.S. Chang, and M. Oka, *A two year in vivo study of polyvinyl alcohol-hydrogel (PVA-H) artificial meniscus*. Biomaterials, 2005. **26**(16): p. 3243-8.
108. Kobayashi, M., J. Toguchida, and M. Oka, *Development of an artificial meniscus using polyvinyl alcohol-hydrogel for early return to, and continuance of, athletic life in sportspersons with severe meniscus injury. I: mechanical evaluation*. Knee, 2003. **10**(1): p. 47-51.
109. Veth, R.P., et al., *Experimental meniscal lesions reconstructed with a carbon fiber-polyurethane-poly(L-lactide) graft*. Clin Orthop Relat Res, 1986(202): p. 286-93.
110. Veth, R.P., et al., *An experimental study of reconstructive procedures in lesions of the meniscus. Use of synovial flaps and carbon fiber implants for artificially made lesions in the meniscus of the rabbit*. Clin Orthop Relat Res, 1983(181): p. 250-4.
111. Veth, R.P., et al., *Repair of the meniscus. An experimental investigation in rabbits*. Clin Orthop Relat Res, 1983(175): p. 258-62.
112. Arnoczky, S.P., *Building a meniscus. Biologic considerations*. Clin Orthop, 1999(367 Suppl): p. S244-53.
113. Klompaker, J., et al., *Porous polymer implant for repair of meniscal lesions: a preliminary study in dogs*. Biomaterials, 1991. **12**(9): p. 810-6.
114. Klompaker, J., et al., *Porous implants for knee joint meniscus reconstruction: a preliminary study on the role of pore sizes in ingrowth and differentiation of fibrocartilage*. Clin Mater, 1993. **14**(1): p. 1-11.
115. Klompaker, J., et al., *Meniscal repair by fibrocartilage? An experimental study in the dog*. J Orthop Res, 1992. **10**(3): p. 359-70.
116. Klompaker, J., et al., *Meniscal replacement using a porous polymer prosthesis: a preliminary study in the dog*. Biomaterials, 1996. **17**(12): p. 1169-75.
117. Klompaker, J., et al., *Meniscal repair by fibrocartilage in the dog: characterization of the repair tissue and the role of vascularity*. Biomaterials, 1996. **17**(17): p. 1685-91.
118. de Groot, J.H., et al., *Use of porous polyurethanes for meniscal reconstruction and meniscal prostheses*. Biomaterials, 1996. **17**(2): p. 163-73.
119. de Groot, J.H., et al., *Meniscal tissue regeneration in porous 50/50 copoly(L-lactide/epsilon-caprolactone) implants*. Biomaterials, 1997. **18**(8): p. 613-22.

120. Welsing, R.T., et al., *Effect on tissue differentiation and articular cartilage degradation of a polymer meniscus implant: A 2-year follow-up study in dogs*. Am J Sports Med, 2008. **36**(10): p. 1978-89.
121. van Tienen, T.G., et al., *Tissue ingrowth and degradation of two biodegradable porous polymers with different porosities and pore sizes*. Biomaterials, 2002. **23**(8): p. 1731-8.
122. Tienen, T.G., et al., *A porous polymer scaffold for meniscal lesion repair--a study in dogs*. Biomaterials, 2003. **24**(14): p. 2541-8.
123. Tienen, T.G., et al., *Replacement of the Knee Meniscus by a Porous Polymer Implant: A Study in Dogs*. Am J Sports Med, 2005.
124. Tienen, T.G., et al., *Meniscal replacement in dogs. Tissue regeneration in two different materials with similar properties*. J Biomed Mater Res B Appl Biomater, 2005.
125. van Tienen, T.G., G. Hannink, and P. Buma, *Meniscus replacement using synthetic materials*. Clin Sports Med, 2009. **28**(1): p. 143-56.
126. Chiari, C., et al., *A tissue engineering approach to meniscus regeneration in a sheep model*. Osteoarthritis Cartilage, 2006. **14**(10): p. 1056-65.
127. Kon, E., et al., *Tissue engineering for total meniscal substitution: animal study in sheep model*. Tissue Eng Part A, 2008. **14**(6): p. 1067-80.
128. Kang, S.W., et al., *Regeneration of whole meniscus using meniscal cells and polymer scaffolds in a rabbit total meniscectomy model*. J Biomed Mater Res A, 2006. **77**(4): p. 659-71.
129. Baker, B.M. and R.L. Mauck, *The effect of nanofiber alignment on the maturation of engineered meniscus constructs*. Biomaterials, 2007. **28**(11): p. 1967-77.
130. Aufderheide, A.C. and K.A. Athanasiou, *Comparison of scaffolds and culture conditions for tissue engineering of the knee meniscus*. Tissue Eng, 2005. **11**(7-8): p. 1095-104.
131. Stone, K.R., et al., *Meniscal regeneration with copolymeric collagen scaffolds. In vitro and in vivo studies evaluated clinically, histologically, and biochemically*. Am J Sports Med, 1992. **20**(2): p. 104-11.
132. Stone, K.R., et al., *Future directions. Collagen-based prostheses for meniscal regeneration*. Clin Orthop Relat Res, 1990(252): p. 129-35.
133. Stone, K.R., et al., *Regeneration of meniscal cartilage with use of a collagen scaffold. Analysis of preliminary data*. J Bone Joint Surg Am, 1997. **79**(12): p. 1770-7.
134. Stone, K., *Meniscal replacement*. Clin Sports med, 1996. **15**: p. 557-71.
135. Rodkey, W.G., J.R. Steadman, and S.T. Li, *A clinical study of collagen meniscus implants to restore the injured meniscus*. Clin Orthop Relat Res, 1999(367 Suppl): p. S281-92.
136. Reguzzoni, M., et al., *Histology and ultrastructure of a tissue-engineered collagen meniscus before and after implantation*. J Biomed Mater Res B Appl Biomater, 2005. **74**(2): p. 808-16.
137. Steadman, J.R. and W.G. Rodkey, *Tissue-engineered collagen meniscus implants: 5- to 6-year feasibility study results*. Arthroscopy, 2005. **21**(5): p. 515-25.
138. Genovese, E., et al., *Follow-up of collagen meniscus implants by MRI*. Radiol Med, 2007. **112**(7): p. 1036-48.
139. Zaffagnini, S., et al., *Arthroscopic collagen meniscus implant results at 6 to 8 years follow up*. Knee Surg Sports Traumatol Arthrosc, 2007. **15**(2): p. 175-83.
140. Buma, P., T. van Tienen, and R. Veth, *The collagen meniscus implant*. Expert Rev Med Devices, 2007. **4**(4): p. 507-16.

141. Han, B., et al., *Proanthocyanidin: a natural crosslinking reagent for stabilizing collagen matrices*. J Biomed Mater Res, 2003. **65A**(1): p. 118-24.
142. Martinek, V., et al., *Second generation of meniscus transplantation: in-vivo study with tissue engineered meniscus replacement*. Arch Orthop Trauma Surg, 2005: p. 1-7.
143. Buma, P., et al., *Tissue engineering of the meniscus*. Biomaterials, 2004. **25**(9): p. 1523-32.
144. Bourke, S.L., J. Kohn, and M.G. Dunn, *Preliminary development of a novel resorbable synthetic polymer fiber scaffold for anterior cruciate ligament reconstruction*. Tissue Eng, 2004. **10**(1-2): p. 43-52.
145. Bellincampi, L.D., et al., *Viability of fibroblast-seeded ligament analogs after autogenous implantation*. J Orthop Res, 1998. **16**(4): p. 414-20.
146. Caruso, A.B., *A Collagen Fiber Tissue Engineering Scaffold for Anterior Cruciate Ligament Reconstruction*, in *Dept. of Biomedical Engineering/Dept. of Orthopaedic Surgery*. 2004, Rutgers University/University of Medicine and Dentistry of New Jersey: New Brunswick. p. 148.
147. Caruso, A.B. and M.G. Dunn, *Functional evaluation of collagen fiber scaffolds for ACL reconstruction: cyclic loading in proteolytic enzyme solutions*. J Biomed Mater Res, 2004. **69A**(1): p. 164-71.
148. Dunn, M.G., et al., *Anterior cruciate ligament reconstruction using a composite collagenous prosthesis. A biomechanical and histologic study in rabbits*. Am J Sports Med, 1992. **20**(5): p. 507-15.
149. Dunn, M.G., et al., *Development of fibroblast-seeded ligament analogs for ACL reconstruction*. J Biomed Mater Res, 1995. **29**(11): p. 1363-71.
150. Stenzel, K.H., T. Miyata, and A.L. Rubin, *Collagen as a biomaterial*. Annu Rev Biophys Bioeng, 1974. **3**(0): p. 231-53.
151. Malone, J.D., M. Richards, and J.J. Jeffrey, *Recruitment of peripheral mononuclear cells by mammalian collagenase digests of type I collagen*. Matrix, 1991. **11**(4): p. 289-95.
152. Albin, A. and B.C. Adelman-Grill, *Collagenolytic cleavage products of collagen type I as chemoattractants for human dermal fibroblasts*. Eur J Cell Biol, 1985. **36**(1): p. 104-7.
153. Adair-Kirk, T.L. and R.M. Senior, *Fragments of extracellular matrix as mediators of inflammation*. Int J Biochem Cell Biol, 2008. **40**(6-7): p. 1101-10.
154. Postlethwaite, A.E. and A.H. Kang, *Collagen-and collagen peptide-induced chemotaxis of human blood monocytes*. J Exp Med, 1976. **143**(6): p. 1299-307.
155. Doillon, C.J., et al., *Collagen-based wound dressings: control of the pore structure and morphology*. J Biomed Mater Res, 1986. **20**(8): p. 1219-28.
156. Lee, C.H., A. Singla, and Y. Lee, *Biomedical applications of collagen*. Int J Pharm, 2001. **221**(1-2): p. 1-22.
157. Radu, F.A., et al., *Modeling of drug release from collagen matrices*. J Pharm Sci, 2002. **91**(4): p. 964-72.
158. Weadock, K.S., D. Wolff, and F.H. Silver, *Diffusivity of 125I-labelled macromolecules through collagen: mechanism of diffusion and effect of adsorption*. Biomaterials, 1987. **8**(2): p. 105-12.
159. McPherson, J.M., *The utility of collagen-based vehicles in delivery of growth factors for hard and soft tissue wound repair*. Clin Mater, 1992. **9**(3-4): p. 225-34.
160. Weadock, K.S., et al., *Physical crosslinking of collagen fibers: comparison of ultraviolet irradiation and dehydrothermal treatment*. J Biomed Mater Res, 1995. **29**(11): p. 1373-9.

161. Wissink, M., et al., *Endothelial cell seeding on crosslinked collagen: effects of crosslinking on endothelial cell proliferation and functional parameters*. Thromb Haemost., 2000. **84**(2): p. 325-31.
162. Gorham, S.D., et al., *Effect of chemical modifications on the susceptibility of collagen to proteolysis. II. Dehydrothermal crosslinking*. Int J Biol Macromol, 1992. **14**(3): p. 129-38.
163. Weadock, K., R.M. Olson, and F.H. Silver, *Evaluation of collagen crosslinking techniques*. Biomater Med Devices Artif Organs, 1983. **11**(4): p. 293-318.
164. Olde Damink, L., et al., *Glutaraldehyde as a crosslink agent for collagen-based biomaterials*. J Mat Sci: Mat Med, 1995. **6**: p. 460-72.
165. Huang-Lee, L., D. Cheung, and M. Nimni, *Biochemical changes and cytotoxicity associated with the degradation of polymeric glutaraldehyde derived crosslinks*. J Biomed Mater Res., 1990. **24**(9): p. 1185-201.
166. Weadock, K.S., et al., *Effect of physical crosslinking methods on collagen-fiber durability in proteolytic solutions*. J Biomed Mater Res, 1996. **32**(2): p. 221-6.
167. Bourke, S.L. and J. Kohn, *Polymers derived from the amino acid L-tyrosine: polycarbonates, polyarylates and copolymers with poly(ethylene glycol)*. Adv Drug Deliv Rev, 2003. **55**(4): p. 447-66.
168. Brocchini, S., et al., *Structure-property correlations in a combinatorial library of degradable biomaterials*. J Biomed Mater Res, 1998. **42**(1): p. 66-75.
169. Jaffe, M., et al., *Process-structure-property relationships of erodable polymeric biomaterials: II - long range order in poly (desaminotyrosyl arylates)*. Polymer, 2003. **44**(19): p. 6033-6042.
170. Jaffe, M., et al., *Process-structure-property relationships of erodable polymeric biomaterials, I: Poly (desaminotyrosyl arylates)*. Polymers for Advanced Technologies, 2002. **13**(10-12): p. 926-937.
171. Gilles, M.A., A.Q. Hudson, and C.L. Borders, Jr., *Stability of water-soluble carbodiimides in aqueous solution*. Anal Biochem, 1990. **184**(2): p. 244-8.
172. Olde Damink, L.H., et al., *Cross-linking of dermal sheep collagen using a water-soluble carbodiimide*. Biomaterials, 1996. **17**(8): p. 765-73.
173. Richards, C., *A Novel Approach to Measurement of Human Meniscal Strain*, in *Department of Biomedical Engineering*. 2002, Rutgers University: Graduate School of New Brunswick: New Brunswick. p. 100.
174. Freshney, R., *Culture of Animal Cells: A Manual of Basic Technique*. 2 ed. 1987, New York: Alan R. Liss, Inc.
175. Tikku, M.L., et al., *Class II histocompatibility antigen-mediated immunologic function of normal articular chondrocytes*. J Immunol, 1985. **135**(5): p. 2923-8.
176. Webber, R.J., *In vitro culture of meniscal tissue*. Clin Orthop Relat Res, 1990(252): p. 114-20.
177. Mueller, S.M., et al., *Meniscus cells seeded in type I and type II collagen-GAG matrices in vitro*. Biomaterials, 1999. **20**(8): p. 701-9.
178. *CellTiter 96® AQueous Non-Radioactive Cell Proliferation Assay: INSTRUCTIONS FOR USE OF PRODUCTS G5421, G5430, G5440, G1111 AND G1112*. 2007, Promega Corporation.
179. Lohmander, L.S., et al., *Temporal patterns of stromelysin-1, tissue inhibitor, and proteoglycan fragments in human knee joint fluid after injury to the cruciate ligament or meniscus*. J Orthop Res, 1994. **12**(1): p. 21-8.
180. Amiel, D., et al., *Injury of the anterior cruciate ligament: the role of collagenase in ligament degeneration*. J Orthop Res, 1989. **7**(4): p. 486-93.
181. Fox, D.B., et al., *Fibrochondrogenesis of free intraarticular small intestinal submucosa scaffolds*. Tissue Eng, 2004. **10**(1-2): p. 129-37.

182. Mankin, H.J. and L. Lippiello, *Biochemical and metabolic abnormalities in articular cartilage from osteo-arthritic human hips*. J Bone Joint Surg Am, 1970. **52**(3): p. 424-34.
183. Newman, A.P., et al., *Mechanics of the healed meniscus in a canine model*. Am J Sports Med, 1989. **17**(2): p. 164-75.
184. Liu, X., et al., *Type III collagen is crucial for collagen I fibrillogenesis and for normal cardiovascular development*. Proc Natl Acad Sci U S A, 1997. **94**(5): p. 1852-6.
185. Chiquet, M., et al., *The chick and human collagen alpha1(XII) gene promoter--activity of highly conserved regions around the first exon and in the first intron*. Eur J Biochem, 1998. **257**(2): p. 362-71.
186. Tissakht, M. and A.M. Ahmed, *Tensile stress-strain characteristics of the human meniscal material*. J Biomech, 1995. **28**(4): p. 411-22.
187. Upton, M.L., et al., *Transfer of macroscale tissue strain to microscale cell regions in the deformed meniscus*. Biophys J, 2008. **95**(4): p. 2116-24.
188. Upton, M.L., et al., *Differential effects of static and dynamic compression on meniscal cell gene expression*. J Orthop Res, 2003. **21**(6): p. 963-9.
189. Imler, S.M., A.N. Doshi, and M.E. Levenston, *Combined effects of growth factors and static mechanical compression on meniscus explant biosynthesis*. Osteoarthritis Cartilage, 2004. **12**(9): p. 736-44.
190. Fink, C., et al., *The effect of dynamic mechanical compression on nitric oxide production in the meniscus*. Osteoarthritis Cartilage, 2001. **9**(5): p. 481-7.
191. Fermor, B., et al., *The effects of cyclic mechanical strain and tumor necrosis factor alpha on the response of cells of the meniscus*. Osteoarthritis Cartilage, 2004. **12**(12): p. 956-62.
192. Shin, S.J., et al., *Regulation of matrix turnover in meniscal explants: role of mechanical stress, interleukin-1, and nitric oxide*. J Appl Physiol, 2003. **95**(1): p. 308-13.
193. Hunter, C.J., et al., *Mechanical compression alters gene expression and extracellular matrix synthesis by chondrocytes cultured in collagen I gels*. Biomaterials, 2002. **23**(4): p. 1249-59.
194. Bourke, S.L., *A Tissue Engineering Approach to Anterior Cruciate Ligament Reconstruction*, in *Biomedical Engineering*. 2000, Rutgers University - Graduate School of New Brunswick: New Brunswick. p. 95.
195. Caruso, A.B. and M.G. Dunn, *Functional evaluation of collagen fiber scaffolds for ACL reconstruction: cyclic loading in proteolytic enzyme solutions*. J Biomed Mater Res A, 2004. **69**(1): p. 164-71.
196. Caruso, A.B. and M.G. Dunn, *Changes in mechanical properties and cellularity during long-term culture of collagen fiber ACL reconstruction scaffolds*. J Biomed Mater Res A, 2005. **73**(4): p. 388-97.
197. Richards, C., C. Gatt, and N. Langrana. *Functional Evaluation of the Human Meniscus*. in *Annals of Biomedical Engineering*. 2001.
198. Richards, C., et al. *Quantitative measurement of human meniscal strain*. in *Transactions of the 49th Annual Meeting of the Orthopaedic Research Society*. 2003.
199. Ahmed, A.M. and D.L. Burke, *In-vitro measurement of static pressure distribution in synovial joints--Part I: Tibial surface of the knee*. J Biomech Eng, 1983. **105**(3): p. 216-25.
200. Jones, R.S., et al., *Direct measurement of hoop strains in the intact and torn human medial meniscus*. Clin Biomech (Bristol, Avon), 1996. **11**(5): p. 295-300.

201. Radin, E.L. and R.S. Bryan, *The effect of weight-bearing on regrowth of the medial meniscus after meniscectomy*. J Trauma, 1970. **10**(2): p. 169-75.
202. Nakata, K., et al., *Human meniscus cell: characterization of the primary culture and use for tissue engineering*. Clin Orthop Relat Res, 2001(391 Suppl): p. S208-18.
203. Webber, R.J., M.G. Harris, and A.J. Hough, Jr., *Cell culture of rabbit meniscal fibrochondrocytes: proliferative and synthetic response to growth factors and ascorbate*. J Orthop Res, 1985. **3**(1): p. 36-42.
204. Bhargava, M.M., et al., *The effect of cytokines on the proliferation and migration of bovine meniscal cells*. Am J Sports Med, 1999. **27**(5): p. 636-43.
205. Pangborn, C.A. and K.A. Athanasiou, *Growth factors and fibrochondrocytes in scaffolds*. J Orthop Res, 2005. **23**(5): p. 1184-90.
206. Lietman, S.A., et al., *Effects of selected growth factors on porcine meniscus in chemically defined medium*. Orthopedics, 2003. **26**(8): p. 799-803.
207. Anderson, G.A., Hanson SR, Harker LA, Johnson RJ, Merritt K, Naylor PT, Schoen FJ, *Host Reactions to Biomaterials and Their Evaluation*, in *Biomaterials Science*, H.A. Ratner BD, Schoen FJ, Lemons JE, Editor. 1996, American Press. p. 165-173.
208. Tienen, T.G., et al., *Replacement of the knee meniscus by a porous polymer implant: a study in dogs*. Am J Sports Med, 2006. **34**(1): p. 64-71.
209. Schultz, G.S. and A. Wysocki, *Interactions between extracellular matrix and growth factors in wound healing*. Wound Repair Regen, 2009. **17**(2): p. 153-62.
210. Bruns, J., et al., *Autologous perichondral tissue for meniscal replacement*. J Bone Joint Surg Br, 1998. **80**(5): p. 918-23.
211. Kohn, D., et al., *Medial meniscus replacement by a tendon autograft. Experiments in sheep*. J Bone Joint Surg Br, 1992. **74**(6): p. 910-7.
212. Kelly, B.T., et al., *Hydrogel meniscal replacement in the sheep knee: preliminary evaluation of chondroprotective effects*. Am J Sports Med, 2007. **35**(1): p. 43-52.
213. Canham, W. and W. Stanish, *A study of the biological behavior of the meniscus as a transplant in the medial compartment of a dog's knee*. Am J Sports Med, 1986. **14**(5): p. 376-9.
214. Cook, J.L., et al., *Kinetic study of the replacement of porcine small intestinal submucosa grafts and the regeneration of meniscal-like tissue in large avascular meniscal defects in dogs*. Tissue Eng, 2001. **7**(3): p. 321-34.
215. Kelly, B.T., et al., *Meniscal allograft transplantation in the sheep knee: evaluation of chondroprotective effects*. Am J Sports Med, 2006. **34**(9): p. 1464-77.
216. Mundy, A., *Political Lobbying Drove FDA Process*, in *Wall Street Journal*. 2009: Washington.
217. Fluck, M., et al., *Tensile stress-dependent collagen XII and fibronectin production by fibroblasts requires separate pathways*. Biochim Biophys Acta, 2003. **1593**(2-3): p. 239-48.
218. Hooiveld, M., et al., *Short-term exposure of cartilage to blood results in chondrocyte apoptosis*. Am J Pathol, 2003. **162**(3): p. 943-51.
219. Jansen, N.W., et al., *Degenerated and healthy cartilage are equally vulnerable to blood-induced damage*. Ann Rheum Dis, 2008. **67**(10): p. 1468-73.
220. Jansen, N.W., et al., *Very rapid clearance after a joint bleed in the canine knee cannot prevent adverse effects on cartilage and synovial tissue*. Osteoarthritis Cartilage, 2009. **17**(4): p. 433-40.
221. Roosendaal, G., et al., *Cartilage damage as a result of hemarthrosis in a human in vitro model*. J Rheumatol, 1997. **24**(7): p. 1350-4.

222. Hiraoka, Y., et al., *Fabrication and biocompatibility of collagen sponge reinforced with poly(glycolic acid) fiber*. Tissue Eng, 2003. **9**(6): p. 1101-12.
223. Pieper, J.S., et al., *Development of tailor-made collagen-glycosaminoglycan matrices: EDC/NHS crosslinking, and ultrastructural aspects*. Biomaterials, 2000. **21**(6): p. 581-93.
224. Murray, M.M., et al., *Enhanced histologic repair in a central wound in the anterior cruciate ligament with a collagen-platelet-rich plasma scaffold*. J Orthop Res, 2007. **25**(8): p. 1007-17.
225. Murray, M.M., et al., *Collagen-platelet rich plasma hydrogel enhances primary repair of the porcine anterior cruciate ligament*. J Orthop Res, 2007. **25**(1): p. 81-91.
226. Murray, M.M., et al., *Use of a collagen-platelet rich plasma scaffold to stimulate healing of a central defect in the canine ACL*. J Orthop Res, 2006. **24**(4): p. 820-30.

**APPENDIX 1**

The following is the pattern layout for meniscus scaffolds. For each pattern, a double stranded, continuous length of polymer fiber is used. The first pattern listed is laid down first, the second next, and so on.

MS500 Scaffolds:

Order	Pattern ID
1	Pattern # 1 157.5°
2	Pattern # 6 33.75°
3	Pattern # 2 123.75°
4	Pattern # 6 33.75°
5	Pattern # 1 157.5°
6	Pattern # 6 33.75°
7	Pattern # 3 101.25°
8	Pattern # 6 33.75°
9	Pattern # 4 78.75°
10	Pattern # 1 157.5°
11	Pattern # 1 157.5°
12	Pattern # 5 56.25°
13	Pattern # 2 123.75°
14	Pattern # 5 56.25°
15	Pattern # 1 157.5°
16	Pattern # 4 78.75°
17	Pattern # 5 56.25°
18	Pattern # 3 101.25°
19	Pattern # 5 56.25°
20	Pattern # 1 157.5°
21	Pattern # 1 157.5°
22	Pattern # 4 78.75°
23	Pattern # 2 123.75°
24	Pattern # 1 157.5°

25	Pattern # 4 78.75°
26	Pattern # 3 101.25°
27	Pattern # 4 78.75°
28	Pattern # 2 123.75°
29	Pattern # 1 157.5°
30	Pattern # 3 101.25°
31	Pattern # 1 157.5°
32	Pattern # 2 123.75°
33	Pattern # 3 101.25°
34	Pattern # 2 123.75°
35	Pattern # 3 101.25°
36	Pattern # 1 157.5°
37	Pattern # 2 123.75°
38	Pattern # 3 101.25°
39	Pattern # 2 123.75°
40	Pattern # 1 157.5°
41	Pattern # 2 123.75°
42	Pattern # 1 157.5°
43	Pattern # 2 123.75°
44	Pattern # 1 157.5°
45	Pattern # 2 123.75°
46	Pattern # 1 157.5°
47	Pattern # 1 157.5°
48	Pattern # 1 157.5°
49	Pattern # 1 157.5°

MS1000 scaffolds:

Order	Pattern ID
1	Pattern # 1 157.5°
2	Pattern # 6 33.75°
3	Pattern # 2 123.75°
4	Pattern # 6 33.75°
5	Pattern # 5 56.25°
6	Pattern # 1 157.5°
7	Pattern # 6 33.75°
8	Pattern # 3 101.25°
9	Pattern # 6 33.75°
10	Pattern # 4 78.75°
11	Pattern # 1 157.5°
12	Pattern # 6 33.75°
13	Pattern # 2 123.75°
14	Pattern # 6 33.75°
15	Pattern # 4 78.75°
16	Pattern # 1 157.5°
17	Pattern # 6 33.75°
18	Pattern # 3 101.25°
19	Pattern # 6 33.75°
20	Pattern # 1 157.5°
21	Pattern # 5 56.25°
22	Pattern # 2 123.75°
23	Pattern # 5 56.25°
24	Pattern # 1 157.5°
25	Pattern # 4 78.75°
26	Pattern # 5 56.25°
27	Pattern # 3 101.25°
28	Pattern # 5 56.25°
29	Pattern # 1 157.5°
30	Pattern # 2 123.75°
31	Pattern # 5 56.25°
32	Pattern # 4 78.75°
33	Pattern # 5 56.25°
34	Pattern # 1 157.5°
35	Pattern # 3 101.25°
36	Pattern # 5 56.25°
37	Pattern # 2 123.75°
38	Pattern # 5 56.25°
39	Pattern # 1 157.5°
40	Pattern # 4 78.75°
41	Pattern # 2 123.75°
42	Pattern # 1 157.5°
43	Pattern # 4 78.75°

44	Pattern # 3 101.25°
45	Pattern # 4 78.75°
46	Pattern # 2 123.75°
47	Pattern # 1 157.5°
48	Pattern # 4 78.75°
49	Pattern # 3 101.25°
50	Pattern # 4 78.75°
51	Pattern # 2 123.75°
52	Pattern # 1 157.5°
53	Pattern # 4 78.75°
54	Pattern # 3 101.25°
55	Pattern # 4 78.75°
56	Pattern # 1 157.5°
57	Pattern # 3 101.25°
58	Pattern # 1 157.5°
59	Pattern # 2 123.75°
60	Pattern # 3 101.25°
61	Pattern # 2 123.75°
62	Pattern # 3 101.25°
63	Pattern # 1 157.5°
64	Pattern # 2 123.75°
65	Pattern # 3 101.25°
66	Pattern # 2 123.75°
67	Pattern # 3 101.25°
68	Pattern # 1 157.5°
69	Pattern # 2 123.75°
70	Pattern # 3 101.25°
71	Pattern # 2 123.75°
72	Pattern # 1 157.5°
73	Pattern # 2 123.75°
74	Pattern # 1 157.5°
75	Pattern # 2 123.75°
76	Pattern # 1 157.5°
77	Pattern # 2 123.75°
78	Pattern # 1 157.5°
79	Pattern # 2 123.75°
80	Pattern # 1 157.5°
81	Pattern # 2 123.75°
82	Pattern # 1 157.5°
83	Pattern # 2 123.75°
84	Pattern # 1 157.5°
85	Pattern # 1 157.5°
86	Pattern # 1 157.5°

## CURRICULUM VITA

**Eric Andrew Balint**

### EDUCATION

- May 2002      **B.S.**, Mechanical Engineering  
Rutgers University, School of Engineering  
New Brunswick, New Jersey
- October 2009      **Ph.D.**, Biomedical Engineering  
Rutgers University/University of Medicine and Dentistry of New Jersey  
New Brunswick, New Jersey

### EXPERIENCE

- 1999-2002      **Laboratory Technician**  
Nanopowder Enterprises Inc  
Piscataway, New Jersey
- 2002-2009      **Graduate Research Assistant**  
Department of Orthopaedic Surgery  
Robert Wood Johnson Medical School  
University of Medicine and Dentistry of New Jersey  
New Brunswick, New Jersey

### PUBLICATIONS AND PRESENTATIONS

- 2008      **Balint EB**, Dunn MG, Gatt CJ. Development of a Tissue Engineered Meniscus Replacement. Presented at the 9<sup>th</sup> New Jersey Symposium on Biomaterials Science and Regenerative Medicine; New Brunswick, NJ.
- 2008      **Balint EB**, Dunn MG, Gatt CJ. Development of a Tissue Engineered Meniscus Replacement. Presented at the 26<sup>th</sup> Army Science Conference; Orlando, FL.
- 2009      **Balint EB**, Dunn MG, Gatt CJ. Development of a Tissue Engineered Meniscus Replacement. Presented at the 2009 Armed Forces Institute of Regenerative Medicine (AFIRM) All Hands Meeting; Tampa, FL.
- 2009      **Balint EB**, Dunn MG, Gatt CJ. Development of a Fiber Reinforced Meniscus Scaffold. Presented at the 55<sup>th</sup> Annual Meeting of the Orthopaedic Research Society; Las Vegas, NV.

- 2009 University of Medicine and Dentistry of New Jersey, Gatt CJ, **Balint EB**, Dunn MG. Tissue Engineered Fibrocartilage Replacement. Patent Pending, International Application Number PCT/US09/45985, filed 2 June 2009.
- 2009 **Balint EB**, Dunn MG, Gatt CJ. Mechanical Evaluation of a Fiber-Reinforced Scaffold for Meniscus Replacement. Submitted for publication.
- 2009 **Balint EB**, Dunn MG, Gatt CJ. *In Vitro* and Preliminary *In Vivo* Evaluation of a Fiber-Reinforced Scaffold for Meniscus Replacement. Submitted for publication.